SUPPLEMENTO
AL VOLUME XV, SERIE X, DEL
NUOVO CIMENTO
A CURA DELLA SOCIETÀ ITALIANA DI FISICA

1960 | Iº Trimestre | N. 2

Fading of Minimum Tracks in Ilford G-5 and K-5 Emulsions.

B. JUDEK

Division of Pure Physics, National Research Council - Ottawa

(ricevuto il 12 Maggio 1959)

Summary. — The fading of plateau electron tracks in Ilford G-5 and K-5 emulsions, stored after exposure at temperatures of 20 °C, — 1 °C, — 18 °C and — 40 °C, has been compared. It has been found that the same initial grain densities are obtained on tracks in both G-5 and K-5 emulsions with identical development one day after the exposure, while the rate of fading is lower in K-5 than G-5 emulsions. The results also show that the rates of fading in both emulsions are much higher at 68 °F than at the lower temperatures. After four weeks at 20 °C there is a marked effect, the reduction in blob densities being 41% in G-5 and 38% in K-5 emulsions. In emulsions stored at 0 °F, on the other hand, even for 2½ months after the exposure, easily recognizable electron tracks have been obtained with blob densities reduced by only 18% and 13.5% respectively. No significant difference between the rates of fading at — 1 °C, — 18 °C and — 40 °C could be detected. It was also found that fading is much more rapid during the first two weeks after the exposure than during a later period.

1. - Introduction.

In work involving exposures of stacks of nuclear emulsions a delay between exposure and processing is often unavoidable, due, either to the necessity of transportation or to inadequate facilities for processing of the whole stack at once. Such a delay usually causes a reduction of grain densities of tracks in the emulsion due to fading of the latent image. A number of investigations (1) have been made, especially on fading of α-particle and proton tracks

(1) P. DEMERS: *Ionographie* (Montreal, 1938), p. 186.

in the region in which the specific energy loss of the particles exceeds several times that at minimum ionization. These have shown that, in general, high temperature, humidity and oxidation cause an increase in the rate of fading. Measurements of long term fading of tracks (over a period of about one year) of particles with about minimum ionization in G-5 emulsions have been made by BARRON and WOLFENDALE [2], using 950 MeV protons and cosmic ray μ-mesons.

The purpose of the present work was to study the reduction of grain densities due to delay of processing on tracks of particles at minimum ionization in Ilford G-5 and especially in the more recently introduced K-5 emulsions, and to determine for how long the exposed emulsions can be kept without processing and at what temperature they should be stored in order to minimize the fading effects. The observations were carried out up to a period of seventy-seven days after exposure.

2. – Experimental details.

Several small stacks of Ilford G-5 and K-5 stripped emulsions, 600 μm thick, have been exposed to (300÷700) MeV electrons and positrons from the Cornell synchrotron. At the time of the exposure the emulsions were three weeks old and most of the time prior to the exposure they had been stored at — 1 °C. The exposure itself took place at room temperature. After the exposure the emulsions were transported under refrigeration (in an insulated box containing solid CO_2). In order to prevent any variations in the moisture content of the emulsions and to protect them from oxidation, the stacks were kept all the time during exposure, transport and subsequent storage in air-tight polythene bags.

One G-5 and one K-5 emulsion were developed on the day following the exposure. The remaining emulsions were placed in rooms kept at controlled temperatures of 20 °C, — 1 °C and — 18°C. One emulsion from each stack of G-5 and K-5 emulsions was processed after two weeks and again after four weeks. Some emulsions stored at — 18 °C were kept until eleven weeks after the exposure. In order to obtain a comparison between the amount of fading at — 18 °C and at — 40 °C, a few G-5 and K-5 emulsions, which had previously been stored at — 18 °C, were placed in — 18 °C and — 40 °C rooms and developed after eight weeks. A standard method of development was used throughout. It consisted of presoaking the emulsions for two hours in distilled water at 3 °C, three hours in amidol developer with boric acid [3] at 3 °C, a dry

---

[2] W. C. BARRON and A. W. WOLFENDALE: *Brit. Journ. Appl. Phys.*, **8**, 297 (1954).

[3] C. C. DILWORTH, G. OCCHIALINI and L. VERMAESEN: *Bulletin du Centre de Physique Nucleaire de l'Université de Bruxelles*, Note 13*a* (1950).

warm stage of development of 45 minutes at 24 °C followed by a 1% acetic acid stop bath for two hours at 3 °C. The emulsions were mounted on glass shortly ((30 ÷ 60) minutes) before processing in order to reduce any additional fading which might be caused by moisture introduced at this stage.

About 5000 blobs were counted on the electron tracks in each plate. Care was taken that they should be evenly distributed throughout the whole depth of emulsion.

3. – Results and discussion.

The values of the blob densities on the electron tracks obtained in emulsions stored for different times at different temperatures are given in Tables I and II. The fading curves for G-5 and K-5 emulsions stored at room tem-

TABLE I. – *Blob densities* (*) *on plateau electron tracks in Ilford* G-5 *and* K-5 *emulsions stored at different temperatures.*

Time after exposure	Type of emulsion	Storage temperatures		
		20 °C	— 1 °C	— 18 °C
1 day	G-5		23.0 ± 0.3	
	K-5		23.3 ± 0.3	
2 weeks	G-5	15.0 ± 0.3	20.1 ± 0.3	20.4 ± 0.3
	K-5	16.3 ± 0.3	21.3 ± 0.3	20.3 ± 0.3
4 weeks	G-5	13.5 ± 0.3	19.7 ± 0.3	19.8 ± 0.3
	K-5	14.5 ± 0.3	21.2 ± 0.3	21.1 ± 0.3
11 weeks	G-5			18.9 ± 0.3
	K-5			20.2 ± 0.3

(*) Blobs per 100 μm.

TABLE II. – *Blob densities* (*) *on plateau electron tracks in Ilford* G-5 *and* K-5 *emulsions stored for eight weeks at* — 1 °C *and* — 40 °C.

Type of emulsion	Storage temperatures	
	— 18 °C	— 40 °C
G-5	20.3 ± 0.3	20.8 ± 0.3
K-5	22.1 ± 0.3	22.7 ± 0.3

(*) Blobs per 100 μm.

perature 20 °C and the lower temperatures (with results for —1 °C and —18 °C combined since there is no significant difference between them) are shown in Fig. 1. It can be noticed that the blob density in the K-5 emulsions stored for two weeks at —18 °C in Table I appears to be slightly too low, and all four values of blob densities in Table II too high, in comparison with other values shown in the Tables. These discrepancies could be attributed to accidental variations in the development or moisture content during storage of the emulsions concerned, but they do not affect the general conclusions.

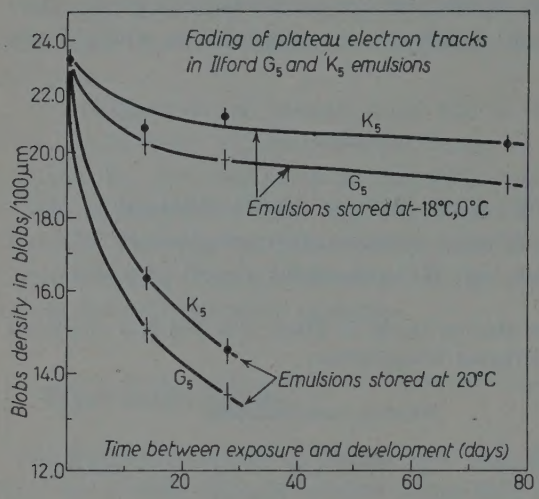

Fig. 1.

These results show that:

1) The rate of fading is much higher during the first two weeks after the exposure than during a later period. The present results for G-5 emulsions, in so far as they are comparable, are in satisfactory agreement with those of BARRON and WOLFENDALE [2].

2) With the same development, the same initial grain densities on minimum tracks are obtained in G-5 and K-5 emulsions. The rate of fading, on the other hand, is under thes ame conditions lower in K-5 that G-5 emulsions.

3) Fading is much more rapid at 20 °C than at —1 °C or lower temperatures. After four weeks at 20 °C the plateau electron tracks have almost vanished; the reduction in blob densities was 41% in G-5 and 38% in K-5 emulsions. With storage at —1 °C or —18 °C, on the other hand, the blob densities were reduced only by 14% and 8% respectively. Further, the results for emulsions kept for eleven weeks at —18 °C show that even with such a long delay of processing, good minimum tracks can be obtained in both G-5 and K-5 emulsions if they have been stored at a low temperature.

4) There appears to be no significant difference in the rates of fading at —1 °C, —18 °C and —40 °C.

Qualitative examination of the plates has also shown some deterioration of the clarity of emulsions if processing is delayed. This appears to be due

mainly to accumulation of background tracks. It seems also that more development fog is formed.

I may be concluded that, although there is a definite advantage, both in higher grain densities and in the quality of the processed emulsions, in developing emulsions very soon after exposure, sufficient grain densities on minimum tracks can be obtained in G-5 and K-5 emulsions processed two and one-half months, or even longer, after the exposure if the emulsions are kept at — 1 °C or at a lower temperature and are protected from moisture. There does not seem to be, on the other hand, any further advantage in storing exposed emulsions at temperatures lower than — 1 °C.

* * *

I wish to thank Dr. P. Connolly and Dr. G. Lynch, High Energy Laboratory, Cornell University, for arranging the exposure of the emulsion stacks at the electron synchrotron.

RIASSUNTO (*)

È stata messa a raffronto l'attenuazione delle tracce di elettroni di soglia su emulsioni G-5 e K-5, emulsioni conservate, dopo esposizione, alle temperature di 20 °C, — 1 °C, — 18 °C e — 40 °C. Si è riscontrato che si ottengono le stesse densità iniziali dei granuli sia sulle tracce dell'emulsione G-5 che su quelle dell'emulsione K-5, con identico sviluppo un giorno dopo l'esposizione, mentre il grado di attenuazione è minore nelle emulsioni K-5 rispetto a quelle G-5. I risultati mostrano anche che i gradi di attenuazione in entrambe le emulsioni, sono molto più elevati a 20 °C che a temperature più basse. Dopo quattro settimane, a 20 °C, vi è un effetto rimarchevole, in quanto la riduzione delle densità dei blob è del 41% per l'emulsione G-5, e del 38% per l'emulsione K-5. D'altra parte, nelle emulsioni conservate a — 18 °C, si sono ottenute anche due mesi e mezzo dopo l'esposizione, tracce facilmente riconoscibili di elettroni con densità dei blob ridotte rispettivamente del 18 e del 13.5%. Non si è potuta rivelare alcuna significativa differenza fra i gradi di attenuazione a — 1 °C, — 18 °C e — 40 °C. Si è anche trovato che l'attenuazione è molto più rapida durante le prime due settimane dopo l'esposizione, di quanto non lo sia durante l'ultimo periodo.

(*) *Traduzione a cura della Redazione.*

SUPPLEMENTO AL VOLUME XV, SERIE X
DEL NUOVO CIMENTO

N. 2, 1960
1° Trimestre

A Simple Finder Attachment to a Microscope. Useful in the Examination of Grid-Backed Nuclear Emulsion Plates, or Glass Slides.

W. B. LASICH

Physics Department, University College - London

(ricevuto il 15 Luglio 1959)

Summary. — A microscope attachment which facilitates the reading of the position coordinates associated with nuclear events located in photographic emulsions is described. By diversion of light into a small finder telescope an image corresponding to the plane of the reference grid may be independently sighted, thus eliminating the need for readjustments of the microscope.

To assist in the location of microscope events it is common for glass backed nuclear emulsions to be provided with a numbered grid attachment to the reverse side. It is usual practice to read off map co-ordinates from this grid with the assistance of a long focus objective. Alternatively, a specially constructed eyepiece may be inserted temporarily for this purpose.

In work of high precision (*e.g.* the grain counting or scattering of nuclear emulsion tracks) it is inconvenient however if in the course of the measurements the image has to be displaced while objective or eyepiece is changed.

The present arrangement obviates these difficulties. It requires the use of a reflex microscope head (with tilting mirror), such as is available from a number of makers. This facility is normally intended to provide the means for projection of the image, or for microphotography. In normal operation the observer sights through the inclined eyepiece E_1 (Fig. 1) which receives the light beam from the face of the mirror diagonal (M). With the mirror swung aside into the position M', a vertical light beam is available through an aperture cen-

tered on the optical axis of the objective. In the present application the light pencil from the objective is reconverged with a positive lens (L) of about 10 cm focal length, so that a real image of the object plane AA' (located at the position of the grid) may be examined with the aid of an auxiliary finder

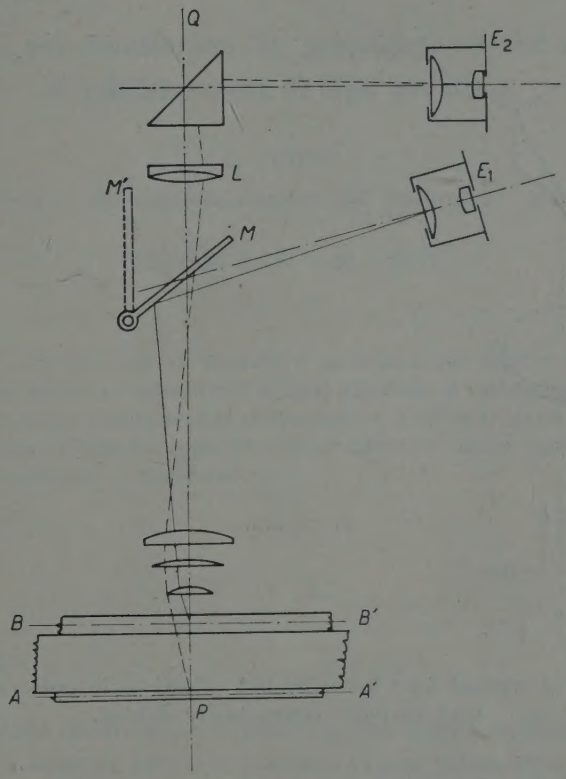

Fig. 1. – The arrangement by which a finder eyepiece (shown at E_2) may be used to view the rear grid (at AA').

eyepiece E_2, while the normal eyepiece E_1 provides an image corresponding to the focal plane BB' at some point within the photographic layer.

Since the finder operates at a comparatively low magnification the image brightness is such that if a small part only of the light is allowed past the inclined mirror via PQ, the grid may be clearly visible without the necessity of switching the beam from the normal eyepiece. When the finder is correctly adjusted the grid should remain substantially in focus over the normal working range of the objective. If different objectives however are to be employed, a refocussing of the image of the grid will then be necessary. This

can be effected by provision for displacement of L, or by use of a subsidiary lens.

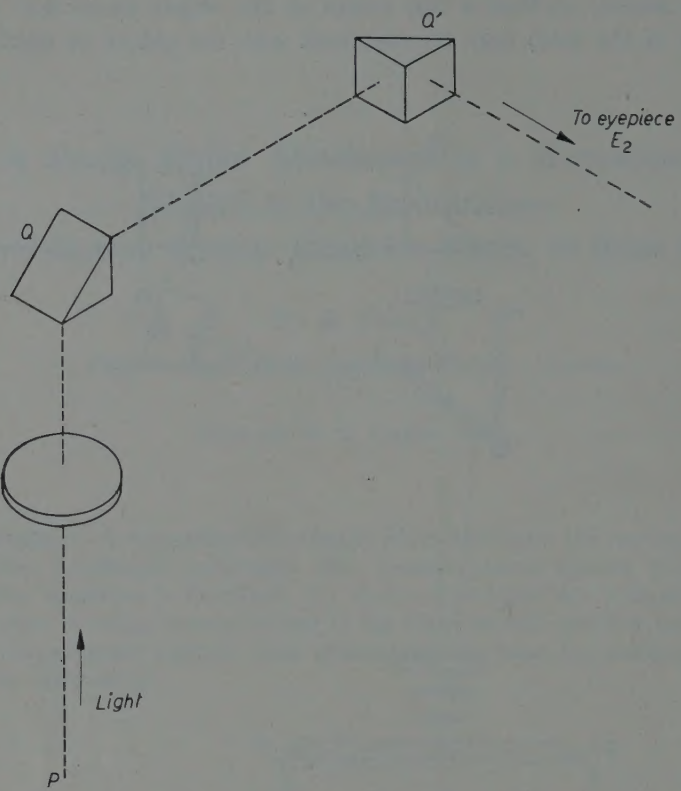

Fig. 2. – Folding of vertical light beam by 90° reflections in order that the eyepiece may be more conveniently sighted.

In order to bring the finder eyepiece into a convenient position the light path may be folded around with the use of a pair of right-angle reflector prisms (as in Fig. 2). If swivel movements of the finder tube are provided about axes PQ and QQ', the eyepiece can be adjusted in position so as to suit individual requirements.

RIASSUNTO

Si descrive un accessorio per il microscopio che facilita la lettura delle coordinate degli eventi nucleari che hanno luogo nelle emulsioni fotografiche. Deviando la luce in un piccolo cannocchiale localizzatore si può osservare indipendentemente un'immagine corrispondente al piano del reticolo di riferimento, eliminando così la necessità di spostare la messa a fuoco del microscopio.

SUPPLEMENTO AL VOLUME XV, SERIE X
DEL NUOVO CIMENTO

N. 2, 1960
1° Trimestre

Circuiti per accelerare la propagazione del riporto in addizionatori di tipo parallelo.

L. DADDA

Istituto di Elettrotecnica Generale del Politecnico - Milano

(ricevuto il 16 Luglio 1959)

Riassunto. — Dopo aver richiamato il problema del riporto negli addizionatori per macchine calcolatrici di tipo parallelo, si riassumono i metodi finora proposti per accelerarne la propagazione. Inoltre si espone un nuovo metodo basato sull'uso di organi di commutazione di comportamento simile ai relé, per esempio i transistori.

1. – Introduzione.

Nelle calcolatrici elettroniche numeriche, due sono i modi con cui i numeri (rappresentati da impulsi elettrici) possono venire trasmessi e manipolati: la trasmissione di tipo *serie*, in cui gli impulsi rappresentanti le cifre significative (binarie) si succedono nel tempo a cominciare dalla cifra meno significativa, utilizzando una unica linea; la tramissione di tipo *parallelo*, in cui i vari impulsi vengono trasmessi contemporaneamente su altrettante linee.

A parità di tipo di circuiti usati, le macchine di tipo parallelo risultano più veloci delle macchine di tipo serie: queste ultime, d'altra parte, risultano in generale più economiche, poichè lo stesso circuito può servire per la manipolazione delle successive cifre, mentre nelle macchine di tipo parallelo sono necessari tanti circuiti quante sono le cifre componenti il numero.

La velocità delle macchine parallelo non risulta però, rispetto a quelle di tipo serie, proporzionalmente maggiore per tutti i tipi di operazioni che si eseguono nelle calcolatrici. Mentre infatti in certi casi, per esempio nella estrazione o nella registrazione di un numero nella memoria, le macchine di tipo

serie impiegano in generale, a parità di tipo di circuito, un tempo n volte maggiore (essendo n il numero delle cifre binarie componenti il numero) delle macchine parallelo, in altre operazioni, esempio tipico nella somma di due numeri, il rapporto tra i due tempi risulta molto minore di n. Ciò è dovuto, come è ben noto, al fatto che il riporto, eventualmente prodotto nella somma delle cifre meno significative, può influire sulle cifre più significative della somma, propagandosi attraverso tutte le cifre intermedie.

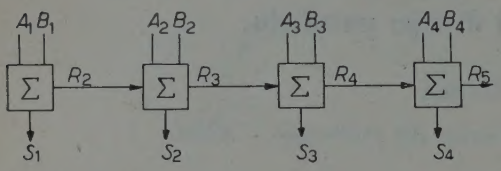

Fig. 1.

Il processo della somma di due numeri binari può venire infatti realizzato, nella sua forma più semplice, come è mostrato schematicamente nella Fig. 1 cioè mediante il collegamento di tanti « sommatori binari completi », ciascuno atto a produrre una cifra della somma, S_i, e l'eventuale riporto R_{i+1}, mediante le cifre corrispondenti, A_i e B_i degli addendi, ed il riporto, R_{i+1}, dal sommatore precedente. Le equazioni di funzionamento del sommatore binario semplice, scritte per esempio nella forma canonica di Boole, sono le seguenti (1):

$$(1) \qquad \begin{cases} S_i = A_i\bar{B}_i\bar{R}_i + \bar{A}_iB_i\bar{R}_i + \bar{A}_i\bar{B}_iR_i + A_iB_iR_i\,, \\ R_{i+1} = A_iB_iR_i + A_iB_i\bar{R}_i + \bar{A}_iB_iR_i + A_i\bar{B}_iR_i\,. \end{cases}$$

Tali equazioni, od altre che si ricavano da esse, sono realizzabili con vari tipi di circuiti.

Di questi ci interessa mettere qui in evidenza il ritardo con cui si produce il segnale di uscita rispetto all'istante in cui si applicano i segnali di entrata. Tale ritardo è dovuto a varie cause: nei circuiti con tubi e raddrizzatori, alle capacità parassite ed alle costanti di tempo con queste associate; nei circuiti a transistori, oltre alle capacità parassite ed alle costanti di tempo, alla dipendenza dalla frequenza dei parametri dei transistori; nei circuiti in cui il transistore viene portato in saturazione, al tempo (« storage time ») necessario a libe-

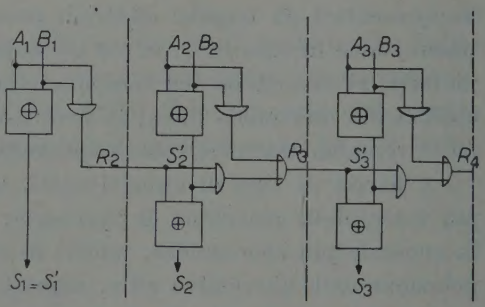

Fig. 2.

(1) Vedi per esempio: R. K. Richards: *Arithmetic operations in digital computers.* (New York, 1955)

rare la base dall'eccesso di cariche minoritarie; nei circuiti utilizzanti nuclei magnetici, al cosiddetto tempo di inversione (« switching time »).

Nella Fig. 2 è riportato uno dei possibili schemi con cui si può realizzare il sommatore binario parallelo: in esso si fa uso dei circuiti atti a realizzare la somma ed il prodotto logico di variabili binarie, nonchè di circuiti per ottenere la « somma modulo due ».

La struttura del circuito discende immediatamente dalla seguente forma delle equazioni del sommatore, nelle quali si fa uso del simbolo della operazione di somma modulo due ($\oplus$) [2]:

$$(2)\qquad \begin{cases} S_i = (A_i\cdot\bar{B}_i + \bar{A}_i\cdot B_i)\cdot\bar{R}_i + (\bar{A}_i\cdot\bar{B}_i + A_i\cdot B_i)\cdot\bar{R}_i = \\ \quad = (A_i \oplus B_i)\cdot\bar{R}_i + \overline{(A_i \oplus B_i)}\cdot R_i = (A_i \oplus B_i) \oplus R_i\,, \\ R_{i+1} = A_i\cdot B_i\cdot(R_i + \bar{R}_i) + (A_i\bar{B}_i + \bar{A}_iB_i)\cdot R_i = \\ \quad = A_i\cdot B_i + (A_i \oplus B_i)\cdot R_i\,. \end{cases}$$

Dalla osservazione della seconda delle (2), o dei circuiti che la realizzano, si vede come il segnale rappresentante il riporto che si produce in uno stadio generico, l'i-esimo, possa dipendere anche dalle cifre meno significative A_1, B_1, degli addendi. Con altre parole il riporto eventualmente prodotto nel primo stadio del sommatore (Fig. 2.) può influire sul valore del riporto all'ultimo stadio, attraverso una catena di circuiti, tanto più lunga quanto maggiori sono le cifre binarie rappresentanti i numeri da sommare.

Tale è il caso quando i due numeri da sommare siano i seguenti:

$$A = 1\ 1\ 1\ 1\ 1\,,$$

$$B = 0\ 0\ 0\ 0\ 1\,.$$

È importante osservare che, comunque si manipolino le equazioni del sommatore per trasformare i relativi circuiti, si può mostrare come il segnale di riporto attraversa sempre almeno due circuiti per ogni stadio del sommatore: nel caso della Fig. 2, tali circuiti sono costituiti da una somma logica e da un prodotto logico. Pertanto, e a meno di ricorrere ad espedienti di vario tipo, che verranno illustrati brevemente nel successivo punto, se si vuole

---

[2] Si ricorda che valgono le seguenti relazioni:

$$A \oplus B = A\cdot\bar{B} + \bar{A}\cdot B; \qquad \overline{(A \oplus B)} = \bar{A}\cdot\bar{B} + A\cdot B\,.$$

aumentare la velocità di funzionamento del sommatore parallelo, si devono realizzare i circuiti di propagazione del riporto in modo da minimizzare il ritardo introdotto da ciascuno.

2. – Metodi per accelerare il funzionamento del sommatore binario di tipo parallelo.

Da quanto detto al punto precedente, risulta come il massimo intervallo di tempo da assegnare alla propagazione del segnale di riporto sia quello relativo alla intera catena di stadi, di cui è composto il sommatore. In una macchina sincrona, cioè in una macchina in cui gli intervalli di tempo assegnati a ciascuna operazione sono prefissati ed indipendenti dalla particolare struttura dei numeri in ogni singola operazione, il tempo impiegato per l'addizione dovrà perciò tener conto di tale intervallo, anche quando, per esempio, vi siano da sommare due numeri di struttura tale da non produrre riporto in nessuno degli stadi del sommatore.

Burks, Goldstine e von Neumann ([3]) hanno mostrato come, nella somma di due numeri binari di 40 bit, il riporto si propaga in media solamente di 4,62 posti, per cui, nella macchina sincrona con tempo di operazione fisso, l'addizione risulta in media molte volte più lunga del necessario.

È infatti possibile pensare ad un circuito, il quale segnali di volta in volta il completamento del processo di propagazione del riporto, in modo che il tempo di esecuzione della somma dipende dalla effettiva struttura dei numeri: si ha così, nel processo di addizione, un funzionamento detto asincrono. Tale possibilità è stata realizzata da Gilchrist, Pomerene e Wong ([4]).

Il circuito proposto da questi autori non risolve tuttavia completamente il problema del sommatore parallelo rapido, in quanto il riporto, quando esso deve propagarsi, è ancora soggetto ai ritardi introdotti dai circuiti del sommatore.

Una soluzione teoricamente completa del problema è stata invece proposta da Weinberger e Smith ([5]), e si basa sulla seguente considerazione. Il riporto, R_{i+1}, prodotto da uno stadio, l'i-esimo, del sommatore dipende: dalle cifre A_i e B_i dei numeri da sommare relative allo stesso stadio, e dal riporto R_i

([3]) A. W. Burks, H. H. Goldstine and J. von Neumann: *Preliminary discussion of the logical design of an electronic computing instrument* (Princeton, 1946).

([4]) B. Gilchrist, J. H. Pomerene e S. Y. Wong: *Fast carry logic for digital computers*. IRE Trans. on Electronic Computers, vol. EC-4, no. 4, p. 133 (Dicembre 1956).

([5]) A. Weinberger e J. L. Smith: *A one microsecond adder using one microsecond circuitry*. IRE Trans. on Electronic Computers, vol. EC-5, no. 2, p. 65 (Giugno 1956).

prodotto dallo stadio precedente. Quest'ultimo, a sua volta, dipenderà da A_{i-1}, B_{i-1} e da R_{i-1}, e così via.

Pertanto R_{i+1} è funzione, oltre che di A_i e B_i, delle cifre A_{i-1}, A_{i-2}, A_{i-3}, ..., A_1; B_{i-1}, B_{i-2}, ..., B_1. Supponendo allora di aver scritto tale funzione per ciascun R_i, e di avere realizzato i relativi circuiti, si vede come tutti i riporti possano essere determinati simultaneamente.

In pratica non è però possibile realizzare completamente tale idea, per la complessità dei circuiti necessari.

Tuttavia, anche sfruttandola parzialmente, è possibile realizzare un sommatore parallelo molto rapido, e si rimanda alla bibliografia per maggiori particolari.

Infine, un'altra soluzione del problema di cui si tratta merita di essere qui illustrata: quella realizzata nella macchina recentemente costruita nella Università dell'Illinois ([6]).

Tale soluzione si basa sulle seguenti considerazioni: si supponga, di introdurre, nel circuito sommatore della Fig. 2, degli elementi di memoria binari (flip-flop), in modo che i riporti R_i generati nella prima fase della somma, anzichè essere « assimilati » con le cifre della semisomma per fornire la somma, vengano ivi accumulati. L'insieme degli elementi di memoria R_i costituisce un registro, il registro dei riporti. Analogamente, le cifre della semisomma sono accumulate in un apposito registro, S'.

Il numero rappresentante la somma è così dato dall'insieme delle cifre contenute nei registri R ed S': per ottenerlo esplicitamente, occorre procedere all'assimilazione dei riporti, operazione nella quale si può avere la propagazione dei riporti stessi.

È ora importante notare che, se si vuole sommare un altro numero al numero contenuto in R ed S', per ottenere ancora in R ed S' la somma in forma non assimilata, *non si produce propagazione del riporto*. Pertanto, dovendo sommare molti numeri, conviene prima determinare la somma in tale forma: per ottenerla nella forma consueta occorrerà una sola volta, alla fine, produrre la assimilazione del riporto.

Per maggiori particolari sul principio, qui appena enunciato, si rimanda alla bibliografia ([6]). Si deve però osservare che la soluzione basata sulla rappresentazione dei numeri binari con riporto non assimilato offre effettivi vantaggi solamente quando occorra fare la somma di più di due numeri: esempio tipico nel processo di moltiplicazione di due numeri binari, ottenuta per somme successive del moltiplicando opportunamente incolonnato. Inoltre si deve osservare che il sommatore esige l'uso di un numero doppio di celle di memorie binarie per la rappresentazione della somma in forma « non assimilata ».

([6]) *On the design of a very high-speed computer.* University of Illinois Digital Computer Laboratory, Report no. 80, p. 194 e seg (Ottobre 1957).

3. – Una nuova soluzione del problema del sommatore parallelo rapido.

Elencati così i progressi finora compiuti per la soluzione del problema del sommatore parallelo, se ne illustrerà una nuova soluzione, che sembra offrire significativi vantaggi rispetto alle precedenti (7).

Per illustrare il principio su cui essa è basata, si consideri la Fig. 3, che rappresenta un sommatore parallelo. Per confronto con lo schema della Fig. 2, si osserva che i due tipi di sommatori differiscono per il modo con cui è realizzato il circuito di propagazione del riporto, per il resto essi sono identici.

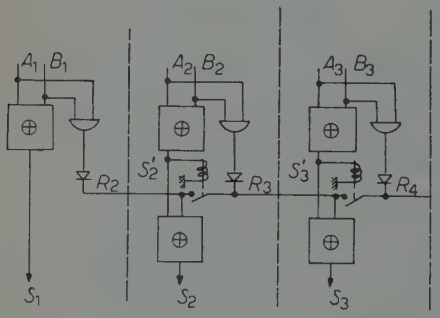

Fig. 3.

Nel sommatore della Fig. 3, il circuito di propagazione del riporto è costituito dal collegamento in serie di vari contatti di relè, uno per ciascuno stadio; ciascuno di tali contatti risulta chiuso se il valore della rispettiva semisomma S' vale 1, altrimenti è aperto. Il suddetto circuito verrà indicato nel seguito come « sbarra di propagazione dei riporti » o « sbarra dei riporti ».

Si osserva subito che si suppone qui di usare dei relé al solo scopo di illustrare più chiaramente il principio di funzionamento del sommatore; per ottenere una maggiore velocità di funzionamento, nella pratica i relé saranno sostituiti da un circuito con transistori, che si illustrerà più avanti.

I circuiti, producenti i riporti in ciascuno stadio, alimentano la sbarra di propagazione dei riporti attraverso dei diodi, che nella Fig. 3 risultano connessi per il caso che gli impulsi rappresentanti i riporti siano positivi.

La somma finale viene ottenuta dalla fila inferiore dei circuiti « $\oplus$ », alimentati ciascuno dalla rispettiva semisomma S'_i, e dalla sbarra di propagazione dei riporti.

Descritta così la costituzione del sommatore parallelo, ecco ora come esso funziona.

In seguito alla applicazione simultanea dei segnali rappresentanti i numeri A_i e B_i, vengono prodotti i segnali S'_i, la semisomma, ed R_{i+1}, i riporti.

La somma finale S_i può essere ottenuta dalla semisomma S'_i e dai riporti R_i con le seguenti regole:

---

(7) Da un intervento di KILBURN al recente Congresso sul trattamento automatico delle informazioni (Parigi, Giugno 1959) risulta che una soluzione simile a quella che si esporrà è in istudio anche presso l'Università di Manchester.

Tutte le volte che $R_{i+1} = 0$, la somma S_{i+1} nello stadio successivo $(i+1)$ uguaglia la semisomma S'_{i+1}. Infatti, in tale caso non si ha propagazione del riporto, essendo questo nullo.

Tutte le volte che $R_{i+1} = 1$ conviene distinguere il caso in cui S'_{i+1} vale 0 da quello in cui S'_{i+1} vale 1.

Per il caso $S'_{i+1} = 0$, con $R_{i+1} = 1$, si ha $S_{i+1} = 1$, cioè S_{i+1} si ottiene da S'_{i+1} per complementazione, appunto per effetto del riporto dallo stadio precedente. Anche in questo caso non si ha una vera e propria propagazione del riporto, in quanto questo non influisce sugli stadi successivi.

Per il caso $S'_{i+1} = 1$, con $R_{i+1} = 1$, non solo si deve complementare S'_{i+1} per ottenere S_{i+1} $(= 0)$, ma si devono complementare anche tutte le cifre binarie della semisomma consecutive ad S'_{i+1}, che valgono 1, ed anche la prima cifra della semisomma che vale 0. In questo caso, cioè, si ha la propagazione del riporto.

Le regole esposte sono illustrate dal seguente esempio di somma:

i	1	2	3	4	5	6	7	8
A_i	0	1	1	0	1	1	0	0
B_i	0	0	1	0	1	0	1	0
R_{i+1}	0	0	1	0	1	0	0	0
S'_i	0	1	0	0	0	1	1	0
S_i	0	1	0	1	0	0	0	1

Le regole enunciate equivalgono a dire che, allorquando si produce un riporto $R_{i+1} = 1$ esso deve sempre modificare la cifra S'_{i+1} della semisomma per ottenere la cifra della somma S_{i+1}; allorquando $S'_{i+1} = 1$, vanno modificate anche tutte le cifre, S'_{i+2}, e seguenti, che valgono 1, ed anche la prima cifra della semisomma che vale 0.

Si vedrà ora come il funzionamento del circuito della Fig. 3 obbedisca alle regola sopra esposte.

Si noti innanzitutto come i circuiti per la somma modulo 2, usati nella costituzione del sommatore parallelo di Fig. 3 riproducano dei segnali S_i, identici al segnale di entrata S'_i, quando l'altro segnale di entrata, proveniente dalla sbarra di propagazione dei riporti, vale 0, mentre producono un segnale S_i pari al complemento $\overline{S}'_i$ di S'_i quando il segnale della sbarra dei riporti vale 1.

Per il modo con cui sono alimentati i relé, i cui contatti costituiscono la

sbarra dei riporti, allorquando, in seguito alla applicazione delle cifre A_i e B_i, si producono le cifre S'_i della semisomma, alcuni dei contatti della sbarra rimarranno aperti ($S'_i = 0$), gli altri verranno, *contemporaneamente*, chiusi.

La sbarra viene così suddivisa in tante porzioni, separate da relé aperti, che individuano i gruppi di successivi 1 che appaiono nella semisomma S'_i: all'inizio di ciascuna di tali porzioni di sbarra ($S'_i = 0$) può apparire sia $R_{i+1} = 0$, sia $R_{i+1} = 1$. Nel primo caso le entrate di tutti i circuiti « somma modulo 2 » che vengono alimentati da tale sbarra riproducono dei segnali S_i uguali ad S'_i, come deve essere. Invece, quando si abbia $R_{i+1} = 1$, tali circuiti producono dei segnali S_i pari al complemento dei segnali di entrata S'_i.

È importante notare che in ciascuna porzione di sbarra, l'unico riporto che può valere 1 è quello iniziale, cioè quello applicato immediatamente dopo un contatto aperto, dato che R_{i+1} può valere 1 solo se S'_i vale 0 (contatto aperto).

Come risulta dalla descrizione fatta, nel sommatore parallelo della Fig. 3 attraverso il gioco dei contatti della sbarra dei riporti, la propagazione di questi avviene su di una vera e propria linea metallica, e perciò con ritardi piccolissimi, dovuti al solo tempo di propagazione di segnali elettrici su di essa. Tali ritardi sono perciò determinati dalla lunghezza della linea stessa, che nella pratica si cercherà perciò di rendere la più piccola possibile, compatibilmente con le esigenze costruttive. È comunque da notare che su 30 cm di linea elettrica supposta priva di dissipazioni, si ha un ritardo di 1 nano-secondo solamente, e che tale ritardo è, allo stato attuale della tecnica dei componenti per calcolatrici, nettamente inferiore al ritardo offerto dai più rapidi circuiti binari conosciuti.

Si noti ancora come l'uso dei relé nel circuito della Fig. 3 benchè fatto a scopo esemplificativo (si mostrerà nel successivo punto come si possono costruire circuiti puramente elettrici per la sbarra dei riporti) sia utile per mostrare come la propagazione rapida del riporto venga ottenuta, nello schema proposto, mediante un organo di commutazione lento, come il relé, ma dotato di particolari proprietà, che conviene mettere in evidenza: infatti esse serviranno da guida nella scelta di un organo puramente elettrico, atto a sostituire il relé negli schemi illustrati.

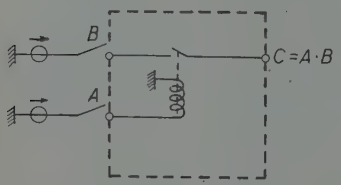

Fig. 4.

La proprietà del relé che viene qui sfruttata è illustrata nella Fig. 4 ove viene messo in evidenza come il relé possa essere considerato come un organo binario atto a realizzare la operazione di prodotto logico tra le due variabili, A e B, rappresentate rispettivamente dalla tensione (o corrente) alimentante la bobina, e la tensione applicata ad un morsetto del contatto. La tensione che appare all'altro morsetto dello

stesso contatto rappresenta la variabile

$$C = A \cdot B \,.$$

Ora è importante osservare che, mentre rispetto alla variabile A (tensione di eccitazione del relé) il funzionamento dell'organo risulta lento, rispetto invece alla variabile B il funzionamento è praticamente istantaneo. Con altre parole, se si suppone assegnato alla variabile B il valore 1 (contatto B chiuso) la variabile di uscita $C = 1 \cdot A = A$ segue il valore di A con il ritardo dovuto al funzionamento del relé; invece, se si suppone assegnata alla variabile A il valore 1 (relé eccitato) la variabile di uscita $C = 1 \cdot B = B$ segue il valore della variabile B praticamente senza ritardo, dato che tra il morsetto B ed il morsetto C esiste un corto circuito.

Pertanto, la soluzione qui proposta per la propagazione rapida del riporto, si basa proprio sulla esistenza di organi, come il relé, atti a realizzare l'operazione di prodotto logico, che offrono ritardi trascurabili rispetto ad almeno una delle variabili di entrata. Il ritardo del funzionamento rispetto all'altra variabile non influisce direttamente sul tempo di propagazione del riporto, in quanto essa viene applicata, *nello stesso istante*, in tutti gli stadi del sommatore. Converrà, naturalmente, che tale ritardo sia il più possibile piccolo, per poter sfruttare completamente le proprietà del circuito, ed è per questo che, come si mostrerà nel successivo punto, converrà sostituire il relé con circuiti elettrici che si comportino in modo analogo, ma siano più veloci.

La soluzione del problema della rapida propagazione del riporto è stata illustrata per ragioni di chiarezza, con riferimento allo schema di Fig. 3 ma i concetti esposti sono applicabili anche ad altri tipi di schemi.

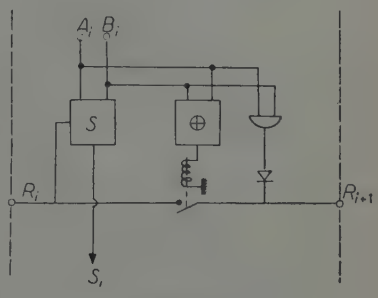

Fig. 5.

In particolare, si consideri lo schema della Fig. 5: essa rappresenta un solo stadio di un sommatore binario semplice, che produce la cifra S_i della somma come funzione delle cifre A_i e B_i dei due addendi, ed R_i, riporto dallo stadio precedente, trasmesso sulla sbarra dei riporti. Il circuito indicato con S produce una cifra della somma, S_i, come funzione delle cifre A_i e B_i degli addendi e del riporto R_i dallo stadio precedente.

Per la sbarra dei riporti, si osservi che essa è di struttura identica a quella della Fig. 3: infatti essa è costituita dal collegamento in serie di contatti di relé, eccitati con tensioni rappresentanti la funzione $A_i \oplus B_i$; inoltre la sbarra stessa è alimentata tramite un raddrizzatore, dalla funzione $A \cdot B$.

Tale struttura della sbarra dei riporti, che nella Fig. 3 è stata illustrata

in diretto riferimento alle regole di propagazione dei riporti, può anche essere ricavata direttamente dalla seconda delle (2).

Nel circuito della Fig. 5 il termine $(A \oplus B) \cdot R$ appare subito a destra del contatto del relé, e vale 1 (cioè il riporto viene trasmesso al successivo stadio) quando $A \oplus B = 1$, cioè quando A e B sono diversi.

Il termine $A \cdot B$ vale 1 quando il riporto è prodotto nello stesso stadio; in tale caso il secondo termine vale 0, perchè $A \oplus B = 0$, ed il relativo contatto risulta aperto.

4. – Circuiti per la propagazione rapida del riporto.

Nel precedente punto si è illustrato lo schema di principio di un sommatore atto ad ottenere la propagazione rapida del riporto, e si è per semplicità supposto di usare dei relé.

Allo scopo di realizzare grandi velocità di funzionamento è possibile, come si mostrerà ora, realizzare circuiti che si comportano in modo simile al circuito con relé prima illustrato. Il modo più spontaneo per ottenere il risultato è quello di usare dei transistori a giunzione, che, come è ben noto, hanno la proprietà di offrire una piccolissima impedenza tra collettore ed emettitore quando vengano saturati e di comportarsi praticamente come un circuito aperto quando vengano bloccati.

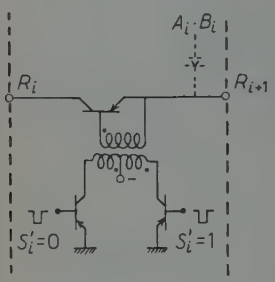

Fig. 6.

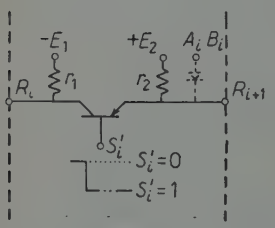

Fig. 7.

Pur non essendo compito della presente nota di illustrare anche la parte realizzativa, ma solo di mostrare il principio di una nuova soluzione del problema della propagazione del riporto, si accennerà a due possibili modi per realizzare mediante transistori un circuito di funzionamento simile a quello con relé della Fig. 3. Essi sono tracciati nelle Fig. 6 e 7. Nella Fig. 6 i segnali S'_i (semisomma) provocano la saturazione (chiusura) del transistore (per $S'_i = 1$) o la sua apertura ($S'_i = 0$), attraverso un segnale applicato tra emettitore e base, tramite un trasformatore. Il primario di questo può essere alimentato da un circuito il cui schema di principio è quello della Fig. 6.

Il circuito della Fig. 7 è invece composto di soli transistori e resistori: con valori opportunamente scelti dei parametri e delle ampiezze dei segnali esso può funzionare come è necessario per gli scopi voluti.

Questo secondo circuito è stato sperimentato, usando transistori del tipo 0C44, e realizzando una catena di 10 stadi. Studi ed esperimenti sono in corso per de-

terminare il comportamento del circuito, e per lo studio di altri circuiti per la realizzazione della propagazione rapida del riporto.

Fra le più importanti questioni che devono essere considerate per l'uso dei circuiti proposti, si segnala qui quella relativa ai circuiti destinati ad alimentare con i segnali di riporto la sbarra di propagazione: nel caso delle Fig. 3 e 4 si tratta dei circuiti di prodotto logico alimentanti la sbarra tramite dei raddrizzatori.

Occorre infatti tener conto che la sbarra dei riporti risulta caricata in corrispondenza di ciascuno stadio, con una ammettenza complessiva pari alla somma delle seguenti ammettenze:

— ammettenza di entrata al morsetto Fig. 3 del circuito « somma modulo due » che genera la somma S_i;

— ammettenza di uscita del circuito generante il riporto;

— ammettenza dovuta alle capacità parassite della sbarra verso la massa.

Si noti allora che, nel caso più sfavorevole, quando la sbarra dei riporti comprende tutti gli stadi, e debba essere trasmesso un riporto già dal primo stadio, il relativo circuito generatore del riporto deve alimentare, tramite la sbarra, una ammettenza complessiva pari alla somma delle ammettenze di tutti gli stadi. Esso deve perciò essere capace di imprimere alla sbarra, anche in tale caso, un impulso di tensione rappresentante il riporto da trasmettere, con tempi di salita e di discesa sufficientemente piccoli e prefissati.

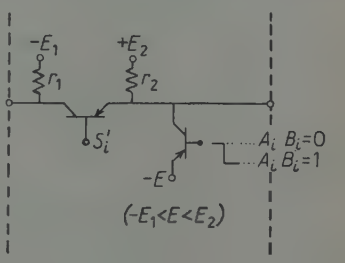

Fig. 8.

Tra le soluzioni che si possono proporre per la realizzazione di tale circuito, una sembra particolarmente interessante, ed è rappresentata nella Fig. 8. In essa si sfrutta ancora la proprietà del transistore di offrire una bassissima impedenza tra collettore ed emettitore quando venga portato a saturazione.

Un'altra questione, relativa alla realizzazione della sbarra dei riporti con transistori, è data dall'effetto della ammettenza tra collettore ed emettitore del transistore quando esso sia bloccato, cioè quando, nello schema di Fig. 3 si vuole che esso si comporti come un circuito aperto.

Di tale ammettenza, importa particolarmente la componente capacitiva, data essenzialmente dalla capacità esistente tra base e collettore. Essa provoca un indesiderabile accoppiamento tra due sezioni adiacenti di sbarra, che si desidera siano elettricamente separate, in quanto su una può trovarsi applicato un segnale di riporto, mentre sull'altra tale segnale non viene applicato.

Per effetto della capacità in discorso l'impulso di riporto può trasmettersi alla sbarra adiacente, e ciò naturalmente non deve accadere.

Una tra le soluzioni più semplici di tale problema, consiste nell'alimentare la base del transistore, quando si vuole che esso risulti bloccato, con un circuito a bassa impedenza di uscita: infatti, così facendo, la base funge, sia pure imperfettamente, da schermo tra emettitore e collettore, eliminando così l'effetto nocivo della capacità.

Queste ed altre questioni devono ancora essere approfondite, per realizzare un efficiente circuito di propagazione rapida del riporto. Tuttavia i risultati finora raggiunti inducono a ritenere che la soluzione proposta offra sensibili vantaggi rispetto a quelle precedentemente note, e meriti perciò di essere ulteriormente perfezionata.

SUMMARY

The problem of carry propagation in adders for parallel digital machines is outlined, and various methods proposed and used to reduce the delay in carry propagation are exposed. A new method is illustrated that uses switching elements which behave like relais, e. g. transistors.

SUPPLEMENTO AL VOLUME XV, SERIE X
DEL NUOVO CIMENTO

N. 2, 1960
1° Trimestre

A Possible Method of Specific Charge Identification from Profile Measurements in Nuclear Emulsions (*).

R. G. AMMAR

The Enrico Fermi Institute for Nuclear Studies
The University of Chicago - Chicago, Ill.

(ricevuto il 25 Luglio 1959)

Summary. — This is a discussion of a method of specific charge identification in nuclear emulsions (*e.g.* 1200 μm thick K-5 pellicles processed unmounted) requiring ~ 50 μm projected range. Using a constant cell length t, the width of the track T_n was measured at each residual range nt, yielding a distribution $\{T_n\}$. Typically $\{T_n\}$ consisted of 100 measurements made at a basic cell length $t \approx 0.57$ μm. Each track was subjected to about three such measurements in order to estimate the measurement errors. The mean $\overline{T}$ and standard spread σ of this distribution, which are conventional charge sensitive parameters, often require normalizations for best results. A search amongst the dimensionless parameters associated with the distribution $\{T_n\}$ indicates that the third moment of the distribution, $\alpha_3 \equiv \sum_n (T_n - \overline{T})^3/\sigma^3$, is a charge sensitive parameter. A truncated distribution $\{T_n'\}$ with mean $\overline{T}'$, spread σ' and skewness $\alpha(p\sigma')$ is derived from $\{T_n\}$ by replacing all $T_n > \overline{T}' + p\sigma'$ by $\overline{T}' + p\sigma'$. $\alpha(p\sigma')$ with $p = 3.75$ is found to be the most sensitive parameter of those tried. It is presumed that its ability to discriminate is based on the presence of « sub δ-rays » and the tendency to form gaps. The principal limitation arises at present from the rather large measurement errors. The observed efficiency of discrimination (~ 80%) is consistent with what would be expected from these errors only. The possibility of utilizing α together with the mean track thickness in order to infer the mass of the particle, is also discussed.

(*) Research supported by the U. S. Air Force Office of Scientific Research, Contract no. AF 49(638)-209.

1. – Introduction.

In nuclear emulsion work one is often faced with the problem of determining the charge of a particle from the characteristics of a rather short (300 μm or less) track. The standard methods of charge identification, such as δ-ray and blob or gap density *vs.* residual range are in general not useful in this connection, particularly for saturated tracks such as one obtains in G-5 and K-5 Ilford emulsions.

Various authors have used the thickness or the area of the track, again measured as a function of residual range, for charge discrimination on short tracks ([1-4]). The Milan group ([2]) has pioneered the use of a Clausen micrometer eyepiece (« Poohstrolino ») for precise track profile measurements. They measure the track thickness T_n at residual ranges nt, using a constant cell length t, and generally refer to the mean thickness, $\overline{T}$, as a quantitative parameter of discrimination. In several recent investigations ([2-4]), $\overline{T}$ has been used specifically for charge discrimination in emulsions not exceeding 600 μm in thickness. One shortcoming of this method is the fact, shown by ALVIAL *et al.* ([2]), that $\overline{T}$ is sensitive both to *a*) emulsion parameters, and *b*) the conditions of observation. The parameters *a*) include the degree and gradient of development as well as the dip and depths of the track in the emulsion, while *b*) includes the intensity of illumination and the fatigue of the observer. Furthermore, the results appear somewhat too subjective. Thus it is in general necessary to perform extensive calibrations on known tracks having the same location and configuration, and under identical conditions of observation. All these difficulties may be increased both by the use of emulsions thicker than 600 μm, such as are currently used in this laboratory, and the technique used in processing free pellicles ([5]).

([1]) J. CRUSSARD: Thesis presented to the Faculty of Sciences at the University of Paris (1952); D. H. PERKINS: *Proc. Roy. Soc.*, A **203**, 399 (1950); O. SKJEGGESTAD: *Arch. Math. Naturvid.*, B **54**, no. 1 (1956).

([2]) G. ALVIAL, A. BONETTI, C. DILWORTH, M. LADU, J. MORGAN and G. OCCHIALINI: *Suppl. Nuovo Cimento*, **4**, 244 (1956).

([3]) S. NAKAGAWA, E. TAMAI, H. HUZITA and K. OKUDAIRA: *Journ. Phys. Soc. Japan*, **11**, 191 (1956); S. LIMENTANI, P. SCHLEIN, P. STEINBERG and J. ROBERTS: *Bull. Am. Phys. Soc.*, **4**, 289 (1959); A. BARKOW: private communication.

([4]) R. AMMAR, R. LEVI SETTI, W. E. SLATER, S. LIMENTANI, P. E. SCHLEIN and P. H. STEINBERG: *Mesic decays of hypernuclei from* K^-*-capture* - I: *Binding energies*, to be published in *Nuovo Cimento*.

([5]) EFINS emulsion laboratory procedures: unpublished. See also A. ROSENFELD, M. BACKUS, J. FRIEDMAN, W. FRY, D. HASKIN, J. LACH, R. LUX, M. ORANS, J. OREAR, E. SILVERSTEIN, W. SLATER, F. SOLMITZ, R. SWANSON and H. TAFT: *How to develop emulsion*, unpublished.

The method of discrimination here proposed was stimulated by the desire to find some parameter, derived from thickness measurements, as independent as possible from the above factors. A consideration of the various moments associated with the distribution $\{T_n\}$ has led us to conclude that its skewness (*i.e.* its third moment) is a particularly useful dimensionless parameter for charge discrimination. This parameter can be invoked for rather short tracks (~ 50 μm) and does not seem to require local calibrations.

2. – Experimental details.

2·1. *Apparatus.* – The microscope used in these measurements was equipped with a Clausen eyepiece micrometer and 100 × Koristka objective. The overall magnification was about 3000 ×, a value which was found to give satisfactory results for the emulsion used (~ 1200 μm unglued pellicles). A 30 × Koristka objective served as the condenser, with immersion oil providing the optical contact to the glass plate upon which the pellicle was placed. The condenser was then rigidly coupled to the vertical motion, thus ensuring that the image of the diaphragm remained always in the focal plane of the objective.

As each track involved several measurements it was found convenient to record the readings using a tape recorder which could be activated by a pedal, The measurements were performed in the dark to improve contrast and reduce fatigue. The illumination was maintained constant by means of a photocell located in the eyepiece; this is particularly necessary if $\overline{T}$ is used as the sensitive parameter.

2·2. *Selection of tracks for measurement.* – A total of 29 tracks were investigated. Of these, one group consisted of 4 protons from the decay of Σ^+'s at rest, as well as 11 uniquely identified hyperfragments of charge 1. Another group consisted of 13 uniquely identified hyperfragments, of charge 2. The identification of these events was based entirely on decay kinematics, except for one event which was identified by a combination of the method described here with kinematic considerations. In addition, one event, involving the emission of a neutron, and which was believed to be uniquely identified charge 1 at the time it was measured, could not be placed in either charge group because of ambiguity in the decay kinematics.

2·3. *The emulsion stack.* – The tracks selected were all contained in the EFINS stack of the EFINS-NU collaboration experiment [4] which consisted of ~ 1200 μm thick K-5 pellicles processed unmounted. These presented a lateral shrinkage of about 10% in addition to a vertical shrinkage factor of about 1.9. The plateau ionization was about 16.5 blobs/100 μm, and the last

50 μm of the tracks investigated showed on the average only about one or two gaps of about 0.25 μm mean width.

2·4. *Method of measurement.* – A basic cell length $t \approx 0.57$ μm was chosen, and the track width T_n was measured at each residual range nt. Each width T_n was obtained as the difference between two readings, setting first on one side of the track and then on the other. As the individual T_n were not immediately derived, it was necessary to guard against gross errors by indicating explicitly those regions which were exceptionally thick or thin.

The last 1.5 μm of each track were omitted since this region is often obscured by the decay tracks of the hyperfragments. In all, about 100 readings, requiring approximately 57 μm of projected range, were made on each track yielding a set $\{T_n(t)\}$. On several tracks, measurements were made at cell lengths $t/2$ yielding another set $\{T_n(t/2)\}$. These readings were later split up into two subsets $\{T_n(t/2)\}_{n\,\mathrm{even}}$ and $\{T_n(t/2)_{n\,\mathrm{odd}}$, equivalent to two measurements each with a basic cell t but shifted relative to each other by $t/2$.

3. – Analysis of the measurements.

3·1. *Definitions and conventions.* – For the distribution $\{T_n(t)\}$ consisting of N observations it is useful to define a mean $\overline{T}$, a standard deviation σ, and a skewness α_3 as follows:

$$\overline{T} = \sum_n^N T_{n/N} \,, \tag{1}$$

$$\sigma = \sqrt{\sum_n^N \Delta_n^2/(N-1)} \,, \tag{2}$$

$$\alpha_3 = \sum_n^N \Delta_n^3/\sigma^3 \,, \tag{3}$$

where

$$\Delta_n = T_n - \overline{T} \,. \tag{4}$$

In the relatively rare instances where a gap was encountered and $T_n = 0$, the reading was discarded and not considered as belonging to the distribution $\{T_n\}$. This admittedly results in some waste of the information available.

3·2. *Conventional parameters for charge discrimination.* – The mean thickness $\overline{T}$ is shown in Fig. 1*a* as a function of dip for the various tracks measured. It is seen that no separation into two groups is readily discernable. No attempt was made to normalize these $\overline{T}$ to the mean thickness of K^- tracks similarly

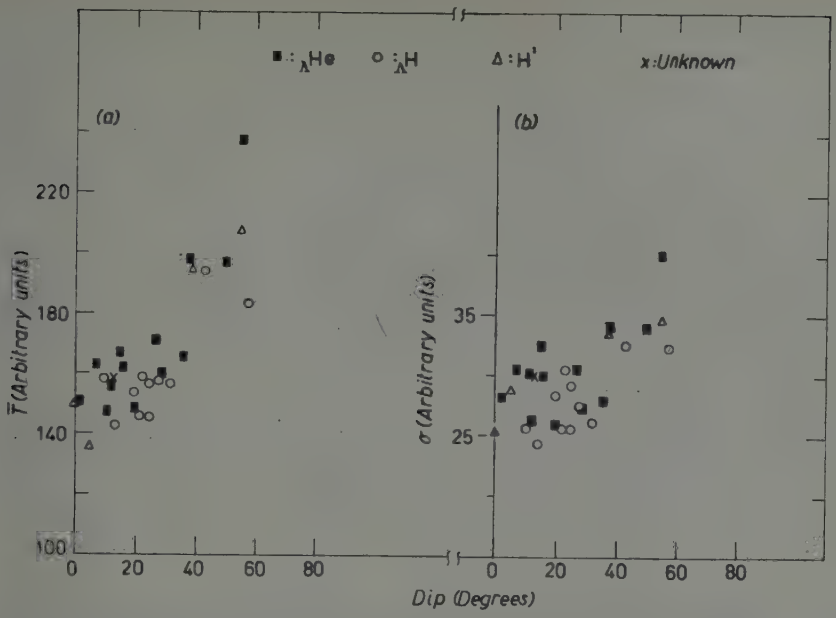

Fig. 1. – *a*) Mean thickness $\overline{T}$ (unnormalized) *vs.* dip. *b*) Standard deviation σ (unnormalized) *vs.* dip.

located and oriented in the emulsion. A similar plot for σ, shown in Fig. 1*b*, likewise does not effect a separation into two charge groups. The dimensionless combination $\sigma/\overline{T}$ (not illustrated) also does not discriminate.

3·3. *The third moment*: α_3. – Fig. 2 shows a histogram of the residuals Δ_n

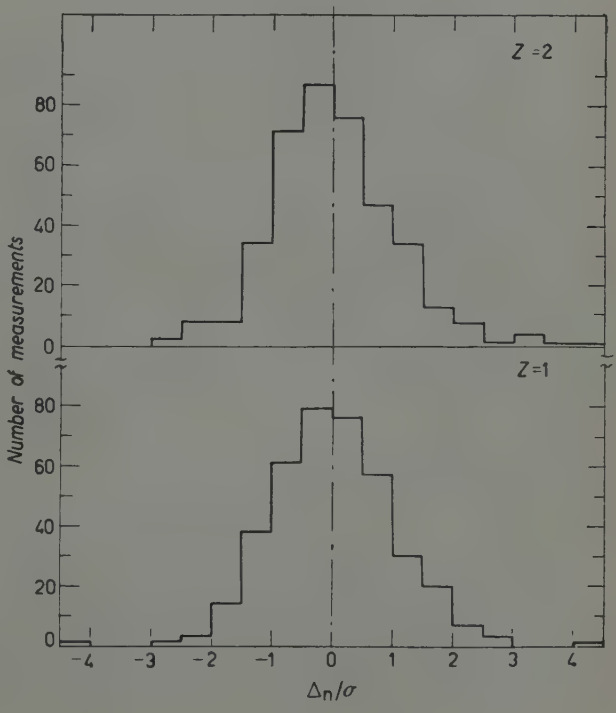

Fig. 2. – Δ_n/σ (residuals in units of σ) for the distribution $\{T_n\}$ both for events with $Z=1$ and $Z=2$. Each charge group consists of the measurements from four tracks.

in units of σ for $Z=1$ and $Z=2$; each charge group consists of measurements on 4 separate tracks, there being approximately 100 measurements on each track. It can be seen that the distribution for $Z=2$ has a more pronounced tail corresponding to large T_n. These can probably be attributed to « sub δ-rays ». Since the $Z=2$ distribution is more skew than the one for $Z=1$ the dimensionless parameter α_3 (« skewness ») suggests itself for discriminating between $Z=1$ and $Z=2$ on an *individual basis.*

Fig. 3*a* shows the distribution of α_3 as a function of dip for the same events as were used in Fig. 1. Some discrimination is seen to be achieved here. There remains the task of finding a suitable function of α_3 which optimizes this discrimination.

3·4. *The truncated distribution*: α. – It may reasonably be expected that the distribution of α_3 will itself be skew, displaying a tail towards high values; this is consistent with Fig. 3*a*.

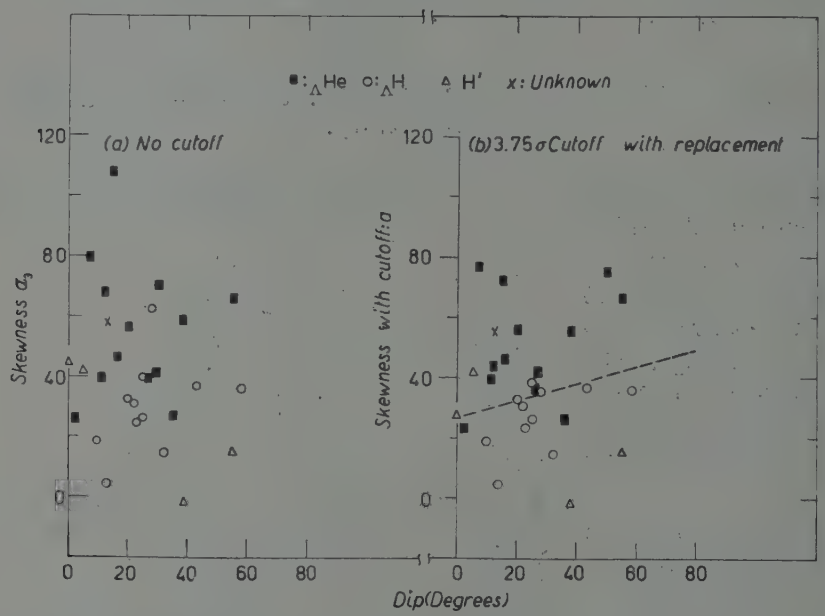

Fig. 3. – *a*) Skewness α_3 *vs.* dip. *b*) Skewness α of the truncated distribution (cut off at 3.75 σ with replacement) *vs.* dip. See Sect. 3·4.

To achieve optimum discrimination it is useful to consider the truncated distribution $\{T_n'\}$ which differs from $\{T_n\}$ in that all $T_n > \overline{T}' + p\sigma'$ have been replaced by $\overline{T}' + p\sigma'$ where T' and σ' are the mean and the spread of the truncated distribution. $\alpha(p\sigma')$ is then defined as the skewness of the trun-

cated distribution:

$$\alpha(p\sigma') = \sum_n (\Delta'_n/\sigma')^3 , \tag{3'}$$

where

$$\Delta'_n = T'_n - \overline{T}' . \tag{4'}$$

From Fig. 2 it is seen that the two distributions differ primarily by the presence of a tail at large Δ_n/σ for $Z = 2$. Hence the problem of finding an optimum value for p is that of restricting the tail in the distribution of α_3 without at the same time destroying the power of charge discrimination.

The values $p = 3$, 3.5, 3.75 and 4 were tried. It was found that a value of 3.75 gave the best results although there was little variation for $3.5 < p < 4$. It is possible that a different value of p would be appropriate for discriminating between $Z = 2$ and $Z = 3$; however little work has been done so far on tracks with $Z > 2$. A scatter plot of $\alpha(3.75\sigma)$, henceforth called simply α, is shown in Fig. 3*b*.

3·5. *Computer programmed calculation.* – The ideas exposed above have been incorporated into a program for UNIVAC. The individual T_n are the input data, and the computer is instructed first to calculate $\overline{T}$, σ and α_3. The $T_n > T + p\sigma$ are next replaced by $\overline{T} + p\sigma$; the value p is left as a program parameter and may be adjusted as desired. The computer then calculated the new mean. Since the value of α_3 is extremely sensitive to the value of the working mean, the machine ascertains whether the change $\mathrm{d}T$ in the mean is smaller than some program constant which is chosen so as to make the maximum error (*) in α_3 about 2. If this is the case as it most frequently is, the old $\overline{T}$ is retained; if not the new mean is used. The new spread is then calculated and the data are again checked for those residuals which are p times larger than the new spread. This must be repeated until convergence is achieved. With the distributions encountered here, rapid convergence was achieved since at most one or two readings exceeded the cut-off, and the number of readings in the neighborhood of the cut-off are also small. This iteration was terminated at the end of three cycles. The distribution that

(*) If the working mean differs from the true mean by $\mathrm{d}T$ then it can be shown that, to first order in $\mathrm{d}T$, the correction to α_3 is:

$$\mathrm{d}\alpha_3 = 3(N-1)\left(\frac{\mathrm{d}T}{\sigma}\right),$$

where N is typically of the order of 100.

remains was taken as the truncated distribution $\{T_n'\}$ referred to earlier; the computer calculated the spread σ' and skewness α for this distribution. In addition the machine split the data $\{T_n\}$ into two sets corresponding to even and odd values of n and repeated the entire calculation. This reduced the data taken at a cell length $t/2$ to standard cell length t.

Finally the machine printed out the mean, spread, and skewness for $\{T_n\}$ and $\{T_n'\}$ and for each of these, the same three quantities corresponding to even and odd n's.

4. – Errors.

The standard error of measurement $\delta\alpha$ or $\delta\alpha_3$ to be assigned to a given measurement of α or α_3 was determined directly by repeated measurements on the same track. 89 measurements were performed on the 29 tracks reported here, averaging about 3 measurements per track. These measurements consisted typically of one run at a cell length of $t/2$, with subsequent decomposition into two sets of cell length t, together with one run at the standard cell length t. The errors so obtained are given in Table I for $Z=1$ and $Z=2$, along with mean values of the skewness for each charge group.

TABLE I. – *Mean value of the individual* α_3's *and* α's *for each charge group as well as the standard measurement errors* $\delta\alpha_3$ *and* $\delta\alpha$.

Charge	No cut-off		3.75σ cut-off	
	$\bar{\alpha}_3$	$\delta\alpha_3$	$\bar{\alpha}$	$\delta\alpha$
1	28.4	24.7 ± 3.5	25.6	21.7 ± 2
2	54.9	28.2 ± 9	49.6	21.0 ± 4

One can also estimate the error $\delta\alpha_3$ in α_3 due to the measurement errors directly. Assuming, as in customary, that the setting error is normally distributed with a standard deviation ε, one obtains readily

$$\delta\alpha_3 = 3\sqrt{\sum_n (\Delta_n/\sigma)^4(\varepsilon/\sigma)^2 + \alpha_3^2\left(\frac{\delta\sigma}{\sigma}\right)^2}, \tag{5}$$

where $\delta\sigma$ is the standard error in σ due to measurement errors. In general the second term is much smaller than the first, and consequently

$$\delta\alpha_3 \approx 3\sqrt{\sum_n (\Delta_n/\sigma)^4}(\varepsilon/\sigma) \equiv 3\sqrt{\alpha_4}(\varepsilon/\sigma)\,. \tag{5'}$$

The error ε may be determined by repeated settings on a given grain. From measurements on 5 tracks (3 charge 1 and 2 charge 2), we find $\alpha_4 \sim 300$. The value obtained from (5′) was about 26, in good agreement with the value 26.2 ± 7 obtained from Table I.

Since the magnitude of $\delta\alpha_3$ is governed by the fourth power of the largest residuals, this error will be considerably reduced, as can be seen from Table I, as a cut-off is imposed.

In later stages of work it was found possible to reduce the setting errors by a factor of ~ 1.5 over the value reported here simply by optimizing intensity and contrast so as to minimize fatigue.

5. – Discussion.

5·1. *General.* – Since each track received on the average three measurements, the typical measurement error to be assigned to each point in Fig. 3*b* is about 12.6. This value is too large to permit one to draw clear-cut conclusions on two items of considerable interest, *i.e.*, *a*) variation of α with dip and *b*) confidence level.

a) Variation of α with dip. – All one can infer from Fig. 3*b* is a general trend favoring an increase in α with dip, particularly for $Z = 2$. This might reasonably be expected, especially for saturated tracks. The less pronounced variation of α with dip for $Z = 1$ may presumably be attributed to the less saturated nature of these tracks.

b) Confidence level. – For given charge and dip, and assuming arbitrarily large precision in measurement, tracks should still yield different values of α due to the statistical fluctuations in the ionization process. The separation of the two charge groups at a fixed dip in units of this natural spread is essentially a measure of the inherent confidence level of our method. The large measurement errors encountered preclude an accurate measurement of this level. The mean values of α and α_3 given in Table I, although reflecting the particular selection of dip angles present in their parent populations, are nevertheless useful in discussing the observed overlap. The separation between the mean value of all the α's for $Z = 1$ and for $Z = 2$ is 24, while the typical error is of the order of 12.6. Two Gaussians with means separated by two standard deviations have an overlap of about 15%. The observed overlap of the two charge distributions in Fig. 3*b* is not inconsistent with this simple picture in which the variation with dip has been neglected and the distribution of the points taken as a normal one.

The inherent confidence level is thus of the order of that introduced by the errors of measurement, namely about 80%. The fact that only 29 events were used obviously limits somewhat the validity of this statement.

5·2. *Critique.* – In addition to those discussed above, certain other factors may limit the use of α, *viz.*,

a) The population of the charge group $Z = 1$ used here is not the most general one possible. For example, no measurements were made on the tracks of K or π mesons. At a given residual range particles with smaller mass will have a higher velocity and consequently be more likely to produce « sub δ-rays ». Furthermore, the increased scattering may tend to simulate the presence of such rays. In fact, of the 4 proton tracks measured, 2 yielded an α value which crosses the separation line. Currently we are testing whether this is indeed a real effect. The possibility of using α together with the normalized $\overline{T}$ in order to infer both the mass and charge, is an interesting one (6).

b) Background grains may come in chance coincidence with the track. The probability of this happening will, of course, vary with the development and background intensity for each stack.

c) The measurements involved in our method are somewhat lengthy. A typical run, consisting of about 100 observations, takes approximately one hour to perform if it is desired to minimize fatigue.

Among the advantages inherent in the use of α we mention the following:

a) Under conditions where the conventional parameters would require normalization, the usefulness of a dimensionless parameter such as α is particularly obvious. Such conditions apparently are obtained with the use of extremely thick emulsions, and may be due to the technique used in processing free pellicles.

b) Discrimination appears to be possible even for rather steep tracks; in fact it appears to improve with increasing dip. This behaviour is not difficult to explain. For given projected range the actual range increases with dip. In addition, we might expect that the inclusion of gaps would tend to decrease the value of α in much the same way that the prescence of « sub δ-rays » would tend to make α large. The small gaps yielding $T_n = 0$ which are neglected for flat tracks now yield non-zero values of T_n and hence contribute information. Thus at these dips α is also a measure of the « undetectable » gaps contained in the track.

(6) R. AMMAR: *Hyperfragments produced by* K^-*-capture in nuclear emulsion:* π^0 *decay modes*, to be published in *Nuovo Cimento*. This possibility has received further confirmation subject however to the qualification outlined there.

c) There does not appear to be any observational subjectivity in this parameter provided that due care is exercised in making the measurements. Fourteen of the tracks reported here were also measured by a second observer. Within the experimental errors the α's obtained by the two observers showed no systematic differences. (The mean α's of the two groups of 14 events are separated by about 7%, while the error in the mean for each group is about 10%.) In addition, the standard deviation of the α's for each observer about the mean for both was calculated for each track; the mean standard deviation was found to be quite consistent with the known errors of measurement.

We note in concluding that the most serious practical limitation either in using α or in extending the investigation of its properties is imposed by the measurement errors. It is thus desirable to develop a way for reducing the setting errors further.

* * *

I would like to thank Professor R. Levi Setti and Professor V. L. Telegdi for many enlightening discussions in connection with this problem. In addition I wish to thank Professor Telegdi for his aid in writing the manuscript.

It is a pleasure to thank Dr. A. Orden and Dr. R. Graves of the Operations Analysis Laboratory for making available the facilities of the computer laboratory. In addition I should like to thank Kevin Tait for programming the calculations for UNIVAC and for processing the events.

I would also like to thank J. Mott for assisting with the observations, N. Crayton for help in data taking and calculating, and P. Gygi for technical aid in setting up the profile microscope and its environs.

RIASSUNTO (*)

Si discute un metodo per la identificazione della carica specifica nelle emulsioni nucleari (p. es. pellicole K-5 dello spessore di 1200 μm trattate senza montatura) che richiede un raggio d'azione di ~ 50 μm in proiezione. Usando una lunghezza di cellula, t, costante, la larghezza della traccia T_n è stata misurata per ogni raggio d'azione residuo nt, ottenendo una distribuzione $\{T_n\}$. Nel caso tipico $\{T_n\}$ consisteva di 100 misure eseguite su una lunghezza base di cellula $t \sim 0.57$ μm. Ogni traccia è stata sottoposta a circa tre di queste misure al fine di stimare gli errori di misura. La media $\bar{T}$

(*) *Traduzione a cura della Redazione.*

e la dispersione tipica σ di questa distribuzione, che sono parametri convenzionali sensibili alla carica, spesso esigono, per il miglioramento dei risultati, la normalizzazione. Una ricerca fra i parametri senza dimensione associati alla distribuzione $\{T_n\}$ indica che il terzo momento della distribuzione, $\alpha_3 = \sum_n (T_n - T)^3/\sigma^3$, è un parametro sensibile alla carica. Una distribuzione tronca $\{T_n'\}$ con media T', dispersione σ' e $\alpha(p\sigma')$ si deduce da $\{T_n\}$ sostituendo tutti i $T_n > \overline{T}' + p\sigma'$ con $\overline{T}' + p\sigma'$. Si è trovato che $\alpha(p\sigma')$ con $p = 3.76$ è il parametro più sensibile fra quelli esaminati. Si presume che la sua capacità di discriminazione dipenda dalla presenza di « raggi sub-δ ». Questa limitazione principale sorge attualmente dagli errori di misura piuttosto grandi. La capacità di discriminazione osservata ($\sim 80\%$) corrisponde a quella che si aspetterebbe soltanto da questi errori. Si discute anche la possibilità di utilizzare α in unione con lo spessore medio della traccia per dedurne la massa della particella.

SUPPLEMENTO AL VOLUME XV, SERIE X
DEL NUOVO CIMENTO

N. 2, 1960
1° Trimestre

Model Experiments on the Design of Solid Iron Magnets for use in Cosmic Ray Spectrographs.

H. W. BENNETT

College of Advanced Technology - Loughborough

W. F. NASH

Department of Physics - University of Nottingham

(ricevuto il 29 Luglio 1959)

Summary. — The high magnetic field available in a magnetised block of iron may be used to measure the momentum of non-interacting particles such as μ-mesons, provided that the line integral of the magnetic induction is known with sufficient accuracy. Model « picture frame » magnets were constructed in order to investigate the effects of geometry and of degree of magnetisation on the uniformity of the magnetic induction. The relative merits of passing the particles through the energising coils or the open ends are considered. It is found that high inductions, with uniformity of $\pm 3\%$, may easily be obtained over 90% of the available volume for comparatively low power dissipation.

1. – Introduction.

The technique most widely used for the determination of the momenta of fast cosmic ray particles is that of magnetic deflection. On account of the comparatively low intensity of cosmic rays, and the natural interest in particles of high momentum, magnetic fields of high intensity and large volume are required. For the study of strongly interacting particles it is necessary that the particles should be deflected in the air gap of a permanent magnet or an electro-magnet. Particles of weak interaction, in particular the most common particles at ground level, μ-mesons, can be deflected in magnetized iron. The

advantages of a magnetized iron system are obvious; high inductions and large volumes for low power of excitation since the effective vector acting on a particle, in a magnetized medium is the magnetic induction, B (RASETTI [1]). Although the probability of a μ-meson suffering a nuclear interaction in such a magnet is negligible the multiple scattering is not and this sets the limit to which the momentum of a single particle may be determined. At constant field over a trajectory of length L the magnetic deflection increases as L and the r.m.s. angle of scattering varies as $L^{\frac{1}{2}}$. The fractional error in a single determination therefore varies as $L^{-\frac{1}{2}}$. Increasing L also increases the maximum detectable momentum so that a high value of L is desirable in every way. A useful value of L is of the order of 1 metre.

The use of magnetized iron is not a new idea. ROSSI [2] suggested the method of magnetic lenses for the partial separation of positive and negative mesons. The method was used with success by BERNARDINI *et al.* [3] in measurements of the positive excess at sea level and in the experiments of CONVERSI, PANCINI and PICCIONI [4].

The present work describes measurements made on small model magnets, the object of which was to determine the variation of magnetic induction through the magnets for a variety of geometrical designs and operating conditions.

The performance of a full scale magnet, incorporating the results of the model experiments, is discussed in the following paper by O'CONNOR and WOLFENDALE (1959).

2. – Measurements on the scale model.

2·1. *Construction and preliminary tests.* – General considerations of particle rates and momentum resolution indicated that the full-scale magnet should have, very approximately, 120 plates of $\frac{1}{2}$ inch steel, each 1.5 m square with a 0.5 m square hole, as shown in Fig. 1. A one-tenth scale model of the proposed magnet was constructed using plates of thickness of 1/20 inch. The steel was made to British Standard 24, Part 6, Specification 18. The plates were held in a brass clamp and wound with two coils, each having 250 turns of 20 S.W.G. cotton covered wire.

The total magnetic flux passing through the unwound side A (Fig. 1) was measured by means of a search coil and fluxmeter. With a current of 3 A.

---

(1) F. RASETTI: *Phys. Rev.*, **66**, 1 (1944).

(2) B. ROSSI: *Nature London*, **128**, 300 (1931).

(3) G. BERNARDINI, M. CONVERSI, E. PANCINI, E. SCROCCO and G. C. WICK: *Phys. Rev.*, **68**, 109 (1945).

(4) M. CONVERSI, E. PANCINI and O. PICCIONI: *Phys. Rev.*, **68**, 232 (1945).

the total flux was 1188 kilolines, the average value of B being 16.5 kG. The fractional change of B with current is given by the expression $I\,\mathrm{d}B/B\,\mathrm{d}I$ which was found to be 0.1. This indicates that with this level of magnetization small variations in current are unimportant.

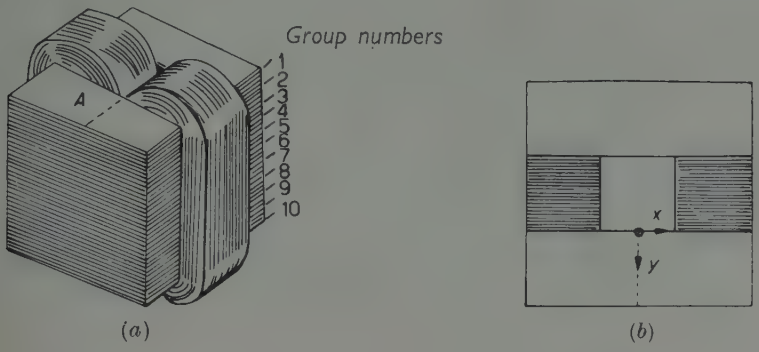

Fig. 1. – View and plan of 1/10 scale magnet.

The leakage flux above and below was measured by direct reading and null methods out to distances of 8 cm from the model. The results of both methods gave the total leakage flux as 0.2% of that in the iron.

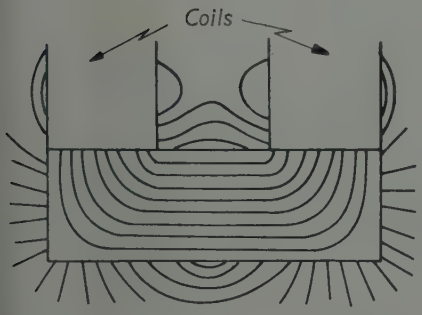

Fig. 2. – Leakage flux of model magnet.

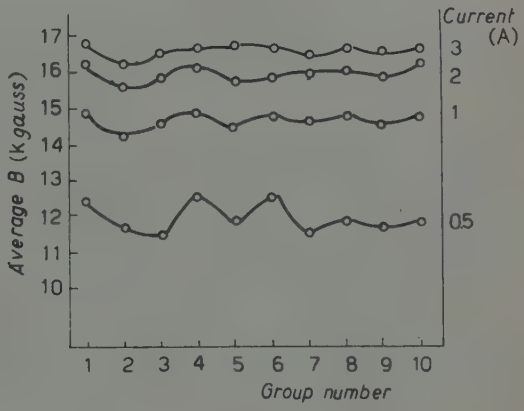

Fig. 3. – Vertical variation of flux of 1/10 scale magnet.

The leakage flux was also investigated by means of iron filings set in waxed paper. This method presents the direction of the horizontal component only but gives a useful indication of the area over which the direction of the field is uniform. Fig. 2 shows the direction of the filings at one end of the model.

2·2. *Vertical variation of the flux.* – The plates were divided into ten equal groups, numbered as in Fig. 1(*a*), and search coils were wound around each group in the position *A*. The results are shown in Fig. 3, and it will be seen that with an excitation current of 3 A. the variation is quite small. In order to demonstrate that these variations are real, the flux was measured at three lower values of current, when dB/dH is greater. This method of magnifying the variations was also used in later measurements.

The variations appear to indicate variation in the composition of the plates since if they were due to differences in the dimensions of the plates, they would not decrease with increasing current.

The group flux was, at an excitation current of 3 A, within 1% of the mean in every case except one, when it was 3%. It may therefore be concluded that the variation in *B* throughout the working volume resolves itself into a two-dimensional problem. This justifies the use of flat models to investigate the horizontal variation of *B*.

3. – Measurements on the flat square model.

3·1. *Construction and preliminary tests.* – A magnet was made from ½ inch steel in the shape shown in Fig. 4, wound with two coils of 250 turns each. The corners were rounded on one side to find whether this improved the uniformity of the flux distribution. The horizontal dimensions indicated that a current of 5.25 A was necessary to produce the same field as that in the previous model.

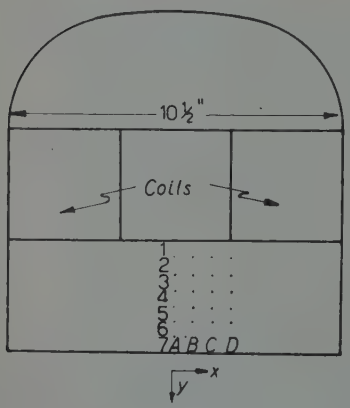

Fig. 4. – Plan of flat square model.

With this current the total flux in the iron was measured at different points. The average value of *B* in the region of the coils was 17.2 kG, falling to 16.1 in position *A* (Fig. 4). The latter value is close to that of 16.5 in a similar position on the scale model, if allowance is made for a greater leakage of flux from the flat model.

3·2. *Use of magnetic potentiometer.* – Since it is impossible to investigate the variation of B_x in the O_y direction (Fig. 4) of a full-scale magnet, it was decided to carry out measurements with a magnetic potentiometer, the object being to test whether the values of *H* measured at the surface of the steel were in agreement with the corresponding values of *B*. If so, it would afford a method of checking the values in the full-scale magnet.

MARGERISON and SUCKSMITH [5] have described a modern form of magnetic potentiometer, which must be small if it is to indicate variations in H over a small area. The instrument, which is a semi-circular coil, measures the magnetic potential difference $\left(\int H \, dL\right)$ between its feet, and the output from it depends on its size and number of turns. The size of the models necessitated the construction of very small instruments, and the very small galvanometer deflection which they produced was amplified by means of a photo-electric cell, cathode follower, D.C. amplifier and pen recorder.

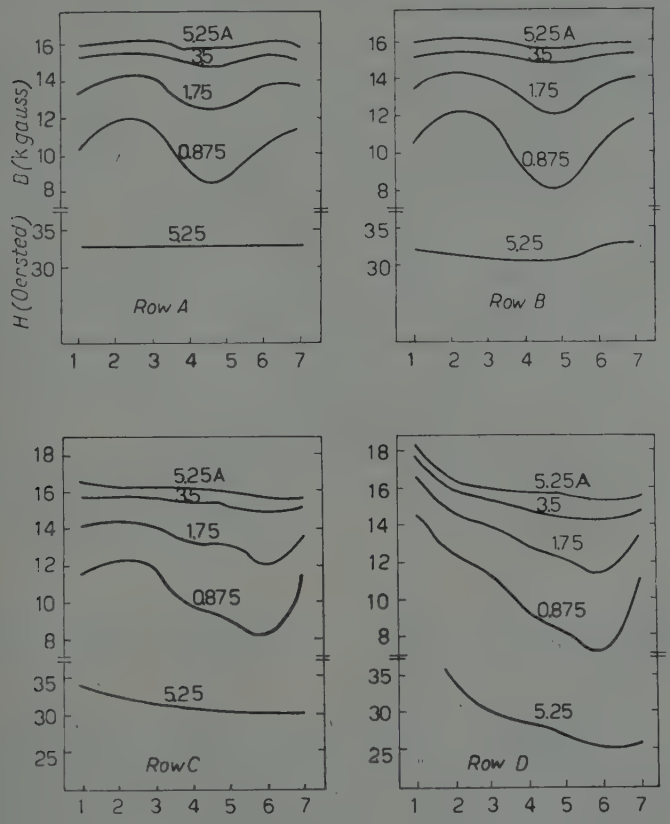

Fig. 5. – B and H distributions in flat square model.

Before the holes shown in Fig. 4 were drilled, the values of H between their positions were measured and the variation along the four rows is shown in the graphs of Fig. 5. From these values and the measured B-H curve, the variation of B_x in the model can be obtained.

(5) T. MARGERISON and W. SUCKSMITH: *Journ. Sci. Instr.*, **23**, 182 (1946).

3·3. *Measurement of magnetic induction.* – Holes approximately 0.8 mm in diameter were drilled in four rows, in the positions shown in Fig. 4. Search coils of fine enamelled wire were wound between adjacent holes in order to measure the flux in each section, this being done at the standard current of 5.25 A and at three lower values. The average values of B_x between holes is shown in the graphs of Fig. 5. The slight variations in the values of B as a function of position were shown ot be real, and not due to experimental inaccuracy, by carrying out measurements at lower values of the magnetizing currents. At the lower values of excitation these variations appeared in a more pronounced form, indicating that they were due to inhomogeneities in the magnetic material.

It is again clear that although B does not increase directly with H, the maximum possible value of H is desirable in order to produce a satisfactory uniformity in B. With a current of 5.25 A the value of B_x was uniform within $\pm 1.5\%$ in rows A and B, and $\pm 2.5\%$ for C. The greater variation towards the corners is small enough for allowance to be made in calculation of trajectories.

Within the limits imposed by the accuracy of the magnetic potentiometer measurements, the variations in B obtained by the two methods follow the same general pattern. It appears therefore that the potentiometer could be useful in showing the presence of significant variations in B in a full-scale magnet, especially if a larger potentiometer were used.

Similar measurements of B and H were made on the opposite face of the model. The effect of the rounded corners is to increase the variation in B as the corners are approached. Square corners appear therefore to be more effective.

4. – Rectangular models.

4·1. *Construction and preliminary tests.* – Two rectangular magnets were made from $\frac{1}{2}$ inch steel, as shown in Figs. 6 and 7. As will be seen the difference between them is that the first model has rounded inside corners whereas the second has square cut corners. The coils contained totals of 510 and 538 turns respectively. With this type, interest is centred on the variations in B beneath the coils, which were wound in separate sections so that rows of holes could be drilled in the positions indicated. It should be noted that it is impossible to use a magnetic potentiometer due to the presence of the coils.

The currents calculated to give the same value of H as in the previous model were 4.8 A and 4.18 A respectively. Using these currents the average value of B in the exposed sides was 16.1 kG in both models, being the same value as that on the square model. This confirms that for different

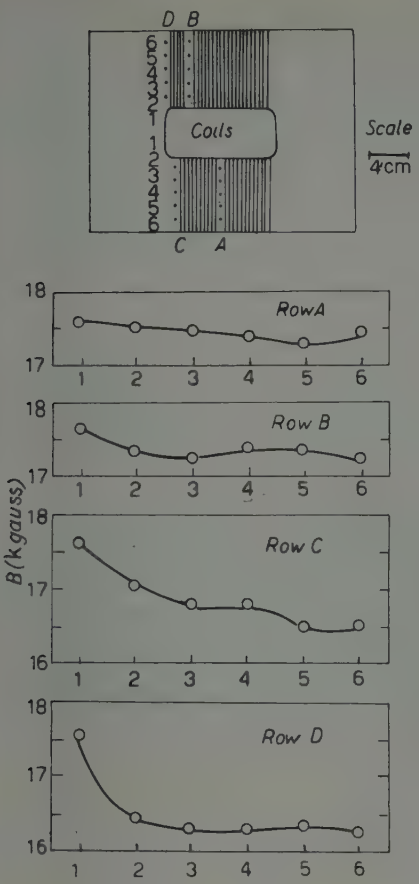

Fig. 6. – Plan and distribution of B in rectangular model with rounded inside corners.

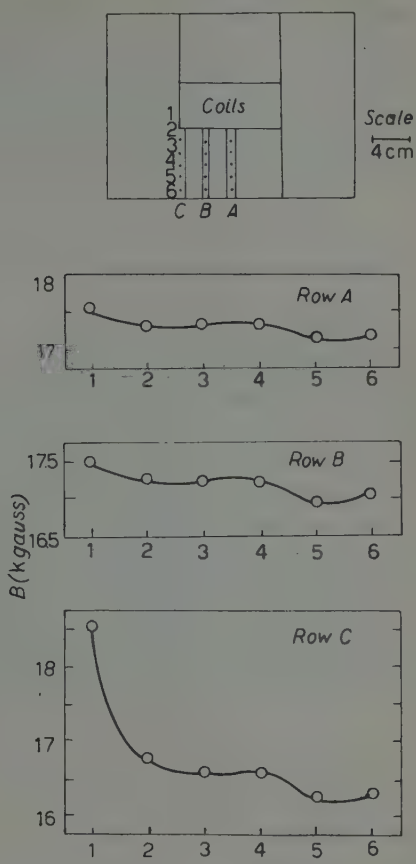

Fig. 7. – Plan and distribution of B in rectangular model with square-cut corners.

shapes of magnet the value of H depends on the number of ampereturns in the coils, and the mean path-length around the magnet. The actual value of H varies considerably around the magnetic circuit, and cannot be calculated by elementary circuit theory. The average value of B under the coils was 17.2 kG.

4·2. *Measurement of B.* – Using search coils wound between adjacent holes, the flux was measured in the same way as before, and the resulting values of B are shown in Figs. 6 and 7.

It is seen that the flux density rises abruptly near the inside corners, but less when they are rounded. It is obvious, therefore, that rounded corners are preferable.

With the model shown in Fig. 6 a useful area would be that under the coil bounded on one side by C with a margin of 1/12-th of the width of the coil at each end. The maximum variation in B is from 16.5 to 17,2 kG along row C, *i.e.* $\pm 2.1\%$ from the mean. The r.m.s. variation over the whole useful area is only $\pm 1\%$

5. – Stability measurements.

The flux density in the iron may be increased by 2 to 3% by a large increase in the magnetizing current, followed by reduction to the original value. If this temporary increase in current is obtainable, it is desirable to know whether the increase in flux is permanent.

It was not found possible to measure any decrease in flux while the normal steady current flowed, but the decrease was measured after the current was switched off, by using one of the magnetizing coils of the original model (Fig. 1) as a search coil connected to a sensitive galvanometer. The decay in the residual flux was found to be exponential and when integrated to infinite time gave a total decrease of 0.03%. It is therefore concluded that any increase in flux obtained by the method described will be stable.

6. – Conclusion.

Sufficient data have been accumulated from model experiments to permit the design of a full-scale solid iron magnet for accurate experimental work

The main conclusions are:

1) Either the region covered by the exciting coils or the open sides (or both) can be used as the deflecting volume. The advantage of the higher induction under the coils is offset to some degree by the greater degree of uniformity in the open side and the ease with which induction measurements can be made there.

2) Care must be taken with the rounding of the inside corners if the useful region of induction is to approach the corners.

3) Even at comparatively low degrees of excitation the variation of $\int B\,\mathrm{d}l$ over most of the selected side is not large.

* * *

The authors are grateful to Professor L. F. BATES, F.R.S. for the facilities of his laboratories, and one of us (H.W.B.) is indebted to Dr. H. L. HASLEGRAVE for permission to undertake work at Loughborough College of Technology.

We also wish to thank Dr. A. W. WOLFENDALE for many useful discussions and Mr. H. CLOW and Dr. P. GRIFFITHS for their valuable technical assistance in magnetic potentiometer measurements.

RIASSUNTO (*)

Si può usare l'intenso campo magnetico che si forma in un blocco di ferro massiccio magnetizzato per misurare l'impulso di particelle non interagenti quali i mesoni μ, purchè sia noto con sufficiente esattezza l'integrale lineare dell'induzione magnetica. Si sono costruiti modelli di magneti per indagare sugli effetti della geometria e del grado di magnetizzazione sull'uniformità dell'induzione magnetica. Si considerano i vantaggi che si hanno facendo passare le particelle attraverso gli avvolgimenti di eccitazione o attraverso le estremità libere del magnete. Si trova che si possono facilmente ottenere induzioni elevate con l'uniformità del $\pm 3\%$ nel 90% del volume disponibile con dissipazioni relativamente basse.

(*) *Traduzione a cura della Redazione.*

SUPPLEMENTO AL VOLUME XV, SERIE X
DEL NUOVO CIMENTO

N. 2, 1960
1° Trimestre

The Characteristics of a Solid Iron Magnet for use in a Cosmic Ray Spectrograph.

P. V. O'Connor and A. W. Wolfendale

Department of Physics The Durham Colleges, - University of Durham

(ricevuto il 29 Luglio 1959)

Summary. — Many advantages are gained by deflecting weakly interacting cosmic rays in magnetised iron instead of the conventional air gap of an electromagnet. A solid iron magnet has been constructed in the form of a rectangular transformer core with excitation windings on opposite sides of the core. The design is based on the results of model experiments by Bennett and Nash (1) on the variation of induction throughout the iron and the leakage field above and below the magnet. When the magnet is operated at a power of 2 kW (mean $\int B\,dl = 982$ kG cm), the variation of integrated magnetic induction for vertical particle trajectories, is less than $\pm 3\%$

1. – Introduction.

A discussion has already been given, in the preceeding paper by Bennett and Nash (1) (denoted by I), of the main advantages to be gained by deflecting cosmic ray particles in magnetized iron.

The present work describes the design, construction and properties of a magnet suitable for accurate measurements of the momentum spectra of cosmic ray μ-mesons.

2. – The design of the magnet.

The results of the model experiments described in I are useful in that they give some idea of the performance to be expected from typical designs. In practice the design is a compromise governed by a large number of factors

(1) H. W. Bennett and W. F. Nash: *Suppl. Nuovo Cimento*, **15**, 193 (1959).

of which the most important are: particle collection rate, the line integral of the magnetic induction, the signal to noise ratio for individual particle deflections, and the cost of the apparatus.

If L is the height of a magnet (and length of the trajectory of a vertical particle) for which the plan area and magnetizing current are constant, the signal to noise ratio varies as $L^{+\frac{1}{2}}$, the maximum rate of collection as L^{-2} and the cost approximately as L. The temperature rise, with natural convertion, is nearly independent of L. Where low momentum particles are to be considered the momentum loss in penetrating the iron is important; this varies approximately as L.

Since the experiments to be carried out in the present application concern measurements of spectra a large signal to noise ratio is not necessary; the effect of scattering can be allowed for accurately when a large number of trajectories is considered. It is expected that a factor of 3 or 4:1 can be tolerated.

A compromise dimension of 25 in. was chosen for which the signal to noise ratio is 3.74 at an excitation current of 16 A. The magnetic deflection is 1.68° for a particle of momentum 10 GeV/c, and the momentum loss in penetrating the iron is 0.89 GeV/c.

3. – The construction of the magnet.

For ease of assembly the magnet was fabricated from boiler plate of nominal thickness 0.5 in. and weight 4.2 cwt per plate. The constitution of the iron is given in Table I. The magnet consists of 50 such laminations mounted horizontally and held in place by vertical steel pegs through opposite corners.

TABLE I. – *Chemical constitution of iron used in magnet.*

Element	C	S	P	Mn	Si	Cr	Ni	Cu	Sn	Co	As	V	Al	Mo	Fe
% by weight	.07	.026	.01	.36	.01	.021	.11	.20	.026	.017	.031	.01	.038	.015	remainder

The general arrangement isshown in Fig. 1*a*. The intention is that the sides B and C shall be used for the deflection of cosmic rays. Side C is shown in detail in Fig. 1*b*.

Provision for measurement of the magnetic flux within the magnet was made by the insertion of insulated wires between selected plates. These wires were inserted between successive groups of five plates along the central axes

of each side. In addition wires were inserted between successive plates in group *C*2.

The coils consist of 250 turns of 14 SWG copper wire on each of the sides *B* and *C*. The total resistance is 7.2 Ω when cold and the self inductance 210 mH (at 1 kHz). With the comparatively small number of ampere-turns needed to produce a high magnetic induction natural convection provides sufficient cooling. The maximum permissible current for which the temperature rise is not excessive is 16 A. Here the power dissipated is 2kW, the temperature of the magnet coils 50 °C and the magnet iron 28 °C for an initial ambient temperature of 19 °C.

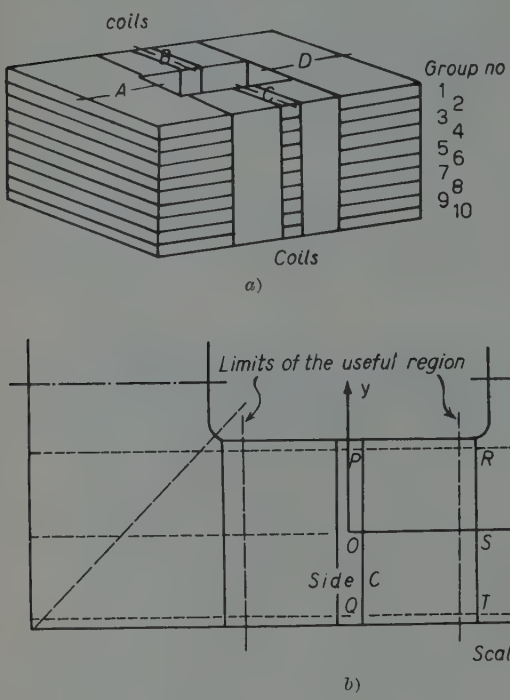

Fig. 1. – Schematic diagrams of the magnet.

4. – The magnetic measurements.

4·1. *The measurements required.* – A basic requirement of a magnet is stability of flux against variations of various parameters. By far the most important parameter is the excitation current and measurements have been made of the variation of induction with current.

In principle it is necessary to determine the line integral of the magnetic induction in the direction *Ox* for many trajectories distributed throughout the useful volume of magnet. Considering side *C* of Fig. 1*b* it is hoped that the useful volume will be only a little less than the volume contained by the two coils on that side. It is comparatively easy to measure the line integral $\int H_x \, dz$ arising from the leakage flux above and below the magnet but measurement within the magnet presents difficulties. The measurements that can be made are $\int_n B_x \, dA$ over each group at the centre of each side, $\int B_x \, dA$ over each

plate within group $C2$ and the variation of $\int_{\Sigma n} B_x \mathrm{d}A$ over the whole side as a function of x. An important quantity not measurable here is the variation of B_x with y.

Before going further it is important to consider reasons for non uniformity of B. These can be divided into two classes i) the geometry of the system and ii) the variation of magnetic properties from plate to plate.

In case i) the main variation is the change in B_x with y arising from the gradient of magnetising field within the coils. Since this variation is almost entirely geometrical the result of experiments on the small scale model at equivalent excitation can be taken over. BENNETT and NASH have shown that the variation of $\int_n B_x \mathrm{d}z$ with y is $\sim \pm 2\%$ over the useful area and this result is considered to be applicable to the full-size magnet.

In case ii) measurements on the full-size magnet are necessary. Variations over one plate are expected to be small but some change from plate to plate might be expected. The measurement of $\int B_x \mathrm{d}A$ enables this variation to be studied. It should be noted that this variation is not very important in practice as the deflection, and displacement, of particle trajectories can be calculated if the variation is accurately known.

Measurements of the leakage flux are useful for two reasons. Firstly they give the contribution to $\int H_x \mathrm{d}z$ and secondly some information can be derived on the direction of the lines of force within the iron. A detailed account is given of the leakage measurements.

The flux measurements were made using a calibrated flux-meter. For the measurement of induction in the iron the magnet current was reversed and for the leakage flux measurements the search coil was reversed in the steady field.

4·2. *The variation of flux with excitation current.* – The flux was measured in one group of plates ($C4$) as a function of the excitation current over the range $(12 \div 17)$ A. Using the mean thickness of the plate the data of Fig. 2 were derived. The diameters of the circles represent the errors, which arise mainly from the lack of complete reproducibility of the flux-meter deflections.

At a mean current of 15 A the variation of induction with current is $\partial B/B\,\partial I = 1.19\%\ \mathrm{A}^{-1}$. A more useful quantity in practice is the ratio of the fractional change in induction

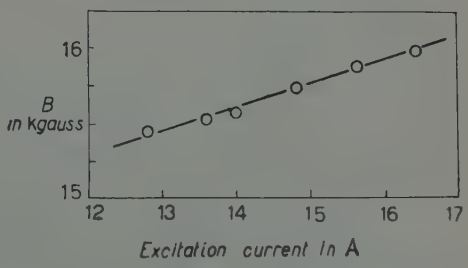

Fig. 2. – Variation of the mean induction in group $C4$ with excitation current.

to that in current, *viz*:

$$\left(\frac{I\partial B}{B\partial I}\right)_{15\text{ A}} = 0.178\,.$$

It is apparent that this degree of stability is satisfactory.

4·3. *The variation of flux with group number.* – Measurements were made at an excitation current of 15 A for each group on side *C* and side *D*. A limited number of measurements of plate thickness were made on a number of plates and a mean thickness derived. The results of Fig. 3 were calculated using this value. The errors shown are derived from the apparent spread in thickness of the plates. It is immediately obvious that there is a significant variation in induction of similar magnitude for both sides *C* and *D*. It is possible that the variation of thickness both over one plate and from plate to plate has been underestimated but this seems an unlikely explanation of the sinusoidal variation. Variation of composition would give the correlation of low and high values but the sinusoidal variation is again unlikely, particularly in view of the fact that each group contains five plates and the plates were stacked in a random manner. The variation remains unexplained but it is not considered to be of great importance; as mentioned in Section **5** its effect can be allowed for.

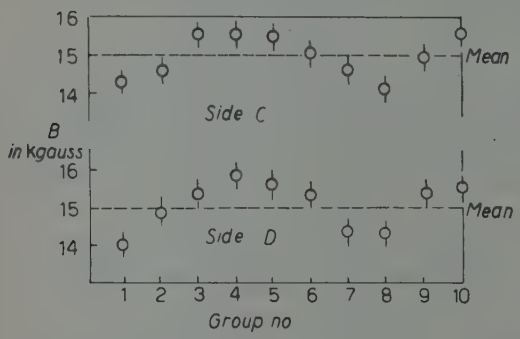

Fig. 3. – The mean induction as a function of group number for sides *C* and *D*.

4·4. *The variation of total flux along the Ox axis.* – A reduction in flux is expected with increasing distance from the centre of the side, proceeding along *Ox*, on account of the increasing leakage. The leakage occurs mainly from the inside edge. The results of measurements with the search coil comprising a single loop round the entire side are shown in Fig. 4. As before the induction, *B*, has been derived using a mean plate thickness. The maximum variations from the means are $\pm 1.4\%$.

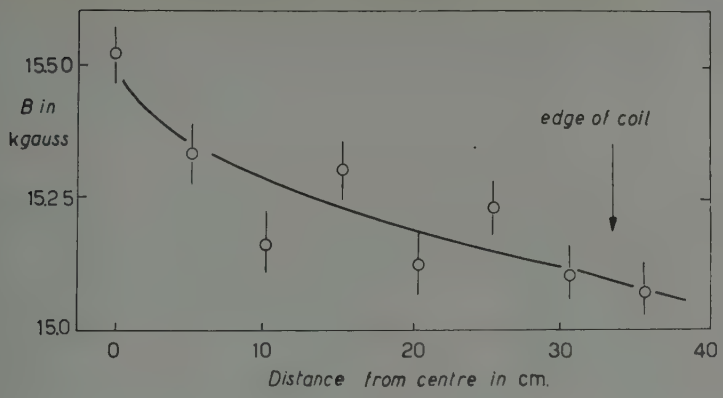

Fig. 4. – Variation of the mean induction in the whole of side C with distance from the centre, O, along Ox.

4·5. *The variation of leakage flux with height.* – Measurements were made of the leakage flux in three mutually perpendicular directions, *i.e.* x, y and z, at points on various axes and at different heights.

The variation of H_x with height above the magnet is shown in Figs. 5*a* and 5*b*. The points through which the vertical axes are drawn are shown in Fig. 1*b*. The variation of $\int H_x \mathrm{d}z$ with distance from the Oy axis is shown in Fig. 6. The average contribution to the line integral of the field is approximately 2×6 kOe cm compared with a mean

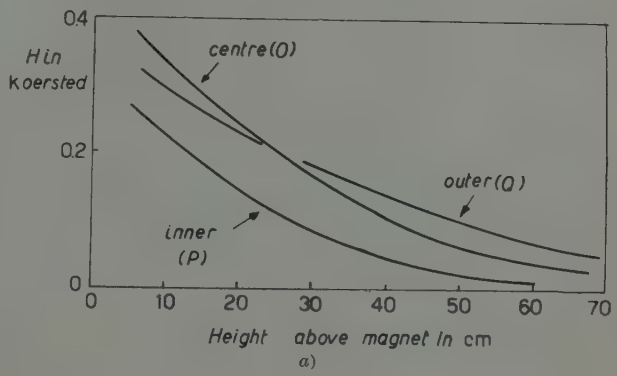

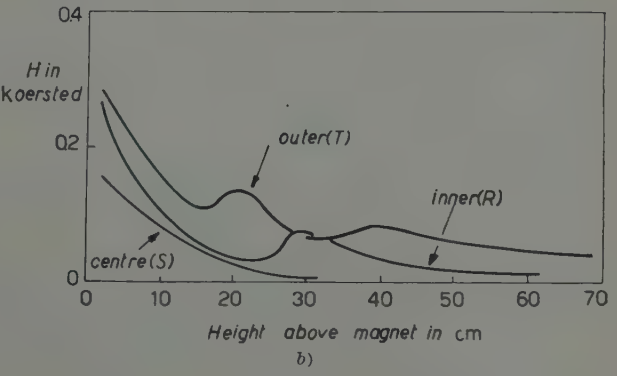

Fig. 5. – Variation of the horizontal component of the leakage field, H_x, with height above the magnet. The positions are as marked on Fig. 1*b*.

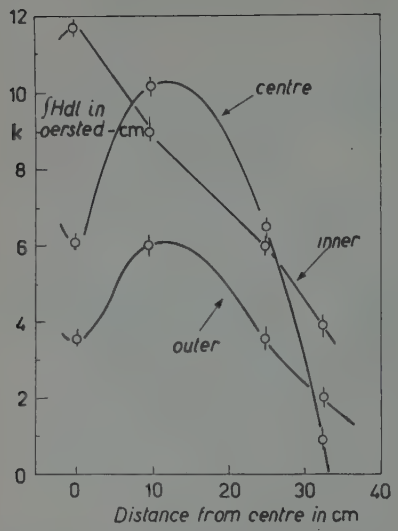

Fig. 6. – The integrated leakage field as a function of distance from the Oy axis, along PR (inner), OS (centre) and QT (outer).

value of $\int B_x \mathrm{d}z = 960$ kG cm for the same excitation, (16 A) *i.e.* a fraction of 1.25% (the direction of the leakage field is, of course, opposite to that of the induction in the iron).

4·6. *The variation of integrated field strength over the useful area of the magnet.* – Considering the variation of the mean $\int B_x \mathrm{d}z$ over the width of the magnet (Oy direction), with distance along Ox, it is seen that the effect of the leakage flux is to compensate somewhat for the fall off of induction in the iron for distances greater than about 15 cm from the centre.

The net result of the variation is to give extreme limits from the mean $\int H_x \mathrm{d}z$ of $\pm 1.7\%$. Taking into account the variation in $\int H_x \mathrm{d}z$ along the Oy axis, which can be inferred only from the results on the scale model, a reasonable estimate of the extreme limits of $\int H_x \mathrm{d}z$ for vertical trajectories over the whole of the useful region is $\pm 3\%$.

3·7. *The direction of the magnetic induction inside the magnet.* – A knowledge of the directions of the lines of force within the magnet is useful for two

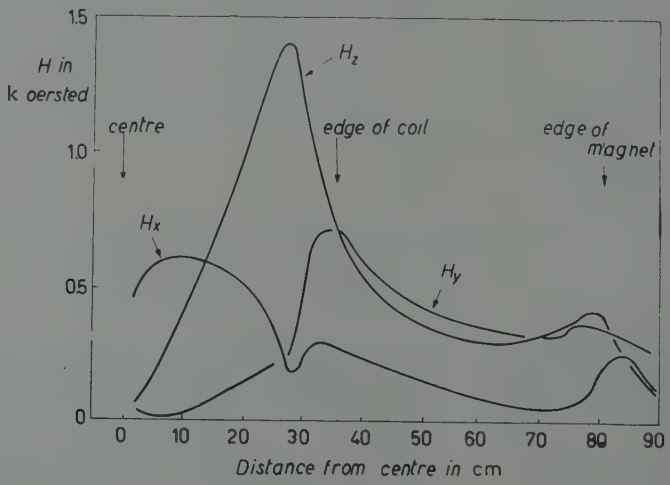

Fig. 7. – The various components of the leakage field, at a height of 3 cm above the magnet, as a function of the distance from O along Ox.

reasons. Firstly it enables a check to be made on the induction measurements and secondly it is necessary for very accurate measurements of particle deflections. The second reason is connected with the fact that the trajectory of an incident vertical particle will be a spiral if $H_y \neq 0$.

A direct determination of directions is not possible but some idea can be found from leakage measurements just above the top plate. Unfortunately measurements near the coils are profoundly modified by the effect of the coils themselves and are not expected to give much information on the flux in the iron beneath. This is apparent from Fig. 7 which shows the variation along the Ox axis, where the effect of the small gap between the coils is quite marked. However an equivalent part of the magnet can be chosen which does not contain a coil. Fig. 8 shows the results from such a part. The vectors represent the magnitude and direction of the leakage flux at a height of 3 cm above the magnet. The leakage flux is the horizontal component and is compounded of H_x and H_y.

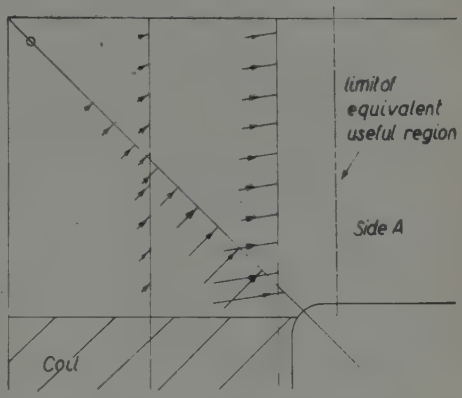

Fig. 8. – A vector diagram of the leakage field in a horizontal plane 3 cm above the magnet.

It is clear from the figure that the obliquity of the lines of force within the useful region should not be large and the effect on particle trajectories will not be serious.

5. – Conclusion.

The conclusion of this work is that the solid iron magnet can be used for accurate spectrum measurements on weakly interacting particles. The main limitation of the technique is the « noise » introduced by multiple scattering but this is reduced as the size of the magnet is increased. The effect of scattering, and the small variations in integrated field strength referred to above, can be allowed for accurately on a statistical basis when a large number of particles is recorded.

It is likely that this technique is the only one possible on economic grounds for producing appreciable deflections in the trajectories of μ-mesons in the important energy region above 1000 GeV.

* * *

The authors wish to thank Professor G. D. ROCHESTER F.R.S. for the facilities of his laboratories and for his interest in the work.

The authors are grateful to the sponsors of this research: the Geophysics Research Directorate of the Air Force Cambridge Centre, Air Research and Development Command, United States Air Force, under contract AF 61(052)-27, through the European Office, ARDC.

The Directors of the Consett Iron Co. Ltd. are thanked for their generous help, and the Head of the Research Department, M. T. F. PEARSON, is thanked for his helful advice.

The authors also wish to thank Dr. W. F. NASH and Mr. H. W. BENNETT for their most helpful co-operation and Mr. J. L. LLOYD for many stimulating discussions.

Messrs. K. RICHARDS and E. ANDERSON gave valuable technical assistance.

RIASSUNTO (*)

La deflessione di raggi cosmici debolmente interagenti entro ferro magnetizzato anzichè nell'intraferro di un elettromagnete presenta vari vantaggi. Si è costruito un magnete massiccio in forma di un nucleo di trasformatore rettangolare con avvolgimenti di eccitazione da lati opposti del nucleo. Il progetto è basato sui risultati degli esperimenti eseguiti con un modello da BENNETT e NASH [1] sulla variazione dell'induzione attraverso il ferro e sul campo di fuga sopra e sotto il magnete. La variazione dell'induzione magnetica integrata per traiettorie verticali delle particelle al disopra della regione utile di $2.52 \cdot 10^3$ cm^2 è meno di $\pm 3\%$ applicando al magnete la potenza di 2 kW per la quale l' $\int B\,dl$ medio è 982 kG cm.

(*) *Traduzione a cura della Redazione.*

SUPPLEMENTO AL VOLUME XV, SERIE X
DEL NUOVO CIMENTO

N. 2, 1960
1° Trimestre

A Compact Processing Plant for Thick Nuclear Emulsions.

J. E. HOOPER, E. DAHL-JENSEN and E. B. NEERGAARD

Institute for Theoretical Physics - University of Copenhagen

(ricevuto il 10 Settembre 1959)

Summary. — A compact processing plant for large nuclear emulsion stacks is described. A « wet » development procedure, which has been found to yield satisfactory results is discussed, together with certain more specific problems, such as the surface deposit of silver and the rate of silver removal from the emulsion during fixation.

1. – Introduction.

The general principles which should be observed when processing thick nuclear emulsions ($\geqslant 100$ μm) are already well known, and have been described by many authors [1-4]. A temperature cycle is usually used in the development stage to ensure even development throughout the depth of the emulsion, the whole thickness of the emulsion being filled with cold, relatively very inactive developer before the temperature is allowed to rise and the development proper to begin.

At all stages the aim must be to keep the swelling of the emulsion layer to a minimum, thus reducing the probability of bubbling or distortion. This is done during development by using slightly acid developer, ($p_H \approx 6.5$) and in the fixing and washing stages by keeping the temperature low (about 5 °C) and by controlling carefully the composition and flow of the liquids used.

---

(1) C. C. DILWORTH, G. P. S. OCCHIALINI and R. M. PAYNE: *Nature*, **162**, 102 (1948).
(2) C. C. DILWORTH, G. P. S. OCCHIALINI and L. VERMAESEN: *Bull. C.P.N.U.L. Brux.*, **13**, (1950).
(3) A. D. DAINTON, A. R. GATTIKER and W. O. LOCK: *Phil. Mag.*, **42**, 396 (1951).
(4) P. DEMERS: *Ionographie* (Montreal, 1958).

A typical procedure for processing a 600 μm electron sensitive emulsion would thus consist of the following steps: presoak (to soften the gelatine) in distilled water for 2 hours — temperature from room temperature to 5 °C. Soak in cold developer for 3 hours at 5 °C — hot stage 50 min at 25 °C — stop in ½% acetic acid for two hours at 10 °C, fix for 72 hours at 5 °C and wash for 72 hours at 5 °C. During the first part of the washing sodium sulphate may be added to the water to reduce the chance of bubble formation. How much influence the sodium sulphate has on the bubble formation is still an open question when the procedure described below is used, as the emulsion swells very slowly when the washing is started.

Summing up, it may be said that the most vital requirements of any plant for processing thick nuclear emulsions are adequate temperature control and suitable provision for controlled agitation of the solutions at all stages. Other points of importance are accessibility for cleaning and repair, ease of operation, and reliability. In general, development and fixing should be carried out in separate dark rooms, preferably interconnected, but, where this is not possible, one should avoid making up hypo solutions in the room in which the development is carried out, as the dust from the dry hypo crystals might otherwise cause difficulties to arise. Within the limits of these more fundamental requirements many variations are possible to suit the more particular requirements of any given laboratory.

2. – Special requirements.

When the present plant was first discussed, the most obvious special circumstance which had to be taken into account, was a lack of suitable space in respect of the desired capacity, which had to be such that an immediate problem of developing 200 emulsion sheets, 600 μm thick and of (28×31) cm² surface each, could be managed within a reasonable time. Large parts of the laboratory building could immediately be ruled out as unsuitable, in as much as the general level of radioactivity, originating from the cyclotron and Van der Graaf machines, was higher than could be desired. The only other possibility was a pair of small basement rooms, connected to each other and to the passage outside by a small entrance hall, which could be used as a light lock. These rooms were a good 50 m from the nearest sources of radiation, and in a part of the building where experimental work with radioative materials was not usual.

Lacking other possibilities, these rooms have been pressed into service, and in spite of their very small size (total useful area about 15 m² - see Fig. 1). It was clear that the apparatus would have to be built very compactly, in several storeys. Again, the hot-plate method, often used when developing by

the temperature cycle technique, would be very difficult to adapt to the available space, in so far as the plates, on being taken from the cold developer, are spread out on a temperature controlled « hot-plate » during the warm stage of the development.

Another, more general, argument against the « hot-plate » technique is that the surface of the emulsion must be mopped dry of free solution between removal from the cold stage and the commencement of the hot stage — this could amount to a very considerable operation if large areas of emulsion are to be simultaneously developed, and the requirements of strict temperature control are to be observed. Finally, there is the general point that the handling of the emulsion should be reduced to a minimum; the « hot-plate » technique is not particularly satisfactory in this respect.

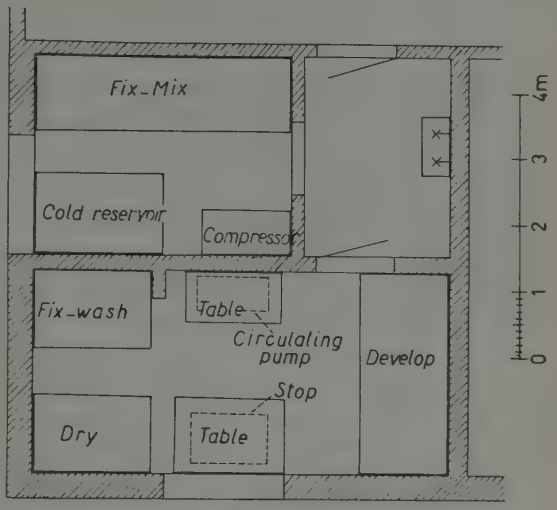

Fig. 1.

3. – Wet development.

In view of the difficulties involved in « hot-plate » development it was decided to build a plant based on the so-called « wet-development » technique, in which the plates are kept submerged in liquid throughout all stages of the development. BARKAS and his colleagues in Berkeley had used this method with considerable success ([5]).

The main problem of wet development is that of preventing under-development of the bottom layers of the emulsion. This effect is caused during the hot stage by fresh developer diffusing into the surface layers of the emulsion, where it replaces used developer which diffuses out. After some time, there is thus a considerably higher concentration of fresh developer near the surface of the emulsion than there is near the glass. BARKAS solved this problem by lowering the concentration of the development bath by a factor of approximately two during the hot stage. (The exact dilution does not seem to be

([5]) W. BARKAS: private communication (1957).

critical ([5])). Our own solution of the problem is a variant of Barkas' method and is described in greater detail in Section **9** below.

Apart from the fact that wet-development equipment is very much more compact, for a given capacity, than hot-plate equipment, there are several other advantages. Of these can be mentioned simplicity of operation, and the fact that the plates do not have to be moved between the time when they first enter the development tank for presoaking and that when they are transferred to the stop bath. Another advantage, the most important, is that it is very much easier to reproduce and control the development conditions from bath to bath so exactly that variations within the stack do not arise. A disadvantage of the method is that there is a tendency, when using developers in which silver has a certain solubility (*e.g.* the ordinary amidol-sulphite mixtures), for a deposit of silver to be formed on the emulsion surfaces. Methods for preventing the formation of this layer are at present being investigated.

4. – General description of equipment.

For the purpose of description it will be convenient to divide the equipment into parts and describe these separately. There are three main blocks of equipment: development plant, fixing and washing equipment, and the drying tanks. In addition there is a tank containing the stop bath. These various parts are served by a common refrigeration system and electrical system, the controls of which are mounted on a single panel.

The minimum capacity of the plant was decided by the immediate need of equipment capable of processing a stack of 200 emulsion sheets, of $(31 \times 28)\,\mathrm{cm}^2$ area, and 600 μm thickness, within a reasonable period of time. In this connection it was decided that a « reasonable period » would be of the order of six to eight weeks, as otherwise the last portion of the stack to be developed might be expected to gather too much background grain-density and to show appreciable fading. The complete processing time for a single plate, from the beginning of the development to the end of the final washing, is just under a week for a 600 μm thick emulsion. Thus, equipment capable of processing simultaneously batches of 40 plates would fulfil the above requirements. While awaiting development the emulsion could be stored in a refrigerator placed in a bunker under three metres of earth and concrete. (There exist no mines or caves in the immediate vicinity of Copenhagen). Both fading and the accumulation of background could thus be appreciably slowed down.

The maximum capacity of the plant was decided on the grounds that the use of very much larger stacks of emulsion than the one mentioned above does not seem probable in the foreseeable future. There might, in certain

circumstances, be use for emulsion sheets in which the one or the other dimension was slightly larger, and the apparatus was therefore designed a little on the large size with respect to immediate needs, being capable of processing plates of dimensions up to (37×40) cm² (area of the glass plates on which the emulsions are mounted). The relative dimensions of the fixing and washing equipment with respect to the development equipment are determined by the fact that the former two processes take a very much longer time than the latter. While it is necessary to fix and wash the whole batch of 40 large emulsion sheets more or less simultaneously, the emulsions may be divided into smaller batches for development. Two development tanks, with common associated equipment, each capable of taking 10 large plates at a time, were therefore used; four batches, forty plates in all, can be developed in a single day's run, and thereafter be fixed and washed together during the following five or six days.

Once the dimensions of the various components had been determined, it was possible to consider the best possible disposition of the various components in the available space. It was quickly realized that one of the most economical dispositions possible was that shown in Fig. 1.

The tank in which the fixing solutions were to be made up was placed in the adjacent room, to avoid the possibility of contamination of the equipment used for development by hypo dust. This room also contains the refrigeration plant and an ion-exchange water softener which provides water for the fixing and washing baths. (Copenhagen water is exceptionally hard, containing calcium and magnesium equivalent to about 190 mg CaO/l).

Extensive use has been made of modern plastic material throughout. In particular, 0.8 cm thick hard P.V.C. sheet has been used for the construction of all those tanks which come into direct contact with photographic solutions, with the exception of the twin developer tanks, which are of stainless steel. Likewise, use has been made of $\frac{1}{2}$ in. diameter P.V.C. piping where there would be contact with photographic solutions, and the same material has been used to build several of the heat-exchanging spirals. Although the thermal conductivity of P.V.C. is low ($4 \cdot 10^{-4}$ cal/s cm °C as compared to steel $1000 \cdot 10^{-4}$ cal/s cm °C), it was found that, in those instances where space presented no particular problem, long lenghts of P.V.C. piping could provide sufficient heat exchange at a lower cost than stainless steel piping. At the same time, the fact that a very much larger cooling area is used reduces appreciably the problem of obtaining a uniform temperature within the vessel, despite the fact that stirring must be kept within strict limits.

The frames on which the various pieces of equipment were mounted were construncted of « Handy » steel profile, which is supplied in standard lengths already provided with bolt holes. The profile is quickly and easily assembled and of more than sufficient strength for the present purpose. All the steel

frames were given an extra coat of rust protecting paint after assembly, to reduce the risk of corrosion.

All the various tanks, with the exception of that in which the fixing solutions are made up, have been enclosed in fibre-board boxes, which in turn are lined with a 4.5 cm thick layer of polystyrene foam heat insulating material. This material is particularly suitable for this use because it is completely impervious to water, and therefore does not lose its excellent heat insulating properties even when thoroughly drenched. Lids for the various tanks were likewise built of fibreboard, enclosing a sheet of polystyrene foam, suitably strengthened with extra wooden supports where an electric motor or other equipment was to be mounted. The exterior surfaces of both boxes and lids were given three layers of paint to protect them from splashes. In addition, all lengths of piping carrying liquids at temperatures other than room temperature have likewise been insulated with polystyrene foam.

The total cost of the installation (excluding the authors' time) was about D.kr. 30000 ($ 4400 at the present rate of exchange).

As mentioned above, it is often advantageous to be able to process the emulsion as soon as possible after exposure. While in many instances the background and fading resulting from the journey from the accelerator laboratory to the home laboratory would not involve serious consequences, there are certain experiments in which a low background and a high grain-density would be particularly desirable. In such instances, it might be worth considering the possibility of taking the processing plant to the accelerator laboratory. The total space occupied by the present equipment is such that this would present no serious problems, in so far as the whole plant could easily be built into a large furniture van, and used there.

5. – The racks.

Several points were considered when designing the racks in which the plates were to be held during the processing. Of these particular weight was placed on simplicity — they should be easy to take apart and clean — and adjustability — it should be possible to use the same racks for emulsions of all sizes up to the maximum, in such a way that the plant as a whole can always be used at almost full capacity, provided, of course, that the total volume of emulsion to be processed is not too small.

Another important consideration is the effect of the racks and plates on the circulation of liquids within the various tanks in which they are placed. Their design should be such that the desired circulation is encouraged, while undesirable eddy currents are prevented from reaching the surfaces of the emulsion.

The very simple form chosen is shown in Fig. 2. The rack itself consists

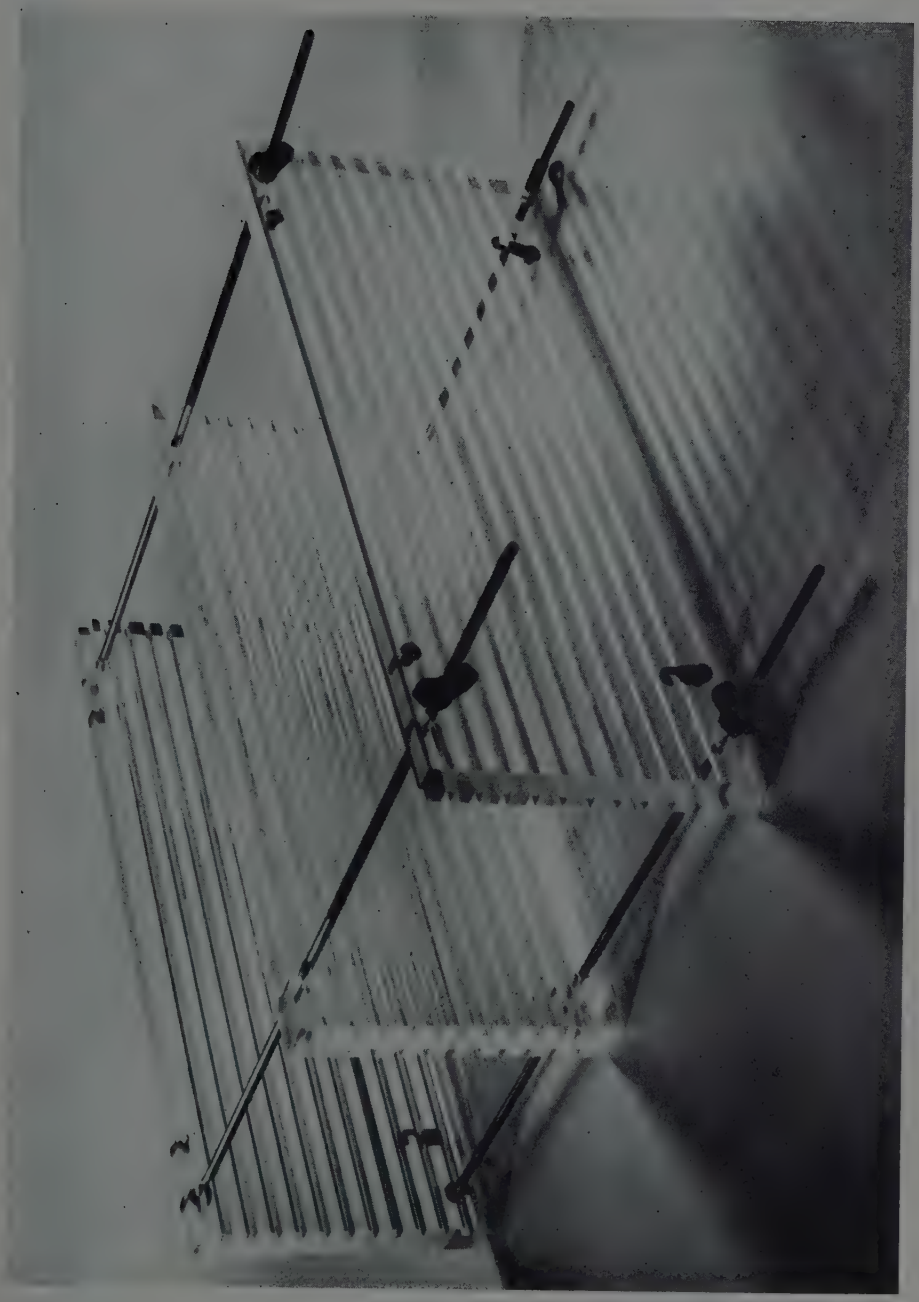

Fig. 2.

of two perspex end pieces, each of which is provided with eleven parallel horizontal grooves, of (5×2) mm² cross-section, cut into the inner surface. The plates slide into these grooves. The two end pieces are held together by four long stainless steel rods, with long screw threads cut into them, on which wing nuts can run. When the width of the plates to be processed is less than half the maximum width for which the racks are designed, a centre piece of perspex, with grooves cut into both surfaces, can be used to double the number of plates which can be processed in one batch. Note that the top groove is always filled with a piece of plain glass so that each emulsion surface is at the same distance from an overlying glass surface. Each rack can thus hold ten large plates or twenty or forty smaller ones.

The question of the control of the circulation is discussed individually for the development and fixing in Sections **8** and **13**.

6. – The refrigeration system.

The refrigeration system, which serves both the developing equipment and that used for fixing and washing, has to have a considerable capacity, as the peak load during development, when the fixing solution is being simultaneously cooled, can be as high as $(3000 \div 4000)$ kcal/hour. However, calculations on specific programmes showed that the *average* load over one day, during which four batches of emulsions were developed, was considerably lower, being approximately 1500 kcal/hour. Taking into account the heat gained from the surroundings, and that produced by pumping, a refrigeration unit of capacity 2000 kcal/hour was chosen. To cope with the peak load, this unit was installed in connection with a « cold » reservoir containing 400 l of 30% ethyl alcohol solution, the temperature of which is normally maintained between -4 °C and -10 °C. During periods of peak load, the temperature is allowed to rise to 0 °C, thus providing a reservoir of approximately 2000 kcal.

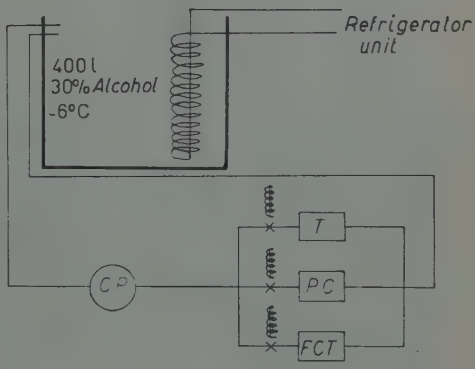

Fig. 3.

Liquid from the « cold » reservoir is circulated, as required, by a centrifugal pump to the various parts of the equipment to be cooled (Fig. 3). The flow is controlled by « Danfoss » solenoid valves, which in turn are controlled by the contact thermometers regulating the temperature of the various baths

in question. Starting and stopping of the centrifugal pump is controlled automatically by a « Danfoss » relay connected in such a way that the pump motor is switched on as long as one or more of the solenoid valves is open, and switched off again as soon as all the solenoid valves are closed. The relevant circuit is shown in Fig. 4.

7. – The electrical system.

All the electrical control units are collected on a common panel, on which are also placed the various lamps and switches connected with the alarm systems. This panel is shown in Fig. 4. Each piece of electrical equipment is connected in parallel with a small neon discharge lamp, or in series with a filament lamp of suitable size, which is also often used instead of a fuse. A glance on the panel can thus provide information on what equipment is functioning at any time.

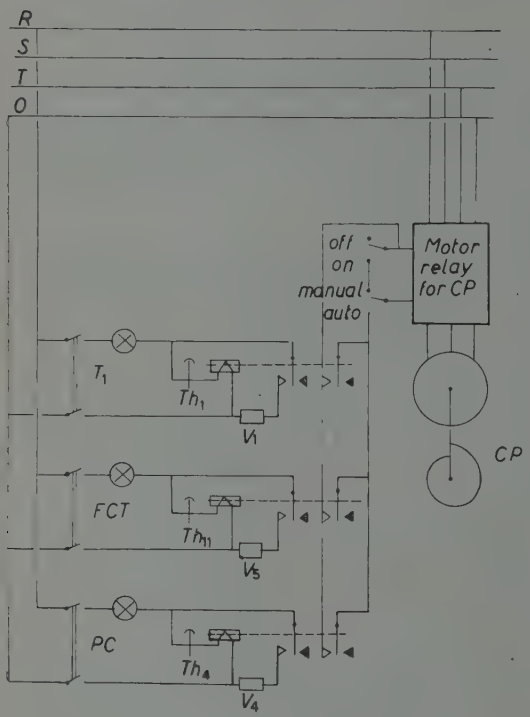

Fig. 4.

There are four main sets of controls on the panel. Firstly there are the switches, rheostats, and filament lamps, which act as fuses, serving the five stirrer motors. Note that all the filament lamps used on the panel are placed behind small windows constructed of suitable orange-red darkroom filter.

Secondly, there is a group of five switches and filament lamps serving the five thermostat systems. (Marked « termostater » on Fig. 5). These are made in such a way that the closing of the contact in a thermometer opens or shuts the circuit to a corresponding solenoid valve. The three cooling circuits are connected in such a way that the centrifugal pump which drives the cooling liquid around is, provided switch is placed at « auto », automatically switched on as soon as one or more of the three solenoid valves is opened. The circuit used is sketched in Fig. 4. Note that the lamps connected with

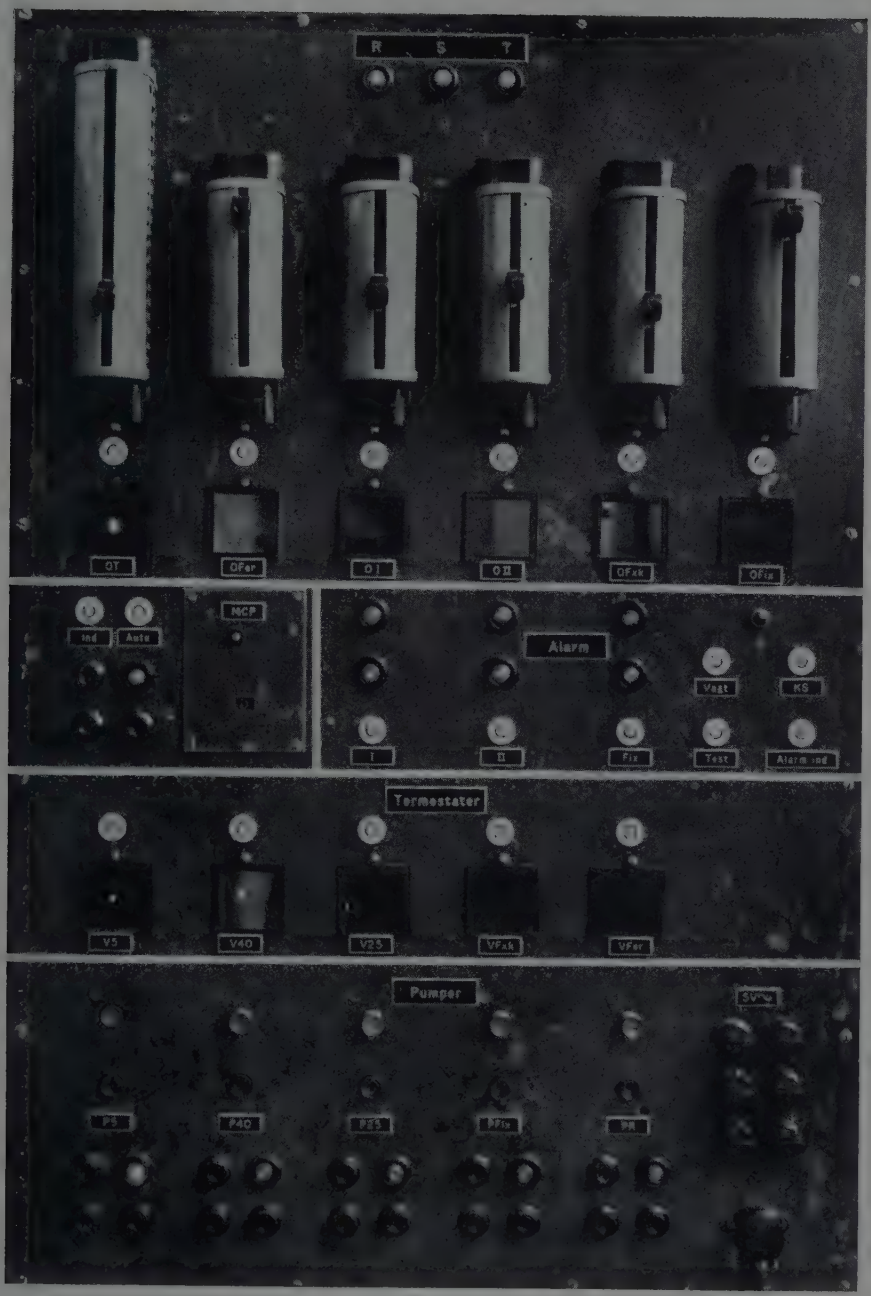
R
S
T
OT
OFør
OI
OH
OFxk
OFix
Ind
Auto
NCP
Alarm
Vakt
KS
I
II
Fix
Test
Termostater
V3
V40
V25
VFxk
VFør
Pumper
P3
P40
P25
PFix
PH

Fig. 5.

these five circuits show that the solenoid valve in question is open, not that the thermostatic control is switched on. They thus indicate that the true temperature is *not* that desired.

The third set of controls is the on-off switches serving the motors of the neoprene rotor pumps, of which there are five; three circulating water from the thermostats T_{1-3} (Section **8**), one circulating fix (Section **13**), and a mobile pump, the use of which is described in Section **9**. All these pumps are driven by $\frac{1}{4}$ hp 3-phase motors. Associated with each switch is a discharge lamp showing when the one phase « *R* » is switched on, and a separate fuse for each of the three phases.

The fourth and last group of switches and lamps gives information or controls the warning systems. At the top of the panel are three discharge lamps, one for each phase, which indicate that the panel is connected to the power supply. Lower on the panel are the alarm systems proper. Two pairs of discharge lamps, each served by a switch so that they can be put out of operation if desired, monitor the temperature of the developer solution during the « hot » stage, as described in Section **8** below. Another set of lamps and switches to the right of these provides visual warning when the temperature in the fix tank rises above a predetermined level, or when the power supply fails. In

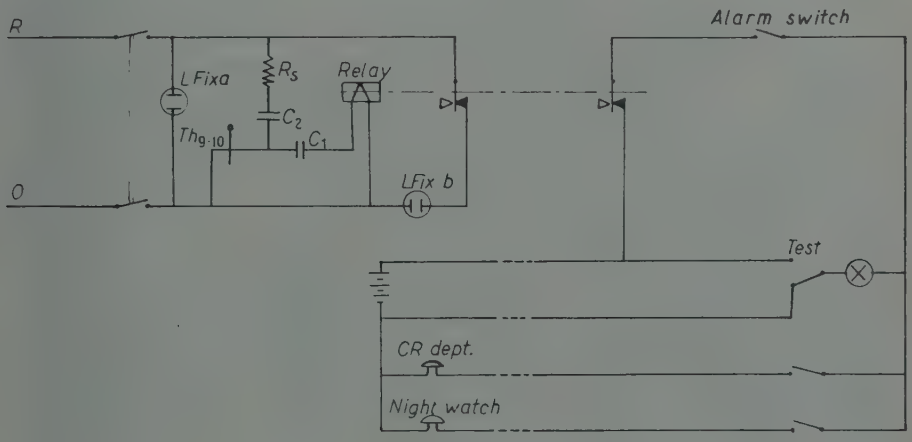

Fig. 6.

addition, two battery operated bells, the one placed in the part of the building where the emulsion group has its main laboratories (at some considerable distance from the darkroom), the other placed in the night watchman office, can be switched in as needed. This alarm circuit is shown in Fig. 6.

8. – Development equipment.

8·1. *General.* – Fig. 7 is a schematic diagram of the apparatus built for the development itself, while a photograph showing the arrangement of the various components with respect to each other is shown in Fig. 8.

The main parts of the development equipment are the three thermostates, T_1, T_2 and T_3, which are normally used at temperatures of 2 °C, 45 °C and 27 °C respectively, a precooler thermostat, *PC*, and the two developer tanks, *D* I and *D* II. The temperature in these two last mentioned tanks may be controlled by circulating water from the three thermostats through built-in heat-exchangers, the circulation being achieved by means of the three neoprene rotor pumps P_1, P_2 and P_3, each of which works in connection with the corresponding thermostat.

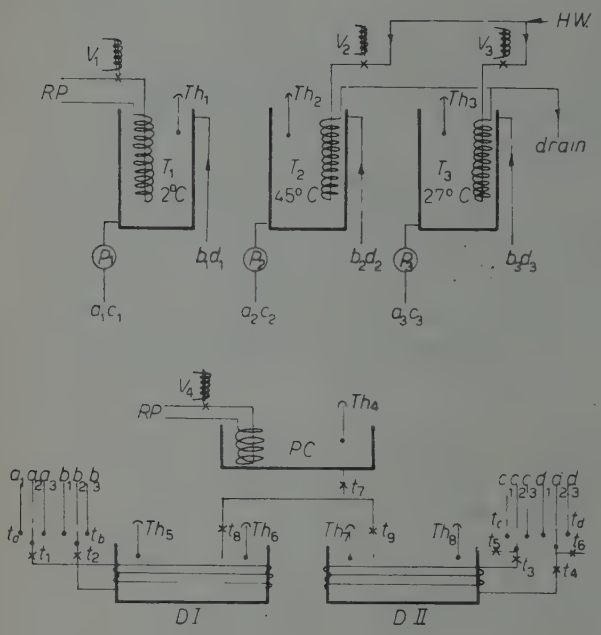

Fig. 7.

8·2. *Thermostats.* – Three large aluminium tanks, each of 100 litres capacity, are used in the construction of the thermostats. Each is equipped with an aluminium spiral of 10 m total length, and 10 mm inside diameter, and a contact thermometer, $Th_{1,2 \text{ or } 3}$, which is connected in a suitable circuit in such a way that it can control the circulation of cooling (warming) liquid through the spiral by opening or shutting the corresponding solenoid valve, $V_{1,2 \text{ or } 3}$. A single 1000 W electric motor driving three rotating paddles, one for each tank, through O-rings, provides adequate stirring.

T_1 is cooled by liquid from the central refrigeration plant described in Section 6 above. T_2 and T_3 are warmed by circulating water from the laboratory's hot water system through their aluminium spirals.

Before going further, a word of warning is necessary. The spirals, which are of drawn aluminium tubing, bent into shape, are not entirely satisfactory

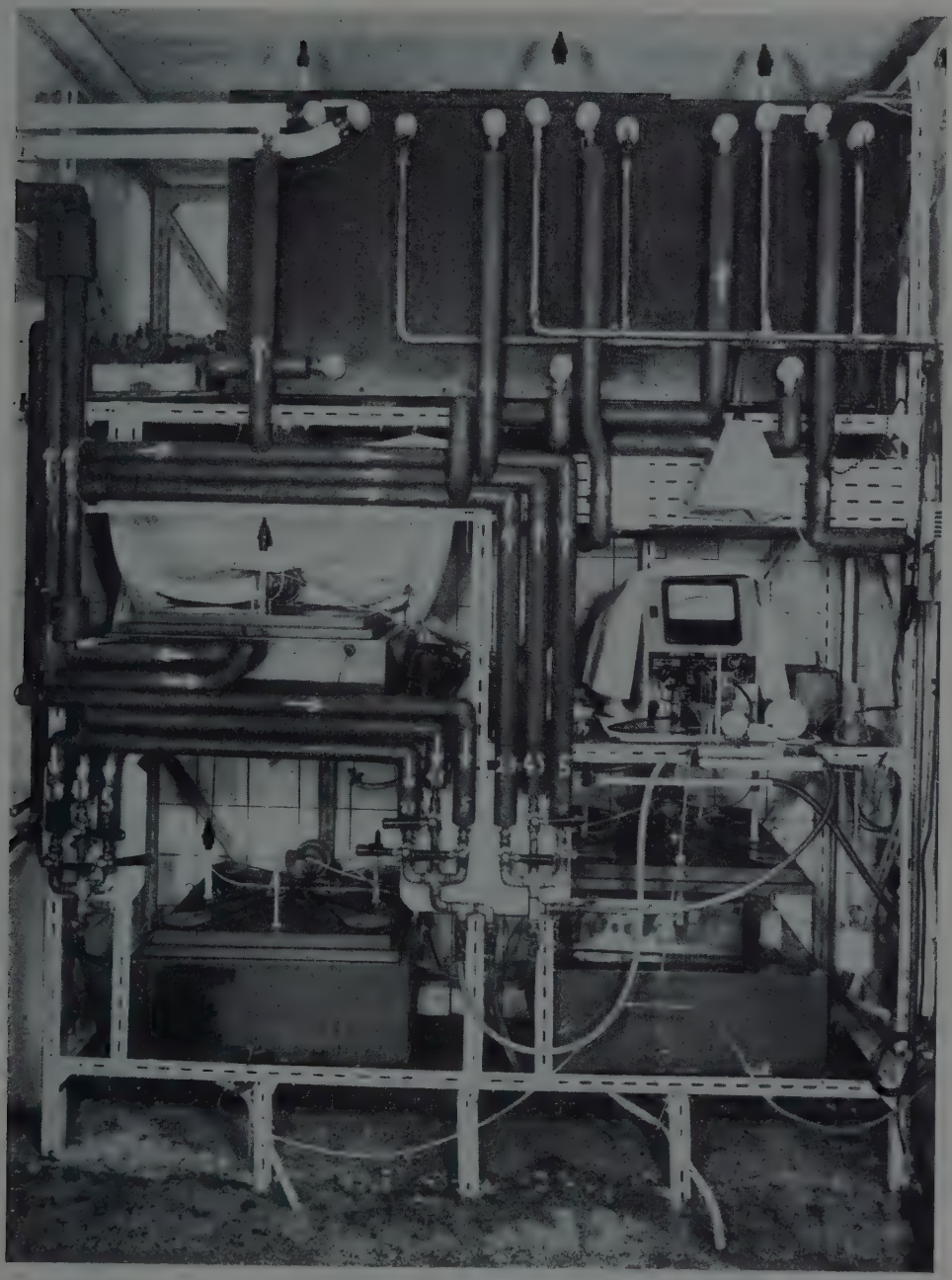

Fig. 8.

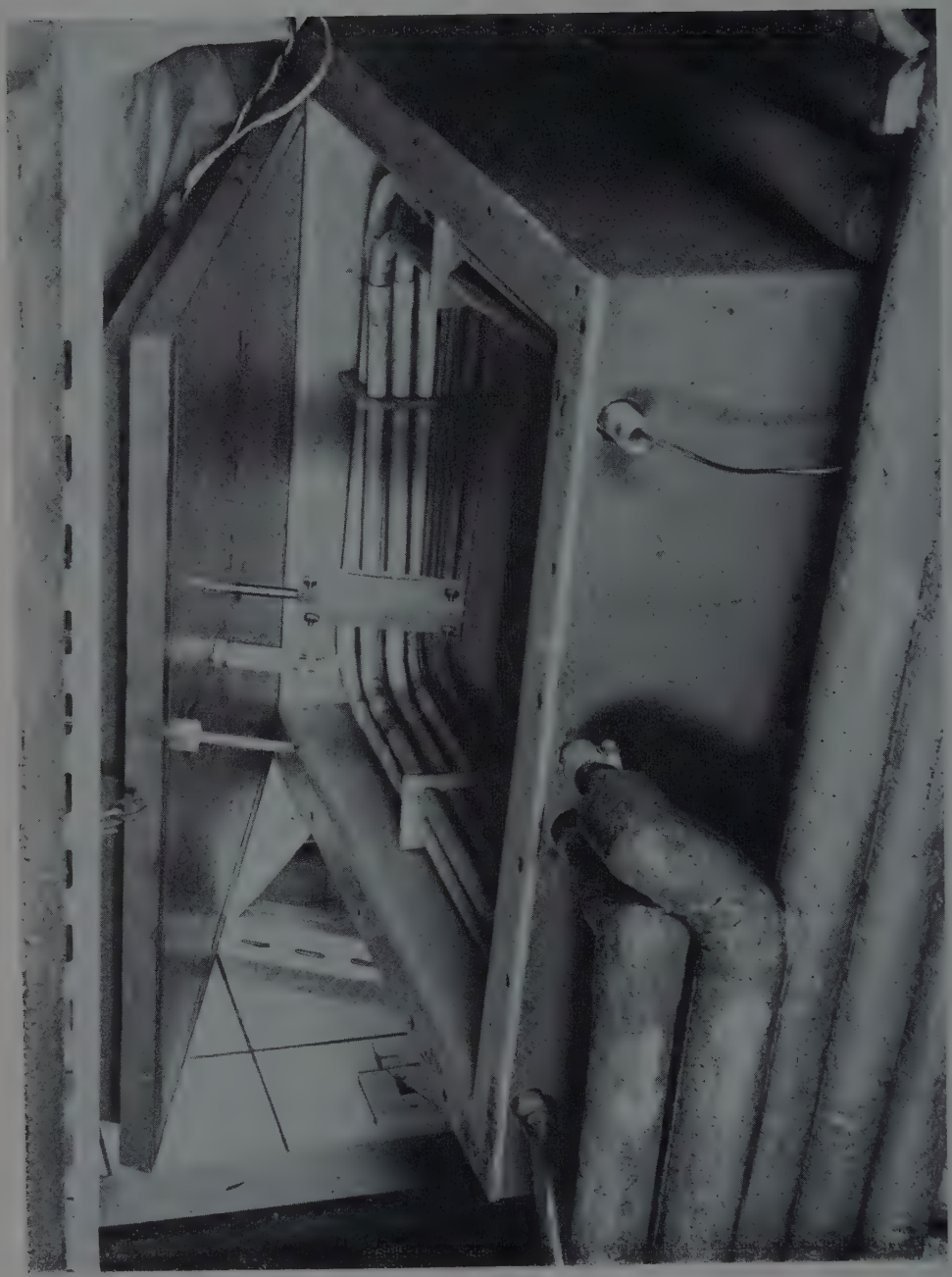

Fig. 9.

in thermostate T_2 and T_3. After about one year of use the metal is beginning to recrystallize, so that it will probably be necessary to replace them in the not very distant future.

8·3. *Precooler.* – The precooler thermostat is a 35 litre flat tank built of chemically resistant hard P.V.C. Cooling is achieved by circulating cooling liquid from the central refrigeration plant through a 10 m spiral of $\frac{1}{2}$ in. hard P.V.C. tubing (Fig. 9). As mentioned above, the temperature is controlled by a contact thermometer, Th_4, which regulates the opening and shutting of the solenoid valve V_4. Stirring is provided by a paddle which is driven directly by a geared down 600 W motor mounted on the lid of the tank.

8·4. *The developer tanks.* – The tanks in which the development is actually carried out, D I and D II, are built of 1 mm thick polished 18/8 stainless steel plate, welded at the corners (Fig. 10). The inside dimensions of each tank are $(50 \times 50 \times 15)$ cm³ (effective volume about 33 litres). Thermal contact between the contents of the tanks and those of the thermostats is achieved by circulating water from the thermostats through 10 m of $\frac{1}{2}$ in. copper tubing soldered directly to the outside of the developer tank. This arrangement has been found to provide adequate heat transfer.

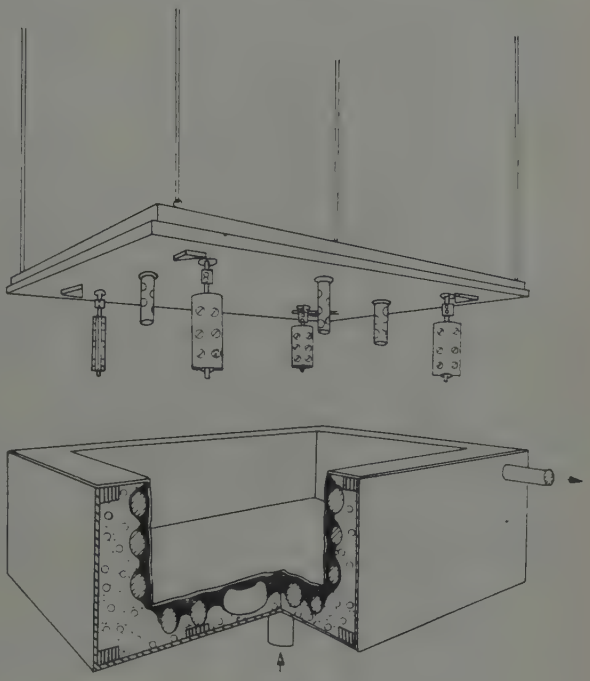

Fig. 10.

The effective heat transfer is easily calculated from the temperature-time curve as measured over the interval between the cold stage and the warm stage. A typical curve, taken during a trial run, is shown in Fig. 11. It should be remarked that the temperature of T_2 falls during the heating period from 45 °C to $(36 \div 37)$ °C, but, despite this fall, the temperature-time curve is extremely constant from run to run. The measured heat transfer is found from the curve to be 1.5 kcal/min °C.

The flow of liquid between the thermostats and the copper spirals is controlled by four three-way sets of taps, t_a, t_b, t_c and t_d. These are arranged in such a way that it is easy to see which are open and which are closed, so that the chance of making a mistake and sending water from one thermostat back to another one is considerably reduced.

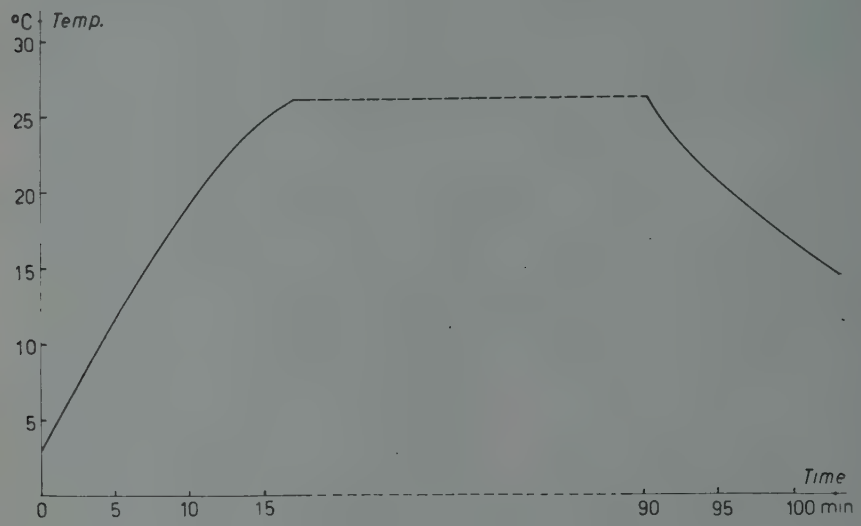

Fig. 11.

Additional taps, t_{1-4}, allow each of the copper spirals to be closed off completely when the corresponding tank is not in use. Taps t_5 and t_6, just under the three-way taps sets t_c and t_d, lead to nozzles to which can be connected tubing leading to other apparatus which is to be temperature controlled (*e.g.* a small developer tank for experimental work) (see Fig. 8).

Suitable stirring within the developer tanks must fulfil certain conditions. In the first palce, it must be adequate to ensure that at no time there can exist appreciable temperature gradients in the solution. On the other hand, if it is too violent, there is a risk of producing distortion in the emulsion, especially during the hot stage. At the same time, the paddles used must be placed in such a way, and be of such a size, that they occupy the least possible space within the tank.

The following solution has been found satisfactory. On the lid of each of the tanks are mounted four paddles, which can be rotated about a vertical axis. Each paddle blade consists of two pieces of hard P.V.C. sheet, of surface area (10×5) cm², clamped onto a stainless steel axle. These are mounted as near the corners of the tank as possible and driven by a single 600 W electric

motor, the speed of which can be continuously altered, in such a way that two of them rotate clockwise and two anticlockwise (see Fig. 12). Placing the racks so that the position of the end pieces with respect to the paddles is as shown in the figure ensures a smooth horizontal « figure of eight » flow in the solution, with a minimum of turbulence.

During the cold stage and the hot stage, when the temperature of the solution in the tank is being held stable, sufficient motion of the liquid is obtained by allowing the paddles to rotate at about (30÷40) r.p.m. Between these stages, and at the end of the hot stage, the temperature is changed rapidly, and, to ensure uniform temperature and good heat transmission, somewhat more vigourous stirring is required. Good results have been obtained by driving the paddles at (80÷90) r.m.p.

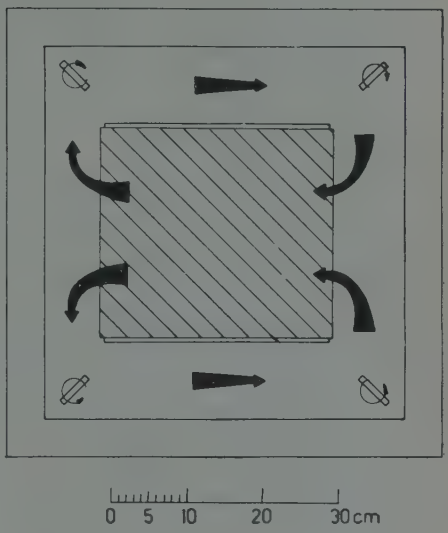

Fig. 12.

Accurate control of the temperature of the developer during the hot stage is of the utmost importance if strictly reproducible results are to be obtained. To provide adequate warning should the temperature begin to wander during this stage, each of the developer tanks is equipped with two contact thermometers, connected in such a way that the first lights a discharge lamp on the electrical control panel as soon as the temperature of the developer solution has reached a temperature lying just below that desired, while the second thermometer lights another discharge lamp when the temperature of the solution passes a value lying a little above the desired development temperature. The temperature interval within which one works may be made as small as the accuracy of the thermometers permits. In practice, an interval of about 0.5 °C has been found satisfactory.

9. – Use of the development equipment.

When the equipment is to be used at full capacity (*i.e.* forty (30×30) cm^2 or an equivalent number of smaller emulsions are to be fixed in the same batch), it is necessary to develop four racks of plates in as short a time as possible. This involves overlapping the use of the two developer tanks in such a way that full use is made of the precooler tank, and this in turn demands

a strict time- table, the details of which depend to some extent on the nature of the development to be carried out.

The procedure which we describe below has been found suitable for 600 μm thick Ilford G-5 emulsions.

The developer solutions used are dissolved in 60 l glass carboys befo starting the development or between runs. In practice it is convenient make up the solutions well before starting, without the amidol, which is add dry about half an hour before the solution in question is to be used. Two solutions are used in each development. These are made up as shown in Table I.

TABLE I.

	A	*B*
Amidol (hydrocloride)	4.5 g	1.9 g
Boric Acid (am.)	35 g	35 g
Sodium Sulphite (sicc. 85%)	18 g	18 g
Pot. Bromide	0.8 g	1.6 g
Distilled water to 1 liter	pH = 6.4	pH = 6.6

30 litres of each solution are made up. Solution A is the standard Brussels recipe for thick emulsions. Solution B has been found to give a flatter variation of the grain density with depth in G-5 emulsion than the use of the usual watered down A solution, and it has the particular advantage that the pH is nearly the same as that of the strong solution A used in the cold stage. Its use was first tried following a suggestion of Prof. OCCHIALINI ([6]).

Transport and mixing of the various developer solutions is carried out with the aid of a small mobile pumping unit, consisting of a « Jabsco » neoprene rotor pump in a bakelite housing, mounted together with a suitable electric motor in a wooden box which can be rolled on small furniture castors (Fig. 13). Solutions to be mixed are stirred very simply by inserting both hoses from the pump into the carboy. Provided both nozzles are placed under the surface of the liquid, little air which can oxidise the developing agent will be mixed in. When the solutions are to be used they are pumped directly from the carboy to the precooler tank, *PC*.

The plates to be developed, held in a rack (Section **5**), are placed in one of the developer tanks which has already been filled with distilled water at room temperature. This is then cooled over a period of about one hour to 2 °C by circulating water from thermostat T_1. After two hours the distilled water is drained off, and the tank is refilled with the developer solution A which has

([6]) G. P. S. OCCHIALINI: private communication (1958).

Fig. 13.

been cooled to 2 °C in the precooler tank during the previous hour. The temperature of solution A is kept at 2 °C during three hours, at the end of which time it is replaced by solution B (at 2 °C) from the precooler tank. The circulation of water from T_1 is then stopped, and replaced by a circulation from T_2 (45 °C). At the same time the speed of rotation of the stirring paddles in the developer tank is approximately doubled. The temperature of the solution in the tank now increases smoothly (see Fig. 11), until it reaches the temperature chosen for the hot stage of the temperature cycle (26 °C), when the circulation from T_2 is replaced by that from T_3, which stabilizes the temperature of the solution, and the stirring speed is again reduced. At the end of the hot stage (which lasts from 50 to 80 min at 26 °C), circulation from T_3 is again replaced by circulation from T_1, the contents of the tank being cooled to $14 \div 15$ °C. The rack of plates is then removed from the developer tank and transferred to the stop bath, which is kept at a temperature of 11 °C.

10. – Development: results.

The procedures described in Section **9** above have been found to be well suited to the development of Ilford G-5 emulsions. The variation of blob

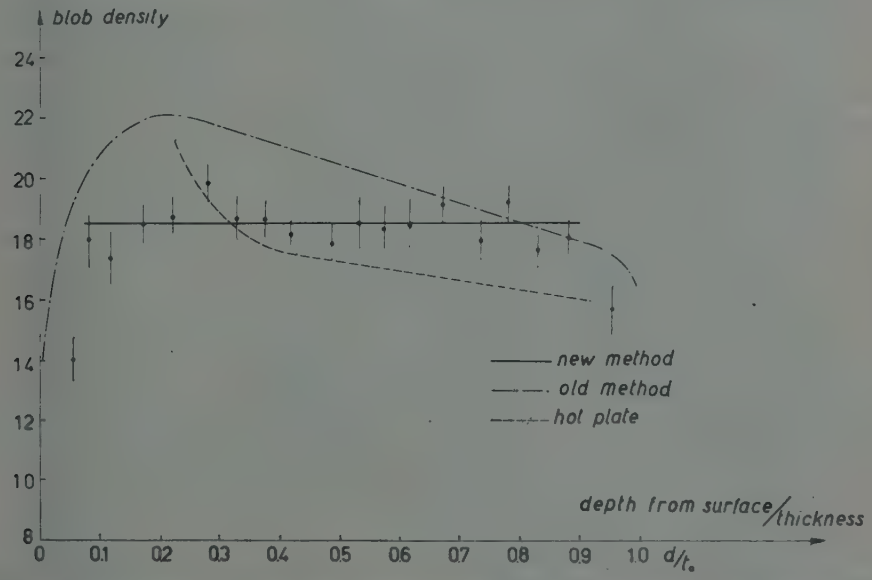

Fig. 14. – Hot plate: A Bristol development from 1954. Old method: Solution A diluted with an equal volume of water during the hot stage. New method:9 As described in the text.

density with depth for a typical 600 μm G-5 emulsion is shown in Fig. 14, the tracks counted being those of 240 MeV π-mesons. Through the greater

part of the thickness of the emulsion the curve is seen to be extremely flat, the value of the blob-density here being (18.4 ± 0.3) blobs/100 μm, corresponding to a plateau blob-density of about 20 blobs/100 μm. The absolute value here in these plates must be considered satisfactory in view of the fact that they were shipped across the Atlantic without being frozen down, and the restriction on too heavy a development inherent in the rather heavy slow electron background which they contained. The figure also shows that the blob-count falls off rapidly close to the surfaces of the emulsion. It is not at present clear whether this is an effect due to the conditions of development. A possible cause, could, for example, be accelerated fading in the layers close to the surfaces resulting from the fact that these layers absorb considerable quantities of water when the emulsion is dipped into gelatine solution prior to mounting on the glass plate ([7]). Another possibility which has been considered is the so-called « Herschel » fading, which would result from excessive exposure to the dark-room lamps. However, the intensities which have previously ([8]) been found to be necessary to produce the effect in nuclear emulsions are greatly in excess of those arising from the lamps which we have used. At the same time, such an effect would be expected to lead to a considerable difference between the top and the bottom of the emulsion, which are, in fact, surprisingly alike.

With respect to the variation of the blob-density from batch to batch, the results are very satisfactory. The variation between 16 different batches of 10 plates each (fixed in four batches of 40 plates each, over a period of four weeks), is less than 5%. This indicates that the temperature control used is sufficiently good, and secondly, that at the temperature of about 5 °C, at which the plates were stored, there is no appreciable fading over a period of a month.

11. – The stop bath.

After an initial cooling to 14 °C, the development is finally stopped by soaking the emulsions in a standard 0.5% acetic acid bath, which is contained in a hard P.V.C. tank of inside dimensions (50 × 50 × 15) cm³, exactly similar to that used for the precooler tank. The temperature of the bath is maintained at about 10 °C, by passing running water from the city supply through a suitable plastic cooling « mat », lying on the bottom of the tank. The mat is constructed of a large number of fine parallel plastic tubes of comparatively small inside diameter, which are fed and drained from heavier P.V.C. tubes

([7]) G. P. S. Occhialini: *CERN Rep.* 59-13, 17 (1959).
([8]) H. Souvenier and L. Winand: *Bull. Soc. Roy. Sci. Liège*, **18**, 156 (1949).

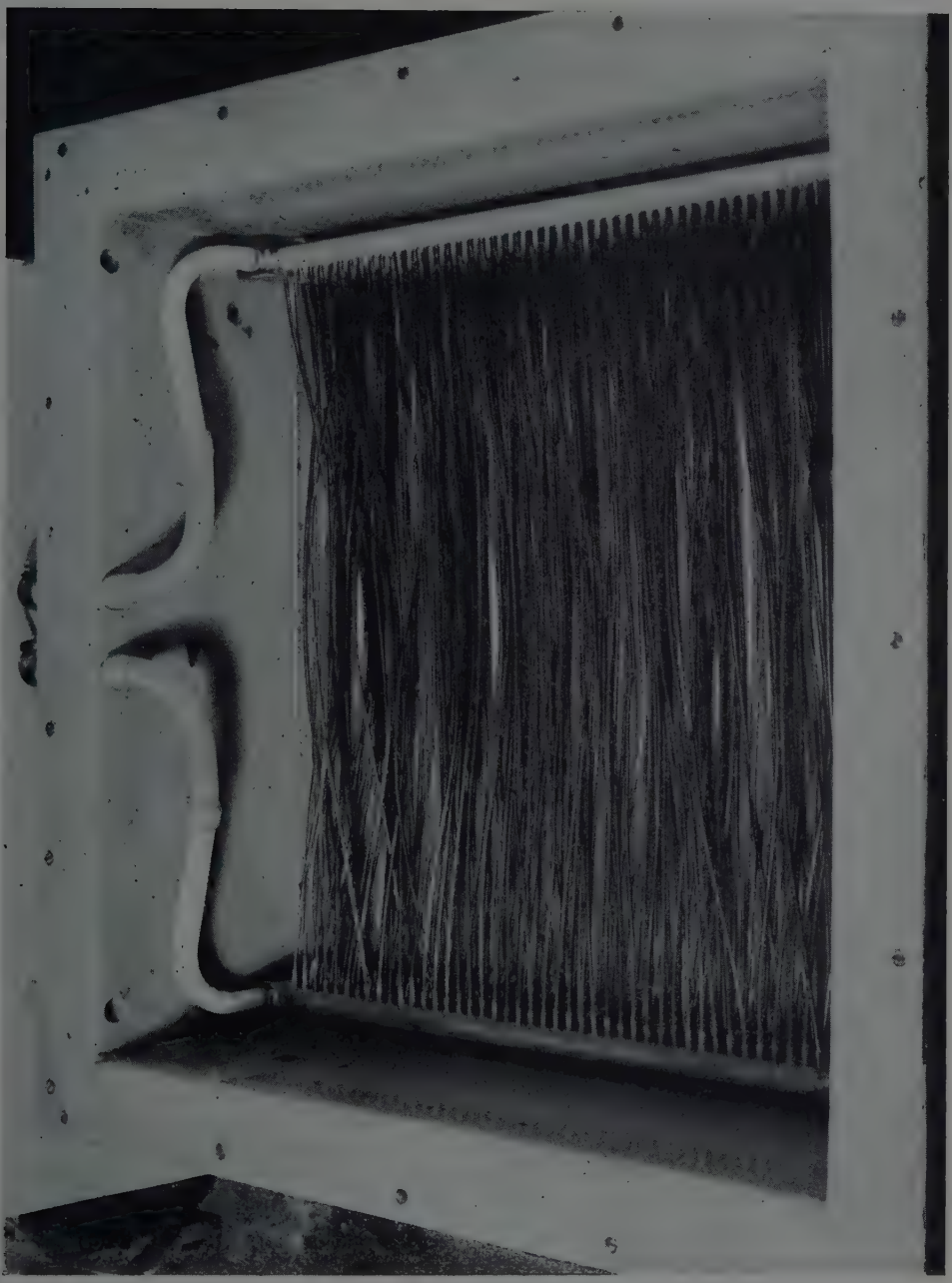

Fig. 15.

at the ends (Fig. 15). This arrangement provides a large and well-distributed cooling surface in the minimum of space and with the minimum of resistance to the flow of the cooling water.

12. – The removal of the silver deposit.

The high concentration of silver present in nuclear emulsions often results in the formation of a silver deposit on the surface of the emulsions during development. The effect is particularly marked when amidol is used as the developing agent, and is further aggravated when a « wet » hot stage is used. Occhialini [6] has used silver coins facing the plates during the initial cold stage, and found that this greatly reduces the silver deposit. We have tried silver plates during the hot stage, but have not found any appreciable improvement. The reason is perhaps that the materials used in the two instances were different. While Occhialini's tank is built of silver plated copper, ours was built of polished stainless steel. It is thus possible that the one arrangement acts as a weak galvanic element, removing excess silver from the solution. To test these ideas we have carried out the following experiment. Five 100 μm thick G-5 emulsions were strongly developed in a plastic vessel, the usual developer being used. Above four of them a thin sheet of metal was placed parallel to the surface, being about 2 mm above it. The fifth plate was left free. The results of the experiments are set out in Table II.

Table II.

Plate no.	Metal	Density of surface silver
1	Cu	0
2	Al	1
3	18/8 steel	3
4	Ag	10
5	—	3

These results confirm Occhialini's and at the same time show why the addition of a silver plate in an 18/8 tank helps very little. In this connection it is perhaps worth remarking that the widespread fear of copper or brass in contact with the developer is, in our experience, absolutely unfounded. We have made extensive use of a small test tank which is milled from a solid

brass (*) block, and have obtained results which are in no way inferior to those obtained when using stainless steel, plastic or glass tanks.

Once the deposit is formed, one may either remove it by gentle rubbing while the plates are still wet, or wait until the emulsions are finally dried, when it may be removed by much more vigorous rubbing with a chamois leather soaked in xylol. The former procedure has certain advantages, in that the silver is much more easily removed from the wet emulsion. On the other hand the emulsion is soft, and one risks introducing distortion if one rubs too hard. In addition, one might believe that there was a risk of removing some of the surface emulsion together with the silver. However, in practice both these effects are found to be very small. One should, of course, choose the point after development at which the emulsion is most firm. This is immediately after the stop-bath, the acidity of which causes the gelatine to contract and harden. At this stage the emulsion still retains its « skeleton » of silver bromide, which also helps to maintain the rigidity. We have therefore mopped the silver off at this stage with medical cotton wool. Our measurements suggest that the layer of emulsion removed from the surface by rubbing is almost certainly under 1 μm thick. Likewise, we have not been able to find evidence for serious distortion or scratching of the surface, resulting from the rubbing.

13. – Fixing and washing equipment.

The equipment built for fixing and washing the emulsions consists of three large tanks built of hard P.V.C. — one (FT) in which the emulsions are actually fixed and washed, one (FCT) in which the solutions are cooled before being circulated to FT, and one (FMT) in which the large quantities of solution can be made up prior to use. In addition, a Jabsco neoprene rotor pump with a bakelite housing is used to circulate the cold solutions between the fix cooling tank (FCT) and the fixing tank (FT). Fig. 16 is a diagrammatic sketch of the apparatus, showing the interrelation of the various parts. Note that all the piping used in this part of the equipment is of hard P.V.C.

13·1. *The fixing tank.* – The fixing tank, built of 0.8 cm thick hard P.V.C., has interior dimensions (100×50) cm^2 $\times 30$ cm deep. It is divided into two equal compartments, each of bottom area about (50×50) cm^2, by a wall of P.V.C. This enables a considerable reduction in the minimum quantities of solutions which can be used when the quantity of material being processed is less than half the maximum capacity of the equipment.

(*) 67 Cu 33 Zn.

Stirring in each of the halves of the tank is provided by a propeller of very high pitch (Fig. 17) mounted vertically in one corner. This is driven very

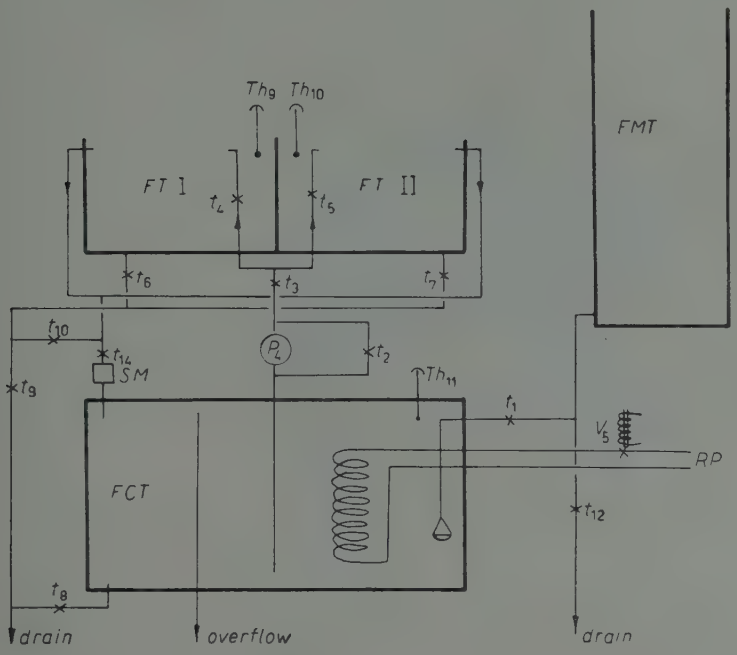

Fig. 16.

slowly (60 ÷ 100) r.p.m. and its main purpose is to ensure that the heavy silver salts do not sink to the bottom of the bath.

13·2. *The fix-cooling tank.* – The fix cooling tank, FCT, is built of hard P.V.C., 0.8 cm thick, with interior dimensions $(100 \times 50 \times 50)$ cm³. It is equipped with a large stirring paddle of dimensions (25×15) cm², mounted on a vertical rotating axle of stainless steel driven by a 600 W electric motor (geared down 1/20) mounted on the lid of the tank. In addition, the tank is provided with a 40 m spiral of hard P.V.C. piping (diameter $\frac{1}{2}$ in.) through which cooling liquid from the central refrigeration system may be circulated, the circulation being controlled by a contact thermometer in connection with a solenoid valve, as described above in Section **7**.

13·3. *Fix mixing tank.* – A large tank (FMT) of steel reinforced P.V.C. of dimensions $(230 \times 50 \times 90)$ cm³ is used for making up the various solutions used for fixing and washing. The dimensions of the tank, which is not heat insulated, are determined by the condition that it should be possible to make

up sufficient fix solution to clear all the emulsion in the fixing tank when it is filled to capacity. Assuming that one begins with a silver concentration of 2 ‰ and that the concentration is to be held under 6 ‰ the required capacity is about 1000 l, the capacity of the equipment being about 2 l of emulsion. This tank is placed in the room adjacent to the main darkroom, together with the central refrigeration plant. In this way it is possible to avoid thiosulphate dust in the air around the developing equipment.

To shorten the time required to dissolve the salts used, tank FMT is equipped with a powerful stirrer, consisting of a marine propeller of nylon (diameter about 30 cm), driven by a 1000 W electric motor (geared down 1/20). In addition, a 200 m spiral of $\frac{1}{2}$ in. hard P.V.C. piping is built into the tank. This can be connected to either the hot or cold water supply as desired: thus heat may be provided while the salts are being dissolved, while the solutions may later be cooled prior to their arrival in the fix cooling tank, thus reducing the load on the central refrigeration plant. This is of particular importance during the occasional spells of hot summer weather which have been known to occur in Denmark.

13·4. *The fix circulation system.* – The fix circulation system is built entirely of $\frac{1}{2}$ in. diameter hard P.V.C. piping. Liquid from tank FMT flows (FMT is placed at a higher level than FCT) through tap t_1 to FCT. Before entering FCT it passes through the filter which removes solid particles. The filter is constructed of a nylon funnel, the mouth of which is covered by several layers of nylon stocking material. Excess liquid in tank FCT is allowed to flow out freely via the overflow.

Cold liquid from FCT is pumped by the neoprene rotor pump P_4 to the two parts of the fix tank FT I and FT II, returning again to FCT via an overflow arrangement. As the pump is run at constant speed, the flow is adjusted by means of a by pass through the tap t_2, which is used in connection with taps t_3, t_4 and t_5. Note that the return flow from the tank FT is led through the electrode holder, SM, of the silver concentration meter.

All three tanks are provided with bottom outlets so that they can be drained. In addition, the outlets from FT are so arranged that both the overflow and the bottom outlet can be directed back to FCT or to the drain as desired.

14. – Fixing procedure.

The four racks of emulsions, constituting a day's processing, come out of the stop bath at different times, spread over about 10 hours. If one wishes to ensure that the fixing time for all the plates be exactly the same, the first

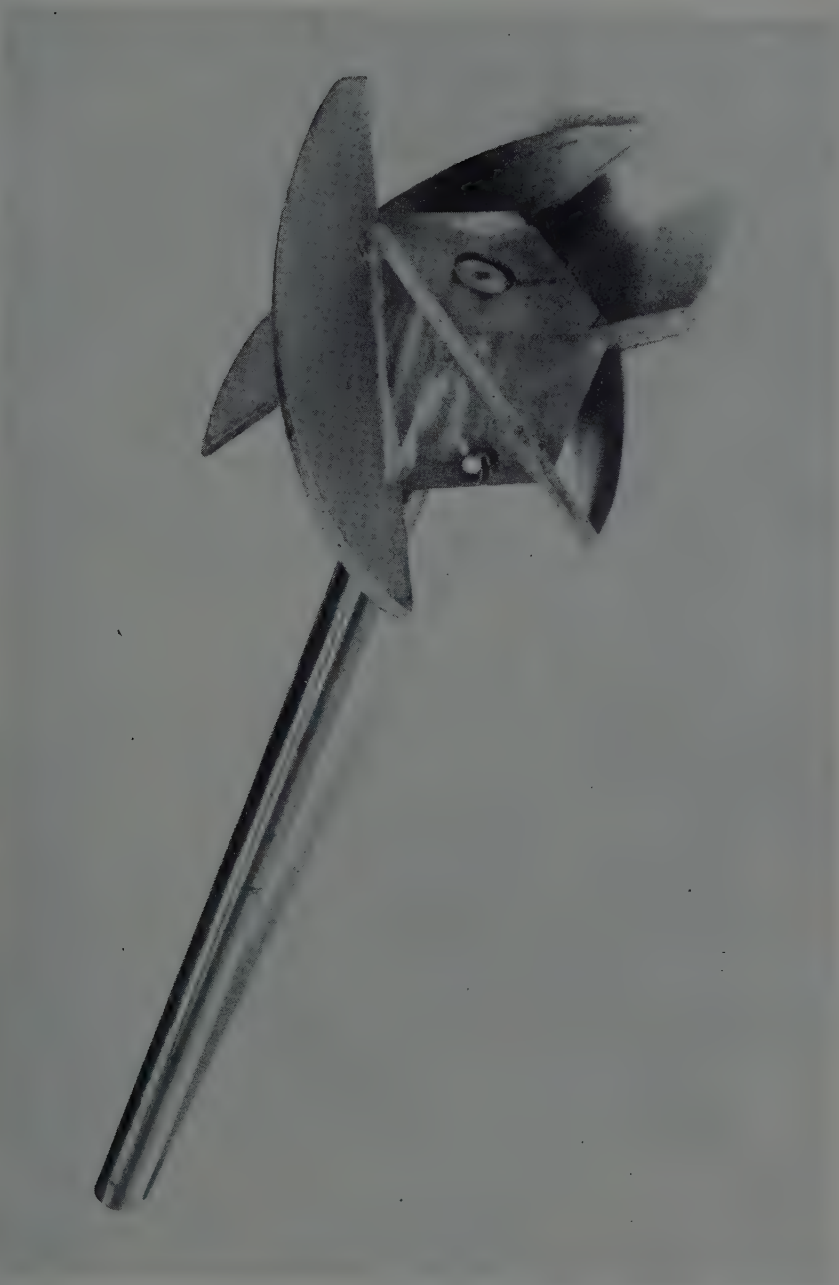

Fig. 17.

three racks may be placed in the fixing tank which is filled with cold water. Three or four hours before the fourth rack is due to be removed from the stop bath, the circulation between FCT and FT is stopped and the water in the former replaced by fix, which is then cooled down to an appropriate temperature. The temperature of the water, in which the plates stand, will, as a result of the heat insulation, rise only one or two degrees during this time. When the last batch of plates has been placed in the fix tank, it may be drained, and the fix pump P_4 started, so that it is filled with fix, which then continues to circulate between the two tanks.

However, there is no evidence that the fixing time is very critical, and we have therefore placed the various batches directly in the fixing solution as they came out of the stop bath. Fixing usually lasts from 70 to 80 hours for 600 μm G-5 emulsions, $1\frac{1}{2}$ times the clearing time. The fix solution is then gradually diluted with a solution of sodium sulphate which in turn is slowly diluted with softened water after 2000 l of the first solution have passed through the apparatus over a period of $(24 \div 36)$ hours. $(3000 \div 4000)$ l of water are passed through the apparatus during the following $(34 \div 48)$ hours, after which a permanganate test usually shows that the washing is completed.

The recipes used in making up the fixing and washing solutions are shown in Table III.

TABLE III.

Sodiumthiosulphate, pentahydrate (kg)	Sodiumbisulphite (kg)	Sodiumsulphate (kg)	Ionexchanged water ad (L)
350	35	—	1000 (pH = 4.7)
—	—	100	1000
—	—	50	1000
—	—	—	$4000 \div 5000$

Both processes are carried out at 5 °C, the alarm system working if the temperature rises above 6 °C. Gentle stirring is provided in the fixing tank until the plates begin to be clear, after which the agitation arising from the circulation of the liquid between the tanks is deemed sufficient. The rate of circulation is such that about 1 l/min flows through each half of the fixing tank.

15. – Silver concentration.

The concentration of silver in a bath used for fixing thick nuclear emulsions must be more carefully controlled than is usually necessary in the case

of that used for fixing ordinary photographic materials. Most writers are agreed that too low a silver concentration entails a danger that the developed silver grains may be etched away. Some writers ([9]) claim that there is evidence that too high a silver concentration can lead to the formation of bubbles or distortion as a result of the formation of large amounts of complex silver salts which cannot escape sufficiently quickly through the surface of the emulsion. Other writers ([10]) do not find evidence that the upper limit to the silver concentration is so critical. It must, of course, be stressed that the whole composition and pH of the fixing bath is important in this respect, and not the silver concentration alone. In our opinion, much experimental work remains to be done on the whole subject of fixing thick emulsions, before an optimum procedure can be laid down. In the work here described, we have followed the recommendations of BURGE *et al.* ([9]) and worked with silver concentrations lying between 2 and 6 g Ag/l.

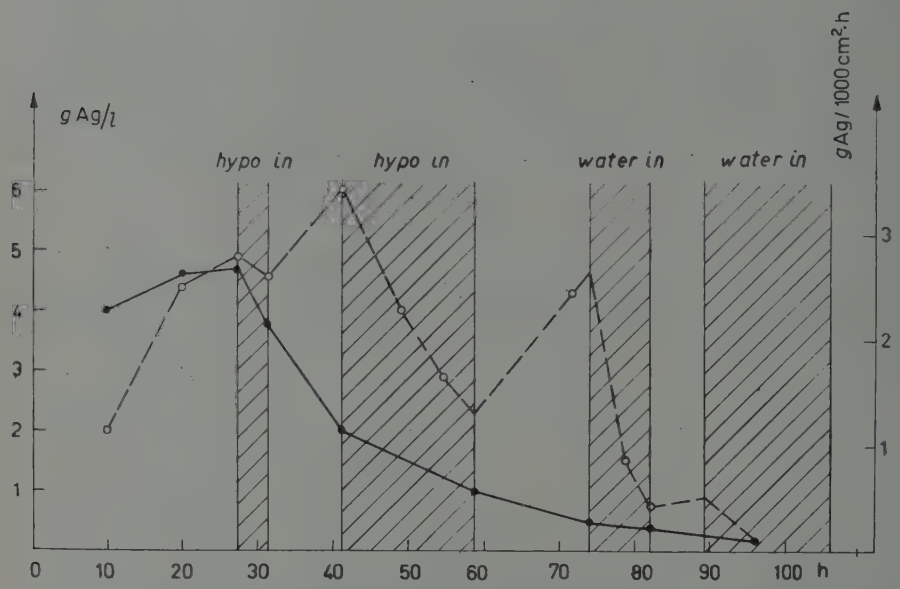

Fig. 18. – ------- g Ag/l in solution; ——— g Ag/l 1000 cm²·h out of plate.

In all work with the present equipment we have made use of an electrolytic silver meter to measure the concentration of silver in the fix solution. This instrument will be described elsewhere.

Our general procedure has been to fill the fixing system with fresh solution

---

([9]) E. J. BURGE, J. H. DAVIES, I. J. VAN HEERDEN and D. J. PROWSE: *Nuovo Cimento*, **5**, 1005 (1957).

([10]) D. HEUGHEBAERT and J. HEUGHEBAERT: *Nuovo Cimento*, **12**, 623 (1959).

prior to beginning fixing, thereafter allowing this to cool down to the desired fixing temperature, or a little below. The circulation is then stopped and the plates put into the fix bath where they are allowed to stand for a couple of hours. Provided that the tank is nearly filled to capacity with emulsion (about 1 l in each half of the tank), the local silver concentration will rise rapidly, so that the necessity of adding silver to the bath before beginning is avoided. The circulation is then restarted, and the silver concentration in the system as a whole is allowed to rise to 6 ‰. At this stage, fresh solution is allowed to run slowly into FCT from FMT, at such a rate that the silver concentration is held constant.

In addition to using the silver meter to carry out routine measurements on the silver concentration, we have investigated in rather more detail the rate at which silver bromide is removed from the emulsion as a function of the fixing time. At the same time, careful checks were made to ensure that the reading of the meter was correct, and that fluctuations of the concentration between different parts of the system were not too great. (They were found to be of the order of 20 % of the mean concentration). The results of these measurements, expressed in g Ag/1000 cm²h are shown in Fig. 18. After a sharp initial rise and plateau, the rate of silver removal decreases approximately exponentially. The shape of the curve may be explained as follows.

At the end of the first 29 hours the fixation proper has been completed; the only remaining process is the diffusion of the silver complex out of the gelatine. At the start the plate contains about 110 g silver. After 29 hours 63.5 g have diffused out, the thickness of the emulsion layer being ~ 2 mm, and the concentration gradient $\mathrm{d}c/\mathrm{d}x$ is $46.5/0.2 = 232.5$ g/cm over 1000 cm² (area of plate). The diffusion rate is given by

$$\frac{\mathrm{d}M}{\mathrm{d}t} = k \frac{\mathrm{d}c}{\mathrm{d}x} .$$

The conditions at $t = 29$ h are

$$\frac{\mathrm{d}M}{\mathrm{d}t} = 2.7 \text{ g Ag/1000 cm}^2 \text{ h} .$$

$$\frac{\mathrm{d}c}{\mathrm{d}x} = 232.5 \text{ g/cm}$$

and

$$k = 0.0116 .$$

At some time $t > 29$ h we find

$$\frac{\mathrm{d}c}{\mathrm{d}x} = 232.5 \cdot \frac{(110 - M)}{46.5} = 5 \cdot (110 - M) ,$$

$$\frac{\mathrm{d}M}{\mathrm{d}t} = 0.0116 \cdot 5 \cdot (110 - M) = 0.0580 \cdot (110 - M) ,$$

$$(110 - M) = \exp [- 0.058\, t + c]$$

and therefore using $(\mathrm{d}M/\mathrm{d}t)_{t=29} = 2.7$

$$\frac{\mathrm{d}M}{\mathrm{d}t} = 0.058 \cdot \exp\left[-0.058t + 5.52\right] \text{ g Ag/1000 cm}^2 \text{ h},$$

which relation provides a good fit to the experimental results.

16. – Silver recovery.

When large stacks of emulsions are processed, the recovery of the silver from the fixing solution can be economically justified, provided the method used is sufficiently cheap. The silver from 10 l of emulsion is, at present prices, more than sufficient to cover all the expenses connected with processing. It was therefore decided to attempt a simple chemical precipitation method using commercial Na_2S. The apparatus used is sketched in Fig. 19.

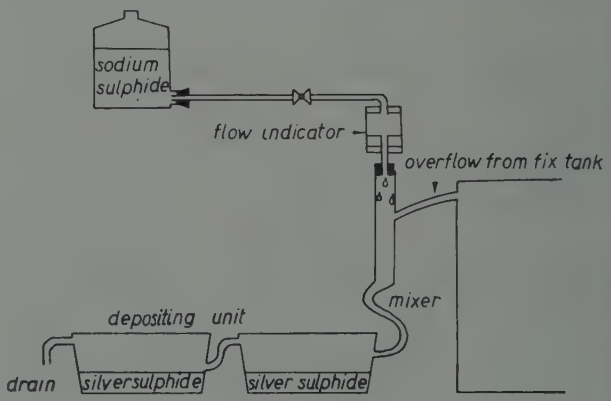

Fig. 19.

Continuous sedimentation from the liquid was necessary as, owing to lack of space, it was not possible to collect the used fix solution in a suitable container and there precipitate the silver. Our experience with this equipment in its present form has been very unsatisfactory, for, apart from the rather low efficiency achieved ($(25 \div 30)\%$), large quantities of H_2S are released into the air. This is extremely unpleasant for those who have to work with the equipment, and very corrosive. Other methods are being investigated.

17. – Drying.

We have chosen the now widely adopted procedure of drying the washed emulsions in a series of alcohol baths of increasing concentration. These are contained in four double walled aluminium tanks which can be cooled to about 10 °C by tap water flowing through the walls. The alcohol concentrations are 25%, 50%, 75% and 95% by volume, respectively. 7% by volume glycerine is added to each of the baths as a plasticizer.

Although cooling of the tanks is possible, it has not been made use of, as no undesirable results have been observed when drying at room temperature. The emulsions are allowed to stand for a few minutes after being taken from the washing solution to reach temperature equilibrium before being placed in the first alcohol bath. It is possible that there would be some advantage in making use of the cooling facilities in an experiment where particularly low distortion was required (*e.g.* less than 20 covans) ([11]).

The plates are allowed to stand for two hours in each of the four baths. On removal from the last they are blotted with filter paper before the alcohol on the surface has time to dry away. This prevents the formation of a surface layer containing a very high glycerine concentration left behind when the surface alcohol evaporates. Neglect of this precaution often results in the thickness of the final plates being very variable.

* * *

We would like to take this opportunity of thanking Prof. G. Occhialini, Milan, who has placed his great experience of emulsion processing at our disposal in the course of several discussions before, during and after the designing and completion of the equipment.

Particular thanks are also due to Danfoss Ltd., of Nordborg, Denmark, who gave us much of the automatic electromechanical equipment used in the apparatus.

One of us (J.E.H.) is grateful to the Ford Foundation for financial assistance during the course of this work.

([11]) M. G. E. Cosyns and G. Vanderhaeghe: *Bull. C.P.N.U.L. Brux.*, 15. (1951).

RIASSUNTO (*)

Si descrive un compatto impianto per trattamento di grandi pacchi di emulsioni nucleari. Si discutono un procedimento di sviluppo « umido », che si è trovato dare risultati soddisfacenti, e alcuni problemi più particolari, come il deposito superficiale di argento e la velocità di asportazione dell'argento dalle emulsioni durante il fissaggio.

(*) *Traduzione a cura della Redazione.*

SUPPLEMENTO AL VOLUME XV, SERIE X
DEL NUOVO CIMENTO

N. 2, 1960
1° Trimestre

Controlled Sensitivity Bubble Chamber with Stabilized Final Pressure (*).

B. Hahn, A. W. Knudsen (**) and E. Hugentobler

Department of Physics, University of Fribourg - Fribourg

(ricevuto il 13 Ottobre 1959)

Summary. — A radiation sensitivity stabilized 2-liter bubble chamber operating with $CBrF_3$ or fluorocarbon gas-liquid mixtures near room temperature is described. Final pressure stabilization is achieved by a method first suggested by Blinov *et al.* [1]. Flat bottomed pressure pulses 30 ms long, and corresponding bubble density plateau with bubble density variations smaller than $\pm 5\%$ have been obtained. The chamber sensitivity is reproducible at any time and can be adjusted instantaneously to the desired bubble density. The chamber is also temperature stabilized. Accurate bubble counting for particle velocity determinations is possible without reference track in each bubble chamber picture. A discussion is presented, on how to minimize undesired pressure oscillations, and on the possibility to pressure stabilize much larger chambers.

1. – Introduction.

The information most readily obtained from bubble chamber photographs are the space co-ordinates of particle tracks, permitting the study of the kinematics of particle collisions and decays. In addition, information on particle velocity can be obtained from the number of bubbles per unit path length along a track, the bubble density, which is roughly inversely proportional to the square of the particle velocity. Reliable bubble density measurements become

(*) This research has been sponsored in part by the Air Research and Development Command, U. S. Air Force, through the European Office, ARDC.

(**) On leave from the High Energy Laboratory, Department of Physics, University of Stanford, Calif.

possible, however, only for well stabilized operating conditions. The bubble density for a particle of known ionizing power depends strongly on temperature as well as on the final pressure reached during expansion. In order to keep the bubble density constant within $\pm 5\%$ for typical operating conditions, *e.g.* for $CBrF_3$, the temperature should be stabilized to better than $\pm 0.1\,°C$, and the final pressure to better than ± 0.05 atmosphere.

While temperature stabilization has been a common enough practice, stabilization of the final pressure has received only little attention. For most of the existing bubble chambers the final pressure is defined only in a somewhat unreliable way, namely by self-recompression due to « wall bubbles » (random bubbles from walls, gaskets, recesses, etc.), and by expansion speed. In such chamber operation it is difficult to do accurate bubble counting without a reference track of known ionizing power in each bubble chamber picture. Attempts at stabilization of the final pressure have first been made by BLINOV *et al.* [1], and by BASSI *et al.* [2], however no constant radiation sensitivity has been reported.

Final pressure stabilization yields a bubble density plateau at each expansion, reproducible bubble density at any time, and provides quick means of adjusting the chamber sensitivity. Adjustement of bubble density by temperature change is usually a slow process.

Besides describing in detail our own stabilization system, we attempt to present some of the necessary conditions for realizing final pressure stabilization for bubble chambers in general.

2. – Method of pressure stabilization.

Pressure stabilization has been achieved by a method very similar to that described by BLINOV *et al.* [1], by providing pressure communication of the chamber liquid with a large volume of compressed air at the stabilization pressure through a flexible diaphragm, as can be seen in detail from Fig. 1. There are three neoprene diaphragms, namely the chamber diaphragm *A*, the stabilization diaphragm *B*, and the main expansion diaphragm *C*. The space *D* enclosed by the three diaphragms is filled by an inert and relatively incompressible liquid, *e.g.* ethyl alcohol.

Prior to expansion the sensitive liquid in the chamber *F* is compressed, and the three diaphragms are in the positions shown in Fig. 1, except for the stabilizing diaphragm *B*, which is pressed against its support plate *E*. Ex-

[1] G. A. BLINOV, I. S. KRESTNIKOV and M. F. LOMANOV: *Žurn. Èksp. Teor. Fiz.*, **4**, 661 (1957).

[2] P. BASSI, A. LORIA, J. A. MEYER, P. MITTNER and I. SCOTONI: *Nuovo Cimento*, **4**, 491 (1956).

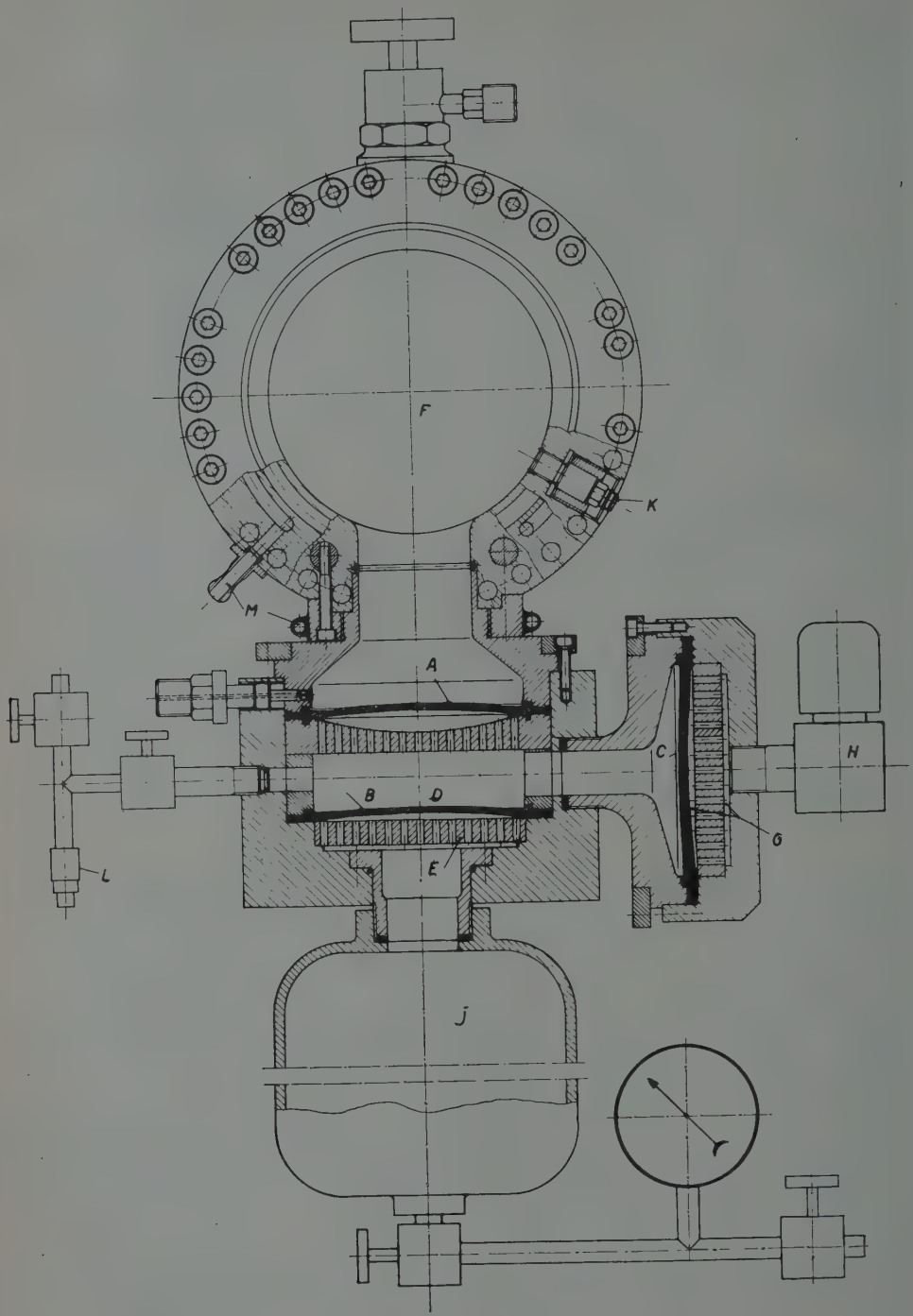

Fig. 1. – Pressure and temperature stabilized bubble chamber.

pansion commences with the release of the compressed air in G by way of the electro-magnetic valve H. The maximum displacement volume available to C is arranged to be two or three times greater than the volume necessary to expand the chamber liquid to the desired final pressure. As soon as this pressure is reached, diaphragm B is free to move, and the stabilizing pressure in tank J will be imposed on the chamber liquid. The motion of diaphragms B and C will occur in a manner to cope with the extra volume taken up by growing vapor bubbles (wall bubbles and radiation bubbles), but will not expand the chamber liquid any further. Diaphragm C eventually will come to the end of its travel, however the stabilization regime will only be terminated, when finally the stabilization diaphragm B hits its stop plate. From that moment on self-recompression due to wall bubbles will set in. In addition fast external recompression with pressurized air through valve H recondenses the vapor bubbles quickly, and a new expansion can be started approximately every second.

Diaphragm A only serves to separate the heavier chamber liquid (*e.g.* $CBrF_3$) from the lighter inert liquid (*e.g.* ethyl alcohol). When a heavy and immiscible inert liquid is used, diaphragm A can be left out. The use of an intermediate « non-bubbling » liquid eliminates wall bubbling in the expansion part, and therefore the stabilization period will be lengthened considerably.

3. – Pressure oscillations.

The sudden pressure stabilization of a fast expanding, highly compressible liquid involves an abrupt change in kinetic energy of the liquid. At least part of this kinetic energy will be available for compression work, resulting in pressure oscillations around the stabilizing pressure and corresponding variations of the chamber sensitivity. By the choice of proper chamber geometry, essentially by avoiding a narrow chamber neck, and by rounding off abrupt pressure changes during expansion, pressure oscillations can be minimized to a tolerable value.

It is possible to estimate roughly the oscillation period and an upper limit for the oscillation amplitude for the two « extreme » cases of a chamber with a pronounced neck and of a chamber with no neck at all. Such an estimate yelds rather good values for the oscillation period, the oscillation amplitude however comes out twice or three times too large compared to the observed one. The discrepancy comes about because presumedly only a small fraction of the kinetic energy goes into pV-work, and not all, as is assumed in the calculations.

3·1. *Chamber with pronounced neck.* – A chamber falls into this category when the kinetic energy of the liquid in the neck is much larger than the

kinetic energy of the liquid in the chamber proper. If this is the case, the chamber represents to a good approximation an oscillatory system, in which the liquid in the neck can be considered as an incompressible mass moving under the restoring force of a massless spring, represented by the compressible liquid in the chamber. The liquid mass in the neck feels on the opposite side to the chamber proper a constant force due to the stabilizing system. The period of such an oscillator can easily be calculated to $T = 2\pi\sqrt{k\varrho lV/A}$, where $k = -((\mathrm{d}V/V)/\mathrm{d}p) =$ compressibility of the chamber liquid, $\varrho =$ liquid density, l and $A =$ length and cross-sectional area of the chamber neck, $V =$ volume of the liquid in the chamber proper. An upper limit to the pressure oscillation amplitude δp can be computed by equating the total kinetic energy of the neck liquid to the pV-work for compressing the liquid in the chamber proper. Thus one obtains $\delta p = \sqrt{k\varrho lV/A}\cdot \mathrm{d}p/\mathrm{d}t = (T/2\pi)\,\mathrm{d}p/\mathrm{d}t$, where $\mathrm{d}p/\mathrm{d}t =$ = expansion speed in terms of pressure change per unit time at the moment when stabilization sets in.

3·2. *Chamber without neck.* – A liquid in a chamber without crossectional restrictions between the chamber proper and the stabilizing system might undergo self-oscillations similar to an open organ pipe. There will be a pressure node at the « open » end where the stabilizing diaphragm is located, and a pressure antinode at the closed opposite side of the chamber. The period of such an oscillator is $T = 2l\sqrt{\varrho k}$, and an average pressure amplitude near the middle of the chamber is $\delta p \sim l\sqrt{k\varrho/3}\,(\mathrm{d}p/\mathrm{d}t)$, where $l =$ height of the chamber.

Case 3·1 applies well to the 16 cm chamber described here, the specifications being given in the following paragraph. The calculated and the measured period come out both to 5.8 ms. The experimental amplitude is approximately three times smaller than the calculated upper limit; $\delta p_{\mathrm{calc}} = \pm 0.15$ atm for $\mathrm{d}p/\mathrm{d}t = 170$ atm/s and $k = 2\cdot 10^{-3}$ atm^{-1}.

4. – Chamber description.

The chamber body (see Fig. 1), 16 cm in inner diameter, and 8 cm long, is machined from a block of corrosion resisting aluminum alloy (anticorodal), and the chamber neck 6.3 cm in diameter, and 5.9 cm long is made from brass. The two chamber windows, 22.5 cm in diameter, and 5 cm thick, are tempered Schott BK-1 Boro-silicate-crown glass plates. All the seal gaskets are neoprene O-rings, and the diaphragms A, B, and C, which are 3, 5, and 3 mm thick respectively, are made from neoprene sheet, and have no Mylar foil backing. The diameter of the unclamped area of the diaphragms is 12 cm and the stiffness of the 3 mm thick diaphragms is negligible.

The space in between the three diaphragms is « tightly filled » with ethyl alcohol, in such manner, that in the expanded state of the chamber, the diaphragms B and C are pressed against their stop plates, and diaphragm A is slightly bulged away from its stop plate. The diaphragm support plates are closely spaced perforated by 3 mm holes. The pressure stabilizing tank, which is filled with pressurized air, has a volume of approximately 10 liters. Pressure variations in the tank due to the displacement of the stabilizing diaphragm do not exceed ± 0.02 atm. The stabilizing tank is provided with temperature stabilization. Located in between the expansion diaphragm C and the electromagnetic valve H, and not shown in Fig. 1, there is an extra valve, to adjust the expansion speed $\mathrm{d}p/\mathrm{d}t$.

The dynamic pressure variations during expansion can be measured by quartz type pressure transducers K and L (SLM, Type PZ 14, Winterthur, Switzerland) directly in the chamber liquid and in the alcohol.

Temperature stabilization is provided by a thermostat-circulator, which pumps ethylene glycol through circular passage ways M in the chamber body and in the chamber neck.

In order to obtain at each expansion a long period of stabilized pressure, and therefore of constant radiation sensitivity all vapor bubbles, which are not due to ionizing particles, have to be minimized, since they cause undesired fast self-recompression of the chamber. All narrow passage ways, connecting an O-ring groove to the main chamber volume, and all small recesses are, during expansion, places of turbulent liquid flow leading to cavitation boiling. We have provided all gaskets with a 1 to 2 mm wide open communication to the chamber, and have avoided recesses at metal joints and on the metal surfaces by polishing.

Several precautions have been taken to reduce the excitation of pressure oscillations during expansion.

A fine meshed wire screen is located between the stabilizing diaphragm D and its support plate E in order to eliminate sealing between the rubber diaphragm and its metal support plate prior to stabilization. Without the screen, undershoot to the stabilizing pressure with subsequent pressure oscillations during the stabilizing period can be observed in the chamber.

A modification of the expansion Barksdale valve effectively « rounds off » the pressure pulse at expansion beginning. This is accomplished by introducing a suitably slit brass ring, which converts the Barksdale valve from a simple poppet valve to a more slowly opening piston valve.

The sudden arrival of the main expansion diaphragm against its stop plate, sometimes during the stabilization regime, is a source of oscillations. By providing a wavy surface for the stop plate, and by expanding the chamber compressed air into a closed volume, to build up a pressure slightly lower than the stabilizing pressure, the oscillations have been eliminated. The « cushioned »

expansion rounds off also the pressure pulse at stabilization beginning and has also shown some promise as stabilization method without a stabilizing diaphragm.

5. – Performance.

With the stabilization system described above, we have obtained flat bottomed pressure pulses as shown slightly schematically in Fig. 2 for the chamber liquid $CBrF_3$ at 36.7 °C. The pressure pulses have been measured directly in the chamber liquid. The numbers attached to the various pressure pulses

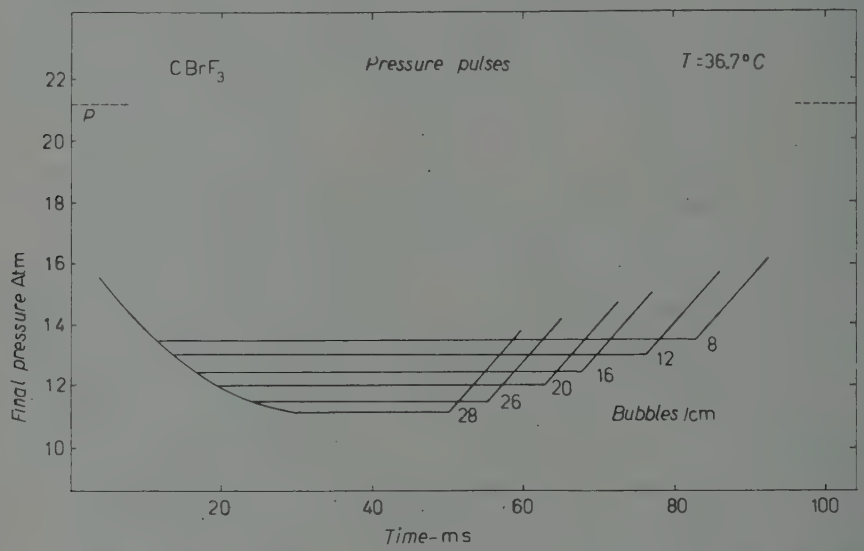

Fig. 2. – Pressure pulses (slightly schematically) for $CBrF_3$ at 36.7 °C with various final pressures. Labelled numbers are corresponding bubble densities found for 30 MeV electrons.

represent the appearing bubble densities measured on 30 MeV electron tracks. The fact that the length of the flat part of the pressure pulse increases with increasing final pressure has to do with the rate of growth of the wall bubbles. The real pressure pulses measured in the chamber are almost identical to those shown in Fig. 2, except for small oscillations of approximately 0.05 atm in amplitude and several ms in period, and for a slightly rising slope near the end of the sensitive time, the latter effect being due to local bubbling at the pressure transducer.

With sensitive times longer than 30 ms at an expansion repetition rate of 1 expansion every three seconds, temperature gradients are introduced in

the chamber due to condensation heat from bubbles reaching the top of the chamber. For sensitive times shorter than 30 ms however, and by applying external fast recompression, bubbles can be recompressed before they reach the top of the chamber and temperature gradients are not severe.

The appearing bubble density produced by 30 MeV electrons has been measured throughout the pressure pulses of various final pressures, for the pure liquids $CBrF_3$ and SF_6, and for the gas-liquid mixture SF_6-C_2ClF_5 [3]. Typical bubble density plateaux for $CBrF_3$ at 36.7 °C and for SF_6-C_2ClF_5

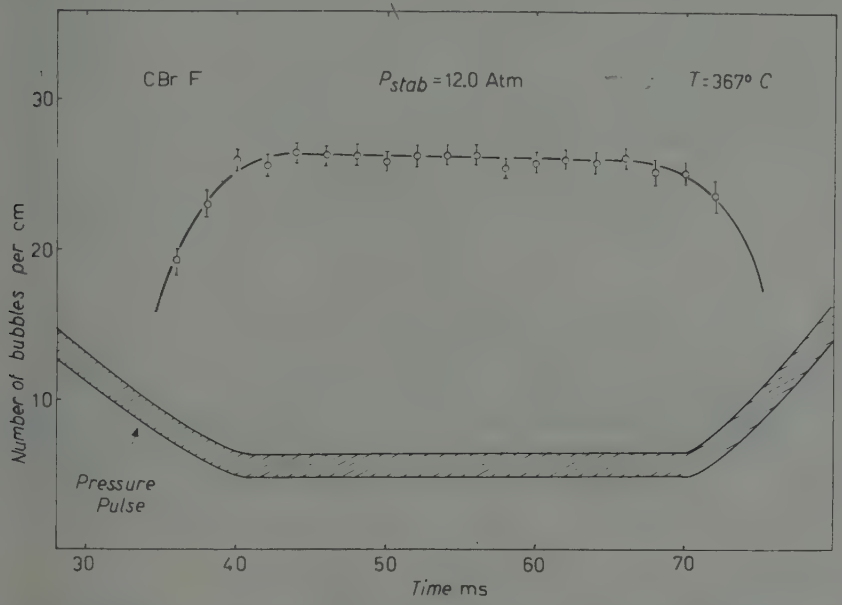

Fig. 3*a*. – Bubble density plateau for $CBrF_3$ obtained for 30 MeV electrons together with corresponding pressure pulse. The errors are statistical errors.

(3:1 mixing ratio by weight) at 23.0 °C are shown in Fig. 3*a*, and Fig. 3*b* respectively. The errors shown, are the statistical errors in bubble counting taking the correction for finite optical resolution and bubble coalescence into account. The observed variations of the bubble density in the plateaux do not exceed significantly the statistical error.

The bubble density for particles of known ionizing power, is reproducible from one expansion to another over a period of several months. The final pressure and therefore the bubble density can be adjusted in a few seconds to the desired value.

An attempt has been made to operate the chamber without the inert

(3) B. Hahn, G. Riepe and A. W. Knudsen: *Rev. Sci. Instr.*, **30**, 654 (1959).

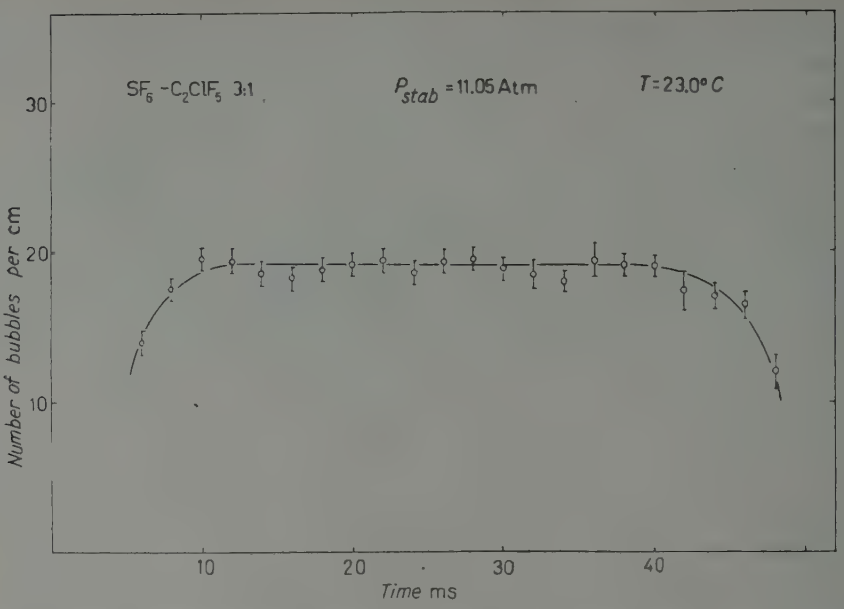

Fig. 3*b*. – Bubble density plateau for SF_6—C_2ClF_5 (3:1 by weight) for 30 MeV electrons. The errors are statistical errors.

liquid and without diaphragm A, but the chamber proper and the expansion part all filled with the sensitive liquid $CBrF_3$. The period of stabilized sensitivity was so reduced from 30 ms to approximately 10 ms.

6. – Discussion.

A sensitivity stabilized bubble chamber not only yields reproducible bubble density and bubble size in each bubble chamber photograph, but also allows to do reliable bubble density measurements by bubble counting or by mean gap length determinations. The bubble density ϱ_b is expected to vary with the particle velocity β approximately as $\varrho_b \sim 1/\beta^2$. The error in momentum determination of particles of known mass is $\Delta p/p = (\gamma^2/2) \cdot \Delta\varrho_b/\varrho_b$; $\gamma^2 = 1/(1-\beta^2)$. As an example, when only 100 bubbles are counted, the momentum of 400 MeV protons can be determined with $\pm 10\%$ accuracy, considering the statistical uncertainty in the number of bubbles counted as the only source of error. The accuracy of momentum measurements by bubble counting in bubble chambers with no final pressure control was limited due to sensitivity variations from one chamber expansion to another [4].

---

[4] D. A. Glaser, D. C. Rahm and C. Dodd: *Phys. Rev.*, **102**, 1653 (1956); W. J. Willis, E. C. Fowler and D. C. Rahm: *Phys. Rev.*, **108**, 1046 (1957).

The possible behaviour of much larger chambers with respect to pressure oscillations might be roughly estimated by the formulas given in Section 3. A chamber with a volume of 200 litres and a neck cross-section of 1000 cm^2, and the remaining quantities being the same as those for our small chamber, would yield oscillation amplitudes, which are 1.6 times those calculated for our chamber. A chamber without neck of 200 liter volume and a chamber height of 50 cm should have pressure oscillation amplitudes not exceeding ours, assuming the same fraction of the kinetic energy to go into compression work.

The construction of large pressure stabilized bubble chambers seems to be feasible, when flexible membranes can be used, which is the case *e.g.* for propane and for many heavy liquids. Since no « resistanceless » diaphragm working at very low temperatures is known, liquid hydrogen or liquid helium bubble chambers have to use different techniques for pressure stabilization. Pressure stabilization might be achieved by « free expansion » of the vapor into a large volume, of a pressure stabilized vapor cushion. In this case no diaphragm is needed.

* * *

The authors wish to thank Mr. H. JUNGO for his great help in constructing the bubble chamber, and Mr. G. FRIESE for his excellent work in designing the electronic timing circuits. It is a pleasure to express appreciation to Professor O. HUBER for his steady interest and criticism and to Mr. G. RIEPE for valuable discussions.

RIASSUNTO (*)

Si descrive una camera a bolle di 2 litri con sensibilità per le radiazioni stabilizzata, funzionante con miscele gas-liquido di $CBrF_3$ o fluorocarbonio in prossimità della temperatura ambiente. La stabilizzazione della pressione finale è ottenuta con un metodo suggerito per la prima volta da BLINOV *et al.* Si sono ottenuti impulsi di pressione a fondo piano della lunghezza di 30 ms, e corrispondenti massimi di densità di bolle con variazioni di questa densità inferiori a $\pm 5\%$. La sensibilità della camera è riproducibile in ogni momento e può essere istantaneamente regolata alla densità di bolle desiderata. La camera è anche stabilizzata rispetto alla temperatura. Un conteggio accurato delle bolle per la determinazione delle velocità delle particelle è possibile senza traccia di riferimento in ogni fotografia della camera. Si discute anche il modo di ridurre al minimo le indesiderabili oscillazioni di pressione e la possibilità di rendere stabili alla pressione camere molto più grandi.

(*) *Traduzione a cura della Redazione.*

SUPPLEMENTO AL VOLUME XV, SERIE X
DEL NUOVO CIMENTO

N. 2, 1960
1° Trimestre

Un metodo ottico-meccanico di ricostruzione stereoscopica.

E. Fiorini e S. Ratti

Istituto di Fisica dell'Università - Milano
Istituto Nazionale di Fisica Nucleare - Sezione di Milano

(ricevuto il 20 Ottobre 1959)

Riassunto. — Viene descritto e discusso un metodo di ricostruzione stereoscopica ottico-meccanica per eventi fotografati in camera a nebbia o in camera a bolle, consistente essenzialmente nella ricostruzione « materiale » degli eventi nello spazio. È stato realizzato un dispositivo che, applicando il metodo, viene attualmente impiegato per la ricostruzione di eventi in camera di Wilson a setti. Viene descritto l'impiego di tale dispositivo e sono stimati gli errori che si commettono nella valutazione della posizione di punti e nella misura di angoli. I vantaggi del dispositivo consistono essenzialmente nella semplicità e nella rapidità delle operazioni di ricostruzione e nella possibilità di *visualizzare* l'evento nello spazio.

Introduzione.

La restituzione nello spazio di eventi fotografati in camera a nebbia o in camera a bolle, che ha avuto notevole sviluppo negli ultimi anni, è stata generalmente ottenuta con metodi o di ricostruzione analitica ([1,2]), o di ricostru-

([1]) P. M. S. Blackett e R. Brode: *Proc. Roy. Phys. Soc.*, A **154**, 537 (1936) e bibliografia ivi contenuta.

([2]) P. Bassi, A. Loria, J. A. Meyer, P. Mittner e I. Scotoni: *Nuovo Cimento*, **5**, 1729 (1957).

zione per riproiezione ([3-7]), o di ricostruzione grafica ([2,8-10]), o infine di ricostruzione per mezzo di stereocomparatori ([11,12]). Non ci risulta che siano stati finora impiegati, almeno in questo campo di ricerche, metodi atti a ricostruire « materialmente » gli eventi nello spazio, pur essendo tali metodi abbastanza diffusi in fotogrammetria. Per questa ragione non ci sembra inutile descrivere un sistema di ricostruzione da noi ideato e recentemente impiegato, che verrà chiamato sistema di ricostruzione ottico-meccanica. Il metodo che unisce ad una certa precisione, non inferiore a quella ottenibile con le ricostruzioni grafiche, una notevole rapidità, permette, forse più di ogni altro, la *visualizzazione* degli eventi nello spazio.

La restituzione ottico-meccanica può essere ottenuta da due soli fotogrammi; naturalmente la possibilità di utilizzare un terzo fotogramma è di grande utilità perchè permette di eseguire tre misure indipendenti sullo stesso evento. L'angolo tra le direzioni di presa può essere quale si voglia; gli assi delle macchine devono però giacere a due a due sullo stesso piano.

Per l'applicazione del metodo è necessario conoscere:

a) la posizione dei due centri di presa rispetto ad un piano di riferimento (per esempio il vetro anteriore della camera oppure il fondo di essa);

b) l'angolo formato dai due assi di presa;

c) *la distanza principale* ([13]) (distanza tra il centro di presa ed il piano del fotogramma) e la posizione del *punto principale sul quadro* ([13]) (piede della perpendicolare calata dal centro di presa sul piano del fotogramma);

d) la direzione dell'intersezione del piano individuato dagli assi delle macchine (piano π) coi piani dei due fotogrammi.

I dati dei punti *c*) e *d*) possono essere ricavati anche *a posteriori* con i semplici procedimenti di autocollimazione e di ricostruzione di più punti noti, comunemente usati in fotogrammetria ([13]).

([3]) D. A. Bromley e R. D. Brandfield: *Rev. Sci. Instr.*, **21**, 191 (1950).

([4]) I. Hamouda, J. Halter e P. Sherrer: *Helv. Phys. Acta*, **24**, 217 (1951).

([5]) K. R. Allen e M. Lipsicas: *Rev. Sci. Instr.*, **24**, 501 (1953).

([6]) M. H. Alston, A. V. Crewe e W. H. Evans: *Rev. Sci. Instr.*, **31**, 253 (1954).

([7]) C. R. Emigh: *Rev. Sci. Instr.*, **25**, 567 (1954).

([8]) J. S. Campbell e D. F. Welch: *Nucleonics*, **10**, 62 (1952).

([9]) G. Mejer, R. Mennega e G. Sizoo: *Physica*, **20**, 301 (1954).

([10]) V. Borelli, P. Franzini, I. Mannelli, A. Minguzzi-Ranzi, R. Santangelo, F. Saporetti, V. Silvestrini, P. Waloschek e V. Zoboli: *Nuovo Cimento*, **10**, 525 (1958).

([11]) L. Grosev, N. Dobrotin e J. Frank: *Compt. Rend. U.S.S.R.*, **3**, 289 (1936).

([12]) K. H. Barker: *Suppl. Nuovo Cimento*, **11**, 309 (1954).

([13]) Vedi per es.: G. Cassinis e L. Solaini: *Note di fotogrammetria*. Milano.

Per raggiungere la massima precisione conviene conoscere la posizione, la forma e l'indice di rifrazione di tutti i materiali rifrangenti posti di fronte alle macchine.

1. – Descrizione del metodo.

Si considerino (Fig. 1) il piano π passante per gli assi delle macchine e l'intersezione, Σ, di π con il volume sensibile della camera. Si riporti Σ su di un foglio e si traccino su di esso i due fasci di rette uscenti dai centri di presa O_1 e O_2 tenendo conto di tutti i materiali rifrangenti percorsi dai raggi luminosi durante la ripresa dei fotogrammi.

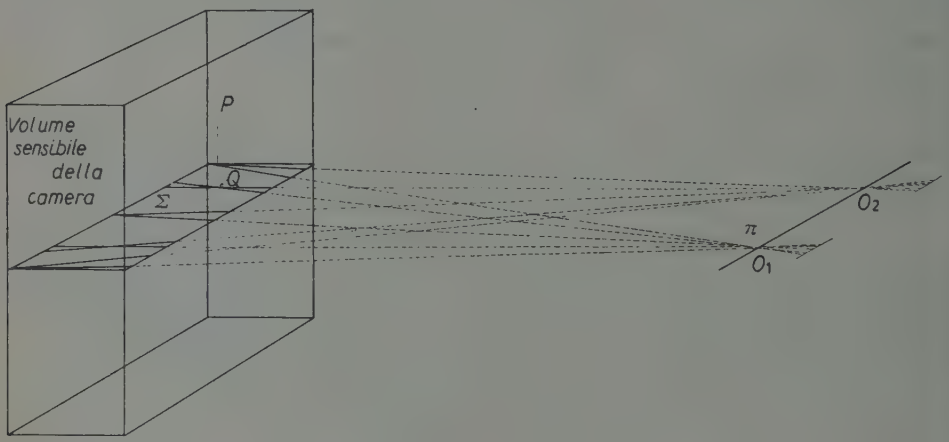

Fig. 1.

Per ricostruire la posizione di un generico punto P occorre individuare la posizione del piede Q della perpendicolare calata da P su Σ e la quota del punto P rispetto al piano π. La posizione del punto Q di Σ è nota quando si conoscano le coordinate che individuano le rette $\overline{x}'$ e $\overline{x}''$, uscenti dai centri di presa O_1 e O_2 che proiettano il punto Q sui due fotogrammi. Si pensi ora di avere (Fig. 2) sovrapposto ad ogni fotogramma, un sistema di coordinate cartesiane ortogonali (O, X, Y) con l'origine nel punto principale e l'asse X coincidente con l'intersezione del piano π col piano del fotogramma.

Di un generico punto P fotografato si hanno due immagini: $P'(x', y')$ nel sistema di riferimento (O', X', Y') e $P''(x'', y'')$ nel sistema di riferimento (O'', X'', Y''); per costruzione risulta $y' = y''$ e questa coordinata, tenuto opportunamente conto dell'ingrandimento e delle correzioni per gli effetti di rifrazione, permette di ottenere la quota di P rispetto a π. Esiste poi una cor-

rispondenza biunivoca tra i valori dell'ascissa x' e le rette uscenti dal centro di presa O_1 ed una corrispondenza biunivoca tra i valori dell'ascissa x'' e le rette uscenti dal centro di presa O_2. Con i valori di x' ed x'' si possono indi-

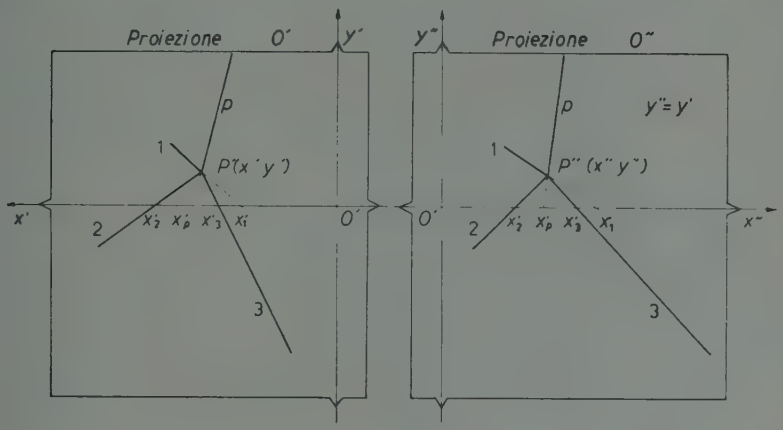

Fig. 2.

viduare le rette $\overline{x}'$ ed $\overline{x}''$ che si intersecano nel punto Q di Σ (Fig. 1).

Risulta così determinata la posizione vera del punto P nella camera.

2. – Realizzazione sperimentale del metodo.

Il metodo è stato impiegato per ricostruire eventi prodotti dai raggi cosmici in una camera di Wilson [14] (volume sensibile $126 \times 126 \times 50$ cm^3) fotografata con due macchine dotate di obiettivo Xenar-Schneider 1:4.5; $f = 150$ mm con centri di presa posti a 4 metri dal vetro anteriore della camera e con assi paralleli alla distanza di un metro.

La figura Σ — un rettangolo di 126×50 cm^2 — è stata riportata in scala 1:1 su una lastra metallica piana e orizzontale, ricoperta con un sottile strato di cementite; sulla lastra è stato tracciato un sistema di rette oblique costituito dalla sovrapposizione nel piano π delle due stelle uscenti dai centri di presa O_1 e O_2 della Fig. 1. Per ottenere una maggior precisione si è tenuto conto della presenza del vetro anteriore della camera traslando ciascuna retta uscente da O_1 e O_2, parallelamente a se stessa di una distanza:

$$s = d \sin \varphi \left(1 - \frac{\cos \varphi}{(n^2 - \sin^2 \varphi)^{\frac{1}{2}}}\right),$$

[14] E. Fiorini, R. Giacconi e C. Succi: *Nuovo Cimento*, **6**, 943 (1957).

dove con d si è indicato lo spessore del vetro, con n l'indice di rifrazione e con φ l'angolo d'incidenza sul vetro della generica retta uscente da O_1 o da O_2 (s assume nel nostro caso valori sensibili per φ maggiore di circa 5°).

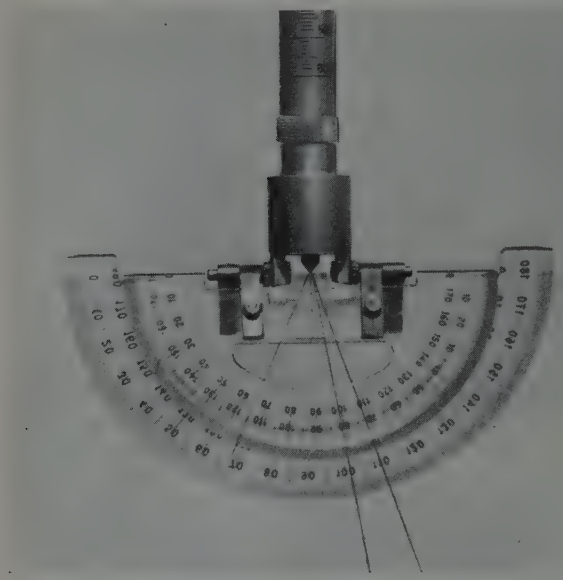

Fig. 3*b*. – Visione ingrandita dei due goniometri M_1 e M_2 centrati nel punto P.

Alla lastra metallica su cui è riportato il rettangolo Σ è stato fissato un supporto ortogonale (Fig. 3) che sostiene un braccio orizzontale a doppio snodo, recante alla estremità una sbarretta verticale graduata S scorrevole senza gioco normalmente al braccio stesso. Gli snodi G_1 e G_2 sono stati montati su cuscinetti a sfere con reggispinta; bloccando con la vite V_3 la sbarretta S rispetto al piano π, il punto P può esplorare interamente il rettangolo Σ, mantenendosi in un piano ad esso parallelo con una incertezza massima di 0.2 mm. Le viti V_1 e V_2 applicate ai rispettivi snodi, permettono di bloccare il punto P sopra un punto qualsivoglia di Σ. La quota massima raggiungibile dal punto P è di 60 cm. Il proiettore T proietta una croce che individua su Σ il piede della perpendicolare calata dalla estremità inferiore della sbarretta S.

I fotogrammi vengono proiettati con un ingrandimento 10 su uno schermo traslucido di vetro smerigliato; su ciascun fotogramma compaiono (Fig. 2) quattro marche che individuano il punto principale (le marche sono state praticate sul pattino anteriore delle macchine fotografiche anzichè sul vetro o sul pistone della camera perchè la determinazione del punto principale sul fotogramma risulta così indipendente da eventuali spostamenti della camera stessa). Le rette congiungenti le coppie di marche opposte si intersecano nei rispettivi punti principali e costituiscono due sistemi di assi cartesiani ortogonali ($O'X'Y'$) ed ($O''X''Y''$) con centro nei punti principali O' e O''. Gli assi X' e X'' risultano approssimativamente appartenenti al piano π. In generale non è necessario che le marche individuino direttamente le direzioni di X' e X''; basta infatti conoscere la posizione dei punti principali sui due fotogrammi ed avere l'immagine di almeno due punti giacenti su di un piano nor-

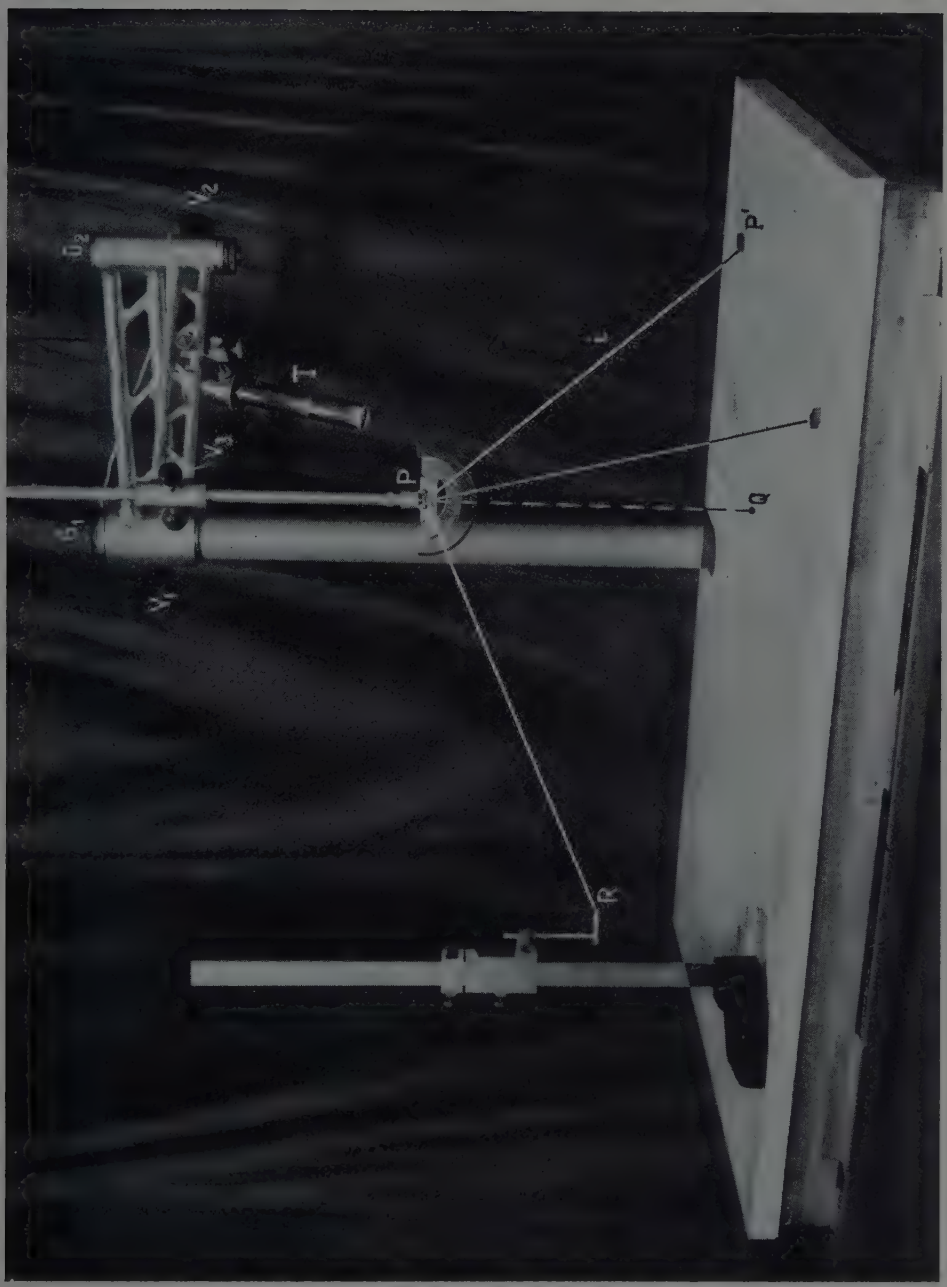

Fig. 3a.

male agli assi di presa: sovrapponendo i due fotogrammi proiettati in modo da far coincidere i punti immagine corrispondenti, la congiungente i due punti principali risulta per costruzione parallela al piano π (tale accorgimento può venire impiegato anche nel caso di presa con assi non paralleli purchè complanari).

Sullo schermo di proiezione si appoggiano due telai mobili che sostengono ciascuno un foglio di plastica millimetrata indeformabile (Astralon) i quali possono essere sovrapposti ai due fotogrammi proiettati; facendo coincidere su ciascuno due assi della millimetratura con gli assi coordinati del fotogramma è possibile leggere direttamente le coordinate x', y' e x'', y'' delle immagini P' e P'' di un generico punto P della zona sensibile della camera (ad esempio del centro di una interazione).

Su Σ è tracciata anche una retta, normale ai due assi di presa, che interseca i due fasci di rette; fra la distanza del punto di intersezione di una retta $\overline{x}$ dal punto di intersezione dell'asse e l'ascissa x letta su un fotogramma vi è una relazione di semplice proporzionalità (salvo la correzione per la rifrazione del vetro); note le ascisse x' e x'' si individuano immediatamente le due rette $\overline{x}'$ e $\overline{x}''$ che si intersecano nel punto Q, piede della perpendicolare calata da P su Σ.

La posizione reale del punto P rispetto alla superficie Σ (vedi Sezione precedente) si individua spostando il braccio del dispositivo di ricostruzione (Fig. 3) fino a far coincidere il centro della crocetta proiettata da T col punto individuato dall'intersezione delle due rette $\overline{x}'$ ed $\overline{x}''$; facendo scorrere la sbarretta graduata S si porta la sua estremità inferiore ad una distanza da Σ uguale alla quota del punto P, ricavata dal valore y' $(= y'')$.

La condizione di uguaglianza tra y' ed y'' permette di controllare la precisione con cui sono state determinate le direzioni dei due assi coordinati X' ed X''.

Ricostruita la posizione del punto di convergenza di due o più rette, risulta molto semplice la ricostruzione nello spazio delle rette e, in particolare, la misura degli angoli tra di loro. A tal fine la sbarretta è stata corredata da due goniometri M_1 ed M_2 incernierati in modo da avere il loro centro nel punto P dal quale escono alcuni sottili fili di cotone.

Per la ricostruzione nello spazio di una generica retta i uscente da P si individua (Fig. 3) il punto P' intersezione della retta (o del suo prolungamento) col piano π, si tende quindi un filo uscente da P verso P' facendolo aderire alla lastra mediante un piccolo magnete. Ripetendo l'operazione su tutte le rette si ricostruisce nello spazio l'intero evento; a mezzo dei goniometri M_1 ed M_2 si possono misurare direttamente gli angoli nello spazio. La verifica della complanarità di tre rette uscenti da uno stesso punto si ottiene immediatamente controllando l'allineamento delle loro intersezioni con Σ.

Può accadere che una retta uscente da P abbia una inclinazione tale da non intersecare la figura Σ; in tal caso per mezzo di un truschino si individua un punto R della retta, che abbia la stessa ordinata nei due fotogrammi e la cui perpendicolare calata su π incontri il piano metallico (Fig. 3).

3. - Precisione e controlli nelle misure.

La precisione nelle misure è stata determinata sistematicamente fotografando fili di 0.2 mm di diametro tesi in modo tale da simulare tracce di particelle nel volume sensibile della camera (*). L'errore quadratico medio nella localizzazione di un punto nello spazio risulta, nei casi più sfavorevoli (come per punti in prossimità degli spigoli orizzontali della camera), non superiore a 0.5 mm; l'errore quadratico medio nella ricostruzione di un angolo, nei casi più sfavorevoli (angoli in un piano normale al vetro anteriore della camera), non supera i 30′, quando il vertice sia ad una quota di almeno 5 cm da π.

Molti eventi sono stati ricostruiti anche analiticamente per stimare in modo approssimato gli errori dovuti alla parte propriamente meccanica del dispositivo di ricostruzione. Si è così costatato che la ricostruzione materiale dell'evento aggiunge un errore trascurabile ($\sim \frac{1}{5}$) agli errori propri della ricostruzione analitica. Le maggiori fonti di errore si possono essenzialmente attribuire a:

1) distorsione degli obbiettivi nella ripresa e nella proiezione;

2) cattiva determinazione dei parametri *a*), *b*), *c*), *d*) di pag. 247;

3) imprecisioni nella lettura delle coordinate.

Indubbiamente nel nostro caso il maggior contributo all'errore è dovuto alla imprecisione nella lettura delle coordinate dato l'ingrandimento relativamente piccolo (1/27) delle macchine fotografiche.

Il sistema di ricostruzione ottico-meccanica si presta particolarmente alla esecuzione di rapidi controlli che permettono di prevenire molti errori sistematici e ad assicurare durante le misura una costante precisione. Basta infatti, di tanto in tanto, ricostruire figure di dimensioni note oppure assicurarsi che i piedi delle perpendicolari calate su Σ da punti qualsiasi appartenenti ad un piano normale a π (per esempio, sul vetro anteriore o sul pistone della camera) giacciano su di una retta; la distanza media dei punti da tale retta permette una valutazione approssimata dell'errore nella ricostruzione di punti appartenenti a Σ.

4. - Osservazioni sul funzionamento del dispositivo.

Il dispositivo è stato impiegato per la ricostruzione di interazioni nucleari di protoni di alta energia nei setti di plexiglas della camera; ma può ovviamente essere usato per la ricostruzione di eventi di altro tipo, fotografati in

(*) Non sono qui compresi, ovviamente, gli errori dovuti alle distorsioni della camera ed allo scattering, errori che vanno attribuiti al rivelatore e non al dispositivo di ricostruzione.

camera a nebbia o in camera a bolle, purchè gli assi di presa siano complanari. Basta cambiare il sistema di coordinate oblique sul piano del tavolo di ricostruzione.

Uno dei più notevoli vantaggi del metodo di ricostruzione ottico-meccanica consiste nella semplicità e rapidità della ricostruzione: la completa restituzione nello spazio di una interazione con 3-4 rami visibili compiuta da due operatori richiede in generale col nostro dispositivo non più di 10 minuti, compresa la lettura delle coordinate e la misura degli angoli nello spazio. Si sta studiando la possibilità di aumentare ulteriormente la rapidità della ricostruzione automatizzando qualche operazione (ricerca dei punti su Σ, regolazione della sbarretta S, ecc.).

Per le sue caratteristiche di semplicità, di rapidità di ricostruzione e specialmente di *visualizzazione* degli eventi nello spazio, ci sembra che il metodo di ricostruzione ottico-meccanica possa in molte applicazioni sostituire vantaggiosamente i metodi di ricostruzione grafica ed i più complessi metodi di ricostruzione per riproiezione. Per l'analisi di un numero molto elevato di eventi è senz'altro preferibile la ricostruzione analitica compiuta mediante calcolatrici elettroniche; in tal caso comunque il metodo ottico-meccanico può essere utilmente impiegato per eseguire rapidi controlli *visivi* e per la ricostruzione di eventi particolarmente interessanti.

* * *

Ci è gradito esprimere la nostra riconoscenza ai professori P. Caldirola, G. P. S. Occhialini e G. Polvani per il costante interessamento al nostro lavoro, ed al prof. C. Succi per le utili discussioni avute.

Un particolare ringraziamento intendiamo rivolgere al prof. M. Cunietti dell'Istituto di Geodesia, Topografia e Fotogrammetria del Politecnico di Milano per gli utili consigli, allo studente G. Bellini ed alla dott. M. di Marco per l'aiuto nello svolgimento delle misure.

SUMMARY

A stereoscopic optical-mechanical method for reconstruction of cloud and bubble chamber events is described. This method consists essentially of a « material » reconstruction of events. A stereoscopic apparatus, based on the method, is at present used to reconstruct multiplate Wilson chamber events. The performance of the apparatus is described and the errors of measurement estimated. The simplicity, quickness of reconstruction and the possibility of « space visualizing » reconstructed events make of this apparatus a valuable help in cloud and bubble chamber researches.

SUPPLEMENTO AL VOLUME XV, SERIE X
DEL NUOVO CIMENTO

N. 2, 1960
1° Trimestre

The High Frequency Properties of a Coaxial Cable and the Distortion of Fast Pulses.

G. FIDECARO
CERN - Genève

(ricevuto il 31 Dicembre 1959)

Summary. — The high frequency properties of a coaxial cable and the distortion of fast pulses are discussed. A convenient way of determining accurately the delay of a coaxial cable is also shown.

1. – Introduction.

Three time of flight experiments have recently been reported on the determination of the $\pi^- - \pi^0$ mass difference ([1,3]). For two of the experiments ([2,3]), the measurements rely on a very accurate absolute calibration of a long stretch of cable. This last fact has prompted the author to re-order some notes which he had worked out during a stay at the Nuclear Physics Research Laboratory of the University of Liverpool, on the properties of coaxial cables and the distortion of fast pulses. It is believed that an appropriate use of the formulae developed here may lead in particular cases to better accuracy.

From a complete knowledge of the response of a transmission line to sinu-

([1]) M. GETTNER, L. HOLLOWAY, D. KRAUS, K. LANDE, E. LEBOY, W. SELOVE and R. SIEGEL: *Phys. Rev. Lett.*, **2**, 471 (1959).

([2]) P. HILLMAN, W. C. MIDDELKOOP, T. YAMAGATA and E. ZAVATTINI: *Nuovo Cim.* **14**, 887 (1959).

([3]) R. P. HADDOCK, A. ABASHIAN, K. M. CROWE and J. B. CZIRR: *Phys. Rev. Lett.*, **3**, 478 (1959).

soidal excitation (4) it is possible to calculate the response to transients. The problem is very complicated from a mathematical point of view, and it does not seem that a complete investigation has ever been published. The explicit solution has been extensively studied only in the case of the low frequency approximation, in which the parameters are considered independent of the frequency (5). This approximation obviously fails if it is necessary to consider Fourier components of sufficiently high frequency in a transient. For example, in this approximation a step function would be propagated with zero rise time.

Here the velocity dispersion and the attenuation are calculated in the high frequency approximation in which it is possible to describe the behaviour of a cable with asymptotic formulae. From these the response to transients is calculated. All the other cases in which the response at intermediate frequency is important are too complicated for a complete analytical investigation and ought to be treated numerically or with special approximations. Fortunately, the asymptotic formulae give a good approximation still at reasonably low frequencies, in such a way as to cover the whole range of interest for time of flight measurements.

Furthermore, the theory refers to cables in which the dielectric has zero conductivity and a dielectric constant independent of the frequency, so that the asymptotic formulae are correct only up to the frequency at which the losses in the conductors become of the same order of magnitude as the losses in the dielectric. For cables in polyethylene this happens at frequencies larger than 1000 MHz.

Some measurements reported here show that a commercial coaxial cable insulated in polyethylene verifies the predictions of the theory in a very wide frequency range.

The same result as given by formula (13) has been found independently by P. BEHREND (6) with more elementary considerations. Some practical graphs based on Behrend's results have been reported in the Counting Handbook of the Radiation Laboratory of the University of California (7). However, it seemed still worth-while to present here a more rigorous treatment, which gives a better understanding of the problem and shows the nature of the approximations involved.

---

(4) A treatment of the electromagnetic theory of coaxial cables and reference to other bibliography can be found in the paper by S. A. SCHELKUNOFF: *Bell Sys. Tech. Journ.*, **8**, 532 (1934).

(5) See for example, A. GHIZZETTI: *Calcolo simbolico* (Bologna, 1944) or B. VAN DER POOL and H. BREMMER: *Operational Calculus* (Cambridge, 1950).

(6) P. BEHREND: *Zeits. f. Angew. Phys.*, **5**, 61 (1953).

(7) Radiation Laboratory of the University of California, Counting Handbook, UCRL-3307, 1st January 1956.

The problem of distortion in long distance cables for television is usually considered from the point of view of designing equalizing networks and repeaters ([8]). However, the requirements of work in nuclear physics do not yet justify the trouble involved in the design of equalizing networks.

2. – The steady state.

The mathematical theory of the coaxial cable merely consists in the solution of the Maxwell equations for cylindrical fields. Some approximations are required, but if the conductivity of the central conductor and the outer shell is very high, as is usually the case, the results are extremely accurate for all the practical applications. Moreover, the range of frequency we are here concerned with corresponds to wavelenghts appreciably larger than the diameter of the cable, so that only the principal mode of propagation has to be considered.

If the Fourier components of the voltage and the current along the line are respectively:

$$(1) \qquad \begin{cases} V_\omega(x, t) = V_\omega(x) \exp[j\omega t], \\ I_\omega(x, t) = I_\omega(x) \exp[j\omega t], \end{cases}$$

t being the time, x the co-ordinate along the cable and $\omega/2\pi = f$, the frequency, the electro-magnetic theory can be summarized by the following two equations:

$$(2a) \qquad \frac{\partial V_\omega(x)}{\partial x} = -(j\omega L + R\langle\omega\rangle)\cdot I_\omega(x),$$

$$(2b) \qquad \frac{\partial I_\omega(x)}{\partial x} = -(j\omega C + G)\cdot V_\omega(x).$$

Here:

$$(3) \qquad L = \frac{\mu_2}{2\pi}\ln\frac{a_2}{a_1}, \qquad C = \frac{2\pi\varepsilon_2}{\ln(a_2/a_1)}, \qquad G = \frac{2\pi\sigma_2}{\ln(a_2/a_1)},$$

are the low frequency inductance, the capacity and the conductance, per unit length and μ_2, ε_2, σ_2, are the permeability, the permittivity and the conductivity of the dielectric, respectively. $R\langle\omega\rangle$ is a complex quantity which has

---

([8]) See for example, P. W. Rounds and G. L. Lakin: *Bell. Sys. Tech. Journ.*, **34**, 713 (1955); T. Kilvington, F. J. M. Laver and H. Stanesby: *Proc. I.E.E.*, **99**, part I, 44 (1952).

the dimensions of impedance/length. If the central conductor and the shell are made of the same metal, of conductivity σ_1, $R\langle\omega\rangle$ is given by the formula:

$$R\langle\omega\rangle = \frac{\sqrt{j}}{\pi a_1^2 \sigma_1} F_1(\omega) + \frac{\sqrt{j}}{\pi a_2^2 \sigma_1} F_2(\omega), \tag{4}$$

where

$$F_1(\omega) = \frac{a_1\sqrt{2}/\delta}{2} \frac{I_0(\sqrt{2j}\,a_1/\delta)}{I_1(\sqrt{2j}\,a_1/\delta)}, \tag{4a}$$

$$F_2(\omega) = \frac{a_2\sqrt{2}/\delta}{2} \frac{I_0(\sqrt{2j}\,a_2/\delta)\cdot K_1(\sqrt{2j}\,a_3/\delta) + K_0(\sqrt{2j}\,a_2/\delta)\cdot I_1(\sqrt{2j}\,a_3/\delta)}{I_1(\sqrt{2j}\,a_3/\delta)\cdot K_1(\sqrt{2j}\,a_2/\delta) - I_1(\sqrt{2j}\,a_2/\delta)\cdot K_1(\sqrt{2j}\,a_3/\delta)}; \tag{4b}$$

δ is the skin depth, given by the usual formula

$$\delta = \frac{1}{(\pi f \mu_1 \sigma_1)^{\frac{1}{2}}}, \tag{5}$$

μ_1 is the permeability of the metal. I_0 and I_1 are the modified Bessel functions of orders zero and one, respectively. K_0 and K_1 the modified Hankel functions of equivalent order. a_1 is the radius of the central conductor, a_2 the internal radius of the shell and a_3 the external radius.

For copper of conductivity $\sigma_1 = 5.8\cdot 10^7$ ohm^{-1} m^{-1} eq. (5) becomes:

$$\delta = \frac{66.15}{f^{\frac{1}{2}}}, \tag{5a}$$

where δ is in mm.

If one expands in series of powers the Bessel functions appearing in eq. (4*a*) and eq. (4*b*), one can show that, as the frequency decreases towards zero, the imaginary part of $R\langle\omega\rangle$ becomes negligible and $R\langle\omega\rangle$ approaches the d.c. resistance per unit length of the cable R_{dc}. If one write R_{dc} in place of $R\langle\omega\rangle$ in eq. (2*a*), eq. (2) become the usual set of equations corresponding to the case mentioned in the introduction of the low frequency approximation, and commonly known as « telegrapher's equations ».

By replacing the Bessel functions in eq. (4*a*) and eq. (4*b*) with their asymptotic expressions, one gets for $R\langle\omega\rangle$ an approximated formula, valid when the frequency is sufficiently high:

$$R\langle\omega\rangle = \frac{\sqrt{j\omega}}{2\pi}\cdot\sqrt{\frac{\mu_1}{\sigma_1}}\left(\frac{1}{a_1}+\frac{1}{a_2}\right) + \frac{1}{4\pi a_1^2 \sigma_1}. \tag{6}$$

This formula is sufficient for the practical considerations reported here. It describes $R\langle\omega\rangle$ rather accurately, also at fairly low frequencies. As a lower

limit for the validity of eq. (6), one could take the frequency at which the skin depth becomes comparable with the radius of the central conductor or the thickness of the outer shell, whichever the tinner. However, the outer shell can often be neglected, especially in the case of high impedance cables, where $a_2 \gg a_1$. In this case, in fact, the resistance of the shell is negligible, in comparison with the resistance of the central conductor at any frequency.

In the range of validity of eq. (6), and with the additional approximation $G = 0$ (*), the solution of eq. (2) in the case of an illimited cable is given by the following formula:

$$V_\omega(x, t) = V_\omega \exp\left[j\omega t - j\omega x\sqrt{LC} - xA\sqrt{j\omega} - xB\right], \tag{7}$$

with a similar expression for the current $I_\omega(x, t)$. Here, V_ω is the amplitude of the sinusoidal excitation at the cable input. A and B are given by the formulae:

$$A = \frac{1}{4\pi Z}\sqrt{\frac{\mu_1}{\sigma_1}}\left(\frac{1}{a_1} + \frac{1}{a_2}\right), \tag{8}$$

and

$$B = \frac{1}{8\pi Z a_1^2 \sigma_1}, \tag{9}$$

where $Z = \sqrt{L/C}$ is the characteristic impedance of the cable (for $R = G = 0$). The attenuation in nepers per unit length is

$$\alpha_f = A\sqrt{\pi f} + B\,. \tag{10}$$

B can be neglected in comparison to $A\sqrt{\pi f}$ if $\delta \ll 2a_1$, as is the case at high frequencies.

The phase velocity is:

$$v = \frac{1}{\sqrt{LC} + A/\sqrt{2\omega}} \simeq v_0(1 - \alpha_f v_0/\omega)\,. \tag{11}$$

The expression for the phase velocity eq. (11) contains a frequency dependent

---

(*) This is not rigorously possible unless $\varepsilon_2 = \varepsilon_0$ (permittivity of vacuum). In fact, the causality principle applied to signals transmitted along a coaxial cable gives the following relation between ε_2 and σ_2:

$$\frac{1}{c}\sqrt{\frac{\varepsilon_2\mu_2}{2}\left[1 + \left(1 + \frac{\sigma_2^2}{\omega^2\varepsilon_2^2}\right)^{\frac{1}{2}}\right]} - 1 = \frac{2}{\pi} P\int_0^\infty \frac{\omega'}{c}\,\frac{\sqrt{\varepsilon_2\mu_2\left[-1 + (1 + \sigma_2^2/\omega'^2\varepsilon_2^2)^{\frac{1}{2}}\right]}}{\omega'^2 - \omega^2}\,\mathrm{d}\omega'.$$

term derived from the imaginary part of eq. (6). To give an idea of its order of magnitude, this term has been evaluated in Table I for a cable having an impedance of 125 Ω, an attenuation of 5.3 db/100 m at 100 MHz, and $v_0 = 0.84$ c. $v_0 = 1/\sqrt{LC}$ is the asymptotic velocity at infinite frequency.

TABLE I.

$\alpha_f v_0/\omega$	MHz
2.45 %	1
0.775%	10
0.245%	100

It should be noted that in the calculation of a transient response this correction cannot be neglected in spite of its smallness, otherwise the causality condition is not satisfied, a signal being present in the cable before any pulse is applied.

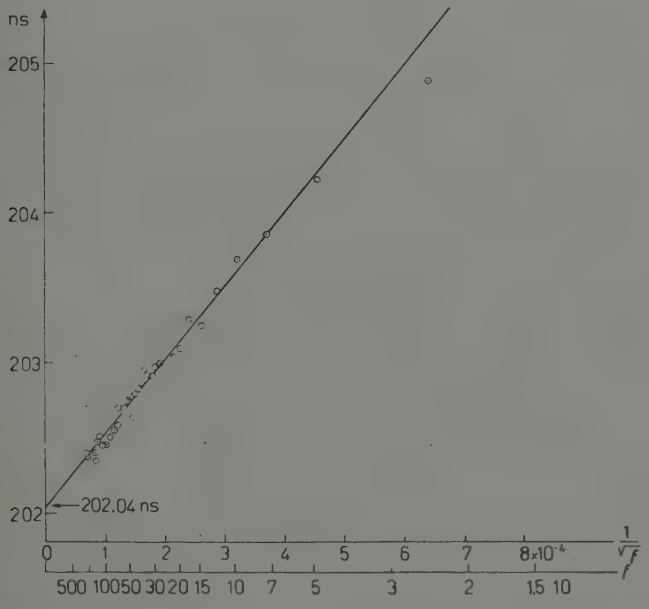

Fig. 1. - Change of measured delay as a function of frequency. The extrapolation gives the delay corresponding to v_0. The solid line has the theoretical angular coefficient.

Eq. (11) has been verified experimentally by measuring with great accuracy the delay of a cable as a function of the frequency. The cable has been short-circuited at one end, and the frequencies at which a « voltage zero » occurs

at the other end of the cable have been measured with a Hewlett and Packard counter (accuracy of 1 part in 10^6). The delay time T is obtained directly from the formulae $T = n/2f$, where n is the length of the cable in half wave lengths. The results are shown in Fig. 1. The straight line has the angular coefficient $L \cdot A/2\sqrt{\pi}$ (L = length of the cable in meters) predicted by eq. (11), and calculated from the known properties of attenuation of the cable. An inspection of Fig. 1 shows clearly that the delay time at infinite frequency is obtained with an accuracy better than 0.1 ns. This is the time taken by the first signal to arrive at the other end of the cable, as will be seen in the next section.

3. – The transient response.

If the transient response of a coaxial cable to sinusoidal excitations is represented by eq. (7), the response to a « unit » step function is given by the following inverse Laplace transform:

$$V(t) = \frac{\exp[-Bx]}{2\pi j} \int \frac{\exp[j\omega(t - x/v_0) - xA\sqrt{j\omega}]}{\omega} \, d\omega \,, \tag{12}$$

calculated along the contour (1) of Fig. 2. For $t < x/v_0$, the integral can be evaluated on a semi-circle of infinite radius in the lower half plane having its centre in 0. For $t > x/v_0$ the integration can be carried out on the contour (2), taking into account that $\sqrt{j\omega}$ is a many-valued function, with a branch point in $\omega = 0$. The result is:

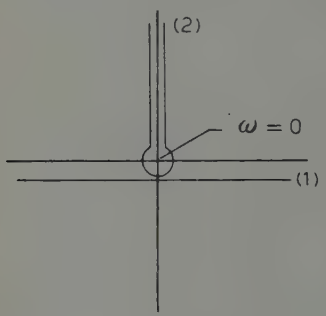

Fig. 2. – Integration contour of eq. (12).

$$\begin{cases} V(t) = 0 & \text{for } t < x/v_0 \\ V(t) = \operatorname{Erfc}\left\{\dfrac{1}{2\sqrt{\tau/\tau_0}}\right\}, & \text{for } t > x/v_0, \end{cases} \tag{13}$$

where

$$\tau = t - x/v_0$$

and

$$\tau_0 = \frac{(x\alpha_f)^2}{\pi f} \,, \tag{14}$$

x is the length of the cable in meters, f is the frequency corresponding to the attenuation α_f in the region of validity of eq. (6).

Erfc (x) is defined by the formula:

$$\operatorname{Erfc}(x) = 1 - \frac{2}{\sqrt{\pi}} \int_0^x \exp[-y^2] \, dy \,. \tag{15}$$

Fig. 3 shows the response of a cable to a unit step function in units of τ_0. Here it has been assumed, as is usually the case, $\exp[-Bx] \simeq 1$. As for $\tau = \tau_0$, $V(t) = 0.48$, τ_0 gives an indication of the rise time of the cable. Eq. (14) shows that this rise time τ_0 increases with the square of the length x.

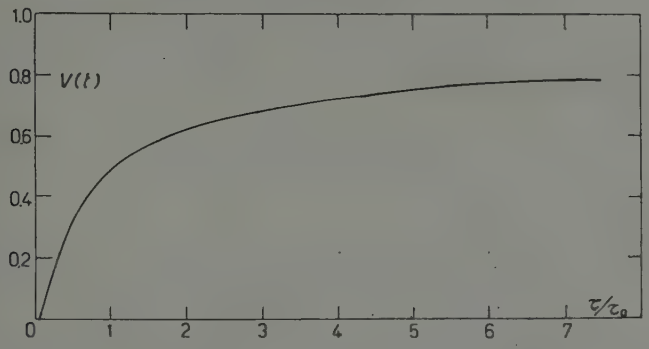

Fig. 3. – Response of a coaxial cable to a unit step function. Time is measured in terms of the rise time τ_0.

τ_0 can be obtained directly from the graph in Fig. 4 if the attenuation of the total length of cable, $x\alpha_f$, is known at any one of the following frequencies: 10, 100 1000, 3000 MHz.

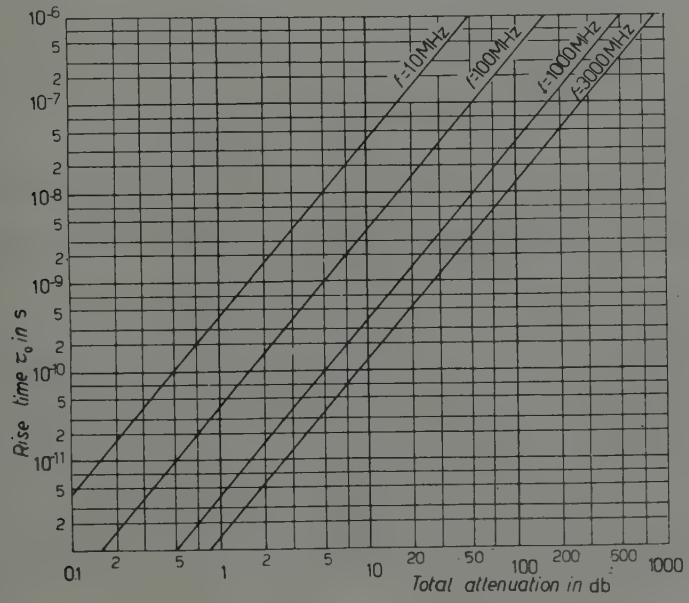

Fig. 4. – Rise time τ_0 of a cable as a function of the total attenuation of the cable in db at 10, 100, 1000 or 3000 MHz.

Approximate expressions to replace eq. (13) can be obtained by means of the inversion formula ([9]):

$$V(t) = \lim_{N\to\infty} \left[\frac{p^{N+1}}{N!} \left(-\frac{\mathrm{d}}{\mathrm{d}p} \right)^N \frac{f(p)}{p} \right]_{p=N/t}. \tag{16}$$

The approximation for $N = 1$ can be considered fairly good for many practical applications. For $N = 1$, eq. (16) becomes:

$$V(t) = \left(1 + \frac{\tau_0}{2\tau} \right) \exp\left[-\sqrt{\frac{\tau_0}{\tau}} \right]. \tag{17}$$

The response to a square pulse is easily obtained from that to a step function. The shape of a square pulse propagated along a cable is a function only of the ratio between the pulse width, Δ, and the cable rise time, τ_0. Fig. 5 shows the response of a cable to a square pulse as a function of the time for different values of the ratio Δ/τ_0.

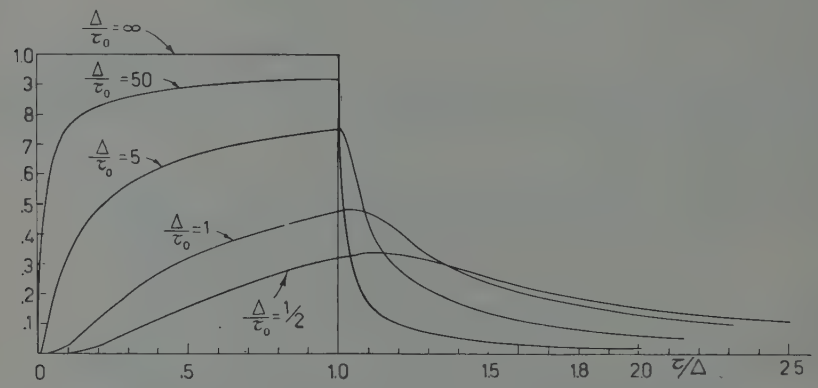

Fig. 5. – Distortion of a square pulse of width Δ transmitted through coaxial cables of different rise times τ_0.

It should be noted that, while the start of the signal is propagated with the asymptotic velocity v_0 as shown by eq. (13), Fig. 5 indicates that the centre of gravity or the peak of a pulse is transmitted with a smaller velocity. Therefore, in the case of precision delay measurements, one should determine, by folding the shape into eq. (13), the change in shape of the original pulse after the transmission through the desired length of cable.

Concluding, we may say that the absolute calibration of a delay cable can

---

([9]) B. Van der Pool and H. Bremmer: ref. ([5]), p. 148.

be done with higher accuracy and increased reliability if eq. (11) is used. To get the delay for pulses of a certain shape it is necessary then to consider the distortion of the pulses by folding the shape of the undistorted pulses in eq. (13). Using this procedure one should be able to reach a very high degree of accuracy without going to the trouble of using special low attenuation cables. For the case experimentally studied in this paper the accuracy of the measurement would be better than 0.05%.

RIASSUNTO

Si discutono le caratteristiche di un cavo coassiale alle alte frequenze, e la propagazione di impulsi rapidi. Viene anche indicato un modo per determinare accuratamente il ritardo in un cavo coassiale.

Direttore responsabile: G. POLVANI

Tipografia Compositori - Bologna

Questo Fascicolo del *Supplemento* è stato licenziato dai torchi il 13-II-1960

SUPPLEMENTO
AL VOLUME XV, SERIE X, DEL
NUOVO CIMENTO
A CURA DELLA SOCIETÀ ITALIANA DI FISICA

1960 1° Trimestre N. 3

Some Results Concerning Heavy Unstable Nuclear Fragments Ejected from Interaction of 4.5 GeV π^- in Emulsion.

M. DE PRETIS and G. POIANI

Istituto di Fisica dell'Università - Trieste
Istituto Nazionale di Fisica Nucleare - Sottosezione di Trieste

(ricevuto il 6 Luglio 1959)

CONTENTS. — **1.** Introduction. 1. Calibration of the emulsions. – **2.** Unstable fragments. Identification of events. 1. ^{8}Li. 2. ^{9}Li. 3. ^{8}Be. 4. ^{8}B. 5. ^{12}C. 6. ^{12}B. – **3.** Frequency of production and energy spectrum of unstable fragments. 1. Production frequency. 2. ^{8}Li, ^{9}Li, ^{8}B. 3. ^{8}Be. 4. ^{8}B, ^{12}C. – **4.** Hyperfragments. – **5.** Conclusions.

1. – Introduction.

The present paper summarizes the results of an investigation carried out on a stack of 600 μm Ilford G-5 emulsions, exposed to 4.5 GeV negative π mesons produced by the Berkeley Bevatron. An area of about 200 cm² has been scanned for interactions of π^- on heavy nuclei. The intensity of the beam in the observed region has been found to be between $(10^5 \div 10^6)$ π's over a cross-section of one cm². About 36000 stars produced by primary π's and associated with at least 5 black prongs have been observed. We have assumed that these were caused by heavy element disintegrations.

The purpose of this work consisted in studying the nature, the emission spectra and angular distributions of unstable nuclear fragments and hyperfragments produced in these type of events.

1'1. *Calibration of the emulsions.* – The experimental methods used in mass and charge determinations do not differ from those currently used by research workers in this field (see *f.i.* CASTAGNOLI *et al.* (1)) and will not be described in any detail. We report here briefly on the calibration curves obtained in

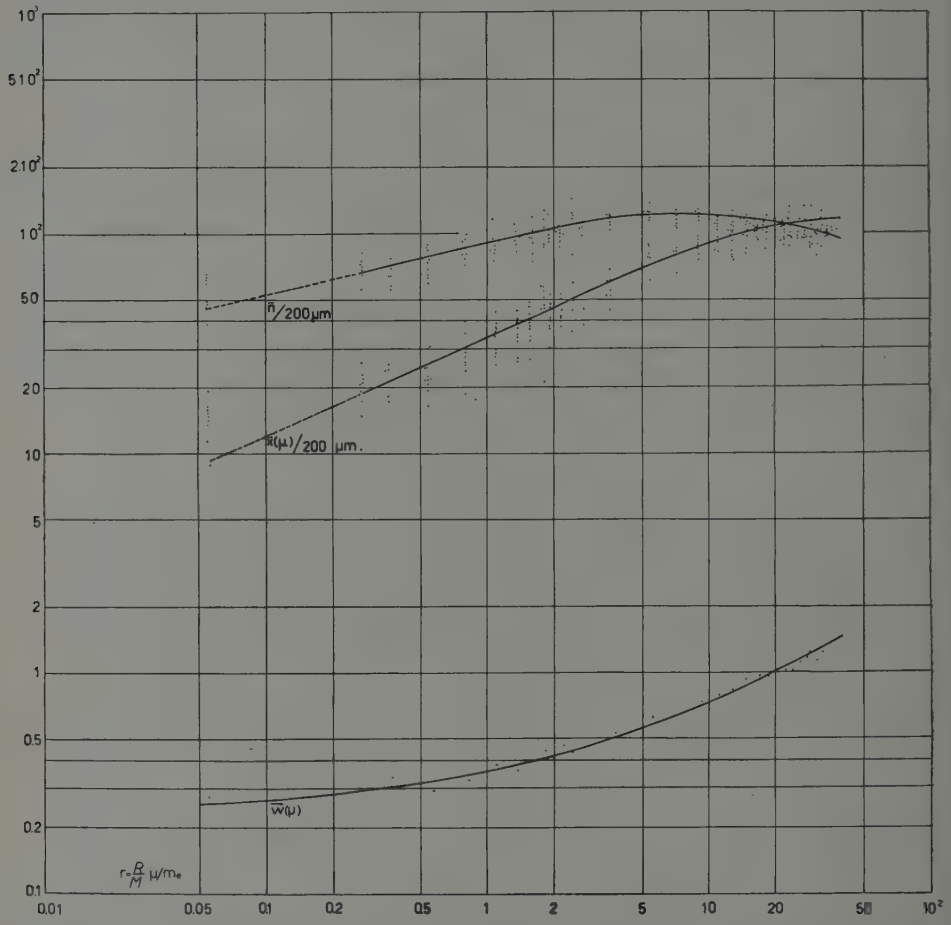

Fig. 1. – Dependence on R/m of the number $\overline{n}$ of gaps, of the total gap length $\overline{X}$ and of the specific gap lenth $\overline{w}$ per 200 μm.

our emulsion, mainly to allow the reader to estimate the weight to be attributed to our results.

Fig. 1. shows the dependence on R/m ($R =$ range in μm, $m =$ mass in electron masses) of the number of gaps per 200 μm ($\overline{n}$), of the total gap length

(1) C. CASTAGNOLI, G. CORTINI and A. MANFREDINI: *Nuovo Cimento*, **2**, 301 (1955).

per 200 μm ($\overline{X}$) and specific gap length ($\overline{w} = \overline{x}/\overline{n}$) *i.e.* the gap length averaged over each interval of 200 μm.

Calibration of the stack for the range-energy relation was carried out by measuring residual ranges of μ-mesons from decay of π^+ at rest. The mean

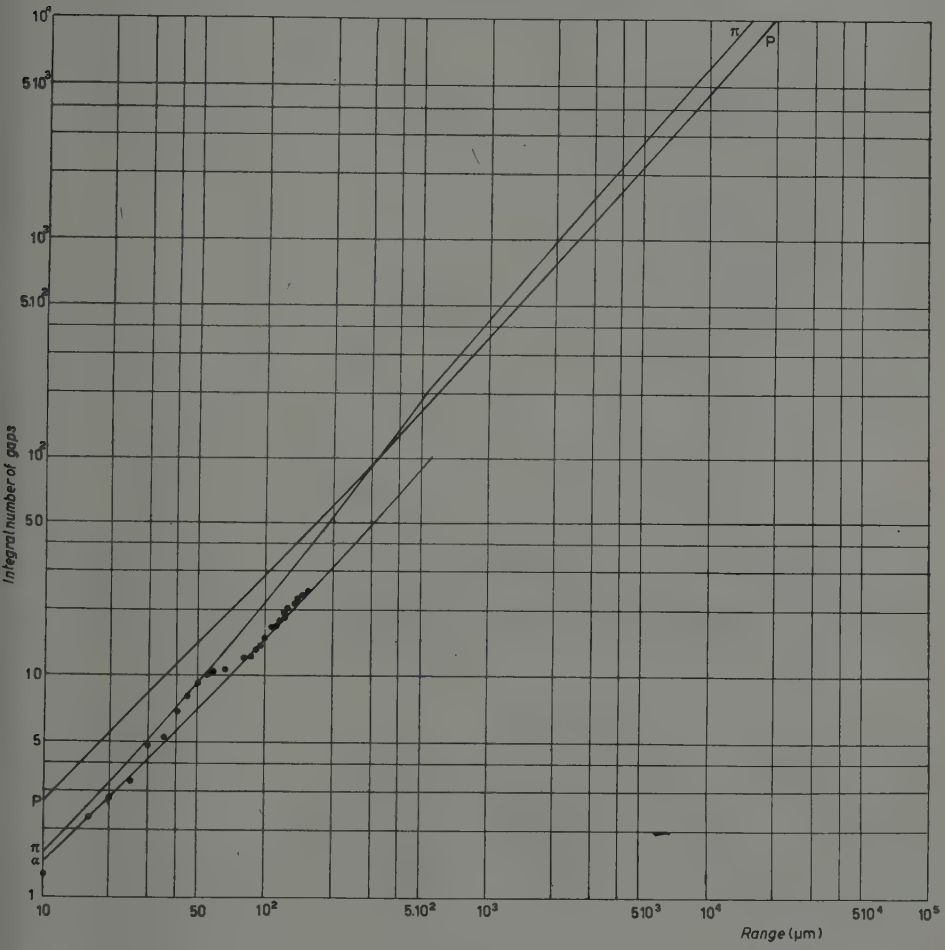

Fig. – 2. Integral number of gaps *versus* residual range.

value obtained is in agreement with the curves computed by WINTZELER on the basis of BARKA's work.

Curves for α-particles, ^{8}Li, ^{8}B have been deduced from it and employed in the present work. Our results have been checked on the range-momentum curves reported by W. E. SLATER (2).

(2) W. E. SLATER: *Suppl. Nuovo Cimento*, **10**, 1 (1958).

The integral number of gaps *versus* residual range has been plotted in Fig. 2. A comparison between the curve obtained for α-particles and those of protons shows agreement with the expected Z-dependence.

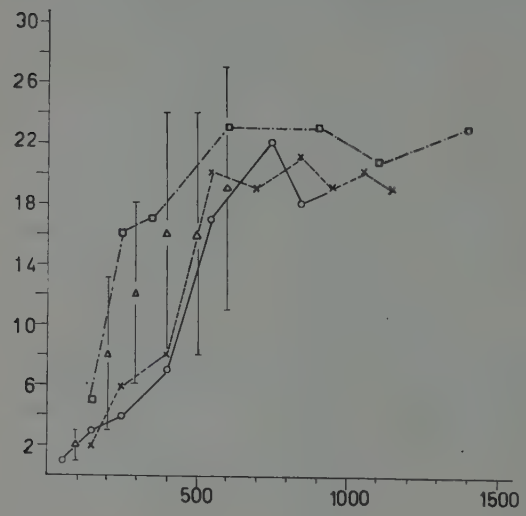

Fig. 3 gives the results of the δ-ray density measured on eight ^{8}B tracks, compared with the results obtained by Sørensen ([3]).

Fig. 3. – δ-ray density measured on ^{8}B tracks: □ ○ x Sørensen data; ▲ present work (8 events).

2. – Unstable fragments (*). Identification of events.

Out of the large variety of fragments which are ejected from high energy nuclear disintegrations, the following ones have been selected and their character studied.

2·1. ^{8}Li. – This type of fragment is responsible for the familiar « hammer tracks » w ich have been identified in energetic disintegrations a long time ago. The lifetime of ^{8}Li for the process: $^8\mathrm{Li} \rightarrow {}^8\mathrm{Be} + e^-$ being about 0.8 s, such a fragment is invariably brought to rest (in emulsion) before it decays. The resulting ^{8}Be is left in the fundamental or sometime in an excited state and in all cases it decays into two α's in a time which is probably much shorter than 10^{-14} s, this being an experimental upper limit ([4]). The allowed transitions are indicated in Fig. 4. For this reason the energy spectrum of the two α's should be expected to show a structure. Our findings seem to confirm this statement. Fig. 5, based on 202 events, shows the well known peak corre-

([3]) S. O. Sørensen: *Meddel.*, **186** (1951).

(*) In this paper unstable fragments are intended to be only those fragments which do not owe their instability to the presence of a hyperon. For the latter the usual name of hyperfragment will be used.

([4]) F. Ajzenberg-Selove and T. Lauristen: *Nucl. Phys.*, **11**, 1 (1959).

sponding to the 2.9 MeV level for the ^{8}Be. The peaks located at (4÷4.5) MeV, and at (6.5÷7) MeV could be taken as an indication for the existence of other levels. Three events may be interpreted as due to transitions from levels of even higher energy (10.8 MeV?).

It is to be noted that not more than three events are probably due to transitions from the ^{8}Be ground level, which is unstable only for ~ 0.1 MeV. This

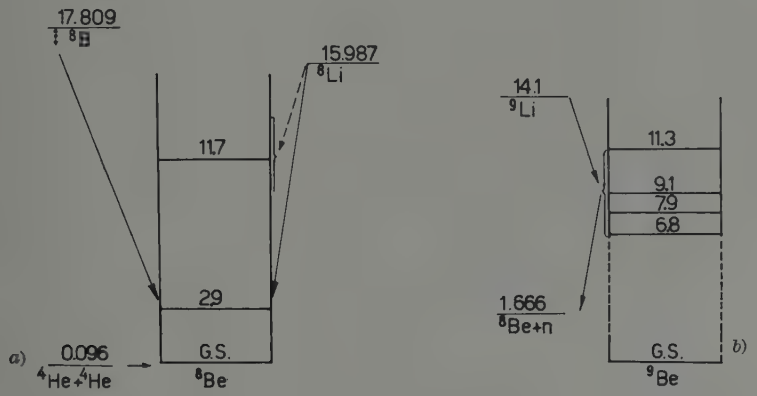

Fig. 4. - Excited levels of ^{8}Be and ^{9}Be nuclei (from F. AJZENBERG and T. LAURITSEN [4]).

transition is however very difficult to detect, since the resulting α-particles have a range smaller than a grain. Thus in most cases they escape detection. For comparison, the established levels of ^{8}Be have been reported (full arrows).

2·2. ^{9}Li. – Events due to decay of ^{9}Li, following the reaction:

$$^9\mathrm{Li} \rightarrow \mathrm{e}^- + {}^9\mathrm{Be}^* \qquad \hookrightarrow \mathrm{n} + {}^8\mathrm{Be} \rightarrow \mathrm{n} + 2\alpha$$

are expected to have a similar appearance. In fact the ^{9}Li ejected in its ground state decays to excited states of ^{9}Be through the emission of a negative electron with a lifetime of ~ 0.17 s. ^{9}Be in turn may decay by neutron emission into ^{8}Be from the unstable state, at which it is created. Thus the event, as seen in the emulsion, will show the electron track and two non-colinear α's, usually having slightly different ranges.

Both the non-colinearity and the range difference are often small and a ^{9}Li event may be taken erroneously to be a ^{8}Li. If the excitation energy of ^{8}Be is calculated from the total range of the two α's, this will introduce a contamination of spurious events in the decay spectrum of ^{8}Be. It is easy to see that the effect of such a misinterpretation leads to an overestimate of the Q-value in the $^8\mathrm{Be} \rightarrow 2\alpha$ decay.

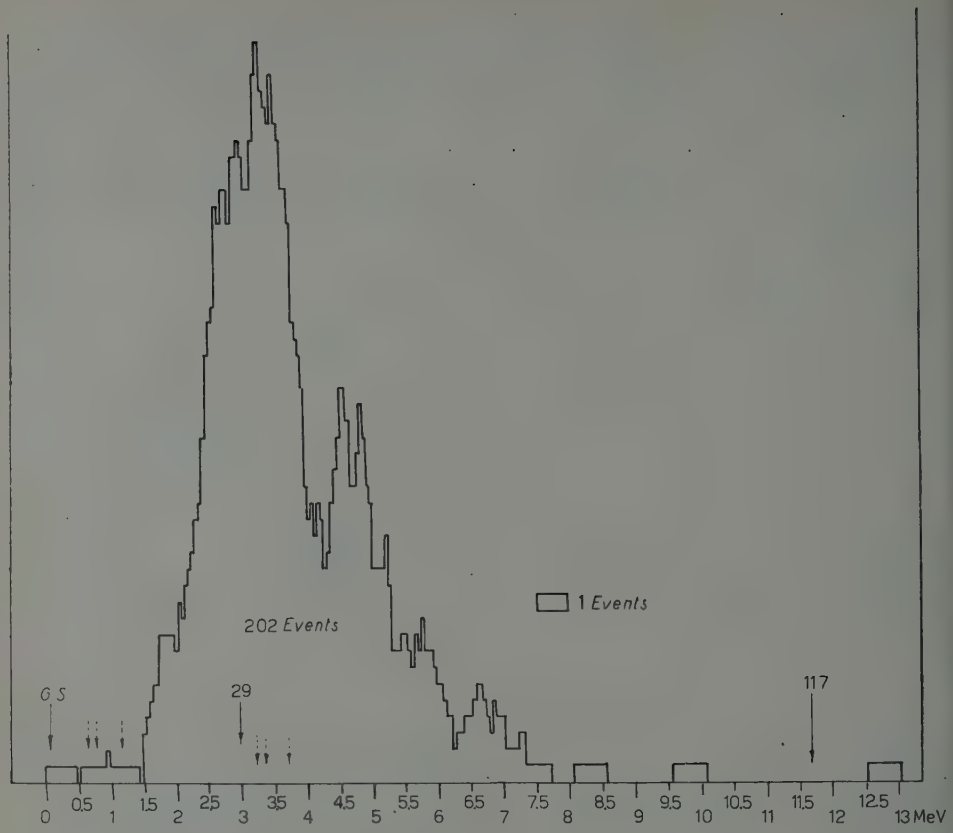

Fig. 5. – Q-spectrum disintegration of ^{8}Be arising from ^{8}Li decays.

Calling Q_{Be} its true value and Q_1 the energy release in $e^9B^* \rightarrow n + {}^8Be$ decay, the apparent Q is:

$$Q_{\mathrm{app}} = Q_{^8\mathrm{Be}} + \tfrac{1}{9} Q_1$$

and is independent of the angle between the two α's (*).

(*) Let P be the momentum of the neutron and the recoiling ^{8}Be in the ^{9}Be* decay. Let also p be the momentum of the two alphas in their c.m. system in the ^{8}Be decay, and P_1 and P_2 the momenta of the two alphas in the laboratory system. Then:

$$p_1^2 = \frac{P^2}{4} + p^2 + Pp\cos\theta\,, \qquad P_2^2 = \frac{P^2}{4} + p^2 - Pp\cos\theta\,,$$

$$Q_{^8\mathrm{Be}} = \frac{p^2}{m_\alpha}\,, \qquad Q_1 = \frac{P^2}{2}\left(\frac{1}{m_{\mathrm{n}}} + \frac{1}{m_{\mathrm{Be}}}\right).$$

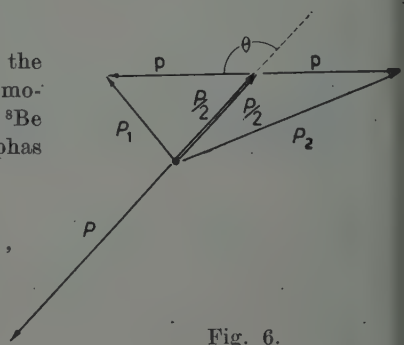

Fig. 6.

Excitation energies (E_9) of known ^{9}Be* levels are reported in Fig. 4 as well as those of ^{8}Be* (E_8). A transition from an E_{9i} level to an E_{8j} will leave an energy

$$Q_1 = E_{9i} - E_{8j} - \Delta$$

to be shared between the neutron and ^{8}Be*, Δ being the difference between the ground states of ^{9}Be and ^{8}Be respectively (*).

Thus we find that we may expect the values for Q_{app} reported in Table I.

TABLE I. – *Apparent Q-values in* $^9\text{Be}^* \rightarrow {}^8\text{Be}^* \rightarrow 2\alpha$ *disintegrations.* (Energies in MeV).

$E_9 =$	11.3	7.9	6.8
$E_8 = 0$ (Gd. st.)	1.17	0.8	0.67
2.9 ± 0.6	3.75	3.37	3.25

Thus, failure to identify ^{9}Li events will lead to some confusion in the interpretation of the ^{8}Be* spectrum. We may attribute to this effect the following peculiarities of the plot shown in Fig. 5.

1) The distribution of events around the 2.9 MeV peak is somewhat broader than expected. In fact this level is known to be associated with a total width of 1.2 MeV, while the observed one exceeds 1.5 MeV. The excess may then be interpreted as due to the apparent Q-values reported in Table I (see also the dotted arrows in Fig. 5).

2) If ^{9}Li is included among the reported events, the alternative mode of decay:

$$\begin{aligned} {}^9\text{Li} &\rightarrow {}^9\text{Be}^* + \text{e} + Q \\ &\quad\quad \rightarrow {}^5\text{He} + {}^4\text{He} + Q_9 \\ &\quad\quad\quad\quad \rightarrow {}^4\text{He} + \text{n} + Q_5 \end{aligned}$$

is to be expected, It may be shown exactly in the same way, as indicated in footnote at page 270, that the total energy of the two resulting α-particles

Hence:

$$Q_{app} = \frac{P_1^2 + P_2^2}{2m_\alpha} = \frac{(P^2/4) + p^2}{m_\alpha} = \frac{1}{9} Q_1 + Q_{^9\text{Be}} .$$

(*) E_9 and E_8 are referred to the ground states of ^{9}Be and ^{8}Be respectively.

(Q_{app}) would be given by the expression

$$Q_{app} = \tfrac{1}{5}Q_5 + \tfrac{16}{15}Q_9 + \tfrac{4}{5}\sqrt{Q_5 Q_9}\cos\theta\,,$$

θ being the decay angle of the ^{4}He and n in the ^{5}He system. Thus for any of the transitions leading from a level E_9 of ^{9}Be* to a level E_5 of ^{5}He one should expect a flat distribution of events within the limits given by the values $\cos\theta = \pm 1$

Assuming that all the ^{9}Be* decays lead to the ^{5}He ground state, the following « apparent Q » values are to be expected (see Table II):

TABLE II. – *Apparent Q-values* (Q_{app}).
in $^9\mathrm{Be}^* \to {}^5\mathrm{He} + {}^4\mathrm{He} \to 2\,{}^4\mathrm{He} + \mathrm{n}$ disintegrations.
(All energies in MeV).

E (^{9}Be*)	13.3	11.3	9.1	7.9
Q_{app}	4.04 ± 0.9	3.4 ± 0.8	2.6 ± 0.7	2.1 ± 0.6

Thus by this assumption we can explain the observed distribution up to an energy of ~ 5 MeV. On the other hand we cannot find an easy explanation for the events included in the region between $(5 \div 8)$ MeV unless the esistence of other not so well established excited ^{8}Be* levels is assumed (*).

2·3. ^{8}Be. – When ^{8}Be* nuclei are directly emitted from an evaporating nucleus, they immediately disintegrate, owing to their very short lifetime. When the ^{8}Be* is ejected in its ground level the event appears as a pair of collimated α-particles of nearly the same energy, their difference depending on the angle of emission of the two α's in the system of the travelling ^{8}Be. On the other hand if the ^{8}Be is in a highly excited state the angular separation is obviously greater and so is the energy difference.

These events have to be identified against the background of randomly (**) ejected α-particles. To minimize the background contamination only α-particles separated by less than 10° have been considered and their Q measured. By this method all the ^{8}Be ground level events have been taken, but drastic losses have been introduced in the high Q region. The results of our search,

(*) Compare f.i.: F. AJZENBERG-SELOVE and T. LAURITSEN: *Rev. Mod. Phys.*, **27**, 91 (1955); *Nucl. Phys.*, **11**, 45 (1959).

(**) We assume that in general the α's ejected in the type of stars we have analyzed are randomly distributed, in so far as their direction is concerned: how true this is, we do not really know. However with regard to this point, this assumption is not critical.

summarized in Fig. 7, clearly show the prominent peak corresponding to the ground level (0.09 MeV), due to 96 events and a distribution of 42 events over a large interval of energy, probably due to transitions from levels other than the ground state.

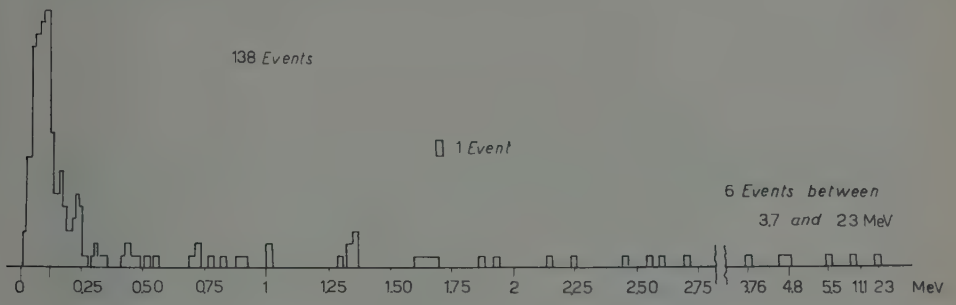

Fig. 7. – Q-Spectrum of ^{8}Be* disintegrations.

2·4. ^{8}B. – This nucleus is known to be unstable for e^+ decay into a ^{8}Be* excited state, with a lifetime of ~ 0.7 s. Thus, if ejected in emulsion it is certainly brought to rest before it decays. The sequence of the various steps:

$$^8\mathrm{B} \rightarrow e^+ + {}^8\mathrm{Be}^*$$

$$\qquad\qquad\qquad\qquad \longrightarrow 2\alpha + Q_{\mathrm{Be}}$$

indicates that the event should produce a track in an emulsion closely similar to the ^{8}Li decay. The two types of events differ essentially for: 1) the sign of the ejected electron which is positive in ^{8}B disintegrations but which cannot in general be established by this technique, 2) also the electron energy, which can be established only in those few lucky cases in which a sufficiently long portion of its track lies flat with respect to the plane of the emulsion, and 3) the charge of the parent nucleus ($Z = 5$ instead of 3). The last parameter is the easiest of the three to be determined in the emulsion and this can be done when the energy of the ejected nucleus exceeds ~ 60 MeV.

Eight of such events have been identified—determining the primary charge by δ-ray counting. The Q-distribution is not very meaningful but is nevertheless consistent with the assumed interpretation (see Fig. 8). From these results we are led to conclude that a considerable number of ^{8}B decays have perhaps been included among the ^{8}Li hammer tracks (see also Section 3·4).

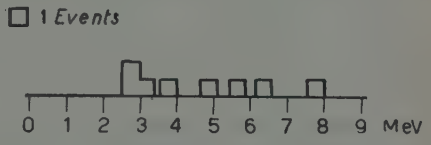

Fig. 8. – Q-spectrum of ^{8}Be arising from $^8\mathrm{B} \rightarrow e^+ + {}^8\mathrm{Be}^*$ decays.

2·5. ^{12}C. – When a $^{12}C^*$ nucleus is emitted in an excited level lying above the threshold for the decay into $^8Be+\alpha$, *i.e.* at an excitation energy greater than 7.37 MeV, the following process becomes possible:

$$^{12}C^* \rightarrow {}^8Be^* + \alpha$$
$$\qquad\quad \hookrightarrow 2\alpha\,.$$

Both steps taking place in a very short time, such an event appears as three α-particles often having comparable ranges and a small angular separation.

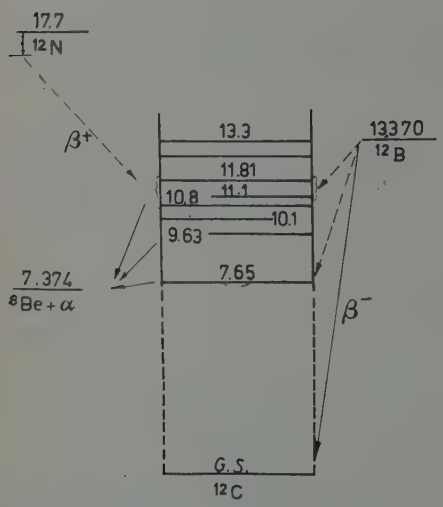

Fig. 9. – Known excited levels of ^{12}C (from F. AJZENBERG and T. LAURITSEN (4)).

The event can be identified by calculating the kinetic energy (in their c.m. system) of the pairs of α's which can be formed out of the three α's. For one pair one should find the Q-value corresponding to one of the levels of $^8Be^*$. These are assumed to arise from the $^8Be^*$ disintegration in flight. Then momentum and energy balance applied to the unpaired α and to the decaying ^8Be should allow a check on the interpretation and determination of the excitation energy of the parent $^{12}C^*$.

However the latter does not—in general—give a great help in the identifictaion of the event, the excited levels of ^{12}C being so many and so close to each other (see Fig. 9).

The angular separation of the three α's and their energy distribution depend on the excitation energies of both $^{12}C^*$ and $^8Be^*$, and therefore are not easy to foresee. Thus losses of good events and contamination due to the background of uncorrelated α's are—in this case—difficult to assert.

The excitation energy of twelve events, interpreted as $^{12}C^*$, are reported in Fig. 10. The results are not inconsistents with what one could reasonably expect. The arrows indicate the known levels of $^{12}C^*$.

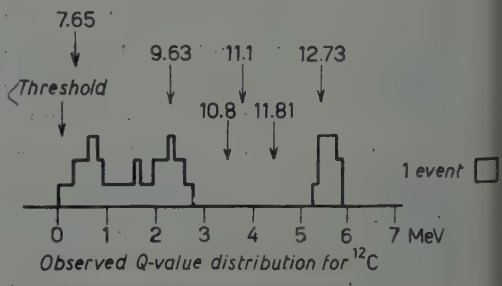

Fig. 10. – Q-spectrum of $^{12}C^*$.

2·6. ^{12}B. – This nucleus is known to be unstable for e^- decay with a lifetime of 0.022 s. In most cases (97%) it decays into the ^{12}C stable ground level. In about 2% of the cases, however, it may decay into one of the $^{12}C^*$ excited levels lying above the $^8Be^* + \alpha$ level (see Fig. 9). Thus the process:

$$^{12}B \rightarrow e^- + {}^{12}C^* \rightarrow {}^8Be^* + \alpha \rightarrow 2\alpha$$

would appear in emulsion as a track stopping in the emulsion and disintegrating into an electron and three α-particles.

Three events consistent with the above interpretation, have been found. The excitation energies of $^{12}C^*$, calculated for each of them, are consistent with this interpretation, It may be worth stressing, in connection with it, that decays from the 7.7 MeV $^{12}C^*$ level are hard to detect, since they would produce α-particles of very short ranges and thus easily escape detection.

Moreover, one might wonder if any of these examples could not be ^{12}N which is also unstable with a lifetime of 0.012 s. This nucleus suffers e^+-decay into $^{12}C^*$, thus producing a similar star. We believe, however, that none of our examples could be ^{12}N since the δ-ray densities which we have measured are definitively too low to support this view.

3. – Frequency of production and energy spectrum of unstable fragments.

3·1. – The frequency of production observed for the events described in the previous Section are reported in Table III (*). It will be noted that for some of them the « observed value » is considerably lower than the estimated « corrected » ones. The difference is due to the fact that some events may be missed altogether during the process of scanning, and to geometrical losses. The estimate of the corrected value, is thus somewhat arbitrary. Frequencies reported in Table III, column 3, are corrected for geometrical losses only. Some comments on the data reported may be appropriate.

3·2. ^8Li, ^9Li, ^8B. – It was mentioned in Sections 2·1. 2·2 and 2·4 that ^8Li, ^9Li, ^8B produce similar tracks, which are not easily distinguishable one from the other. We can, therefore, give only their total frequency of occurrence. Experimental losses have been calculated purely on geometrical considerations, rejecting all the tracks at an angle with the plane of the emulsion

(*) The frequencies reported here refer only to disintegrations associated with at least 5 black prongs.

TABLE III. – *Production frequencies of unstable fragments in disintegrations produced by 4.5 GeV π^- in emulsion.*

Unstable fragment	Observed value (No. per star)	Corrected value (No. per star)	Remarks
1) $^8Li^* \rightarrow e^- + {}^8Be^* + 2\alpha$ 2) $^8B \rightarrow {}^8Be^* \rightarrow 2\alpha$ 3) $^9Li^* \rightarrow n + {}^8Be \rightarrow 2\alpha + n$ 4) $\rightarrow {}^4He + {}^5He \rightarrow 2\alpha + n$	$0.48 \cdot 10^{-2}$	$\sim 0.62 \cdot 10^{-2}$	Transition from the $^8Be^*$ g.l. not excluded.
$^8Be^*$	$0.8 \cdot 10^{-2}$	$\sim 1.5 \cdot 10^{-2}$	Transition from $^8Be^*$ levels other than ground hard to detect.
$^{12}C^*$	$0.1 \cdot 10^{-2}$	difficult to estim.	
$^{12}B^*$	$0.01 \cdot 10^{-2}$	—	—
Hyperfragments (identified with certainty)	$\sim 0.08 \cdot 10^{-2}$	$\sim 0.08 \cdot 10^{-2}$	
Goks	$0.1 \cdot 10^{-2}$	$0.1 \cdot 10^{-2}$	

larger than 70° and those which did not terminate in the same pellicle in which they were created. It was assumed that the azimuthal distribution of these tracks was a constant. Even so the total number of ^8Li may be grossly underestimated: in fact we have no idea of the frequencies of ^8Li decaying into the ^8Be ground state.

The observed energy spectrum is shown in Fig. 11. It rises sharply after 5 MeV, in accordance with the cut-off imposed by the height of the potential barrier of ^8Li in a silver or bromine nucleus. It shows a prominent peak between 10 and 20 MeV, as predicted by the evaporation theory (*). A number of events higher than expected by the same theory has been found between 20 and 30 MeV: if this peak is not due to statistical fluctuations, it could be

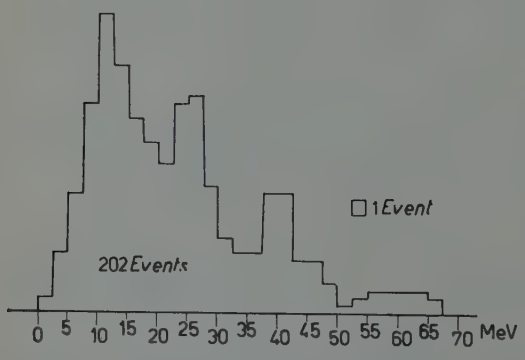

Fig. 11. – Energy spectrum of ejected $^{8,9}Li$ nuclei.

(*) Compare f.i. with S. J. GOLDSACK, W. O. LOCK and B. A. MUNIR: *Phil. Mag.*, **2**, 149 (1957). Earlier literature quoted here. See also O. SKIEGGESTAD and S. D. SØRENSEN: *Phys. Rev.*, **113**, 1115 (1959).

interpreted as a contamination of ^{8}B fragments which could not be resolved from ^{8}Li owing to the shortness of their range.

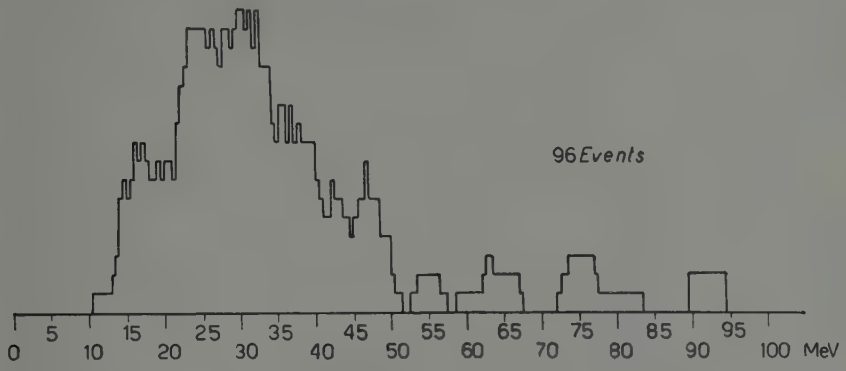

Fig. 12. – Energy spectrum of ejected ^{8}Be (ground state only).

The evaporation theory indicates that ^{8}B fragments should have an energy spectrum with a peak between 40 and 55 MeV. This corresponds to tracks of about 65 to 95 μm. If these are interpreted as ^{8}Li, the energy which will be attributed to them will be (24÷30) MeV, which coincides remarkably with our observations.

Fig. 12 shows angular distribution of ^{8}Li fragments (inclusive of ^{8}B contamination), given as a function of the kinetic energy of the ejected fragment. A definitive asymmetry is visible clearly for fragments having more than 3 MeV per nucleon. The overall forward to backward ratio equals 1.4.

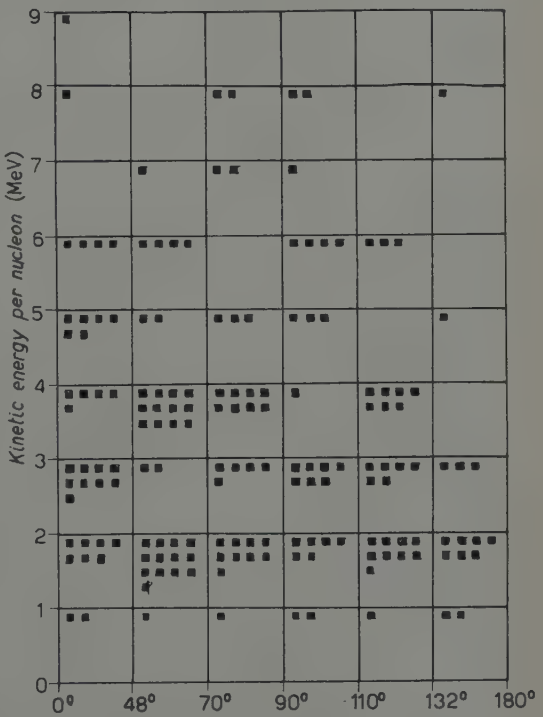

Fig. 13. – Angular distribution of (^{8}Li, ^{9}Li, ^{8}B) nuclei as a function of their energy.

3·3. ^{8}Be. – The energy spectrum (Fig. 13) is strongly biassed against ^{8}Be ejected at low energy. This is because

slow ^{8}Be produce two short α's at a large angle and identification of such an event is often impossible.

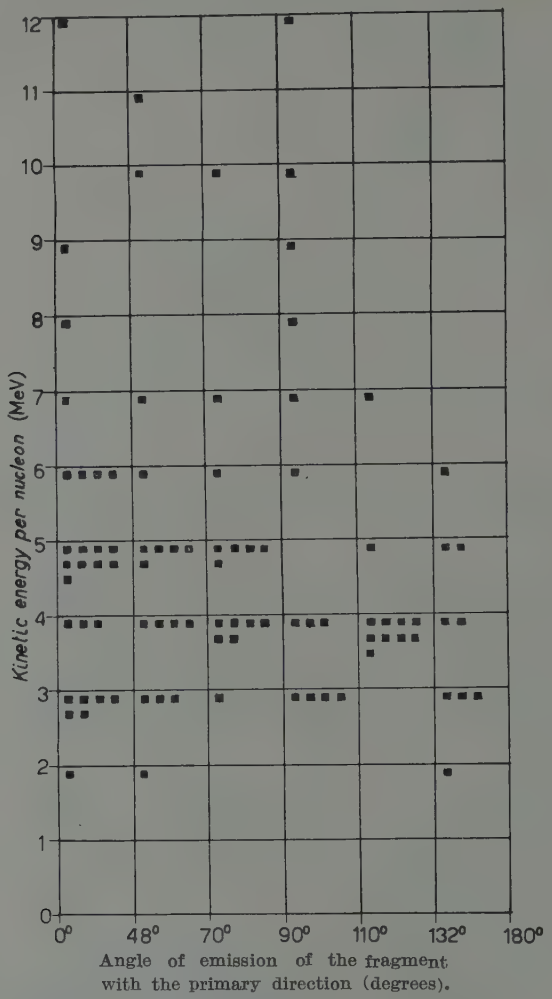

Fig. 14. – Angular distribution of the ejected ^{8}Be.

The angular distribution (Fig. 14) shows departure from anisotropy for energies greater than 4 MeV. The forward to backward ratio is 1,8.

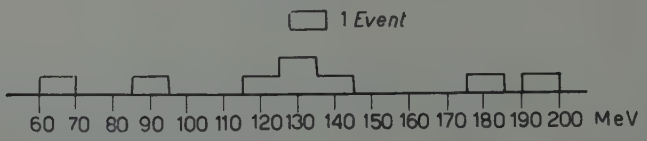

Fig. 15. – ^{8}B energy distribution.

3·4. ^{8}B, ^{12}C. – The energy distributions observed for these fragments are shown in Fig. 15 and 16. ^{8}B—as mentioned above—could not be identified if produced at less than 60 MeV.

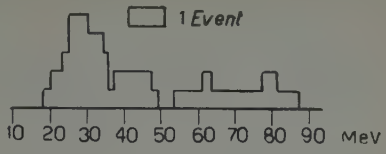

Fig. 16. – ^{12}C energy distribution.

4. – Hyperfragments.

Twenty nine events have been identified with certainty as due to hyperfragment decays, their relevant data are summarized in Fig. 17, 18 and 19, 20.

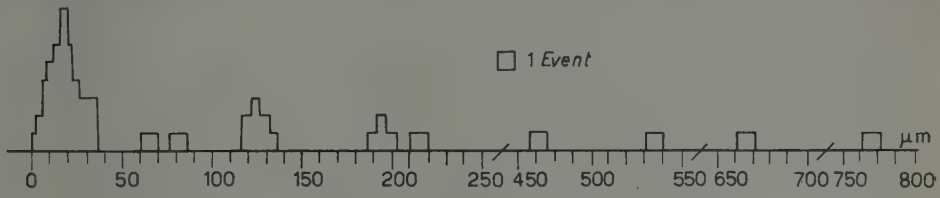

Fig. 17. – Range distribution of hyperfragments.

The data plotted in Fig. 17, 18 and 19 agree with those obtained by other workers. The angular distribution of hyperfragments with respect to the primary π^- direction requires some comments (Fig. 20).

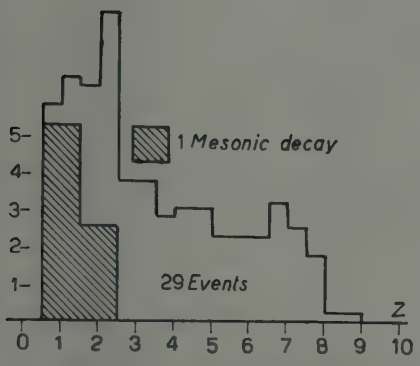

Fig. 18. – Z distribution of hyperfragments.

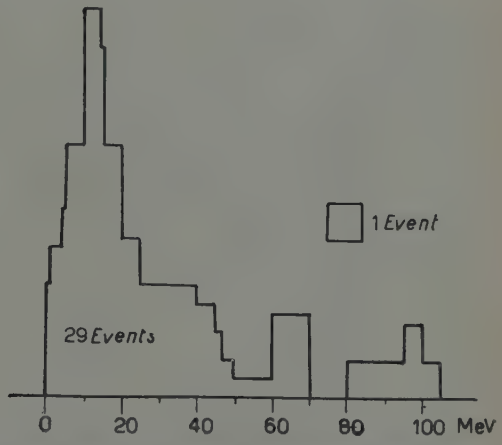

Fig. 19. – Energy distribution of hyperfragments.

The overall forward to backward ratio is 1.6, not too different from that of the unstable fragments analyzed in the previous section. In our opinion

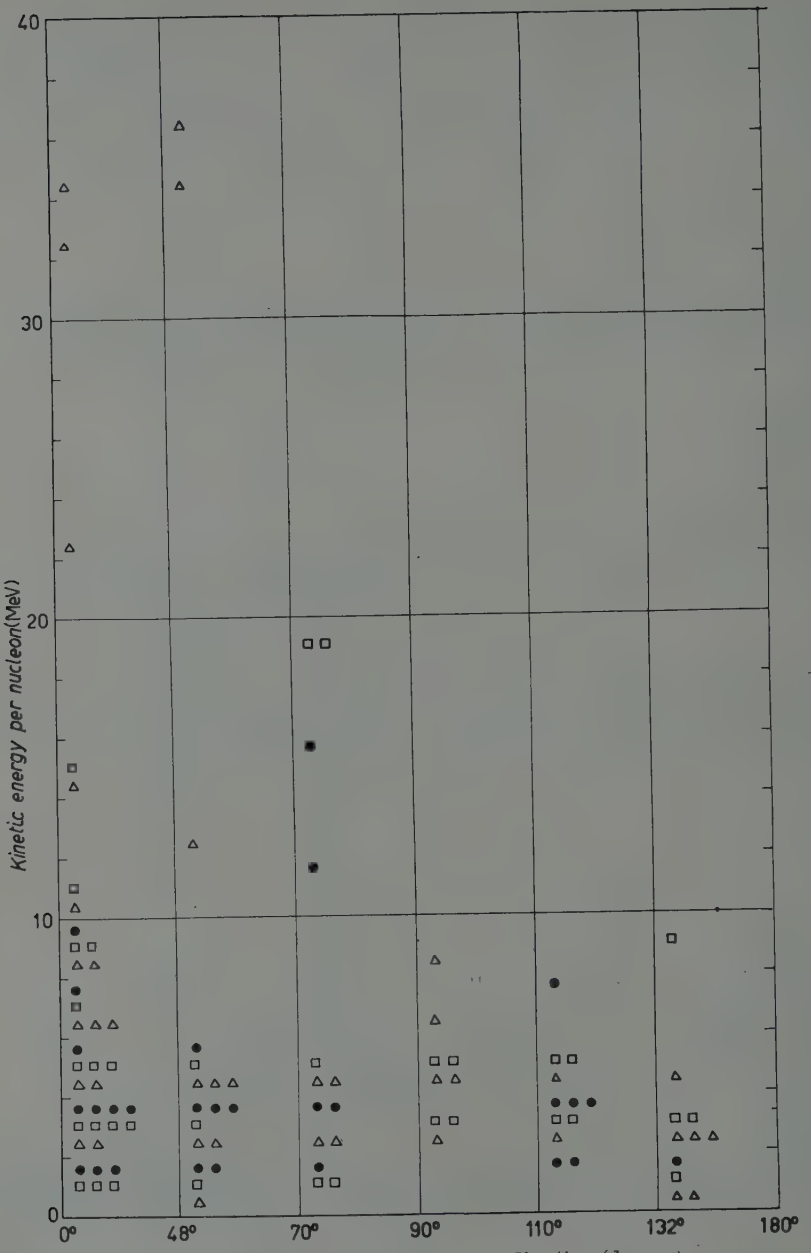

Fig. 20. – Angular distribution of hyperfragments as a function of their energy. ○ present work, □ W. E. SLATER, *Suppl. Nuovo Cimento*, **10**, 1 (1958); ▲ HENNESSY, *Thèse*, Faculté de Science, Paris (1957).

these results do not support Deka's view (*), suggesting that the mechanism which is operative in hyperfragment emission is substantially different from that of normal fragments.

5. – Conclusions.

The analysis of the data discussed in this paper can be summarized as follows:

1) The Q-spectrum due to ^{8}Be* as deduced from the familiar « hammer tracks » contains a contamination due to events ^{9}Be*. The presence of this contamination alters the spectrum by producing a widening of the peaks and may be responsible for a considerable number of tracks associated with apparent Q-values up to ~ 5 MeV.

Also some ^{8}B contribute to produce « hammer tracks ». Only a small energetic fraction of them can be resolved from ^{8}Li. Their presence however does not alter the Q-spectrum in any appreciable way.

2) In addition to the already established ^{8}Li, ^{8}Be, ^{8}B and ^{12}C* fragments we have found evidence for ^{12}B* nuclei β^--decaying into ^{12}C*. Their presence among the particles ejected in energetic disintegrations of nuclei has, to our knowledge, so far not been reported in the literature.

3) The relative frequencies of occurrence of the various types of fragments reported here are to be taken as lower limits and in any case as preliminary. Various reasons mentioned in the preceding pages may cause loss of events. Even so our results seem to indicate that an appreciable number of α-particles and perhaps protons may originate from the decay of heavier unstable fragments of very short lifetime. A deeper study based on much larger statistics will be necessary to determine the true values. Work on this line is being continued.

4) Data on 29 hyperfragments identified with certainty have been briefly reported. Their angular and energy distribution does not support the view that their mechanism of production is substantially different from that of unstable fragments of non hyperonic origin.

* * *

We would like to thank Prof. C. Franzinetti, who suggested the experiment and assisted us during the development of this research, Prof. M. Baldo-Ceolin, of Padua University, who kindly lent us the emulsions on which the events reported here have been found. Thanks are also due to the group of observers of the University of Trieste for their enthusiastic co-operation.

(*) G. C. Deka: *Intern. Conf. on Mesons* (Padua-Venice, 1957), p. II-88.

SUPPLEMENTO AL VOLUME XV, SERIE X
DEL NUOVO CIMENTO

N. 3, 1960
1° Trimestre

Näherungstheorie des rotationssymmetrischen Kreisels mit veränderlicher Masse.

N. ST. KALITZIN

Physikalisches Institut bei der Bulgarischen Akademie der Wissenschaften - Sofia

(ricevuto l'8 Luglio 1959)

Die Theorie des Kreisels mit veränderlicher Masse ist wenig entwickelt. Sie wird eine Anwendung finden bei den rotierenden Sternen, deren Masse sich durch Ausfluß von Materie rasch ändert und bei den Raketen, welche durch Rotation um ihrer Längsachse stabilisiert werden. Bie den Supernovae und auch bei einigen Atomraketen, welche schon ihre Verwirklichung finden, fließt die Materie aus dem Grundkörper mit relativistischen Geschwindigkeiten aus. Es ist daher von Interesse eine Theorie des Kreisels mit veränderlicher Masse zu haben, bei welcher die relativistischen Geschwindigkeiten der ausfließenden Materie berücksichtigt werden.

Wir wollen hier eine Näherungstheorie des rotationssymmetrischen Kreisels mit veränderlicher Masse entwickeln, wobei wir zunächst den Fall der unrelativistischen Geschwindigkeiten der Massenzuwächse betrachten werden, und dann uns zu dem Fall der relativistischen Geschwindigkeiten wenden werden.

1. – Im Falle des rotationssymmetrischen Kreisels mit konstanter Masse ist die folgende Grundformel aus der Näherungstheorie der Kreiselerscheinungen gültig

$$I(\boldsymbol{\omega}_2 \times \boldsymbol{\omega}_1) = \boldsymbol{M}\,. \tag{1}$$

I, das Trägheitsmoment des Kreisels in Bezug auf die Drehachse OO_1; $\boldsymbol{\omega}_1$, Vektor der Winkelgeschwindigkeit des Kreisels um OO_1; $\boldsymbol{\omega}_2$, Vektor der Winkelgeschwindigkeit der Achse OO_1; $\boldsymbol{M}$, Moment der äußeren Kräfte in Bezug auf einen unbeweglichen Punkt auf der Drehachse. Bei der Ableitung der Formel (1) wird vorausgesetzt, daß $\omega_2 \ll \omega_1$ ist und daß ω_1 eine konstante Winkelgeschwindigkeit ist.

Zunächst wollen wir die Formel (1) für einen Kreisel mit veränderlicher Masse verallgemeinern, wobei die Geschwindigkeiten der Massenzuwächse nichtrelativistisch vorauszusetzen sind.

Zu diesem Zweck leiten wir den Drehimpulssatz für ein System bestehend aus n Massenpunkten mit veränderlicher Masse ab. Im Zeitpunkt t betrachten wir das System der Massenpunkte P_i $(i = 1, ..., n)$ mit den Massen m_i, deren Radiusvektoren durch $\boldsymbol{r}_i$ bezeichnet werden und das System der Punkte P_i' mit den Massen $\mathrm{d}m_i$, welche die gleichen Lagen wie die Punkte P_i besitzen Die absoluten Geschwindigkeiten der Punkte P_i bezeichnen wir mit $\boldsymbol{v}_i = \dot{\boldsymbol{r}}_i$ und die der Punkte P_i', mit $\boldsymbol{u}_i$.

Im Zeitpunkt $t+\mathrm{d}t$ wird jedes Paar der Punkte P_i und P_i' als einen Massenpunkt P_i^* mit der Masse $m_i+\mathrm{d}m_i$, die Geschwindigkeit $\boldsymbol{v}_i+\mathrm{d}\boldsymbol{v}_i$ und die Lage $\boldsymbol{r}_i+\mathrm{d}\boldsymbol{r}_i$ betrachtet. Wenden wir den Drehimpulssatz an: im Zeitpunkt t ist der gemeinsame Drehimpuls der Punkte P_i und P_i' in Bezug auf einen beliebigen festen Punkt A gleich

$$\boldsymbol{r}_i \times m_i \boldsymbol{v}_i + \boldsymbol{r}_i \times \mathrm{d}m_i \boldsymbol{u}_i$$

und im Zeitpunkt $t+\mathrm{d}t$ ist der Drehimpuls des Punktes P_i^*

$$(\boldsymbol{r}_i + \mathrm{d}\boldsymbol{r}_i) \times (m_i + \mathrm{d}m_i)(\boldsymbol{v}_i + \mathrm{d}\boldsymbol{v}_i) .$$

Die Zunahme des Drehimpulses ist gleich

$$\boldsymbol{r}_i \times m_i \mathrm{d}\boldsymbol{v}_i + \boldsymbol{r}_i \times \mathrm{d}m_i(\boldsymbol{v}_i - \boldsymbol{u}_i) + \mathrm{d}\boldsymbol{r}_i \times m_i \boldsymbol{v}_i .$$

Dem Fall der abnehmenden Masse entspricht $\mathrm{d}m_i < 0$.

Diese Zunahme des Drehimpulses ist gleich der Größe $\boldsymbol{M}_i \mathrm{d}t + \boldsymbol{M}_i' \mathrm{d}t$, wobei $\boldsymbol{M}_i(\boldsymbol{F}_i)$ das Moment der Resultante $\boldsymbol{F}_i$ der auf den Punkt wirkenden äußeren Kräfte ist, und $\boldsymbol{M}_i'(\boldsymbol{F}_i')$ das Moment der Resultante $\boldsymbol{F}_i'$ der inneren Kräfte. Wir haben also

$$\boldsymbol{r}_i \times m_i \frac{\mathrm{d}\boldsymbol{v}_i}{\mathrm{d}t} + \boldsymbol{r}_i \times \dot{m}_i(\boldsymbol{v}_i - \boldsymbol{u}_i) = \boldsymbol{M}_i + \boldsymbol{M}_i' . \tag{2}$$

Wenn wir (2) über alle Punkte des Systems summieren, so erhalten wir die Formel

$$\sum_{i=1}^{n} \boldsymbol{r}_i \times m_i \frac{\mathrm{d}\boldsymbol{v}_i}{\mathrm{d}t} + \sum_{i=1}^{n} \boldsymbol{r}_i \times \dot{m}_i(\boldsymbol{v}_i - \boldsymbol{u}_i) = \boldsymbol{M} . \tag{3}$$

Hierbei

$$\boldsymbol{M} = \sum_{i=1}^{n} \boldsymbol{M}_i ; \qquad \sum_{i=1}^{n} \boldsymbol{M}_i' = 0 . \tag{4}$$

Der rotationssymmetrische Kreisel mit veränderlicher Masse ist ein starrer Körper mit veränderlicher Masse, welcher Rotationssymmetrie um eine Achse OO_1 besitzt und welcher mit großer Winkelgeschwindigkeit um dieselbe Achse rotiert. Ein starrer Körper mit veränderlicher Masse ist ein Körper in dem die Entfernungen zwischen dessen Punkten unveränderlich bleiben (die Punkte haben veränderliche Massen). Der Zuwachs der Masse des Kreisels für das Zeitintervall dt besitzt ebenfalls Rotationssymmetrie um die Kreiselachse.

Der Kreisel rotiert um seine Symmetrieachse mit der Winkelgeschwindigkeit ω_1. Die Richtung des Winkelgeschwindigkeitsvektors $\boldsymbol{\omega}_1$ fällt mit der Richtung der Achse OO_1 zusammen. Die Achse OO_1 ihrerseits dreht sich mit der Winkelgeschwindigkeit $\boldsymbol{\omega}_2$. In unserer Näherungstheorie nehmen wir an, daß

$$\omega_2 \ll \omega_1 \tag{5}$$

ist. Die Grundannahmen unserer Theorie sind also die folgenden:

a) Der Drehimpuls (der Drall) $\boldsymbol{K}$ des Kreisels, wenn die Winkelgeschwindigkeit ω_2 sehr klein im Verhältnis zu ω_1 ist, bleibt in die Richtung der Kreiselachse OO_1 gerichtet.

b) Bei der Berechnung von $\boldsymbol{K}$ kann man die Winkelgeschwindigkeit $\boldsymbol{\omega}_2$, vernachlässigen, d.h. wir können ansetzen

$$\boldsymbol{K} = I\boldsymbol{\omega}_1 , \tag{6}$$

wobei I das Trägheitmoment des Kreisels in Bezug auf die Achse OO_1 im Zeitpunkt t bedeutet. Wenn wir den Vektor $\boldsymbol{K}$ auf der Achse OO_1 im festen Punkt ansetzen, so haben wir

$$\boldsymbol{K} = \sum \boldsymbol{r}_i \times m_i \boldsymbol{v}_i = I\boldsymbol{\omega}_1 . \tag{7}$$

(Der Einfachheit halber haben wir das Integrieren durch Summation ersetzt).

c) Die Massenabnahme des Punktes P_i soll den Kreisel (die Rakete, den Stern usw.) sofort verlassen. Im Gegenfall sind zu unseren Gleichungen Korrektionsglieder notwendig, welche Glieder die Wechselwirkung des Kreisels mit dem in ihm verweilenden Massenzuwachs darstellen werden. Nach [1], S. 402 aber, sind diese Glieder bei den Raketen so klein, daß sie im Vergleich zu den anderen Gliedern zu vernachlässigen sind. Also ist die letzte Einschränkung nicht wesentlich.

---

[1] L. G. Loitzianski und A. I. Lurie: *Kurs theoretitcheskoi mechaniki*, II, (Leningrad-Moskau, 1948) (russisch).

Nach *b*) kann man die Gleichung (3) in die Form bringen

$$(8) \qquad \sum \boldsymbol{r}_i \times m_i \dot{\boldsymbol{v}}_i + \sum \boldsymbol{r}_i \times \dot{m}_i \boldsymbol{v}_i - \sum \boldsymbol{r}_i \times \dot{m}_i \boldsymbol{u}_i = \frac{\mathrm{d}\boldsymbol{K}}{\mathrm{d}t} - \sum \boldsymbol{r}_i \times \dot{m}_i \boldsymbol{u}_i = \boldsymbol{M} .$$

Die Größen in (8) sind in Bezug auf den festen Punkt auf der OO_1 Achse bestimmt.

Wenn wir

$$(9) \qquad \boldsymbol{\omega}_1 = \omega_1 \boldsymbol{e}_1$$

ansetzen, $\boldsymbol{e}_1$ ein Einheitsvektor, dann haben wir für die von uns betrachtete Drehung der Achse mit der Winkelgeschwindigkeit $\boldsymbol{\omega}_2$

$$(10) \qquad \frac{\mathrm{d}(\omega_1 \boldsymbol{e}_1)}{\mathrm{d}t} = \dot{\omega}_1 \boldsymbol{e}_1 + \boldsymbol{\omega}_2 \times \omega_1 \boldsymbol{e}_1 ,$$

da

$$\frac{\mathrm{d}\boldsymbol{e}_1}{\mathrm{d}t} = \boldsymbol{\omega}_2 \times \boldsymbol{e}_1$$

ist. Aus (7), (8), (9) und (10) ergibt sich

$$(11) \qquad I(\boldsymbol{\omega}_2 \times \boldsymbol{\omega}_1) = \boldsymbol{N} - (\dot{I}\omega_1 + I\dot{\omega}_1)\boldsymbol{e}_1 ,$$

wobei

$$(12) \qquad \boldsymbol{N} = \boldsymbol{M} + \sum \boldsymbol{r}_i \times \dot{m}_i \boldsymbol{u}_i .$$

ist. Gewöhnlich sind bekannt $\boldsymbol{N}$ und $\boldsymbol{e}_1$. Aus Gleichung (11) folgt, dad $\boldsymbol{\omega}_2 \times \boldsymbol{\omega}_1$ in der durch die Vektoren $\boldsymbol{N}$ und $\boldsymbol{e}_1$ bestimmten Ebene liegt.

Wenn wir (11) skalar mit $\boldsymbol{e}_1$ multiplizieren, so ergibt sich

$$(13) \qquad \boldsymbol{N}\boldsymbol{e}_1 = I\dot{\omega}_1 + \dot{I}\omega_1 .$$

Aus (11) und (13) erhalten wit

$$(14) \qquad I(\boldsymbol{\omega}_2 \times \boldsymbol{\omega}_1) = \boldsymbol{N} - (\boldsymbol{N}\boldsymbol{e}_1)\boldsymbol{e}_1 = \boldsymbol{e}_1 \times (\boldsymbol{N} \times \boldsymbol{e}_1).$$

Gleichung (14) ist die gesuchte Verallgemeinerung von Gl. (1) für einen rotationssymmetrischen Kreisel mit veränderlicher Masse. Aus (14) folgt

$$I\omega_1\omega_2 \sin\alpha = |\boldsymbol{N} - (\boldsymbol{N}\boldsymbol{e}_1)\boldsymbol{e}_1| ,$$

wobei α der Winkel zwischen $\boldsymbol{\omega}_2$ und $\boldsymbol{\omega}_1$ ist. Die Beziehung (5) nimmt dann

die Gestalt

$$\omega_2 = \frac{|\boldsymbol{N} - (\boldsymbol{N}\boldsymbol{e}_1)\boldsymbol{e}_1|}{J\omega_1 \sin\alpha} \ll \omega_1$$

an, oder

$$|\boldsymbol{N} - (\boldsymbol{N}\boldsymbol{e}_1)\boldsymbol{e}_1| \ll I\omega_1^2 \sin\alpha \,. \tag{15}$$

Also ist das die Bedingung für $\boldsymbol{N}$, bei welcher die vorliegende Theorie anwendbar ist.

Wenn $\boldsymbol{\omega}_1$, $\boldsymbol{\omega}_2$ und I gegeben sind (Kreisel mit vorbestimmter Präzession), dann können wir aus (14) und (12) die Bedingungen erhalten, welche das Moment $\boldsymbol{M}$ der äußeren Kräfte befriedigen soll. Auf die Vorrichtungen, welche den Kreisel in diese Bewegung setzen werden, wird ein Moment von gleicher Größe wirken, jedoch in der entgegengesetzten Richtung. Den Vektor $\boldsymbol{L} = -\boldsymbol{M}$ bezeichnet man als das gyroskopische Moment. Das gyroskopische Moment gibt uns einen Näherungsausdruck für das Moment der Trägheitskräfte in der betrachteten Kreiselbewegung.

Aus (1), (12) und (14) ist ersichtlich, daß man das gyroskopische Moment $\boldsymbol{L}$ im Falle eines rotationssymmetrischen Kreisels mit veränderlicher Masse durch geeignete Wahl von $\sum \boldsymbol{r}_i \times \dot{m}_i \boldsymbol{u}_i$ größer als das gyroskopische Moment eines Kreisels mit konstanter Masse bei gleichen übrigen Bedingungen machen kann.

2. – Es ist interessant die Formel (14) für den Fall zu verallgemeinern, wenn die Massenzuwächse des Kreisels mit veränderlicher Masse relativistische Geschwindigkeiten besitzen. Diese Verallgemeinerung, wie schon erwähnt, ist von Bedeutung für die rotierenden Supernovae und für die Atomraketen, welche um ihre Längsachse rotieren.

Zu diesem Zweck verallgemeinern wir die Gl. (3) für den Fall, wenn $\mathrm{d}m_i$ relativistische Geschwindigkeit $\boldsymbol{u}_i$ besitzt.

Wir betrachten wieder das System der Massenpunkte P_i mit veränderlicher Masse. Für den Punkt P_i ist nach [2] die folgende Gleichung gültig:

$$\boldsymbol{F}_i + \boldsymbol{F}_i' = \frac{\mathrm{d}}{\mathrm{d}t}\left(\frac{m_i \boldsymbol{v}_i}{\sqrt{1 - (v_i^2/c^2)}}\right) + \tag{16}$$

$$+ \frac{(\mathrm{d}m_i/\mathrm{d}t)c^2\sqrt{1 - (v_i^2/c^2)} + (\boldsymbol{F}_i + \boldsymbol{F}_i')\boldsymbol{v}_i - \mathrm{d}E_i/\mathrm{d}t}{\boldsymbol{u}_i\boldsymbol{v}_i - c^2}\,\boldsymbol{u}_i \,.$$

Hier ist t die Zeit im Koordinatensystem gemessen, in welchem der Punkt P_i die Geschwindigkeit $\boldsymbol{v}_i$ besitzt. $\boldsymbol{F}_i$ und $\boldsymbol{F}_i'$ sind entsprechend die Resultanten der auf den Punkt P_i wirkenden äußeren und inneren Kräfte. $\mathrm{d}E_i$ ist die

[2] N. St. Kalitzin: *Nuovo Cimento*, **8**, 6, 843 (1958).

Energie, die vom Punkte P_i im Zeitintervall dt aus den übrigen Punkten des Systems und aus dem umgebenden Raum aufgenommen wird.

Wir nehmen an, daß $\boldsymbol{v}_i$ nichtrelativistische Geschwindigkeiten sind, d.h.

$$|\boldsymbol{v}_i| \ll c \qquad c \text{ die Lichtgeschwindigkeit,} \tag{17}$$

die $\boldsymbol{u}_i$ sind dagegen relativistisch. Dann kann man in das betrachtete System die gemeinsame Zeit t und den Begriff der Gleichzeitigkeit für alle Punkte P_i einführen. In diesem Spezialfall hat auch der Begriff der auf zwei verschiedenen Punkten des Systems gleichzeitig wirkenden Kräfte einen Sinn, es bleibt auch das dritte Gesetz von Newton für die Wirkung und die Gegenwirkung bestehen. (Dieses Gesetz folgt aus dem Satz der Erhaltung der Bewegungsgröße eines Systems von Massenpunkten in der relativistischen Mechanik bei der Bedingung $|\boldsymbol{v}_i| \ll c$, d.h. wenn ein invariantes Zeitelement Δt für sämtliche Punkte des Systems definiert werden kann. Dann genügt die Zunahme der Bewegungsgröße des Systems durch Δt zu teilen um bei $\Delta t \to 0$ das dritte Gesetz von Newton zu erhalten).

Wir nehmen hier außerdem an, daß dE_i/dt von dergleichen Größenordnung ist wie $(\boldsymbol{F}_i + \boldsymbol{F}_i')\boldsymbol{v}_i$.

(Bei $dm_i/dt = 0$ haben wir $dE_i/dt = (\boldsymbol{F}_i + \boldsymbol{F}_i')\boldsymbol{v}_i$.)

Auf Grund dieser Voraussetzung ergibt sich aus (17) und (16)

$$\boldsymbol{F}_i + \boldsymbol{F}_i' = \frac{d}{dt}(m\boldsymbol{v}_i) - \frac{dm_i}{dt}\boldsymbol{u}_i\,, \tag{18}$$

d.h. die Gleichung von Meschtcherski ($\boldsymbol{u}_i$ relativistische Geschwindigkeit).

Wenn $\boldsymbol{r}_i$ den Radiusvektor des Punktes P_i in Bezug auf einen beliebigen Punkt A des unbewegten Systems bedeutet, dann erhalten wir aus (18)

$$\boldsymbol{M}_i + \boldsymbol{M}_i' = \boldsymbol{r}_i \times m_i \frac{d\boldsymbol{v}_i}{dt} + \boldsymbol{r}_i \times \dot{m}_i(\boldsymbol{v}_i - \boldsymbol{u}_i)\,, \tag{19}$$

d.h. wir erhalten die Gleichung (2). ($\boldsymbol{M}_i$ und $\boldsymbol{M}_i'$ sind entsprechend die Momente der Kräfte $\boldsymbol{F}_i$ und $\boldsymbol{F}_i'$).

Wenn wir (19) über sämtliche Punkten des Systems summieren, so ergibt sich wieder die Gleichung (3). (Dabei benutzen wir auf Grund des dritten Gesetzes von Newton die Gleichung $\sum_{i=1}^{n} \boldsymbol{M}_i' = 0$).

Also wir erhalten für einen rotationssymmetrischen Kreisel mit veränderlicher Masse, wobei die Massenzuwächse relativistische Geschwindigkeiten haben, wieder die Gleichung (14) mit der Definition (12).

3. – Bei der relativistischen Geschwindigkeiten ist die Massenabnahme $\mathrm{d}m_i$ des Punktes P_i im Zeitintervall $\mathrm{d}t$ im allgemeinen nicht gleich der Masse $\mathrm{d}m_i'$, welche aus dem Punkte P_i mit der Geschwindigkeit $\boldsymbol{u}_i$ im gleichen Zeitintervall $\mathrm{d}t$ herausgeworfen wird. (Vergl. auch [2]). Z.B. wenn

$$\boldsymbol{F}_i + \boldsymbol{F}_i' = 0\,, \qquad \frac{\mathrm{d}E_i}{\mathrm{d}t} = 0\,,$$

dann

$$\mathrm{d}m_i' = \mathrm{d}m_i\sqrt{1-(q_i^2/c^2)}\,,$$

wobei $\boldsymbol{q}_i$ die relative Geschwindigkeit der Masse $\mathrm{d}m_i'$ in Bezug auf dem Punkt P_i ist. (Dies entspricht der Tatsache, daß ein Teil der Masse des Punktes P_i in kinetische Energie der wegfliegenden Masse umgesetzt wird.)

Deswegen müßen wir bei der Berechnung von $\sum \boldsymbol{r}_i \times \dot{m}_i \boldsymbol{u}_i$ im vorigen Kapitel die Zuwächse der Massen der Punkte P_i nehmen und nicht die Massen die aus dem Kreisel wegfliegen. Hierin besteht der Unterschied zum Fall der nichtrelativistischen Geschwindigkeiten $\boldsymbol{u}_i$, in welchem Fall man $\mathrm{d}m_i$ auf Grund des Gesetzes der Erhaltung der Massen an den Punkten des Kreisels P_i, wie an den aus dem Kreisel wegfliegenden Massen bestimmen kann.

Man kann die Gleichung (14) bei den Atomraketen mit relativistischen Geschwindigkeiten der Massenzuwächse verwenden.

Ein praktisches Interesse hat auch der Fall, wenn die aus dem Kreisel mit relativistischen Geschwindigkeiten wegfliedenden Massen gemessen werden.

Zu diesem Zweck ist es notwendig die relativistische Verallgemeinerung der Gleichung von Meschtcherski zu haben, welche ähnlich der Gleichung (16) ist, in welcher aber der Massenzuchwachs $\mathrm{d}m_i'$ und nicht $\mathrm{d}m_i$ (die Massenabnahme des Punktes P_i) vorkommt.

Wir bestimmen $\mathrm{d}m$ aus Gl. (7) [2] und setzen in die Gleichung (6) [2] ein. Dann erhalten wir in der dreidimensionalen Darstellung die folgende relativistische Verallgemeinerung der Grundgleichung der Mechanik eines Punktes mit veränderlicher Masse:

$$(20)\quad \boldsymbol{F}_i + \boldsymbol{F}_i' = m_i \frac{\mathrm{d}}{\mathrm{d}t}\left(\frac{\boldsymbol{v}_i}{\sqrt{1-(v_i^2/c^2)}}\right) - \frac{\boldsymbol{v}_i}{c^2 - v_i^2}\left((\boldsymbol{F}_i + \boldsymbol{F}_i')\boldsymbol{v}_i - \frac{\mathrm{d}E_i}{\mathrm{d}t}\right) - \\ - \frac{\mathrm{d}m_i'}{\mathrm{d}t}\,\frac{1}{\sqrt{1-(u_i^2/c^2)}}\left[\boldsymbol{u}_i + \left(\frac{\boldsymbol{u}_i\boldsymbol{v}_i}{c^2} - 1\right)\frac{\boldsymbol{v}_i}{1-(v_i^2/c^2)}\right].$$

Wenn $v_i \ll c$, dann erhalten wir aus (20)

$$(21)\qquad \boldsymbol{F}_i + \boldsymbol{F}_i' = m_i \frac{\mathrm{d}}{\mathrm{d}t}\boldsymbol{v}_i + \frac{\mathrm{d}m_i'}{\mathrm{d}t}\,\frac{1}{\sqrt{1-(u_i^2/c^2)}}\,(\boldsymbol{v}_i - \boldsymbol{u}_i)\,.$$

Gleichung (21) kann man auch direkt aus Gleichung (18) erhalten, wenn man die Beziehung

$$\mathrm{d}m_i = \mathrm{d}m_i' \frac{1}{\sqrt{1-(u_i^2/c^2)}}, \tag{22}$$

welche sich bei $v_i \ll c$ aus Gl. (8) ([2]) ergibt, benutzt. Man kann die Gleichung (21) auf Grund der Gl. (22) in die Form

$$\boldsymbol{F}_i + \boldsymbol{F}_i' = \frac{\mathrm{d}}{\mathrm{d}t}(m_i \boldsymbol{v}_i) - \frac{\mathrm{d}m_i'}{\mathrm{d}t} \frac{1}{\sqrt{1-(u_i^2/c^2)}} \boldsymbol{u}_i \cdot \tag{23}$$

bringen. Dann nimmt die Gl. (19) die folgende Gestalt

$$\boldsymbol{M}_i + \boldsymbol{M}_i' = \frac{\mathrm{d}}{\mathrm{d}t}(\boldsymbol{r}_i \times m_i \boldsymbol{v}_i) - \boldsymbol{r}_i \times \dot{m}_i' \frac{1}{\sqrt{1-(u_i^2/c^2)}} \boldsymbol{u}_i, \tag{24}$$

an, und Gl. (3) nimmt die Form an

$$\boldsymbol{M} = \frac{\mathrm{d}}{\mathrm{d}t} \sum_{i=1}^{n} \boldsymbol{r}_i \times m_i \boldsymbol{v}_i - \sum_{i=1}^{n} \boldsymbol{r}_i \times \dot{m}_i' \frac{1}{\sqrt{1-(u_i^2/c^2)}} \boldsymbol{u}_i \cdot \tag{25}$$

Wenn wir ansetzen

$$\boldsymbol{N} = \boldsymbol{M} + \sum_{i=1}^{n} \boldsymbol{r}_i \times \dot{m}_i' \frac{1}{\sqrt{1-(u_i^2/c^2)}} \boldsymbol{u}_i, \tag{26}$$

so erhalten wir in den Grenzen unserer Näherungstheorie des Kreisels wieder die Formel

$$I(\boldsymbol{\omega}_2 \times \boldsymbol{\omega}_1) = \boldsymbol{N} - (\boldsymbol{N}\boldsymbol{e}_1)\boldsymbol{e}_1 . \tag{27}$$

Hierbei wird $\mathrm{d}m_i'$ weit vom Punkte P_i und außerhalb des Kreisels (der Rakete usw.) gemessen.

SUPPLEMENTO AL VOLUME XV, SERIE X
DEL NUOVO CIMENTO

N. 3, 1960
1° Trimestre

Tables of Eigenvalues and Matrix Elements of Transition Probabilities for an Axial Spin Hamiltonian with $S = \frac{3}{2}$ (*).

R. STAHL-BRADA and W. LOW

Department of Physics, The Hebrew University - Jerusalem

(ricevuto il 18 Agosto 1959)

CONTENTS. — 1. Introduction. – 2. Instructions for the use of Tables I-II.

1. – Introduction.

Trivalent chromium in an axial crystalline field is among the ions which can be used for a three-level solid state Bloembergen maser. Examples are chromium in ruby or in ruby spinel. Operation of a maser at a number of frequencies requires a knowledge of the energy level scheme as well as the relative transition probabilities as a function of the orientation of the external magnetic field with respect to the crystal symmetry axis.

The spin Hamiltonian of Cr^{3+} in a tetragonal or trigonal field of six surrounding charges is given by

$$\mathcal{H}_s = g_{\parallel} H_z S_z + g_{\perp} (H_x S_x + H_y S_y) + D(S^2_z - \tfrac{1}{3} S(S+1)) \,, \tag{1}$$

with a spin number $S = \frac{3}{2}$.

If θ is the angle between the magnetic field and the crystalline axis and φ the angle of the projection of the magnetic field in the xy plane and the x axis, the spin Hamiltonian is transformed into

$$\mathcal{H}_s = g_{\parallel} \beta H \cos\theta S_z + \tfrac{1}{2} g_{\perp} \beta H \sin\theta [S_+ e^{-i\varphi} + S_- e^{+i\varphi}] + D[S_z^2 - \tfrac{1}{3} S(S+1)] \,, \tag{2}$$

where $S_{\pm} = S_x \pm i S_y$.

(*) Supported in part by the U. S. Air Force, Office of Scientific Research, through its European Office, under Contract no. AF 61(052)-59.

This can be written as a 4×4 matrix:

(3)

M	$\frac{3}{2}$	$\frac{1}{2}$	$-\frac{1}{2}$	$-\frac{3}{2}$
	$3x \cos\theta + \frac{1}{2} - W$	$3^{\frac{1}{2}} x \sin\theta e^{-i\varphi}$	0	0
	$3^{\frac{1}{2}} x \sin\theta e^{i\varphi}$	$x \cos\theta - \frac{1}{2} - W$	$2x \sin\theta e^{i\varphi}$	—
	—	$2x \sin\theta e^{i\varphi}$	$x \cos\theta - \frac{1}{2} - W$	$3^{\frac{1}{2}} x \sin\theta e^{-i\varphi}$
	—	—	$3^{\frac{1}{2}} x \sin\theta e^{+i\varphi}$	$-3x \cos\theta + \frac{1}{2} - W$

in which $x = g\beta B/4D$ and $W = E/2D$.

Here $2D$ is the zero field splitting between the two Kramers doublets $M = \pm\frac{3}{2}$ and $M = \pm\frac{1}{2}$. The notation of the quantum number is that of the very strong field case.

The eigenvalues of the matrix are only a function of θ and not of φ.

2. – Instructions for the use of Tables I and II.

We have computed the eigenvalues of the matrix (3) for the angle θ from 5° to 85° in steps of 5°. These eigenvalues for a given angle θ and given x are given by the various rows in Tables $I_{5°}$ to $I_{85°}$. The columns give the eigenvalues for a given angle θ and a given M, for different values of $x = g\beta H/4D$. The values x chosen cover the cases from a very weak to a very strong field. The eigenvalues for $\theta = 0°$ and $\theta = 90°$ are trivial since the matrix factors into two submatrices of 2×2.

Tables $II_{5°}$ to $II_{85°}$ give the square of the matrix elements $|\langle M|J_x|M'\rangle|^2$ and $|\langle M|J_z|M'\rangle|^2$ where M and M' refer to the normalized eigenvectors obtained from solving the matrix (3), for various angles θ and parameters x. In general the transition probability from the state M to M' is given by

$$W_{M \to M'} = \left(\frac{g\beta H_{rf}}{2\hbar}\right)^2 g(\nu - \nu_0) |\langle M|J_i|M'\rangle|^2 .$$

For linear polarization in the x or y direction $J_i = J_x$ or J_y and in the z direction $J_i = J_z$. H_{rf} denotes the amplitude ot the rf field and $g(\nu - \nu_0)$ describes the line shape such that

$$\int g(\nu - \nu_0)\, d\nu = 1 .$$

It is obvious that if these matrix elements are known, the intensity of the transitions can be computed for any given polarization.

Tables II can be used as follows. For a given θ and a given x the resulting matrix gives the values of the elements $|\langle M|J_i|M'\rangle|^2$. The rows and columns of each matrix denote the strong field quantum numbers $M = \frac{3}{2}, \frac{1}{2}, -\frac{1}{2}$ and $-\frac{3}{2}$. Only half of the matrix is written since it is symmetrical with respect to the diagonal.

It should be noted for example, that matrix elements connecting $\Delta M = \pm 2$ for small values of x are vanishingly small for small angles of θ, but can become fairly large at $\theta = 90°$.

Diagrams of computed energy levels but not of the intensity matrices have recently been published by SCHULZ-DUBOIS (1) for various angles θ in steps of 10°.

* * *

We are grateful to Prof. G. RACAH for helping us with the programming of these matrices for the Weiszac computer.

TABLES $I_{5°} \to I_{85°}$. – *Tables of the eigenvalues for various angles of θ, the angle between the magnetic field and the crystalline field. The values are given in units of $E/2D$ as a function of the parameter $x = g\beta H/4D$.*

$\theta = 5°$

X	$W\,\frac{3}{2}$	$W-\frac{1}{2}$	$W-\frac{3}{2}$	$W\,\frac{1}{2}$
10	030494442	— 010493962	— 029505866	009505386
5	015494752	— 005493653	— 014506261	004505162
2	006495410	— 002492418	— 005507550	001504558
1	003496182	— 001488740	— 002511249	000503807
0.9	003196319	— 001387390	— 002212600	000403672
0.8	002896476	— 001285188	— 001914805	000303517
0.7	002596660	— 001180988	— 001619008	000203336
0.65	002446764	— 001127095	— 001472903	000153234
0.6	002296878	— 001070284	— 001329716	000103123
0.55	002147002	— 001006425	— 001193578	000053001
0.5	001997138	— 000924592	— 001075414	000002867
0.45	001847289	— 000812731	— 000987278	— 000047280
0.4	001697457	— 000679401	— 000920615	— 000097441
0.35	001547644	— 000537304	— 000862722	— 000147618
0.3	001397854	— 000391706	— 000808349	— 000197800
0.25	001248093	— 000250000	— 000755617	— 000242476
0.2	001098365	— 000298416	— 000703762	— 000096188
0.15	000948680	— 000348703	— 000652424	000052447
0.1	000799046	— 000399059	— 000601415	000201428
0.05	000649480	— 000449485	— 000550629	000350635

(1) E. O. SCHULZ-DU BOIS: *Bell System. Techn. Journ.*, **33**, 271 (1959).

TABLE I (*continued*). $\theta = 10°$

X	$W\,\frac{3}{2}$	$W-\frac{1}{2}$	$W-\frac{3}{2}$	$W\,\frac{1}{2}$
10	030478510	— 010476262	— 029523847	009521599
5	015479432	— 005474981	— 014525087	004520636
2	006481841	— 002470223	— 005529841	001518222
1	003484830	— 001456844	— 002543257	000515271
0.9	003185367	— 001352228	— 002247884	000414745
0.8	002885987	— 001245063	— 001955068	000314139
0.7	002586712	— 001132679	— 001667468	000213435
0.65	002437122	— 001072623	— 001527538	000163039
0.6	002287570	— 001007806	— 001392373	000112608
0.55	002138061	— 000935153	— 001265049	000062141
0.5	001988602	— 000850314	— 001149920	000011633
0.45	001839200	— 000749574	— 001050708	— 000038918
0.4	001689865	— 000633170	— 000967190	— 000089505
0.35	001540608	— 000505080	— 000895435	— 000140093
0.3	001391446	— 000369821	— 000831171	— 000190453
0.25	001242395	— 000250000	— 000771455	— 000220940
0.2	001093482	— 000294179	— 000714545	— 000084757
0.15	000944735	— 000345040	— 000659435	000059739
0.1	000796198	— 000396354	— 000605528	000205685
0.05	000647927	— 000447996	— 000552460	000352529

$\theta = 15°$

X	$W\,\frac{3}{2}$	$W-\frac{1}{2}$	$W-\frac{3}{2}$	$W\,\frac{1}{2}$
10	+ 030452150	— 010447369	— 029552844	+ 009548062
5	+ 015454162	— 005444673	— 014555497	+ 004546007
2	+ 006459428	— 002434818	— 005565430	+ 001540820
1	+ 003466020	— 001408891	— 002591576	+ 000534448
0.9	+ 003167210	— 001300628	— 002299897	+ 000433314
0.8	+ 002868587	— 001188498	— 002012102	+ 000332013
0.7	+ 002570199	— 001069413	— 001731294	+ 000230507
0.65	+ 002421113	— 001005451	— 001595327	+ 000179665
0.6	+ 002272112	— 000936898	— 001463971	+ 000128757
0.55	+ 002123207	— 000861940	— 001339048	+ 000077781
0.5	+ 001974415	— 000778419	— 001222733	+ 000026737
0.45	+ 001825752	— 000684413	— 001116982	— 000024357
0.4	+ 001677240	— 000579174	— 001022622	— 000075444
0.35	+ 001528907	— 000463754	— 000938852	— 000126301
0.3	+ 001380785	— 000341436	— 000863727	— 000175622
0.25	+ 001232917	— 000250000	— 000795071	— 000187846
0.2	+ 001085357	— 000288504	— 000731055	— 000065798
0.15	+ 000938175	— 000339607	— 000670334	+ 000071766
0.1	+ 000791463	— 000392207	— 000611973	+ 000212717
0.05	+ 000645347	— 000445676	— 000555338	+ 000355667

TABLE I (*continued*). $\theta = 20°$

X	$W\,\frac{3}{2}$	$W-\frac{1}{2}$	$W-\frac{3}{2}$	$W\,\frac{1}{2}$
10	+ 030415972	— 010408264	— 029591763	+ 009584055
5	+ 015419503	— 005403942	— 014596265	+ 004580703
2	+ 006428545	— 002388347	— 005612285	+ 001572087
1	+ 003439949	— 001350303	— 002651064	+ 000561417
0.9	+ 003142023	— 001239135	— 002362412	+ 000459524
0.8	+ 002844428	— 001123536	— 002078251	+ 000357358
0.7	+ 002547249	— 001000706	— 001801415	+ 000254872
0.65	+ 002398851	— 000935143	— 001667203	+ 000203494
0.6	+ 002250604	— 000865669	— 001536960	+ 000152025
0.55	+ 002102530	— 000791155	— 001411847	+ 000100472
0.5	+ 001954656	— 000710326	— 001293191	+ 000048861
0.45	+ 001807013	— 000621998	— 001182283	— 000002732
0.4	+ 001659641	— 000525510	— 001080041	— 000054090
0.35	+ 001512587	— 000421446	— 000986680	— 000104461
0.3	+ 001365912	— 000314500	— 000901625	— 000149787
0.25	+ 001219691	— 000250000	— 000823738	— 000145953
0.2	+ 001074020	— 000282620	— 000751681	— 000039718
0.15	+ 000929022	— 000333143	— 000684200	+ 000088320
0.1	+ 000784862	— 000387037	— 000620255	+ 000222431
0.05	+ 000641755	— 000442722	— 000559048	+ 000360015

$\theta = 25°$

X	$W\,\frac{3}{2}$	$W-\frac{1}{2}$	$W-\frac{3}{2}$	$W\,\frac{1}{2}$
10	+ 030371579	— 010360510	— 029639898	+ 009628829
5	+ 015376616	— 005354491	— 014646163	+ 004624038
2	+ 006389880	— 002333430	— 005668114	+ 001611664
1	+ 003406987	— 001286022	— 002717203	+ 000596238
0.9	+ 003110132	— 001173142	— 002430503	+ 000493513
0.8	+ 002813792	— 001055859	— 002148344	+ 000390411
0.7	+ 002518101	— 000931885	— 001873101	+ 000286885
0.65	+ 002370553	— 000866313	— 001739199	+ 000234960
0.6	+ 002223242	— 000797560	— 001608621	+ 000182938
0.55	+ 002076203	— 000724891	— 001482168	+ 000130855
0.5	+ 001929477	— 000647516	— 001360756	+ 000078795
0.45	+ 001783115	— 000564741	— 001245336	+ 000026962
0.4	+ 001637179	— 000476329	— 001136746	— 000024104
0.35	+ 001491745	— 000383545	— 001035530	— 000072670
0.3	+ 001346907	— 000294276	— 000941789	— 000110842
0.25	+ 001202784	— 000250000	— 000855151	— 000097633
0.2	+ 001059526	— 000277314	— 000774888	— 000007324
0.15	+ 000917325	— 000326324	— 000700091	+ 000109090
0.1	+ 000776431	— 000381267	— 000629851	+ 000234686
0.05	+ 000637174	— 000439338	— 000563364	+ 000365528

TABLE I (*continued*). $\theta = 30°$

X	$W\,\frac{3}{2}$	$W-\frac{1}{2}$	$W-\frac{3}{2}$	$W\,\frac{1}{2}$
10	+ 030319724	— 010305575	— 029695171	+ 009681021
5	+ 015326347	— 005298117	— 014703138	+ 004674908
2	+ 006344079	— 002272763	— 005730251	+ 001658935
1	+ 003367496	— 001219979	— 002786339	+ 000638822
0.9	+ 003071860	— 001106599	— 002500543	+ 000535283
0.8	+ 002776957	— 000989216	— 002219022	+ 000431281
0.7	+ 002482984	— 000866068	— 001943707	+ 000326791
0.65	+ 002336427	— 000801558	— 001809252	+ 000274382
0.6	+ 002190211	— 000734558	— 001677561	+ 000221908
0.55	+ 002044388	— 000664611	— 001549227	+ 000169451
0.5	+ 001899018	— 000591279	— 001424930	+ 000117192
0.45	+ 001754176	— 000514303	— 001305410	+ 000065537
0.4	+ 001609953	— 000434047	— 001191401	+ 000015495
0.35	+ 001466461	— 000352935	— 001093535	— 000029991
0.3	+ 001323836	— 000281161	— 000982224	— 000060451
0.25	+ 001182251	— 000250000	— 000887578	— 000044674
0.2	+ 001041922	— 000272897	— 000799380	+ 000030354
0.15	+ 000903123	— 000319668	— 000717152	+ 000133697
0.1	+ 000766207	— 000375266	— 000640265	+ 000249324
0.05	+ 000631630	— 000435713	— 000568067	+ 000372150

$\theta = 35°$

X	$W\,\frac{3}{2}$	$W-\frac{1}{2}$	$W-\frac{3}{2}$	$W\,\frac{1}{2}$
10	030261837	— 010245270	— 029755760	009739193
5	015269982	— 005236845	— 014765198	004732060
2	006292060	— 002208990	— 005796176	001713106
1	003321999	— 001155142	— 002855764	000688907
0.9	003027669	— 001042317	— 002570015	000584663
0.8	002734324	— 000926096	— 002288126	000479897
0.7	002442237	— 000805209	— 002011660	000374632
0.65	002296775	— 000742496	— 001876147	000321867
0.6	002151779	— 000677947	— 001742934	000269103
0.55	002007319	— 000611330	— 001612477	000216488
0.5	001863481	— 000542504	— 001485304	000164326
0.45	001720368	— 000471624	— 001362011	000113267
0.4	001578108	— 000399678	— 001243236	000064806
0.35	001436853	— 000330047	— 001129602	000022796
0.3	001296796	— 000273006	— 001021657	— 000002133
0.25	001158172	— 000250000	— 000919784	000011612
0.2	001021275	— 000269371	— 000824146	000072243
0.15	000886474	— 000313501	— 000734666	000161693
0.1	000754236	— 000369324	— 000651067	000266155
0.05	000625154	— 000432007	— 000572965	000379818

TABLE I (*continued*). $\theta = 40°$

X	$W\,\frac{3}{2}$	$W-\frac{1}{2}$	$W-\frac{3}{2}$	$W\,\frac{1}{2}$
10	030199769	— 010181626	— 029819901	009801757
5	015209142	— 005172821	— 014830351	004794030
2	006235002	— 002144566	— 005863558	001773122
1	003271198	— 001093688	— 002923457	000745947
0.9	002978187	— 000982252	— 002637120	000641185
0.8	002686440	— 000868137	— 002354180	000535876
0.7	002396317	— 000750517	— 002075900	000430100
0.65	002252013	— 000690096	— 001939055	000377138
0.6	002108317	— 000628454	— 001804125	000324263
0.55	001965324	— 000565550	— 001671470	000271696
0.5	001823149	— 000501500	— 001541514	000219865
0.45	001681931	— 000436812	— 001414748	000169629
0.4	001541841	— 000372941	— 001291720	000122820
0.35	001403086	— 000313654	— 001173019	000083587
0.3	001265919	— 000267831	— 001059230	000061143
0.25	001130652	— 000250000	— 000950887	000070234
0.2	000997672	— 000266612	— 000848407	000117347
0.15	000867451	— 000307995	— 000752046	000192589
0.1	000740579	— 000363650	— 000661889	000284960
0.05	000617786	— 000428349	— 000577892	000388455

$\theta = 45°$

X	$W\,\frac{3}{2}$	$W-\frac{1}{2}$	$W-\frac{3}{2}$	$W\,\frac{1}{2}$
10	030135555	— 010116723	— 029885804	009866972
5	015145637	— 005108162	— 014896628	004859153
2	006174296	— 002081624	— 005930319	001837647
1	003215963	— 001037106	— 002987910	000809052
0.9	002924196	— 000927665	— 002700557	000704025
0.8	002633990	— 000816303	— 002416137	000598450
0.7	002345806	— 000702593	— 002135679	000492466
0.65	002202664	— 000644750	— 001997377	000439462
0.6	002060291	— 000586252	— 001860669	000386631
0.55	001918809	— 000527213	— 001725847	000334250
0.5	001778371	— 000467950	— 001593257	000282835
0.45	001639160	— 000409218	— 001463308	000233367
0.4	001501397	— 000352706	— 001336477	000187786
0.35	001365353	— 000302056	— 001213298	000150001
0.3	001231359	— 000264419	— 001094357	000127416
0.25	001099817	— 000250000	— 000980255	000130438
0.2	000971213	— 000264469	— 000871572	000164828
0.15	000846139	— 000303206	— 000768824	000225891
0.1	000725305	— 000358387	— 000672426	000305508
0.05	000609571	— 000424839	— 000582708	000397976

TABLE I (*continued*). $\theta = 50°$

X	$W\,\frac{3}{2}$	$W-\frac{1}{2}$	$W-\frac{3}{2}$	$W\,\frac{1}{2}$
10	030070471	— 010052336	— 029950819	009932684
5	015080996	— 005044737	— 014961697	004925438
2	006111384	— 002021886	— 005994474	001904976
1	003157296	— 000986301	— 003047895	000876899
0.9	002866605	— 000879242	— 002759275	000771912
0.8	002577774	— 000771012	— 002473154	000666392
0.7	002291381	— 000661523	— 002190374	000560516
0.65	002149343	— 000606359	— 002050597	000507613
0.6	002008246	— 000551038	— 001912147	000454938
0.55	001868253	— 000495788	— 001775262	000402798
0.5	001729555	— 000441063	— 001640232	000351740
0.45	001592390	— 000387752	— 001507401	000302763
0.4	001457045	— 000337577	— 001377182	000257714
0.35	001323868	— 000293798	— 001250060	000219990
0.3	001193280	— 000262078	— 001126593	000195392
0.25	001065788	— 000250000	— 001007408	000191620
0.2	000941997	— 000262808	— 000893182	000213993
0.15	000822619	— 000299129	— 000784619	000261129
0.1	000708483	— 000353626	— 000682422	000327564
0.05	000600558	— 000421559	— 000587293	000408294

$\theta = 55°$

X	$W\,\frac{3}{2}$	$W-\frac{1}{2}$	$W-\frac{3}{2}$	$W\,\frac{1}{2}$
10	030007143	— 009990591	— 030013647	009997094
5	015017503	— 004984478	— 015023988	004990963
2	006048191	— 001966819	— 006054553	001973182
1	003096590	— 000941792	— 003102565	000947767
0.9	002806693	— 000837293	— 002812561	000843162
0.8	002518939	— 000732322	— 002524666	000738050
0.7	002234032	— 000627075	— 002239571	000632614
0.65	002092948	— 000574524	— 002098369	000579945
0.6	001952991	— 000522232	— 001958273	000527514
0.55	001814361	— 000470503	— 001819480	000475622
0.5	001677307	— 000419868	— 001682232	000424793
0.45	001542129	— 000371257	— 001546825	000375953
0.4	001409194	— 000326308	— 001413617	000330730
0.35	001278947	— 000287851	— 001283044	000291948
0.3	001151920	— 000260427	— 001155633	000264139
0.25	001028747	— 000250000	— 001032007	000253260
0.2	000910162	— 000261520	— 000912897	000264254
0.15	000797003	— 000295716	— 000799138	000297851
0.1	000690203	— 000349414	— 000691671	000350882
0.05	000590802	— 000418564	— 000591551	000419313

TABLE I (*continued*).

$\theta = 60°$

X	$W\,\frac{3}{2}$	$W-\frac{1}{2}$	$W-\frac{3}{2}$	$W\,\frac{1}{2}$
10	029947334	— 009933202	— 030072233	010058100
5	014957073	— 004928983	— 015081660	005053571
2	005986688	— 001917513	— 006109158	002039983
1	003035492	— 000903743	— 003151182	001019433
0.9	002746006	— 000801798	— 002859791	000915584
0.8	002458896	— 000700002	— 002570167	000811274
0.7	002175001	— 000598773	— 002282883	000706655
0.65	002034624	— 000548638	— 002140363	000654377
0.6	001895556	— 000499092	— 001998765	000602301
0.55	001758048	— 000450484	— 001858256	000550691
0.5	001622412	— 000403375	— 001719041	000500004
0.45	001489029	— 000358684	— 001581374	000451029
0.4	001358365	— 000317917	— 001445570	000405122
0.35	001230987	— 000283521	— 001312023	000364556
0.3	001107569	— 000259237	— 001181222	000332890
0.25	000988896	— 000250000	— 001053776	000314879
0.2	000875855	— 000260524	— 000930439	000315108
0.15	000769406	— 000292908	— 000812138	000335640
0.1	000670557	— 000345777	— 000700001	000375220
0.05	000580365	— 000415902	— 000595397	000430933

$\theta = 65°$

X	$W\,\frac{3}{2}$	$W-\frac{1}{2}$	$W-\frac{3}{2}$	$W\,\frac{1}{2}$
10	029892781	— 009881730	— 030124707	010113655
5	014901635	— 004879651	— 015133070	005111086
2	005929040	— 001874785	— 006157116	002102860
1	002976071	— 000872104	— 003193152	001089185
0.9	002686529	— 000772549	— 002900460	000986480
0.8	002399514	— 000673670	— 002609247	000883403
0.7	002115985	— 000576048	— 002319988	000780051
0.65	001975957	— 000528039	— 002176298	000728380
0.6	001837401	— 000480868	— 002033381	000676848
0.55	001700624	— 000434907	— 001891379	000625661
0.5	001566014	— 000390721	— 001750468	000575175
0.45	001434050	— 000349190	— 001610870	000526009
0.4	001305328	— 000311688	— 001472864	000479224
0.35	001180571	— 000280352	— 001336808	000436589
0.3	001060640	— 000258371	— 001203156	000400887
0.25	000946517	— 000250000	— 001072497	000375980
0.2	000839265	— 000259760	— 000945591	000366086
0.15	000739966	— 000290645	— 000823423	000374102
0.1	000649653	— 000342721	— 000707266	000400334
0.05	000569314	— 000413606	— 000598761	000443052

TABLE I (*continued*). $\theta = 70°$

X	$W\,\frac{3}{2}$	$W-\frac{1}{2}$	$W-\frac{3}{2}$	$W\,\frac{1}{2}$
10	029845278	— 009837585	— 030169626	010161932
5	014853116	— 004837673	— 015176910	005161467
2	005877538	— 001839220	— 006197520	002159202
1	002920850	— 000846686	— 003228038	001153875
0.9	002630765	— 000749233	— 002934200	001052669
0.8	002343229	— 000652880	— 002641604	000951255
0.7	002059293	— 000558325	— 002350653	000849684
0.65	001919157	— 000512092	— 002205970	000798904
0.6	001780606	— 000466879	— 002061941	000748215
0.55	001644006	— 000423065	— 001918691	000697750
0.5	001509827	— 000381206	— 001776372	000647751
0.45	001378667	— 000342135	— 001635181	000598650
0.4	001251283	— 000307114	— 001495370	000551201
0.35	001128612	— 000278049	— 001357264	000506701
0.3	001011770	— 000257742	— 001221289	000467262
0.25	000902013	— 000250000	— 001088012	000435998
0.2	000800639	— 000259184	— 000958189	000416735
0.15	000708842	— 000288872	— 000832843	000412873
0.1	000627605	— 000340241	— 000713356	000425992
0.05	000557720	— 000411700	— 000601587	000455567

$\theta = 75°$

X	$W\,\frac{3}{2}$	$W-\frac{1}{2}$	$W-\frac{3}{2}$	$W\,\frac{1}{2}$
10	029806880	— 009802109	— 030206224	010201453
5	014813503	— 004804095	— 015212322	005202914
2	005834554	— 001811256	— 006229738	002206440
1	002872843	— 000827268	— 003255541	001209966
0.9	002581807	— 000731532	— 002960759	001110483
0.8	002293196	— 000637219	— 002667034	001011057
0.7	002008083	— 000545103	— 002374717	000911737
0.65	001867346	— 000500265	— 002229239	000862157
0.6	001728219	— 000456572	— 002084325	000812679
0.55	001591114	— 000414405	— 001940086	000763376
0.5	001456576	— 000374304	— 001796657	000714385
0.45	001325328	— 000337062	— 001654217	000665952
0.4	001198315	— 000303853	— 001512996	000618534
0.35	001076750	— 000276418	— 001373294	000572961
0.3	000962122	— 000257298	— 001235515	000530691
0.25	000856111	— 000250000	— 001100206	000494095
0.2	000760376	— 000258764	— 000968116	000466504
0.15	000676252	— 000287539	— 000840289	000451576
0.1	000604548	— 000338327	— 000718183	000451962
0.05	000545662	— 000410202	— 000603833	000468372

TABLE I (*continued*). $\theta = 80°$

X	$W\,\frac{3}{2}$	$W-\frac{1}{2}$	$W-\frac{3}{2}$	$W\,\frac{1}{2}$
10	029778272	— 009776029	— 030232891	010230647
5	014783967	— 004779557	— 015238136	005233726
2	005802057	— 001791115	— 006253094	002242153
1	002835225	— 000813591	— 003275344	001253710
0.9	002543073	— 000719124	— 002979863	001155913
0.8	002253104	— 000626306	— 002685308	001058510
0.7	001966330	— 000535957	— 002391993	000961620
0.65	001824634	— 000492118	— 002245937	000913421
0.6	001684459	— 000449507	— 002100382	000865431
0.55	001546230	— 000408499	— 001955429	000817698
0.5	001410529	— 000369624	— 001811202	000770297
0.45	001278156	— 000333643	— 001667866	000723354
0.4	001150219	— 000301667	— 001525636	000677084
0.35	001028229	— 000275328	— 001384795	000631895
0.3	000914166	— 000257002	— 001245731	000588567
0.25	000810399	— 000250000	— 001108974	000548575
0.2	000719300	— 000258478	— 000975267	000514444
0.15	000642551	— 000286614	— 000845664	000489728
0.1	000580644	— 000336969	— 000721677	000478002
0.05	000533221	— 000409124	— 000605460	000481363

$\theta = 85°$

X	$W\,\frac{3}{2}$	$W-\frac{1}{2}$	$W-\frac{3}{2}$	$W\,\frac{1}{2}$
10	029760531	— 009760052	— 030249009	010248530
5	014765686	— 004764599	— 015253785	005252697
2	005781771	— 001778964	— 006267226	002264418
1	002811089	— 000805464	— 003287278	001281653
0.9	002518020	— 000711775	— 002991369	001185124
0.8	002226885	— 000619867	— 002696309	001089291
0.7	001938590	— 000530587	— 002402387	000994383
0.65	001795953	— 000487348	— 002255980	000947375
0.6	001654685	— 000445383	— 002110038	000900736
0.55	001515181	— 000405064	— 001964654	000854536
0.5	001377993	— 000366911	— 001819946	000808865
0.45	001243902	— 000331669	— 001676072	000763839
0.4	001114033	— 000300409	— 001533236	000719612
0.35	000990015	— 000274703	— 001391714	000676401
0.3	000874174	— 000256831	— 001251880	000634537
0.25	000769664	— 000250000	— 001114256	000594592
0.2	000680195	— 000258312	— 000979579	000557696
0.15	000608830	— 000286070	— 000848911	000526151
0.1	000556189	— 000336160	— 000723790	000503761
0.05	000520489	— 000408475	— 000606445	000494431

TABLES $II_5 \rightarrow II_{85°}$ – *Tables of the square of the matrix elements* $|\langle M|J_x|M'\rangle|^2$ *and* $|\langle M|J_z|M'\rangle|^2$ *for various angles of* θ *and as a function of the parameter* $x = g\beta H/4D$.

$\theta = 5°$

	$\lvert\langle M\lvert J_z\rvert M'\rangle\rvert^2$				$\lvert\langle M\lvert J_x\rvert M'\rangle\rvert^2$			
X	M $\frac{3}{2}$	$\frac{1}{2}$	$-\frac{1}{2}$	$-\frac{3}{2}$	$\frac{3}{2}$	$\frac{1}{2}$	$-\frac{1}{2}$	$-\frac{3}{2}$
	0234				0015			
10	0005	0247			0744	0002		
	0000	0007	0248		0000	0992	0001	
	0000	0000	0006	2231	0000	0000	0743	0018
	2235				0014			
5	0004	0247			0745	0003		
	0000	0007	0249		0000	0992	0000	
	0000	0000	0007	2228	0000	0000	0742	0021
	2239				0010			
2	0003	0246			0746	0004		
	0000	0007	0252		0000	0991	0000	
	0000	0000	0010	2219	0000	0000	0737	0030
	2242				0007			
1	0002	0244			0747	0007		
	0000	0007	0264		0000	0987	0006	
	0000	0000	0021	2183	0000	0005	0715	0066
	2242				0007			
0.9	0002	0244			0747	0008		
	0000	0007	0270		0000	0984	0012	
	0000	0000	0027	2167	0000	0008	0704	0082
	2243				0006			
0.8	0002	0244			0747	0008		
	0000	0007	0281		0000	0978	0025	
	0000	0000	0036	2137	0000	0014	0682	0112
	2244				0005			
0.7	0001	0244			0747	0009		
	0000	0007	0307		0000	0962	0062	
	0000	0000	0058	2068	0000	0030	0629	0179
	2244				0005			
0.65	0001	0244			0747	0010		
	0000	0007	0336		0001	0943	0106	
	0000	0000	0080	1993	0000	0049	0571	0250
	2244				0005			
0.6	0001	0244			0747	0010		
	0000	0007	0401		0001	0901	0199	
	0000	0000	0122	1845	0000	0092	0456	0386
	2245				0004			
0.55	0001	0243			0747	0011		
	0000	0006	0577		0001	0792	0396	
	0000	0001	0198	1518	0000	0201	0227	0646

TABLE II (*continued*). $\theta = 5°$

	$\lvert\langle M\lvert J_z\rvert M'\rangle\rvert^2$				$\lvert\langle M\lvert J_x\rvert M'\rangle\rvert^2$			
X	M $\frac{3}{2}$	$\frac{1}{2}$	$-\frac{1}{2}$	$-\frac{3}{2}$	$\frac{3}{2}$	$\frac{1}{2}$	$-\frac{1}{2}$	$-\frac{3}{2}$
	2245				0004			
0.5	0001	0243			0747	0011		
	0000	0004	1068		0000	0534	0597	
	0000	0003	0252	0919	0000	0460	0000	0898
	2246				0003			
0.45	0001	0243			0747	0012		
	0000	0002	1725		0000	0244	0397	
	0000	0005	0152	0460	0001	0751	0223	0648
	2246				0003			
0.4	0001	0243			0747	0013		
	0000	0001	2051		0000	0108	0170	
	0000	0006	0063	0313	0001	0889	0485	0346
	2247				0002			
0.35	0000	0243			0747	0014		
	0000	0001	2167		0000	0056	0072	
	0000	0006	0026	0270	0001	0945	0604	0198
	2247				0002			
0.3	0000	0242			0746	0016		
	0000	0002	2210		0000	0033	0031	
	0000	0006	0012	0254	0002	0981	0646	0126
	2248				0001			
0.25	0000	1003			0184	0064		
	0000	0736	0000		0562	0005	0000	
	0000	0000	0012	0248	0002	1484	0182	0088
	2248				0001			
0.2	0000	2241			0000	0007		
	0000	0000	0242		0746	0015	0017	
	0000	0002	0007	0245	0002	0744	0944	0066
	2249				0000			
0.15	0000	2246			0000	0003		
	0000	0000	0242		0746	0011	0019	
	0000	0001	0007	0243	0003	0740	0960	0051
	2249				0000			
0.1	0000	2248			0000	0001		
	0000	0000	0242		0746	0008	0022	
	0000	0000	0007	0242	0003	0741	0966	0041
	2249				0000			
0.05	0000	2249			0000	0000		
	0000	0000	0242		0745	0006	0025	
	0000	0000	0007	0242	0004	0743	0969	0034

TABLE II (*continued*). $\theta = 10°$

	$\lvert\langle M\lvert J_z\rvert M'\rangle\rvert^2$				$\lvert\langle M\lvert J_x\rvert M'\rangle\rvert^2$			
X	M $\frac{3}{2}$	$\frac{1}{2}$	$-\frac{1}{2}$	$-\frac{3}{2}$	$\frac{3}{2}$	$\frac{1}{2}$	$-\frac{1}{2}$	$-\frac{3}{2}$
	2188				0061			
10	0020	0240			0729	0009		
	0000	0030	0244		0000	0969	0005	
	0000	0000	0024	2175	0000	0000	0724	0074
	2193				0056			
5	0018	0238			0731	0012		
	0000	0030	0247		0000	0969	0003	
	0000	0000	0027	2166	0000	0000	0720	0083
	2206				0043			
2	0014	0234			0736	0019		
	0000	0030	0259		0000	0967	0000	
	0000	0000	0038	2132	0000	0002	0703	0117
	2219				0030			
1	0010	0230			0739	0030		
	0000	0030	0304		0002	0951	0019	
	0000	0000	0077	2009	0000	0018	0628	0238
	2221				0028			
0.9	0009	0229			0739	0032		
	0000	0030	0324		0002	0942	0035	
	0000	0000	0092	1960	0000	0027	0595	0287
	2223				0026			
0.8	0008	0228			0739	0035		
	0000	0030	0359		0003	0925	0066	
	0000	0000	0116	1876	0000	0044	0538	0367
	2226				0023			
0.7	0007	0227			0740	0038		
	0000	0029	0431		0003	0889	0133	
	0000	0001	0157	1721	0000	0082	0431	0510
	2228				0021			
0.65	0007	0226			0740	0040		
	0000	0029	0500		0004	0853	0193	
	0000	0002	0188	1591	0000	0118	0342	0623
	2229				0020			
0.6	0006	0226			0740	0043		
	0000	0027	0615		0004	0794	0279	
	0000	0003	0224	1402	0000	0178	0223	0773
	2231				0018			
0.55	0006	0225			0740	0045		
	0000	0026	0811		0004	0699	0381	
	0000	0005	0257	1140	0001	0275	0086	0939

TABLE II (*continued*). $\theta = 10°$

	$\lvert\langle M \lvert J_z \rvert M' \rangle\rvert^2$				$\lvert\langle M \lvert J_x \rvert M' \rangle\rvert^2$			
X	M $\frac{3}{2}$	$\frac{1}{2}$	$-\frac{1}{2}$	$-\frac{3}{2}$	$\frac{3}{2}$	$\frac{1}{2}$	$-\frac{1}{2}$	$-\frac{3}{2}$
	2232				0017			
0.5	0005	0224			0740	0048		
	0000	0022	1115		0004	0558	0444	
	0000	0009	0259	0832	0002	0418	0001	1039
	2234				0015			
0.45	0005	0223			0739	0052		
	0000	0019	1484		0003	0396	0397	
	0000	0013	0209	0561	0003	0583	0054	0969
	2236				0013			
0.4	0004	0222			0739	0057		
	0000	0017	1798		0003	0259	0271	
	0000	0017	0136	0391	0004	0727	0208	0770
	2238				0011			
0.35	0003	0219			0737	0065		
	0000	0018	1995		0003	0167	0151	
	0000	0020	0078	0304	0005	0834	0352	0566
	2240				0009			
0.3	0003	0208			0733	0081		
	0000	0038	2076		0007	0109	0067	
	0000	0020	0044	0262	0007	0939	0416	0413
	2242				0007			
0.25	0000	1011			0178	0220		
	0001	0703	0000		0561	0020	0000	
	0000	0001	0044	0241	0008	1293	0168	0309
	2244				0005			
0.2	0000	2213			0001	0032		
	0001	0006	0221		0737	0056	0054	
	0000	0007	0028	0231	0010	0725	0802	0239
	2246				0003			
0.15	0000	2237			0000	0012		
	0001	0000	0223		0737	0042	0069	
	0000	0003	0027	0226	0012	0712	0856	0190
	2248				0001			
0.1	0000	2245			0000	0004		
	0000	0000	0223		0735	0033	0081	
	0000	0001	0027	0223	0014	0717	0877	0155
	2249				0000			
0.05	0000	2249			0000	0000		
	0000	0000	0222		0732	0026	0095	
	0000	0000	0027	0222	0017	0723	0886	0130

TABLE II (*continued*). $\theta = 15°$

	$\lvert\langle M\rvert J_z\rvert M'\rangle\rvert^2$				$\lvert\langle M\rvert J_x\rvert M'\rangle\rvert^2$			
X	M $\frac{3}{2}$	$\frac{1}{2}$	$-\frac{1}{2}$	$-\frac{3}{2}$	$\frac{3}{2}$	$\frac{1}{2}$	$-\frac{1}{2}$	$-\frac{3}{2}$
	2112				0137			
10	0045	0228			0705	0021		
	0000	0066	0238		0000	0932	0012	
	0000	0000	0055	2084	0000	0000	0693	0165
	2124				0125			
5	0042	0225			0709	0026		
	0000	0067	0244		0000	0932	0008	
	0000	0000	0060	2066	0000	0000	0685	0182
	2151				0098			
2	0032	0216			0718	0041		
	0000	0067	0268		0001	0927	0000	
	0000	0000	0082	1997	0000	0004	0650	0252
	2181				0068			
1	0023	0206			0725	0066		
	0000	0067	0356		0005	0898	0026	
	0000	0000	0146	1779	0000	0033	0522	0465
	2185				0064			
0.9	0021	0204			0726	0072		
	0000	0067	0391		0006	0884	0044	
	0000	0001	0167	1703	0000	0048	0475	0537
	2191				0058			
0.8	0019	0202			0727	0078		
	0000	0067	0448		0007	0860	0078	
	0000	0002	0195	1588	0000	0072	0402	0643
	2197				0052			
0.7	0017	0199			0727	0086		
	0000	0066	0551		0008	0815	0136	
	0000	0003	0233	1408	0000	0118	0290	0800
	2200				0049			
0.65	0016	0198			0727	0091		
	0000	0066	0634		0009	0779	0179	
	0000	0005	0254	1281	0001	0155	0216	0900
	2203				0046			
0.6	0015	0196			0727	0097		
	0000	0065	0752		0009	0728	0228	
	0000	0007	0272	1125	0001	0208	0132	1011
	2207				0042			
0.55	0014	0194			0727	0104		
	0000	0063	0916		0010	0657	0275	
	0000	0011	0281	0940	0002	0280	0053	1112

TABLE II (*continued*). $\theta = 15°$

	$\lvert\langle M\rvert J_z\rvert M'\rangle\rvert^2$				$\lvert\langle M\rvert J_x\rvert M'\rangle\rvert^2$			
X	M $\frac{3}{2}$	$\frac{1}{2}$	$-\frac{1}{2}$	$-\frac{3}{2}$	$\frac{3}{2}$	$\frac{1}{2}$	$-\frac{1}{2}$	$-\frac{3}{2}$
	2211				0038			
0.5	0012	0192			0726	0113		
	0000	0061	1130		0010	0566	0300	
	0000	0015	0271	0743	0003	0375	0004	1170
	2215				0034			
0.45	0011	0188			0725	0124		
	0000	0060	1378		0011	0460	0283	
	0000	0020	0235	0560	0005	0487	0013	1148
	2219				0030			
0.4	0010	0183			0723	0139		
	0000	0062	1617		0012	0353	0221	
	0000	0026	0181	0417	0007	0605	0081	1039
	2223				0026			
0.35	0008	0171			0717	0165		
	0000	0080	1790		0016	0257	0136	
	0000	0029	0127	0321	0010	0724	0168	0879
	2228				0021			
0.3	0006	0124			0693	0235		
	0000	0179	1774		0038	0167	0045	
	0000	0027	0089	0264	0013	0884	0192	0716
	2232				0017			
0.25	0001	1027			0170	0394		
	0004	0659	0000		0559	0040	0000	
	0000	0002	0086	0230	0016	1067	0150	0576
	2237				0012			
0.2	0000	2158			0004	0076		
	0004	0024	0188		0723	0111	0085	
	0000	0013	0059	0212	0020	0690	0629	0465
	2241				0008			
0.15	0000	2221			0000	0028		
	0002	0003	0196		0723	0087	0128	
	0000	0007	0056	0202	0024	0672	0718	0380
	2245				0004			
0.1	0000	2240			0000	0009		
	0001	0000	0195		0719	0068	0159	
	0000	0002	0055	0197	0029	0682	0754	0314
	2248				0001			
0.05	0000	2248			0000	0001		
	0000	0000	0194		0713	0054	0189	
	0000	0000	0055	0194	0036	0695	0771	0263

TABLE II (*continued*). $\theta = 20°$

	$\lvert\langle M\rvert J_z\rvert M'\rangle\rvert^2$				$\lvert\langle M\rvert J_x\rvert M'\rangle\rvert^2$			
X	M $\frac{3}{2}$	$\frac{1}{2}$	$-\frac{1}{2}$	$-\frac{3}{2}$	$\frac{3}{2}$	$\frac{1}{2}$	$-\frac{1}{2}$	$-\frac{3}{2}$
	2008				0241			
10	0080	0213			0671	0037		
	0000	0117	0229		0000	0882	0021	
	0000	0000	0095	1962	0000	0000	0651	0287
	2028				0221			
5	0074	0207			0678	0045		
	0000	0117	0238		0000	0881	0014	
	0000	0000	0104	1934	0000	0000	0639	0315
	2075				0174			
2	0058	0191			0694	0071		
	0000	0117	0277		0003	0873	0001	
	0000	0000	0137	1827	0000	0007	0586	0422
	2127				0122			
1	0041	0174			0706	0115		
	0000	0119	0405		0009	0832	0021	
	0000	0002	0215	1536	0000	0046	0422	0702
	2135				0114			
0.9	0038	0171			0708	0125		
	0000	0120	0451		0011	0815	0037	
	0000	0002	0235	1448	0000	0062	0371	0783
	2144				0104			
0.8	0035	0167			0709	0137		
	0000	0120	0520		0013	0788	0061	
	0000	0004	0259	1327	0000	0089	0300	0890
	2155				0094			
0.7	0031	0162			0709	0153		
	0000	0120	0632		0015	0745	0099	
	0000	0007	0285	1159	0001	0133	0206	1028
	2161				0088			
0.65	0029	0160			0709	0163		
	0000	0121	0712		0017	0712	0122	
	0000	0009	0296	1052	0002	0166	0150	1107
	2167				0082			
0.6	0027	0156			0709	0175		
	0000	0121	0816		0018	0671	0146	
	0000	0011	0303	0930	0002	0209	0093	1186
	2173				0076			
0.55	0025	0152			0708	0189		
	0000	0122	0946		0020	0617	0166	
	0000	0015	0301	0795	0004	0264	0042	1253

TABLE II (*continued*). $\theta = 20°$

	$\lvert\langle M\rvert J_x\rvert M'\rangle\rvert^2$				$\lvert\langle M\rvert J_x\rvert M'\rangle\rvert^2$			
X	M $\frac{3}{2}$	$\frac{1}{2}$	$-\frac{1}{2}$	$-\frac{3}{2}$	$\frac{3}{2}$	$\frac{1}{2}$	$-\frac{1}{2}$	$-\frac{3}{2}$
	2180				0069			
0.5	0022	0147			0706	0207		
	0000	0125	1103		0022	0550	0175	
	0000	0019	0287	0655	0005	0334	0007	1293
	2187				0062			
0.45	0020	0139			0703	0231		
	0000	0132	1276		0025	0472	0163	
	0000	0024	0259	0521	0008	0417	0001	1287
	2195				0054			
0.4	0017	0126			0696	0267		
	0000	0151	1438		0030	0384	0126	
	0000	0029	0217	0406	0011	0513	0026	1224
	2203				0046			
0.35	0014	0098			0680	0332		
	0000	0207	1523		0045	0287	0068	
	0000	0031	0174	0318	0015	0628	0063	1111
	2211				0038			
0.3	0011	0019			0612	0502		
	0001	0448	1259		0110	0147	0006	
	0000	0021	0144	0255	0019	0799	0050	0971
	2219				0030			
0.25	0002	1051			0162	0540		
	0007	0612	0000		0556	0062	0000	
	0000	0003	0130	0215	0025	0862	0130	0827
	2227				0022			
0.2	0000	2079			0010	0137		
	0007	0056	0149		0704	0164	0098	
	0000	0016	0095	0190	0031	0642	0468	0696
	2235				0014			
0.15	0000	2198			0001	0048		
	0004	0008	0165		0708	0138	0178	
	0000	0010	0088	0176	0038	0625	0575	0583
	2242				0007			
0.1	0000	2233			0000	0016		
	0002	0001	0165		0701	0110	0236	
	0000	0004	0086	0168	0047	0641	0623	0489
	2247				0002			
0.05	0000	2246			0000	0003		
	0000	0000	0164		0691	0088	0289	
	0000	0000	0086	0164	0058	0661	0646	0411

TABLE II (*continued*). $\theta = 25°$

	$\lvert\langle M \lvert J_z \rvert M' \rangle\rvert^2$				$\lvert\langle M \lvert J_x \rvert M' \rangle\rvert^2$			
X	M $\frac{3}{2}$	$\frac{1}{2}$	$-\frac{1}{2}$	$-\frac{3}{2}$	$\frac{3}{2}$	$\frac{1}{2}$	$-\frac{1}{2}$	$-\frac{3}{2}$
	1879				0370			
10	0123	0195			0628	0056		
	0000	0178	0217		0000	0820	0034	
	0000	0000	0144	1813	0000	0000	0601	0436
	1907				0342			
5	0114	0185			0639	0068		
	0000	0178	0230		0000	0819	0024	
	0000	0000	0156	1774	0000	0001	0583	0474
	1977				0272			
2	0091	0163			0663	0106		
	0000	0180	0283		0005	0807	0004	
	0000	0000	0197	1634	0000	0009	0515	0614
	2056				0192			
1	0065	0137			0682	0174		
	0000	0185	0439		0015	0756	0011	
	0000	0003	0276	1304	0000	0054	0337	0928
	2069				0179			
0.9	0060	0132			0683	0190		
	0000	0186	0489		0017	0738	0020	
	0000	0004	0292	1216	0000	0071	0289	1005
	2084				0164			
0.8	0055	0126			0685	0209		
	0000	0188	0561		0021	0711	0034	
	0000	0006	0309	1104	0001	0096	0229	1101
	2101				0148			
0.7	0049	0119			0685	0235		
	0000	0192	0666		0025	0669	0053	
	0000	0009	0324	0958	0002	0135	0154	1214
	2110				0139			
0.65	0046	0115			0685	0252		
	0000	0195	0735		0027	0641	0063	
	0000	0011	0328	0872	0003	0163	0114	1274
	2119				0129			
0.6	0043	0109			0684	0272		
	0000	0199	0819		0030	0605	0073	
	0000	0014	0329	0777	0004	0197	0074	1330
	2129				0119			
0.55	0039	0102			0682	0297		
	0000	0205	0918		0034	0560	0080	
	0000	0017	0322	0675	0005	0240	0038	1378

TABLE II (*continued*). $\theta = 25°$

	$\lvert\langle M \lvert J_z \rvert M' \rangle\rvert^2$				$\lvert\langle M \lvert J_x \rvert M' \rangle\rvert^2$			
X	M $\frac{3}{2}$	$\frac{1}{2}$	$-\frac{1}{2}$	$-\frac{3}{2}$	$\frac{3}{2}$	$\frac{1}{2}$	$-\frac{1}{2}$	$-\frac{3}{2}$
	2140				0108			
0.5	0035	0093			0678	0329		
	0001	0216	1028		0039	0505	0079	
	0000	0021	0308	0570	0007	0294	0011	1406
	2152				0097			
0.45	0031	0080			0671	0372		
	0001	0237	1138		0047	0439	0068	
	0000	0024	0284	0468	0010	0359	0000	1405
	2163				0085			
0.4	0027	0060			0657	0439		
	0001	0281	1218		0061	0356	0045	
	0000	0027	0252	0376	0014	0438	0004	1365
	2176				0073			
0.35	0022	0025			0623	0556		
	0002	0390	1181		0093	0246	0013	
	0000	0025	0219	0298	0019	0538	0014	1285
	2189				0060			
0.3	0015	0020			0505	0786		
	0004	0687	0719		0208	0070	0002	
	0000	0010	0197	0239	0025	0676	0002	1172
	2202				0047			
0.25	0004	1082			0155	0642		
	0011	0567	0000		0553	0084	0000	
	0000	0004	0170	0196	0032	0695	0111	1040
	2215				0034			
0.2	0000	1993			0019	0207		
	0010	0093	0111		0683	0208	0095	
	0000	0017	0132	0168	0041	0583	0340	0904
	2227				0022			
0.15	0000	2171			0002	0074		
	0007	0016	0136		0692	0188	0210	
	0000	0012	0120	0150	0052	0575	0447	0775
	2238				0011			
0.1	0000	2225			0000	0024		
	0003	0002	0136		0683	0154	0300	
	0000	0005	0117	0140	0065	0598	0500	0659
	2246				0003			
0.05	0000	2245			0000	0004		
	0001	0000	0134		0668	0124	0381	
	0000	0001	0116	0135	0081	0625	0526	0556

TABLE II (*continued*). $\theta = 30°$

	$\lvert\langle M\rvert J_x\rvert M'\rangle\rvert^2$				$\lvert\langle M\rvert J_x\rvert M'\rangle\rvert^2$			
X	M $\frac{3}{2}$	$\frac{1}{2}$	$-\frac{1}{2}$	$-\frac{3}{2}$	$\frac{3}{2}$	$\frac{1}{2}$	$-\frac{1}{2}$	$-\frac{3}{2}$
	1727				0521			
10	0174	0174			0578	0077		
	0000	0250	0202		0000	0749	0049	
	0000	0000	0200	1643	0000	0000	0543	0606
	1765				0484			
5	0163	0162			0593	0092		
	0000	0250	0219		0001	0747	0036	
	0000	0000	0214	1595	0000	0001	0522	0653
	1859				0390			
2	0132	0133			0625	0143		
	0000	0253	0283		0006	0732	0010	
	0000	0000	0259	1430	0000	0011	0443	0816
	1969				0279			
1	0095	0098			0651	0238		
	0001	0262	0452		0021	0672	0002	
	0000	0004	0329	1092	0000	0057	0269	1132
	1988				0260			
0.9	0088	0092			0654	0261		
	0001	0265	0501		0025	0652	0005	
	0000	0005	0340	1012	0001	0073	0227	1201
	2009				0239			
0.8	0081	0084			0656	0289		
	0001	0270	0566		0030	0625	0010	
	0000	0007	0351	0913	0001	0096	0178	1282
	2033				0215			
0.7	0072	0074			0656	0328		
	0001	0279	0655		0037	0585	0017	
	0000	0010	0357	0792	0003	0130	0121	1371
	2046				0202			
0.65	0068	0068			0655	0352		
	0001	0285	0709		0041	0558	0021	
	0000	0012	0357	0723	0004	0152	0091	1415
	2060				0188			
0.6	0063	0061			0653	0382		
	0001	0294	0772		0046	0524	0023	
	0000	0014	0353	0649	0005	0186	0062	1456
	2075				0173			
0.55	0057	0053			0649	0420		
	0002	0308	0839		0053	0483	0024	
	0000	0017	0345	0570	0007	0214	0036	1490

TABLE II (*continued*). $\theta = 30°$

	$\lvert\langle M\rvert J_z\rvert M'\rangle\rvert^2$				$\lvert\langle M\rvert J_x\rvert M'\rangle\rvert^2$			
	M $\frac{3}{2}$	$\frac{1}{2}$	$-\frac{1}{2}$	$-\frac{3}{2}$	$\frac{3}{2}$	$\frac{1}{2}$	$-\frac{1}{2}$	$-\frac{3}{2}$
	2091				0158			
0.5	0051	0042			0642	0468		
	0002	0329	0906		0063	0432	0021	
	0000	0019	0331	0489	0009	0256	0016	1509
	2107				0141			
0.45	0045	0028			0629	0535		
	0003	0366	0958		0077	0367	0014	
	0000	0021	0311	0410	0012	0308	0003	1509
	2124				0124			
0.4	0038	0010			0605	0632		
	0003	0434	0960		0102	0281	0004	
	0000	0021	0286	0335	0016	0372	0000	1480
	2143				0106			
0.35	0030	0001			0551	0783		
	0005	0568	0820		0155	0160	0000	
	0000	0015	0261	0270	0022	0453	0000	1420
	2161				0087			
0.3	0019	0159			0408	0962		
	0010	0773	0366		0296	0014	0015	
	0000	0003	0240	0216	0030	0549	0003	1329
	2181				0068			
0.25	0006	1119			0149	0705		
	0016	0526	0000		0550	0105	0000	
	0000	0005	0207	0175	0039	0567	0094	1213
	2199				0049			
0.2	0001	1912			0028	0273		
	0015	0128	0079		0663	0241	0086	
	0000	0017	0168	0146	0050	0523	0246	1082
	2217				0032			
0.15	0000	2141			0004	0101		
	0010	0026	0108		0676	0233	0225	
	0000	0014	0151	0126	0065	0527	0340	0946
	2233				0016			
0.1	0000	2215			0000	0033		
	0005	0005	0110		0665	0196	0348	
	0000	0006	0145	0114	0082	0556	0392	0813
	2245				0004			
0.05	0000	2243			0000	0006		
	0001	0000	0108		0646	0160	0460	
	0000	0001	0143	0108	0103	0589	0419	0688

TABLE II (*continued*). $\theta = 35°$

	$\lvert\langle M\lvert J_z\rvert N'\rangle\rvert^2$				$\lvert\langle M\lvert J_x\rvert M'\rangle\rvert^2$			
X	M $\frac{3}{2}$	$\frac{1}{2}$	$-\frac{1}{2}$	$-\frac{3}{2}$	$\frac{3}{2}$	$\frac{1}{2}$	$-\frac{1}{2}$	$-\frac{3}{2}$
	1557				0692			
10	0232	0152			0522	0099		
	0000	0329	0185		0000	0670	0066	
	0000	0000	0261	1458	0000	0000	0481	0791
	1602				0646			
5	0218	0137			0540	0118		
	0000	0329	0204		0001	0667	0052	
	0000	0000	0276	1404	0000	0001	0457	0845
	1720				0528			
2	0180	0103			0580	0180		
	0000	0333	0276		0008	0648	0020	
	0000	0001	0320	1226	0000	0012	0373	1019
	1865				0382			
1	0131	0062			0615	0302		
	0001	0348	0442		0028	0581	0000	
	0000	0005	0375	0903	0001	0057	0214	1315
	1890				0357			
0.9	0122	0054			0618	0332		
	0002	0354	0484		0034	0561	0000	
	0000	0006	0382	0833	0001	0072	0180	1373
	1919				0329			
0.8	0112	0046			0621	0370		
	0002	0362	0538		0041	0532	0000	
	0000	0008	0386	0750	0002	0092	0141	1438
	1951				0296			
0.7	0100	0035			0621	0421		
	0003	0375	0606		0051	0491	0001	
	0000	0010	0386	0651	0003	0120	0098	1506
	1969				0278			
0.65	0093	0029			0619	0454		
	0003	0385	0645		0057	0464	0001	
	0000	0012	0384	0596	0004	0139	0076	1538
	1988				0259			
0.6	0086	0022			0616	0494		
	0003	0399	0685		0066	0432	0001	
	0000	0013	0378	0538	0006	0161	0055	1568
	2009				0239			
0.55	0079	0015			0610	0544		
	0004	0419	0723		0076	0391	0001	
	0000	0014	0369	0476	0008	0189	0035	1591

TABLE II (*continued*). $\theta = 35°$

	$\lvert\langle M\rvert J_z\rvert M'\rangle\rvert^2$				$\lvert\langle M\rvert J_x\rvert M'\rangle\rvert^2$			
X	M $\frac{3}{2}$	$\frac{1}{2}$	$-\frac{1}{2}$	$-\frac{3}{2}$	$\frac{3}{2}$	$\frac{1}{2}$	$-\frac{1}{2}$	$-\frac{3}{2}$
	2030				0217			
0.5	0070	0007			0599	0608		
	0005	0449	0752		0091	0339	0000	
	0000	0016	0356	0413	0010	0222	0019	1604
	2053				0194			
0.45	0061	0000			0581	0692		
	0006	0495	0756		0113	0273	0000	
	0000	0016	0338	0351	0014	0264	0009	1601
	2077				0170			
0.4	0051	0004			0546	0805		
	0008	0570	0700		0149	0186	0002	
	0000	0014	0318	0291	0019	0314	0003	1578
	2103				0145			
0.35	0038	0057			0478	0949		
	0011	0683	0521		0219	0076	0014	
	0000	0008	0296	0237	0025	0377	0002	1530
	2129				0119			
0.3	0023	0349			0338	1025		
	0017	0755	0186		0357	0000	0023	
	0000	0000	0274	0190	0034	0443	0014	1454
	2155				0093			
0.25	0009	1159			0144	0734		
	0022	0489	0000		0546	0125	0000	
	0000	0005	0238	0153	0045	0470	0078	1352
	2181				0067			
0.2	0002	1846			0037	0330		
	0020	0156	0055		0644	0263	0074	
	0000	0016	0199	0124	0059	0465	0178	1229
	2206				0043			
0.15	0000	2110			0007	0129		
	0013	0038	0084		0661	0272	0227	
	0000	0014	0178	0105	0076	0481	0255	1091
	2227				0021			
0.1	0000	2205			0001	0043		
	0006	0007	0088		0648	0236	0379	
	0000	0007	0169	0092	0098	0515	0302	0947
	2243				0006			
0.05	0000	2241			0000	0008		
	0001	0000	0085		0624	0194	0522	
	0000	0001	0166	0086	0124	0555	0329	0803

TABLE II (*continued*). $\theta = 40°$

	$\lvert\langle M\lvert J_x\rvert M'\rangle\rvert^2$				$\lvert\langle M\lvert J_x\rvert M'\rangle\rvert^2$			
X	M $\frac{3}{2}$	$\frac{1}{2}$	$-\frac{1}{2}$	$-\frac{3}{2}$	$\frac{3}{2}$	$\frac{1}{2}$	$-\frac{1}{2}$	$-\frac{3}{2}$
	1373				0876			
10	0294	0129			0461	0122		
	0000	0413	0165		0000	0585	0086	
	0000	0000	0324	1264	0000	0000	0416	0985
	1424				0824			
5	0279	0113			0481	0143		
	0000	0414	0186		0001	0582	0070	
	0000	0000	0339	1207	0000	0002	0391	1042
	1563				0685			
2	0236	0075			0529	0215		
	0000	0419	0260		0010	0561	0035	
	0000	0001	0378	1028	0000	0013	0308	1216
	1742				0504			
1	0175	0031			0573	0360		
	0003	0439	0410		0036	0487	0008	
	0000	0005	0416	0735	0001	0055	0169	1477
	1775				0471			
0.9	0163	0024			0578	0396		
	0003	0446	0444		0043	0465	0006	
	0000	0006	0418	0677	0001	0068	0142	1524
	1812				0434			
0.8	0150	0017			0581	0442		
	0004	0457	0485		0053	0436	0004	
	0000	0007	0418	0609	0002	0085	0112	1574
	1854				0392			
0.7	0134	0009			0580	0505		
	0005	0474	0530		0066	0394	0003	
	0000	0009	0413	0529	0004	0109	0080	1624
	1878				0368			
0.65	0125	0005			0578	0545		
	0005	0486	0554		0075	0367	0003	
	0000	0010	0409	0486	0005	0125	0064	1647
	1903				0343			
0.6	0115	0001			0574	0593		
	0006	0503	0575		0086	0334	0004	
	0000	0011	0402	0440	0007	0143	0048	1668
	1930				0316			
0.55	0105	0000			0566	0652		
	0007	0526	0985		0101	0293	0005	
	0000	0011	0392	0392	0009	0166	0034	1683

TABLE II (*continued*). $\theta = 40°$

	$\lvert\langle M\rvert J_z\rvert M'\rangle\rvert^2$				$\lvert\langle M\rvert J_x\rvert M'\rangle\rvert^2$			
X	M $\frac{3}{2}$	$\frac{1}{2}$	$-\frac{1}{2}$	$-\frac{3}{2}$	$\frac{3}{2}$	$\frac{1}{2}$	$-\frac{1}{2}$	$-\frac{3}{2}$
	1958				0288			
0.5	0093	0002			0552	0724		
	0009	0557	0589		0121	0242	0007	
	0000	0011	0380	0343	0012	0193	0022	1689
	1989				0257			
0.45	0080	0014			0528	0815		
	0011	0602	0561		0151	0178	0012	
	0000	0010	0364	0294	0016	0226	0013	1684
	2012				0225			
0.4	0065	0053			0487	0924		
	0014	0663	0480		0196	0101	0021	
	0000	0008	0346	0246	0021	0266	0008	1663
	2055				0192			
0.35	0048	0177			0414	1028		
	0018	0726	0316		0272	0023	0032	
	0000	0003	0325	0202	0028	0314	0009	1621
	2090				0157			
0.3	0029	0529			0289	1021		
	0024	0702	0098		0396	0009	0025	
	0001	0000	0300	0163	0037	0364	0021	1556
	2126				0122			
0.25	0012	1203			0139	0740		
	0029	0455	0000		0542	0143	0000	
	0001	0005	0265	0130	0049	0396	0063	1464
	2161				0088			
0.2	0003	1797			0044	0373		
	0025	0176	0037		0628	0280	0064	
	0001	0014	0227	0104	0065	0413	0130	1349
	2193				0055			
0.15	0000	2081			0010	0155		
	0017	0049	0064		0647	0304	0221	
	0001	0014	0203	0086	0086	0439	0189	1212
	2221				0028			
0.1	0000	2195			0001	0053		
	0008	0010	0069		0633	0272	0398	
	0000	0008	0191	0073	0112	0478	0230	1061
	2241				0008			
0.05	0000	2238			0000	0010		
	0002	0001	0066		0604	0226	0570	
	0000	0002	0185	0067	0144	0523	0254	0902

TABLE II (*continued*). $\theta = 45°$

	$\lvert\langle M\lvert J_z\rvert M'\rangle\rvert^2$				$\lvert\langle M\lvert J_x\rvert M'\rangle\rvert^2$			
X	$M\ \frac{3}{2}$	$\frac{1}{2}$	$-\frac{1}{2}$	$-\frac{3}{2}$	$\frac{3}{2}$	$\frac{1}{2}$	$-\frac{1}{2}$	$-\frac{3}{2}$
	1180				1069			
10	0360	0107			0397	0144		
	0000	0500	0144		0000	0498	0107	
	0000	0000	0388	1068	0000	0000	0351	1181
	1235				1014			
5	0345	0090			0419	0166		
	0000	0501	0165		0002	0495	0091	
	0000	0000	0401	1011	0000	0002	0326	1237
	1388				0859			
2	0299	0050			0473	0243		
	0001	0506	0236		0012	0472	0056	
	0000	0001	0431	0841	0000	0013	0249	1401
	1601				0643			
1	0227	0010			0526	0405		
	0004	0529	0362		0043	0394	0027	
	0000	0005	0451	0588	0001	0052	0133	1620
	1640				0603			
0.9	0212	0005			0531	0445		
	0005	0537	0387		0052	0372	0024	
	0000	0005	0450	0541	0002	0063	0112	1656
	1686				0557			
0.8	0195	0001			0535	0498		
	0006	0549	0414		0064	0341	0022	
	0000	0006	0446	0486	0003	0078	0089	1692
	1740				0504			
0.7	0175	0000			0536	0568		
	0008	0566	0441		0081	0300	0022	
	0000	0007	0438	0424	0004	0099	0065	1728
	1769				0474			
0.65	0163	0001			0534	0612		
	0009	0579	0451		0093	0273	0022	
	0000	0008	0432	0390	0006	0112	0054	1744
	1801				0442			
0.6	0150	0004			0529	0664		
	0010	0595	0457		0107	0241	0023	
	0000	0008	0425	0354	0007	0127	0042	1756
	1836				0407			
0.55	0136	0013			0519	0726		
	0012	0615	0455		0126	0202	0026	
	0000	0008	0415	0317	0010	0145	0032	1765

TABLE II (*continued*). $\theta = 45°$

	$\lvert\langle M\rvert J_z\rvert M'\rangle\rvert^2$				$\lvert\langle M\rvert J_x\rvert M'\rangle\rvert^2$			
X	M $\frac{3}{2}$	$\frac{1}{2}$	$-\frac{1}{2}$	$-\frac{3}{2}$	$\frac{3}{2}$	$\frac{1}{2}$	$-\frac{1}{2}$	$-\frac{3}{2}$
	1873				0370			
0.5	0120	0031			0503	0800		
	0014	0642	0438		0151	0155	0030	
	0000	0007	0402	0279	0013	0168	0023	1766
	1913				0331			
0.45	0103	0069			0477	0886		
	0017	0674	0396		0186	0101	0036	
	0000	0006	0387	0241	0017	0194	0016	1758
	1955				0289			
0.4	0083	0148			0433	0975		
	0021	0708	0315		0236	0043	0043	
	0000	0004	0370	0203	0022	0227	0013	1736
	1999				0246			
0.35	0061	0322			0362	1035		
	0027	0719	0189		0313	0002	0044	
	0001	0001	0349	0168	0030	0265	0014	1698
	2045				0201			
0.3	0038	0684			0256	0980		
	0033	0643	0054		0420	0029	0025	
	0001	0000	0322	0136	0040	0305	0024	1639
	2092				0155			
0.25	0018	1248			0135	0727		
	0036	0425	0000		0538	0160	0000	
	0001	0005	0288	0108	0053	0340	0051	1556
	2137				0111			
0.2	0006	1764			0050	0401		
	0031	0188	0025		0614	0292	0055	
	0001	0013	0252	0085	0072	0368	0094	1447
	2179				0069			
0.15	0001	2055			0013	0177		
	0021	0059	0048		0634	0329	0211	
	0001	0014	0225	0069	0095	0401	0138	1313
	2214				0034			
0.1	0000	2184			0002	0063		
	0010	0014	0053		0619	0303	0406	
	0001	0008	0209	0058	0125	0444	0172	1157
	2240				0009			
0.05	0000	2236			0000	0013		
	0002	0001	0051		0586	0256	0606	
	0000	0002	0202	0051	0162	0493	0193	0984

TABLE II (*continued*). $\theta = 50°$

	$\lvert\langle M\rvert J_z\rvert M'\rangle\rvert^2$				$\lvert\langle M\rvert J_x\rvert M'\rangle\rvert^2$			
X	M $\frac{3}{2}$	$\frac{1}{2}$	$-\frac{1}{2}$	$-\frac{3}{2}$	$\frac{3}{2}$	$\frac{1}{2}$	$-\frac{1}{2}$	$-\frac{3}{2}$
	0984				1265			
10	0427	0085			0332	0165		
	0000	0587	0122		0000	0411	0129	
	0000	0000	0451	0875	0000	0000	0286	1374
	1039				1210			
5	0414	0069			0353	0187		
	0000	0587	0142		0002	0408	0114	
	0000	0000	0460	0821	0000	0002	0263	1426
	1199				1046			
2	0369	0031			0411	0264		
	0001	0593	0206		0013	0384	0080	
	0000	0001	0480	0669	0000	0013	0195	1571
	1439				0802			
1	0289	0000			0472	0432		
	0006	0615	0304		0049	0306	0053	
	0000	0004	0482	0460	0001	0048	0103	1745
	1486				0754			
0.9	0271	0000			0480	0475		
	0007	0622	0320		0060	0284	0051	
	0000	0004	0478	0422	0002	0058	0087	1771
	1541				0699			
0.8	0251	0002			0485	0529		
	0009	0632	0336		0075	0255	0050	
	0000	0005	0471	0380	0003	0071	0070	1796
	1605				0634			
0.7	0225	0010			0487	0602		
	0011	0646	0348		0095	0215	0049	
	0000	0006	0461	0331	0005	0089	0053	1819
	1642				0597			
0.65	0210	0018			0485	0647		
	0013	0656	0350		0109	0190	0050	
	0000	0006	0454	0305	0006	0100	0044	1829
	1682				0557			
0.6	0194	0032			0481	0699		
	0015	0667	0346		0126	0161	0052	
	0000	0005	0445	0278	0008	0113	0036	1835
	1725				0514			
0.55	0175	0054			0471	0759		
	0017	0681	0335		0148	0127	0054	
	0000	0005	0435	0250	0010	0129	0028	1837

TABLE II (*continued*). $\theta = 50°$

	$\lvert\langle M \lvert J_z \rvert M' \rangle\rvert^2$				$\lvert\langle M \lvert J_x \rvert M' \rangle\rvert^2$			
X	M $\frac{3}{2}$	$\frac{1}{2}$	$-\frac{1}{2}$	$-\frac{3}{2}$	$\frac{3}{2}$	$\frac{1}{2}$	$-\frac{1}{2}$	$-\frac{3}{2}$
	1772				0467			
0.5	0155	0091			0455	0828		
	0021	0697	0311		0177	0088	0057	
	0000	0004	0422	0221	0013	0147	0022	1834
	1823				0417			
0.45	0132	0154			0429	0901		
	0025	0711	0268		0216	0047	0060	
	0000	0003	0407	0192	0018	0170	0017	1823
	1877				0364			
0.4	0106	0267			0386	0967		
	0030	0716	0201		0268	0012	0060	
	0001	0001	0389	0163	0023	0196	0014	1800
	1934				0308			
0.35	0078	0469			0321	0994		
	0036	0688	0113		0341	0001	0050	
	0001	0000	0368	0135	0031	0228	0015	1763
	1993				0251			
0.3	0050	0814			0232	0920		
	0041	0589	0031		0436	0051	0023	
	0001	0000	0341	0109	0042	0263	0022	1708
	2052				0193			
0.25	0025	1292			0132	0701		
	0043	0398	0000		0534	0175	0000	
	0002	0005	0308	0087	0057	0297	0040	1630
	2110				0136			
0.2	0009	1745			0055	0416		
	0037	0194	0017		0602	0301	0048	
	0002	0012	0272	0068	0077	0330	0068	1526
	2163				0085			
0.15	0002	2033			0016	0196		
	0025	0068	0035		0623	0350	0199	
	0002	0013	0243	0054	0103	0367	0100	1395
	2207				0042			
0.1	0000	2175			0003	0071		
	0012	0017	0040		0607	0331	0408	
	0001	0008	0225	0044	0137	0413	0126	1237
	2238				0011			
0.05	0000	2234			0000	0015		
	0003	0002	0038		0569	0283	0632	
	0000	0002	0215	0039	0179	0465	0143	1053

TABLE II (*continued*). $\theta = 55°$

	$\lvert\langle M \lvert J_z \rvert M' \rangle\rvert^2$				$\lvert\langle M \lvert J_x \rvert M' \rangle\rvert^2$			
X	M $\frac{3}{2}$	$\frac{1}{2}$	$-\frac{1}{2}$	$-\frac{3}{2}$	$\frac{3}{2}$	$\frac{1}{2}$	$-\frac{1}{2}$	$-\frac{3}{2}$
	0790				1459			
10	0494	0066			0267	0185		
	0000	0671	0099		0000	0327	0152	
	0000	0000	0510	0691	0000	0000	0226	1558
	0842				1406			
5	0483	0051			0287	0205		
	0000	0671	0117		0002	0324	0138	
	0000	0000	0516	0644	0000	0002	0205	1604
	1000				1244			
2	0444	0017			0345	0277		
	0001	0676	0171		0014	0301	0108	
	0000	0001	0523	0515	0000	0012	0149	1723
	1257				0979			
1	0362	0001			0413	0439		
	0007	0691	0242		0054	0227	0084	
	0000	0003	0509	0349	0001	0045	0077	1853
	1310				0925			
0.9	0342	0005			0422	0480		
	0009	0696	0252		0067	0207	0082	
	0000	0003	0502	0320	0002	0054	0066	1870
	1373				0861			
0.8	0318	0015			0430	0533		
	0012	0702	0259		0083	0180	0081	
	0000	0004	0493	0288	0003	0066	0054	1886
	1449				0784			
0.7	0288	0036			0435	0603		
	0015	0710	0261		0107	0145	0080	
	0000	0004	0481	0252	0005	0081	0041	1899
	1493				0739			
0.65	0270	0053			0434	0645		
	0017	0715	0258		0123	0123	0080	
	0000	0004	0473	0232	0006	0091	0035	1903
	1541				0691			
0.6	0249	0078			0431	0694		
	0020	0719	0250		0142	0099	0081	
	0000	0003	0464	0212	0008	0102	0029	1904
	1594				0638			
0.55	0226	0114			0423	0749		
	0023	0724	0236		0167	0072	0081	
	0000	0003	0452	0191	0010	0115	0024	1901

TABLE II (*continued*). $\theta = 55°$

	$\lvert\langle M\rvert J_z\rvert M'\rangle\rvert^2$				$\lvert\langle M\rvert J_x\rvert M'\rangle\rvert^2$			
X	M $\frac{3}{2}$	$\frac{1}{2}$	$-\frac{1}{2}$	$-\frac{3}{2}$	$\frac{3}{2}$	$\frac{1}{2}$	$-\frac{1}{2}$	$-\frac{3}{2}$
	1652				0581			
0.5	0200	0169			0409	0808		
	0027	0726	0212		0198	0043	0081	
	0000	0002	0439	0169	0014	0131	0019	1894
	1715				0518			
0.45	0170	0254			0384	0868		
	0032	0721	0176		0239	0017	0079	
	0001	0001	0424	0148	0018	0151	0016	1879
	1783				0452			
0.4	0138	0388			0346	0915		
	0038	0702	0126		0292	0000	0071	
	0001	0000	0406	0126	0024	0173	0014	1855
	1855				0381			
0.35	0102	0601			0289	0923		
	0045	0650	0068		0361	0011	0052	
	0001	0000	0384	0105	0032	0200	0015	1818
	1930				0308			
0.3	0067	0922			0213	0848		
	0050	0542	0018		0445	0072	0021	
	0002	0001	0357	0085	0044	0231	0019	1765
	2006				0235			
0.25	0036	1335			0129	0664		
	0051	0373	0000		0531	0188	0000	
	0002	0005	0324	0068	0060	0264	0030	1691
	2079				0165			
0.2	0015	1736			0059	0418		
	0044	0196	0011		0592	0307	0043	
	0002	0010	0290	0053	0081	0299	0048	1591
	2145				0101			
0.15	0004	2016			0019	0208		
	0029	0075	0025		0613	0365	0188	
	0002	0012	0259	0041	0110	0338	0071	1463
	2199				0049			
0.1	0000	2167			0003	0079		
	0014	0020	0029		0595	0355	0406	
	0002	0008	0238	0033	0148	0395	0091	1302
	2236				0013			
0.05	0000	2232			0000	0017		
	0003	0002	0028		0553	0308	0650	
	0000	0002	0226	0028	0195	0440	0104	1110

TABLE II (*continued*). $\theta = 60°$

	$\lvert\langle M\rvert J_z\rvert M'\rangle\rvert^2$				$\lvert\langle M\rvert J_x\rvert M'\rangle\rvert^2$			
X	M $\frac{3}{2}$	$\frac{1}{2}$	$-\frac{1}{2}$	$-\frac{3}{2}$	$\frac{3}{2}$	$\frac{1}{2}$	$-\frac{1}{2}$	$-\frac{3}{2}$
	0605				1643			
10	0558	0048			0205	0202		
	0000	0750	0076		0000	0248	0174	
	0000	0000	0565	0521	0000	0000	0170	1728
	0651				1597			
5	0552	0036			0223	0219		
	0000	0750	0091		0002	0245	0162	
	0000	0000	0566	0482	0000	0002	0153	1765
	0796				1445			
2	0523	0008			0276	0282		
	0002	0752	0134		0014	0225	0137	
	0000	0001	0560	0380	0000	0012	0109	1857
	1054				1175			
1	0447	0008			0348	0425		
	0008	0757	0182		0058	0160	0116	
	0000	0002	0532	0255	0001	0042	0056	1945
	1111				1116			
0.9	0427	0018			0359	0462		
	0011	0758	0187		0071	0142	0114	
	0000	0002	0523	0234	0002	0050	0048	1955
	1181				1044			
0.8	0401	0037			0369	0510		
	0014	0758	0189		0090	0120	0112	
	0000	0002	0513	0210	0003	0061	0040	1963
	1266				0956			
0.7	0367	0069			0377	0572		
	0018	0758	0186		0116	0091	0110	
	0000	0002	0498	0184	0004	0075	0031	1967
	1317				0904			
0.65	0346	0095			0379	0610		
	0021	0756	0181		0133	0074	0108	
	0000	0002	0490	0170	0006	0083	0027	1966
	1373				0847			
0.6	0322	0130			0378	0652		
	0024	0753	0172		0155	0055	0107	
	0000	0002	0479	0155	0008	0093	0023	1963
	1436				0784			
0.55	0293	0180			0373	0700		
	0028	0748	0159		0181	0035	0104	
	0000	0001	0468	0140	0010	0105	0019	1957

TABLE II (*continued*). $\theta = 60°$

	$\lvert\langle M \lvert J_z \rvert M' \rangle\rvert^2$				$\lvert\langle M \lvert J_x \rvert M' \rangle\rvert^2$			
X	M $\frac{3}{2}$	$\frac{1}{2}$	$-\frac{1}{2}$	$-\frac{3}{2}$	$\frac{3}{2}$	$\frac{1}{2}$	$-\frac{1}{2}$	$-\frac{3}{2}$
	1506				0714			
0.5	0261	0249			0362	0749		
	0034	0737	0139		0214	0017	0100	
	0001	0001	0454	0125	0013	0120	0016	1945
	1583				0638			
0.45	0224	0350			0342	0797		
	0040	0716	0112		0256	0003	0092	
	0001	0000	0438	0109	0018	0136	0013	1928
	1668				0555			
0.4	0183	0498			0310	0832		
	0046	0678	0078		0310	0001	0077	
	0001	0000	0419	0093	0024	0157	0012	1902
	1759				0467			
0.35	0138	0712			0262	0832		
	0053	0612	0041		0376	0025	0053	
	0002	0000	0397	0078	0033	0180	0012	1865
	1855				0375			
0.3	0093	1009			0198	0768		
	0059	0502	0011		0452	0090	0020	
	0002	0001	0370	0063	0045	0208	0015	1812
	1952				0284			
0.25	0053	1373			0126	0618		
	0059	0352	0000		0529	0197	0000	
	0002	0005	0338	0050	0062	0239	0022	1740
	2044				0196			
0.2	0024	1733			0062	0410		
	0050	0195	0007		0586	0311	0039	
	0003	0009	0304	0039	0085	0274	0033	1644
	2126				0119			
0.15	0007	2004			0021	0216		
	0034	0080	0017		0605	0377	0177	
	0003	0011	0273	0030	0117	0313	0048	1517
	2191				0057			
0.1	0001	2159			0004	0085		
	0016	0023	0020		0585	0376	0401	
	0002	0008	0249	0024	0158	0361	0063	1356
	2234				0015			
0.05	0000	2230			0000	0018		
	0004	0003	0020		0538	0331	0663	
	0001	0002	0235	0020	0210	0417	0073	1157

TABLE II (*continued*). $\theta = 65°$

	$\lvert\langle M \lvert J_z \rvert M' \rangle\rvert^2$				$\lvert\langle M \lvert J_x \rvert M' \rangle\rvert^2$			
X	M $\frac{3}{2}$	$\frac{1}{2}$	$-\frac{1}{2}$	$-\frac{3}{2}$	$\frac{3}{2}$	$\frac{1}{2}$	$-\frac{1}{2}$	$-\frac{3}{2}$
	0436				1813			
10	0616	0033			0148	0217		
	0000	0821	0055		0000	0177	0195	
	0000	0000	0613	0370	0000	0000	0120	1879
	0472				1775			
5	0616	0024			0162	0230		
	0000	0821	0067		0002	0175	0186	
	0000	0000	0610	0340	0000	0002	0107	1907
	0595				1644			
2	0603	0003			0208	0279		
	0001	0819	0098		0014	0158	0165	
	0000	0000	0592	0264	0000	0011	0075	1972
	0835				1384			
1	0546	0018			0278	0395		
	0009	0811	0128		0060	0106	0146	
	0000	0001	0551	0176	0001	0040	0039	2023
	0892				1324			
0.9	0527	0032			0290	0425		
	0011	0808	0130		0074	0092	0143	
	0000	0001	0541	0161	0001	0047	0033	2026
	0963				1248			
0.8	0502	0057			0302	0464		
	0015	0802	0129		0094	0074	0140	
	0000	0001	0529	0145	0002	0057	0027	2027
	1054				1151			
0.7	0467	0100			0314	0515		
	0019	0792	0125		0122	0052	0135	
	0000	0001	0513	0127	0004	0070	0022	2024
	1109				1094			
0.65	0445	0132			0318	0546		
	0023	0785	0120		0140	0040	0132	
	0000	0001	0503	0117	0005	0078	0019	2020
	1172				1029			
0.6	0418	0175			0320	0581		
	0027	0774	0112		0163	0027	0128	
	0000	0001	0493	0107	0007	0087	0016	2013
	1244				0955			
0.55	0386	0234			0320	0620		
	0032	0759	0102		0191	0014	0122	
	0000	0000	0480	0097	0009	0098	0014	2003

TABLE II (*continued*). $\theta = 65°$

	$\lvert\langle M \lvert J_z \rvert M' \rangle\rvert^2$				$\lvert\langle M \lvert J_x \rvert M' \rangle\rvert^2$			
X	$M \quad \frac{3}{2}$	$\frac{1}{2}$	$-\frac{1}{2}$	$-\frac{3}{2}$	$\frac{3}{2}$	$\frac{1}{2}$	$-\frac{1}{2}$	$-\frac{3}{2}$
	1326				0873			
0.5	0348	0314			0314	0660		
	0038	0737	0087		0226	0004	0113	
	0001	0000	0466	0086	0012	0111	0012	1989
	1419				0780			
0.45	0303	0426			0300	0699		
	0044	0704	0068		0269	0000	0100	
	0001	0000	0449	0076	0017	0127	0010	1969
	1523				0679			
0.4	0252	0580			0276	0727		
	0052	0654	0046		0322	0008	0080	
	0001	0000	0430	0065	0023	0145	0009	1941
	1638				0569			
0.35	0194	0792			0238	0728		
	0060	0578	0024		0386	0038	0052	
	0002	0000	0407	0054	0032	0166	0009	1903
	1760				0454			
0.3	0135	1070			0185	0680		
	0066	0471	0006		0459	0103	0019	
	0002	0001	0381	0044	0045	0192	0011	1851
	1884				0340			
0.25	0080	1401			0123	0564		
	0065	0334	0000		0531	0203	0000	
	0003	0004	0350	0035	0063	0221	0015	1780
	2001				0232			
0.2	0038	1732			0064	0393		
	0056	0192	0004		0583	0312	0036	
	0003	0008	0316	0027	0088	0254	0022	1686
	2104				0137			
0.15	0013	1993			0023	0218		
	0038	0084	0011		0600	0384	0168	
	0003	0010	0284	0021	0122	0292	0032	1561
	2183				0064			
0.1	0002	2153			0005	0089		
	0018	0025	0014		0577	0393	0395	
	0003	0007	0258	0016	0168	0339	0041	1399
	2232				0017			
0.05	0000	2229			0000	0020		
	0004	0004	0013		0524	0352	0671	
	0001	0002	0242	0013	0225	0395	0048	1194

TABLE II (*continued*). $\theta = 70°$

	$\lvert\langle M\rvert J_z\rvert M'\rangle\rvert^2$				$\lvert\langle M\rvert J_x\rvert M'\rangle\rvert^2$			
X	M $\frac{3}{2}$	$\frac{1}{2}$	$-\frac{1}{2}$	$-\frac{3}{2}$	$\frac{3}{2}$	$\frac{1}{2}$	$-\frac{1}{2}$	$-\frac{3}{2}$
	0287				1961			
10	0668	0021			0097	0228		
	0000	0882	0037		0000	0116	0213	
	0000	0000	0654	0240	0000	0000	0078	2008
	0313				1933			
5	0673	0014			0108	0238		
	0000	0882	0044		0002	0114	0206	
	0000	0000	0646	0220	0000	0001	0069	2027
	0406				1830			
2	0680	0000			0143	0272		
	0001	0876	0065		0014	0102	0191	
	0000	0000	0618	0169	0000	0011	0048	2066
	0606				1601			
1	0655	0024			0203	0353		
	0008	0855	0082		0060	0064	0172	
	0000	0001	0567	0112	0000	0038	0024	2085
	0657				1543			
0.9	0642	0040			0215	0375		
	0010	0847	0083		0075	0054	0169	
	0000	0001	0556	0102	0001	0045	0021	2084
	0723				1468			
0.8	0623	0067			0228	0403		
	0013	0836	0081		0095	0042	0163	
	0000	0001	0542	0092	0002	0054	0018	2079
	0812				1370			
0.7	0593	0114			0243	0440		
	0018	0818	0077		0125	0027	0156	
	0000	0000	0525	0081	0003	0067	0014	2070
	0867				1309			
0.65	0573	0149			0249	0463		
	0022	0805	0073		0144	0019	0150	
	0000	0000	0515	0075	0004	0074	0012	2063
	0933				1239			
0.6	0547	0195			0255	0489		
	0026	0788	0068		0168	0011	0144	
	0000	0000	0503	0068	0006	0083	0011	2054
	1010				1157			
0.55	0514	0258			0259	0518		
	0031	0765	0060		0197	0004	0134	
	0000	0000	0490	0062	0008	0094	0009	2041

TABLE II (*continued*). $\theta = 70°$

	$\lvert\langle M\lvert J_z\rvert M'\rangle\rvert^2$				$\lvert\langle M\lvert J_x\rvert M'\rangle\rvert^2$			
X	$M\ \frac{3}{2}$	$\frac{1}{2}$	$-\frac{1}{2}$	$-\frac{3}{2}$	$\frac{3}{2}$	$\frac{1}{2}$	$-\frac{1}{2}$	$-\frac{3}{2}$
	1101				1063			
0.5	0473	0344			0259	0550		
	0038	0734	0051		0233	0000	0122	
	0001	0000	0475	0055	0011	0106	0008	2024
	1208				0954			
0.45	0422	0460			0253	0581		
	0045	0692	0039		0278	0002	0105	
	0001	0000	0458	0048	0015	0121	0007	2002
	1332				0832			
0.4	0359	0618			0238	0605		
	0054	0634	0026		0333	0015	0081	
	0002	0000	0439	0042	0021	0138	0006	1973
	1474				0696			
0.35	0286	0828			0211	0612		
	0063	0553	0013		0397	0048	0051	
	0002	0000	0416	0035	0030	0158	0006	1934
	1630				0552			
0.3	0207	1096			0170	0583		
	0070	0447	0003		0469	0109	0018	
	0003	0001	0389	0028	0043	0181	0007	1882
	1792				0407			
0.25	0129	1409			0118	0501		
	0070	0320	0000		0537	0202	0000	
	0004	0004	0359	0023	0062	0208	0009	1812
	1946				0272			
0.2	0064	1725			0065	0367		
	0061	0189	0002		0586	0307	0033	
	0004	0007	0325	0017	0089	0239	0013	1719
	2077				0158			
0.15	0023	1983			0025	0215		
	0041	0086	0006		0599	0386	0161	
	0004	0009	0293	0013	0127	0276	0019	1595
	2173				0072			
0.1	0005	2148			0005	0092		
	0019	0027	0008		0570	0406	0389	
	0003	0007	0265	0010	0177	0320	0025	1433
	2230				0018			
0.05	0000	2228			0000	0021		
	0004	0004	0008		0511	0371	0677	
	0001	0002	0248	0008	0238	0376	0030	1224

TABLE II (*continued*). $\theta = 75°$

	$\lvert\langle M\lvert J_z\rvert M'\rangle\rvert^2$				$\lvert\langle M\lvert J_x\rvert M'\rangle\rvert^2$			
	M $\frac{3}{2}$	$\frac{1}{2}$	$-\frac{1}{2}$	$-\frac{3}{2}$	$\frac{3}{2}$	$\frac{1}{2}$	$-\frac{1}{2}$	$-\frac{3}{2}$
	0165				2083			
10	0711	0012			0056	0238		
	0000	0932	0021		0000	0066	0228	
	0000	0000	0687	0137	0000	0000	0044	2112
	0181				2065			
5	0721	0007			0062	0243		
	0000	0931	0026		0002	0065	0224	
	0000	0000	0675	0125	0000	0001	0039	2122
	0241				1993			
2	0749	0000			0085	0262		
	0001	0922	0038		0013	0057	0213	
	0000	0000	0638	0095	0000	0010	0027	2139
	0381				1811			
1	0767	0022			0129	0308		
	0006	0888	0046		0060	0034	0194	
	0000	0000	0579	0062	0000	0037	0014	2134
	0420				1761			
0.9	0765	0037			0139	0320		
	0007	0877	0046		0074	0028	0188	
	0000	0000	0567	0057	0000	0044	0012	2128
	0473				1694			
0.8	0758	0061			0151	0337		
	0010	0861	0045		0095	0021	0181	
	0000	0000	0552	0051	0001	0053	0010	2120
	0546				1602			
0.7	0743	0102			0165	0359		
	0014	0837	0042		0125	0012	0171	
	0000	0000	0534	0045	0002	0065	0008	2106
	0595				1544			
0.65	0731	0134			0172	0373		
	0017	0820	0039		0145	0008	0164	
	0000	0000	0523	0042	0003	0073	0007	2097
	0653				1473			
0.6	0713	0177			0180	0389		
	0021	0798	0036		0170	0003	0155	
	0000	0000	0511	0038	0004	0081	0006	2085
	0726				1389			
0.55	0687	0235			0187	0408		
	0026	0771	0032		0201	0000	0143	
	0001	0000	0498	0035	0006	0092	0005	2071

TABLE II (*continued*). $\theta = 75°$

	$\lvert\langle M \lvert J_z \rvert M' \rangle\rvert^2$				$\lvert\langle M \lvert J_x \rvert M' \rangle\rvert^2$			
X	M $\frac{3}{2}$	$\frac{1}{2}$	$-\frac{1}{2}$	$-\frac{3}{2}$	$\frac{3}{2}$	$\frac{1}{2}$	$-\frac{1}{2}$	$-\frac{3}{2}$
	0816				1288			
0.5	0651	0316			0193	0429		
	0032	0735	0026		0239	0000	0128	
	0001	0000	0483	0031	0008	0104	0004	2052
	0928				1167			
0.45	0602	0427			0195	0452		
	0040	0687	0020		0286	0004	0108	
	0001	0000	0465	0027	0011	0118	0004	2028
	1067				1024			
0.4	0534	0581			0191	0472		
	0049	0623	0013		0344	0018	0081	
	0002	0000	0445	0023	0017	0135	0003	1997
	1236				0860			
0.35	0447	0788			0177	0484		
	0059	0540	0006		0411	0049	0050	
	0003	0000	0423	0020	0025	0155	0003	1957
	1434				0679			
0.3	0340	1054			0150	0473		
	0068	0435	0001		0485	0104	0017	
	0004	0001	0396	0016	0038	0177	0004	1905
	1650				0493			
0.25	0224	1370			0110	0425		
	0071	0312	0000		0554	0189	0000	
	0005	0003	0366	0013	0058	0203	0005	1836
	1861				0321			
0.2	0119	1694			0064	0330		
	0063	0188	0001		0600	0293	0031	
	0005	0006	0332	0010	0087	0231	0007	1744
	2038				0180			
0.15	0045	1965			0026	0206		
	0044	0088	0003		0606	0380	0155	
	0005	0007	0299	0007	0129	0265	0010	1621
	2162				0079			
0.1	0010	2141			0006	0092		
	0021	0029	0004		0567	0413	0384	
	0004	0006	0271	0005	0184	0306	0014	1458
	2229				0020			
0.05	0000	2226			0000	0022		
	0004	0004	0004		0499	0388	0680	
	0001	0002	0252	0004	0251	0358	0016	1246

TABLE II (*continued*). $\theta = 80°$

	$\lvert\langle M\lvert J_z\rvert M'\rangle\rvert^2$				$\lvert\langle M\lvert J_x\rvert M'\rangle\rvert^2$			
X	M $\frac{3}{2}$	$\frac{1}{2}$	$-\frac{1}{2}$	$-\frac{3}{2}$	$\frac{3}{2}$	$\frac{1}{2}$	$-\frac{1}{2}$	$-\frac{3}{2}$
	0074				2174			
10	0742	0005			0025	0244		
	0000	0969	0009		0000	0029	0240	
	0000	0000	0712	0061	0000	0000	0020	2187
	0082				2164			
5	0758	0003			0028	0246		
	0000	0967	0011		0002	0029	0237	
	0000	0000	0696	0056	0000	0001	0017	2191
	0111				2120			
2	0804	0000			0039	0253		
	0000	0955	0017		0013	0025	0229	
	0000	0000	0653	0042	0000	0010	0011	2192
	0185				1992			
1	0870	0014			0063	0268		
	0003	0912	0020		0059	0014	0209	
	0000	0000	0588	0027	0000	0036	0006	2168
	0208				1954			
0.9	0882	0023			0069	0273		
	0004	0898	0020		0073	0011	0203	
	0000	0000	0575	0025	0000	0043	0005	2160
	0238				1901			
0.8	0893	0038			0077	0278		
	0006	0879	0019		0094	0008	0194	
	0000	0000	0559	0023	0000	0052	0004	2148
	0284				1826			
0.7	0903	0065			0086	0286		
	0008	0852	0018		0125	0004	0181	
	0000	0000	0540	0020	0001	0064	0003	2132
	0315				1775			
0.65	0906	0086			0092	0291		
	0010	0833	0017		0145	0002	0173	
	0000	0000	0529	0018	0001	0072	0003	2121
	0355				1713			
0.6	0906	0115			0099	0298		
	0013	0809	0015		0171	0000	0162	
	0000	0000	0517	0017	0002	0081	0002	2108
	0407				1636			
0.55	0901	0157			0106	0305		
	0016	0779	0013		0203	0000	0148	
	0001	0000	0503	0015	0003	0092	0002	2092

TABLE II (*continued*). $\theta = 80°$

	$\lvert\langle M \lvert J_z \rvert M' \rangle\rvert^2$				$\lvert\langle M \lvert J_x \rvert M' \rangle\rvert^2$			
X	M $\frac{3}{2}$	$\frac{1}{2}$	$-\frac{1}{2}$	$-\frac{3}{2}$	$\frac{3}{2}$	$\frac{1}{2}$	$-\frac{1}{2}$	$-\frac{3}{2}$
	0476				1539			
0.5	0888	0216			0113	0315		
	0021	0741	0011		0244	0000	0131	
	0001	0000	0488	0013	0004	0104	0002	2072
	0568				1418			
0.45	0862	0302			0120	0325		
	0027	0691	0008		0295	0004	0109	
	0001	0000	0470	0012	0007	0119	0001	2046
	0694				1265			
0.4	0814	0429			0125	0337		
	0034	0627	0005		0358	0015	0081	
	0002	0000	0450	0010	0011	0137	0001	2015
	0866				1077			
0.35	0734	0613			0125	0347		
	0044	0543	0002		0433	0038	0049	
	0003	0000	0427	0008	0017	0158	0001	1974
	1095				0856			
0.3	0611	0872			0116	0349		
	0054	0438	0000		0516	0082	0016	
	0004	0001	0401	0007	0029	0181	0001	1921
	1381				0617			
0.25	0443	1207			0094	0331		
	0061	0317	0000		0592	0154	0000	
	0006	0002	0371	0005	0047	0207	0002	1852
	1690				0390			
0.2	0258	1581			0060	0277		
	0059	0193	0000		0638	0254	0030	
	0006	0004	0338	0004	0078	0234	0003	1761
	1962				0208			
0.15	0106	1912			0026	0188		
	0044	0092	0001		0631	0355	0151	
	0006	0006	0304	0003	0124	0262	0004	1639
	2141				0087			
0.1	0024	2127			0006	0090		
	0021	0030	0002		0573	0411	0381	
	0005	0006	0275	0002	0187	0297	0006	1475
	2227				0021			
0.05	0001	2225			0000	0022		
	0005	0005	0002		0489	0401	0683	
	0002	0002	0255	0002	0263	0343	0007	1261

TABLE II (*continued*). $\theta = 85°$

	$\lvert\langle M \lvert J_z \rvert M' \rangle\rvert^2$				$\lvert\langle M \lvert J_x \rvert M' \rangle\rvert^2$			
X	M $\frac{3}{2}$	$\frac{1}{2}$	$-\frac{1}{2}$	$-\frac{3}{2}$	$\frac{3}{2}$	$\frac{1}{2}$	$-\frac{1}{2}$	$-\frac{3}{2}$
	0018				2230			
10	0762	0001			0006	0248		
	0000	0991	0002		0000	0007	0247	
	0000	0000	0726	0015	0000	0000	0005	2233
	0020				2226			
5	0781	0000			0007	0248		
	0000	0989	0003		0001	0007	0246	
	0000	0000	0709	0014	0000	0001	0004	2233
	0028				2202			
2	0840	0000			0010	0247		
	0000	0975	0004		0013	0006	0239	
	0000	0000	0661	0010	0000	0010	0002	2224
	0049				2117			
1	0945	0004			0017	0241		
	0000	0927	0005		0058	0003	0218	
	0000	0000	0593	0006	0000	0035	0001	2189
	0055				2090			
0.9	0968	0007			0018	0240		
	0001	0912	0005		0072	0002	0211	
	0000	0000	0580	0006	0000	0042	0001	2179
	0065				2052			
0.8	0997	0011			0021	0238		
	0001	0891	0004		0093	0001	0202	
	0000	0000	0564	0005	0000	0052	0001	2166
	0079				1996			
0.7	1034	0020			0024	0236		
	0002	0862	0004		0124	0000	0187	
	0000	0000	0544	0005	0000	0064	0000	2147
	0089				1958			
0.65	1056	0027			0026	0234		
	0003	0843	0004		0145	0000	0178	
	0000	0000	0533	0004	0000	0072	0000	2135
	0103				1909			
0.6	1080	0037			0029	0233		
	0004	0819	0003		0171	0000	0166	
	0000	0000	0521	0004	0000	0081	0000	2121
	0121				1847			
0.55	1106	0052			0032	0231		
	0005	0789	0003		0205	0000	0151	
	0001	0000	0507	0003	0001	0092	0000	2104

TABLE II (*continued*). $\theta = 85°$

	$\lvert\langle M\lvert J_z\rvert M'\rangle\rvert^2$				$\lvert\langle M\lvert J_x\rvert M'\rangle\rvert^2$			
X	M $\frac{3}{2}$	$\frac{1}{2}$	$-\frac{1}{2}$	$-\frac{3}{2}$	$\frac{3}{2}$	$\frac{1}{2}$	$-\frac{1}{2}$	$-\frac{3}{2}$
	0147				1767			
0.5	1133	0074			0035	0229		
	0006	0751	0002		0248	0000	0133	
	0001	0000	0491	0003	0001	0106	0000	2083
	0185				1662			
0.45	1160	0108			0039	0227		
	0009	0703	0002		0303	0002	0110	
	0002	0000	0473	0003	0002	0122	0000	2058
	0244				1523			
0.4	1181	0164			0044	0225		
	0012	0642	0001		0374	0006	0081	
	0002	0000	0453	0002	0003	0142	0000	2025
	0338				1339			
0.35	1184	0258			0049	0222		
	0017	0563	0000		0462	0015	0048	
	0004	0000	0430	0002	0006	0166	0000	1984
	0495				1103			
0.3	1143	0419			0053	0219		
	0024	0463	0000		0567	0035	0016	
	0005	0000	0404	0001	0012	0194	0000	1931
	0760				0816			
0.25	1012	0694			0052	0212		
	0032	0343	0000		0671	0077	0000	
	0007	0001	0374	0001	0024	0227	0000	1862
	1171				0512			
0.2	0744	1125			0042	0194		
	0038	0214	0000		0737	0155	0030	
	0009	0002	0340	0001	0049	0259	0000	1771
	1673				0257			
0.15	0378	1650			0023	0152		
	0035	0102	0000		0717	0268	0149	
	0008	0004	0307	0000	0097	0286	0001	1649
	2060				0098			
0.1	0099	2053			0006	0084		
	0020	0033	0000		0613	0373	0378	
	0006	0004	0277	0000	0174	0306	0001	1486
	2220				0022			
0.05	0007	2219			0000	0022		
	0005	0005	0000		0486	0405	0684	
	0002	0002	0256	0000	0269	0335	0001	1270

SUPPLEMENTO AL VOLUME XV, SERIE X
DEL NUOVO CIMENTO

N. 3, 1960
1° Trimestre

On a Quantum Mechanical Theory of Absolute Reaction Rates (*)(**).

S. GOLDEN

Chemistry Department, Brandeis University - Waltham, Mass.

(ricevuto il 31 Agosto 1959)

CONTENTS. — **1**. Introduction. – **2**. Species classification. – **3**. Construction of classification operators. – **4**. Composition operators and variables. – **5**. Equation of motion. – **6**. Variational considerations. – **7**. Heuristics. – **8**. Theories of chemical reaction rates. – **9**. Remarks.

1. – Introduction.

The phenomenological laws which describe the temporal evolution of a reacting chemical system are sufficiently well known to require little attention here to be given to their exposition (1). Both the concentration dependence of the kinetic equations and the temperature coefficients of the rate constants of these equations are now generally understood in the light of the molecular processes occurring during the course of chemical change. To be sure, questions not fully answered remain. In the realm of theoretical investigations these refer generally to details of the sort necessarily involved in producing quantitatively precise, absolute theories of reaction rates.

To investigate such questions in a ultimate sense, a theory of absolute reaction rates must be based upon quantum mechanics. However, such a theory may assume a form more-or-less expressible in classical mechanical terms when classical mechanics furnishes an adequate description of the system

(*) Supported, in part, by the Office of Naval Research.

(**) Presented at the Symposium on the Theory of Absolute Reaction Rates, University of Wisconsin, March 30-April 1, 1959.

(1) See, for example, A. A. FROST and R. G. PEARSON: *Kinetics and Mechanism* (New York, 1953).

undergoing chemical reactions. Nevertheless, in contemplating either a classical or a quantum mechanical theory, one is forced to the realization that the mechanical description is devoid of any reference to the molecular species which are essential for the chemical description of the system. It is apparent, therefore, that the mechanical description—be it classical or quantum—must be augmented by quantities which make explicit reference to the possible existence of chemical species. In the simplest terms, an immediate question arises: What is meant by a « molecule » as contrasted with simply a collection of fundamental particles, from a mechanical viewpoint? The answer to this question may be expected to have a considerable bearing upon the form of a theory of absolute reaction rates.

Each theory which contemplates chemical change must deal with this question, and the answer employed generally may vary from one theory to another. However, the criteria which have been employed to date in theories of chemical reaction rates are rather limited. Thus, the absolute rate theory of Eyring [2] employs a criterion based upon location in configuration space; thereby, a collection of particles is designated as comprising one set of molecular species or another according to the region of the configuration space in which they are to be found. In addition, the unimolecular rate theory of Slater [3] illustrates a similar sort of criterion; here a critical length of a particular bond of a molecule, or a suitable collection of such bonds, serves to distinguish between a particular chemical species and those which result from rupture of the pertinent chemical bonds. By contrast, the unimolecular theory of Rice-Ramsperger-Kassel [4] employs the criterion by which a critical value of the energy ascribable to a certain bond, or a suitable collection of bonds, must be exceeded to effect the same sort of distinction. The question of what is meant by the term « molecule » is important in any chemical description of a system in which the numbers of each species may not always be fixed, in spite of the fact that the numbers of fundamental particles are. As a result, similar questions have arisen with regard to equilibrium systems, and their constituent *complexes* [5], *clusters* [6], and *metastable molecules* [7] require criteria to be employed which permit these unusual species to be distinguished from the ordinary molecular species compromising the systems.

---

[2] See, for example, S. Glasstone, K. Laidler and H. Eyring: *The Theory of Rate Processes* (New York, 1941).

[3] See, for example, N. B. Slater: *Proc. Camb. Phil. Soc.*, **35**, 56 (1939); *Nature*, **159**, 264 (1947).

[4] O. K. Rice and H. C. Ramsperger: *J.A.C.S.*, **49**, 1617 (1927); **50**, 617 (1928); L. S. Kassel: *Journ. Phys. Chem.*, **32**, 225 (1928).

[5] See, for example, G. Glockler: *Journ. Chem. Phys.*, **2**, 823 (1934).

[6] T. L. Hill: *Statistical Mechanics* (New York, 1956), pp. 156-160.

[7] J. O. Hirschfelder: private communication.

The present paper has as its starting point the introduction of operators which serve to classify a collection of fundamental particles as one set of molecular species or another. These operators are presumed to embody the appropriate criteria upon which a classification may be based. However, only the logical characteristics ofc lassification are utilized explicitly. These operators, termed *species-classification* operators are discussed fully in Section 2. The formal construction of such operators is described in Section 3.

The formal construction of species-classification operators for microscopic systems facilitates the construction of composition operators for macroscopic systems. The macroscopic composition operators are symmetric with respect to exchange of identical fundamental particles. From the composition operators are constructed dynamical variables for the numbers of each chemical species of a macroscopic system. These matters are discussed in Section 4.

In Section 5, the quantum mechanical description of a system is utilized. Heisenberg's equation of motion for a dynamical variable which does not depend explicitly upon the time is applied to obtain operators for the time-rate of change of the composition of a macroscopic mixture. The resulting equations are applied to an ensemble through the introduction of the statistical matrix of von Neumann. Expressions for the time-rate of change of the ensemble averaged number of each species resemble the phenomenological equations of chemical kinetics and permit an identification of the rate constants to be made. The instantaneous rate expression simplicitly involve a knowledge of the value of the statistical matrix at the instant in question and exhibits an explicit compositional dependence corresponding only to unimolecular and bimolecular elementary mechanisms of chemical change. The results of this Section appear to be useful to apply if an estimate can be made of the statistical matrix which is both physically sensible and an insensitive function of the time.

Section 6 is devoted to a consideration of a variational problem, by which a typical quantity identified as a rate constant is subjected to variations of the statistical matrix and the species-classification operators. Apart from certain constraints of normalization together with the projection and orthogonal properties of the classification operators, the variations are arbitrary. The necessary conditions under which the rate constants then are stationary are obtained. These correspond to conditions of *detailed balancing* for the rates of chemical transition in various states of the system, as well as to *microscopic reversibility* of forward and inverse chemical transitions. In these terms, the conditions appear to correspond to stationary values of the statistical matrix. The expression which is obtained for the rate constant under these conditions is shown to be of a form which furnishes an upper bound to the rate constant under the most general conditions.

The rate expressions are considered in an heuristic manner in Section 7. Thereby, identifications are made which relate the rates of chemical transition

to the composition of the macroscopic system and its statistical thermodynamic properties. A kinetic criterion of chemical equilibrium is shown to reduce to the usual statistical thermodynamic one. For conditions presumably « close » to equilibrium, the rate constant depends explicitly upon the equilibrium constant of the reaction.

The results which have been obtained are discussed briefly in Section **8** with reference to extant theories of chemical kinetics.

2. – Species classification.

A physically meaningful description of a system in terms other than those invoking the basic or fundamental particles of which the system is composed implies the existence of measurement processes the results of which are capable of validating such a description. Thus, to justify a description of a system consisting of electrons and nuclei in terms such as *atoms*, *molecules*, *ions*, etc., one requires an act of measurement to yield results which can be attributed to these composite entities. A description of this sort is necessarily approximate—when regarded from a fundamental viewpoint—but has a pragmatic validity.

Measurements which are so designed as to yield the classification of a system in terms of various *species* (*i.e.*, various collections of the basic particles) must possess certain logical characteristics. They must, for example, yield results which: 1) are reproducible, 2) permit different species to be distinguished from one another, and 3) give a complete classification of the system in terms of the several species. These characteristics are conveniently expressed as the mathematical properties of the elements of a Boolean algebra ([8]). When the physical system adequately is described classically, the properties of a Boolean algebra alone permit the selection of logically suitable measurement processes. When the physical system requires a quantum mechanical description, corresponding greater restrictions may be imposed.

For the present purpose, a measurement process which permits a decision to be made as to whether or not a physical system can be regarded as consisting of a certain set of species, say α, will be identified with a projection operator (hermitian) σ_α. The conditional probability that a system with a wave function Ψ is to be described as α will be taken as ([9])

$$\text{(2.1)} \qquad \text{Probability of } \alpha = \frac{\langle \Psi | \sigma_\alpha | \Psi \rangle}{\langle \Psi | \Psi \rangle} .$$

([8]) See, for example, S. GOLDEN: *Suppl. Nuovo Cimento*, **5**, 540 (1957).

([9]) The bracket notation follows P. A. M. DIRAC: *The Principles of Quantum Theory* (Oxford, 1947), p. 18 ff. For simplicity normalizable wave functions are assumed.

Here, Ψ is a function of all of the co-ordinates of the system and the time and is presumed to satisfy Schrödinger's equation

$$H\Psi = i\hbar \frac{\partial \Psi}{\partial t}, \tag{2.2}$$

where H is the Hamiltonian of the system. For simplicity, σ_α will be assumed not to depend explicitly upon the time, corresponding to the physical circumstance where the criteria taken for a species classification do not depend upon the time. Otherwise σ_α depends upon the general co-ordinates and momenta of the system. For other sets of species, β, γ, etc., the associated measurements permitting a decision that the system may be regarded as consisting of them will be identified with projection operators σ_β, σ_γ, etc., and the relevant conditional probabilities defined analogously to eq. (2.1).

The present considerations may be clarified by an explicit chemical illustration. A system consisting of three hydrogen atoms, three deuterium atoms, and three carbon atoms may exist as several different kinds of cyclo-propane and propylene molecules; other arrangements including decomposition products are also possible. In these terms, each of the cyclopropane and propylene molecules would be put into a one-to-one correspondence with the members of a certain set of σ's. An analogous correspondence for a different set of σ's would be attributed to other possible chemical arrangements of this system.

The description of a macroscopic system in similar terms, corresponding to a mixture of the several species introduces no serious formal difficulty. The projection operator corresponding to such a description must be as detailed as one corresponding to a description in terms of a microscopic set of species. Moreover, since different compositions are presumed to be distinguishable, their operators have formal properties identical with those of a microscopic species-set. However, because of the wide range of possible compositions the number of corresponding operators is enormous for macroscopic systems, while the variety of species involved may be relatively small. The macroscopic operators are discussed in detail in Section **4**.

The various σ's will be termed *species-classification* operators. Their mathematical properties (which are those of the elements of a Boolean algebra) have been discussed elsewhere ([10]). For the present purposes, a few of the pertinent properties will be displayed. In accordance with the logical characteristics mentioned above, they are

$$\text{Reproducibility:} \qquad \sigma_\alpha \sigma_\alpha = (\sigma_\alpha)^2 = \sigma_\alpha, \qquad \text{all } \alpha, \tag{2.3}$$

([10]) See, for example, ref. ([8]); also G. Birkhoff and S. MacLane: *A Survey of Modern Algebra* (New York, 1944), Chapter XI.

(2.4) Distinguishability: $\sigma_\alpha\sigma_\beta = \sigma_\beta\sigma_\alpha = \mathbf{0}$, all $\alpha \neq \beta$,

(2.5) Completeness: $\sum_{\text{all } \alpha} \sigma_\alpha = \boldsymbol{I}$.

Here $\mathbf{0}$ and $\boldsymbol{I}$ represent the null and identity elements, respectively, of the algebra. The σ's can be seen to correspond to the *minimal* elements of the algebra ([10]).

Eqs. (2.4) and (2.5) merit some comment. The essential criterion of distinguishability between a species-set α and any other has been taken to be the following: If a system is known certainly to consist of the species-set α (in the extended sense discussed above) it cannot consist of any other distinguishable species-set. While some properties of a species-set may be identical with those of another species-set the measured values of those properties upon which the classification depend are assumed not to be so. In that case, for those wave functions (*) satisfying the eigenvalue relation

(2.6) $$\sigma_\alpha\varphi_i = \varphi_i ,$$

one requires that

(2.7) $$\langle\varphi_i|\sigma_\beta|\varphi_i\rangle = \langle\varphi_i|\sigma_\alpha\sigma_\beta\sigma_\alpha|\varphi_i\rangle = 0 .$$

Furthermore, for those wave functions satisfying the eigenvalue relation

(2.8) $$\sigma_\alpha\varphi_j = 0 ,$$

clearly,

(2.9) $$\langle\varphi_j|\sigma_\alpha\sigma_\beta\sigma_\alpha|\varphi_i\rangle = 0 .$$

But, then, since $\sigma_\alpha\sigma_\beta\sigma_\alpha = (\sigma_\alpha\sigma_\beta)(\sigma_\beta\sigma_\alpha) = (\sigma_\alpha\sigma_\beta)(\sigma_\alpha\sigma_\beta)^\dagger$ it follows that both $\sigma_\alpha\sigma_\beta$ and $\sigma_\beta\sigma_\alpha$ must be null operators, in accordance with eq. (2.4).

The condition of completeness seems more-or-less self-evident. However, the restriction implied by this condition is worth noting. When a particular choice is made of the various σ's, even consistent with eq. (2.4), there is no assurance that the completeness relation will be satisfied automatically. As a result, it is necessary to suppose that there may exist « species » other than those which may have been listed and which serve to provide the desired completeness. The necessity for their introduction into the theory stems from inadequacies inherent in the particular choice which has been made of the various σ's, and their corresponding measurement processes. To illustrate

(*) For simplicity, $\{\varphi_n\}$ is assumed to form a complete orthonormal set of functions.

simply, the selection of a σ_α and a σ_β (satisfying eq. (2.4)) does not assure one that the operator corresponding to « neither species-set α nor species-set β » will be necessarily a null-operator.

The construction of species-classification operators will be discussed in the following section.

For the present, two important properties of these operators will be considered. When a system is not to be accorded a wave-function description, but is to be regarded rather as a member of an ensemble ([11]), eq. (2.1) must be modified. The average probability that a system thus described will consist of the species (set) α is

$$\bar{\sigma}_\alpha = \sum_{n=1}^{\infty} \langle \psi_n | \varrho \sigma_\alpha | \psi_n \rangle = \mathrm{Tr}\, \varrho \sigma_\alpha , \tag{2.10}$$

where $\{\psi_n\}$ is a complete orthonormal set of wave functions and ϱ is the statistical matrix of von Neumann ([12]); for simplicity it has been assumed that $\mathrm{Tr}\, \varrho = 1$. The statistical matrix satisfies the equation

$$i\hbar \frac{\partial \varrho}{\partial t} = H\varrho - \varrho H . \tag{2.11}$$

Clearly, eq. (2.1) corresponds to a specific choice of ϱ in eq. (2.10). Now the uncertainty in the probability $\bar{\sigma}_\alpha$ is given by

$$\{\mathrm{Tr}\, \varrho(\sigma_\alpha - \bar{\sigma}_\alpha)^2\}^{\frac{1}{2}} = \{\mathrm{Tr}\, \varrho(\sigma_\alpha - 2\sigma_\alpha\bar{\sigma}_\alpha + \bar{\sigma}_\alpha^2)\}^{\frac{1}{2}} = \{\bar{\sigma}_\alpha(1 - \bar{\sigma}_\alpha)\}^{\frac{1}{2}} \tag{2.12}$$

so that the uncertainty in the probability $\bar{\sigma}_\alpha$ vanishes if and only if $\sigma_\alpha = 0, 1$. Under these circumstances it can be shown that σ_α and ϱ must commute. To see this, note that ϱ is a positive definite operator and, therefore, $\varrho^{\frac{1}{2}}$ exists. Moreover, σ_α and ϱ commute if and only if σ_α and $\varrho^{\frac{1}{2}}$ commute. Then consider the trace of the following positive definite operator

$$\begin{aligned}
&\mathrm{Tr}\, [\varrho^{\frac{1}{2}}(\sigma_\alpha - \bar{\sigma}_\alpha) - (\sigma_\alpha - \bar{\sigma}_\alpha)\varrho^{\frac{1}{2}}]^2 = \\
&\qquad = \mathrm{Tr}\, [\varrho^{\frac{1}{2}}(\sigma_\alpha - \bar{\sigma}_\alpha)^2\varrho^{\frac{1}{2}}] - \mathrm{Tr}\, [(\sigma_\alpha - \bar{\sigma}_\alpha)\varrho^{\frac{1}{2}}(\sigma_\alpha - \bar{\sigma}_\alpha)\varrho^{\frac{1}{2}}] - \\
&\qquad - \mathrm{Tr}\, [\varrho^{\frac{1}{2}}(\sigma_\alpha - \bar{\sigma}_\alpha)\varrho^{\frac{1}{2}}(\sigma_\alpha - \bar{\sigma}_\alpha)] + \mathrm{Tr}\, [(\sigma_\alpha - \bar{\sigma}_\alpha)\varrho(\sigma_\alpha - \bar{\sigma}_\alpha)] = \\
&\qquad = 2\, \mathrm{Tr}\, \varrho(\sigma_\alpha - \bar{\sigma}_\alpha)^2 - 2\, \mathrm{Tr}\, [\varrho^{\frac{1}{2}}(\sigma_\alpha - \bar{\sigma}_\alpha)\varrho^{\frac{1}{2}}(\sigma_\alpha - \bar{\sigma}_\alpha)]
\end{aligned}$$

([11]) See, for example, E. C. KEMBLE: *Fundamental Principles of Quantum Mechanics* (New York, 1937), p. 320.

([12]) J. VON NEUMANN: *Mathematische Grundlagen der Quantenmechanik* (New York, 1943), p. 157.

because of the properties of the Trace, and

$$\leqslant 2 \operatorname{Tr} \varrho(\sigma_\alpha - \bar{\sigma}_\alpha)^2 + 2 \left| \operatorname{Tr} \varrho^{\frac{1}{2}}(\sigma_\alpha - \bar{\sigma}_\alpha) \varrho^{\frac{1}{2}}(\sigma_\alpha - \bar{\sigma}_\alpha) \right| .$$

The last quantity can be simplified by using Schwartz's inequality. Then it can be shown that

$$\left| \operatorname{Tr} \varrho^{\frac{1}{2}}(\sigma_\alpha - \bar{\sigma}_\alpha) \varrho^{\frac{1}{2}}(\sigma_\alpha - \bar{\sigma}_\alpha) \right| \leqslant \operatorname{Tr} \varrho(\sigma_\alpha - \bar{\sigma}_\alpha)^2$$

so that

$$\operatorname{Tr} [\varrho^{\frac{1}{2}}(\sigma_\alpha - \bar{\sigma}_\alpha) - (\sigma_\alpha - \bar{\sigma}_\alpha)\varrho^{\frac{1}{2}}]^2 \leqslant 4 \operatorname{Tr} \varrho(\sigma_\alpha - \bar{\sigma}_\alpha)^2 \tag{2.13}$$

which vanishes, as shown above, for $\bar{\sigma}_\alpha = 0, 1$. Hence

$$\varrho\sigma_\alpha - \sigma_\alpha\varrho = \mathbf{0} , \qquad \text{if} \quad \bar{\sigma}_\alpha = 0, 1 . \tag{2.14}$$

3. – Construction of classification operators.

The utility of any theory involving species-classification operators depends, at the outset, upon the ease with which they may be constructed. Since the relevant measurement processes which furnish the criteria for the classifications are capable of considerable variety it is desirable to keep the theory general enough to accommodate whatever criteria may be deemed necessary. On the other hand, it is necessary to be explicit to the extent of indicating clearly what must be done—and how—in instances which may arise, even if the procedure is a formal one.

To that end, let the criteria employed in describing the system as consisting of the α species-set comprise certain measured values of a set of commuting observables $\xi_1 \dots \xi_N$. Let such a set of values of these variables be designated by $\boldsymbol{\xi}$. Then if the set of values of these variables taken to identify the species-set α is designated as M_α, one has the statement

$$\text{« species-set } \alpha \text{ »} \leftrightarrow (\boldsymbol{\xi} \in M_\alpha) . \tag{3.1}$$

If the remaining set of values, the complement of M_α, is designated by $M_{\alpha'}$, one has

$$\text{« species-set non-}\alpha \text{ »} = \text{« species-set } \alpha' \text{ »} \leftrightarrow (\boldsymbol{\xi} \in M_{\alpha'}) . \tag{3.2}$$

Clearly, M_α and $M_{\alpha'}$ have been constructed to be disjoint and the set of values $M_{\alpha+\alpha'}$ includes the totality of measured values of the variables.

Now, if $\langle x | \xi_1 \dots \xi_N \rangle$ represents a normalized eigenfunction of the variables

it is evident that the representative (*)

$$S_\alpha(x', x) \equiv \sum_{\xi \in M_\alpha} \langle x \,|\, \xi_1 \dots \xi_N \rangle \langle \xi_1 \dots \xi_N \,|\, x' \rangle \tag{3.3}$$

satisfies, in accordance with eq. (2.3), the relation

$$S_\alpha(x', x) = \int \mathrm{d}x''\, S_\alpha(x', x'')\, S_\alpha(x'', x)\,, \tag{3.4}$$

where it has been supposed that

$$\langle \xi_1' \dots \xi_N' \,|\, \xi_1 \dots \xi_N \rangle = \delta_{\xi', \xi}\,.$$

It can be seen that, with eq. (2.1), eq. (3.3) yields the usual expression for the probability of an observable having a certain range of values (**).

Now, when it comes to a characterization of the β set of species, the previous formalism may be used with the modification

$$\text{« species-set } \beta \text{ »} \leftrightarrow (\xi \in M_\beta)\,, \quad \text{etc.} \tag{3.5}$$

If M_α and M_β are not disjoint it is clearly impossible to satisfy eq. (2.4). However, it readily can be verified when S_β is of the form of eq. (3.3) that

$$S_\alpha S_\beta = S_\beta S_\alpha\,. \tag{3.6}$$

By construction, this relation is an expected one, and represents a necessary condition for S_α and S_β to be elements of a Boolean algebra. If they are not orthogonal the choice of M_α and M_β has been made in such a way as to vitiate any precise distinguishability between these sets of species. In actual fact this may be the case, whereupon no further elaboration of the projection operators is necessary. On the other hand, if distinguishability is regarded as a logical necessity, the operators are clearly unsuitable.

For distinguishable sets of species, the desired orthogonality is that possessed by the minimal elements of the algebra. To achieve this result the choice of either M_α and M_β or both may, of course, be modified. However, if one understands these criteria as they stand to be reasonably good approximations to the desired ones the modification can be effected in a systematic way. The minimal elements of a Boolean algebra consist of the non-null products of each of the elements or its complement. Thus, for an algebra con-

(*) See, for example, ref. (9), pp. 53 and 67.

(**) Ref. (9), p. 47.

sisting of S_α, S_β, I, and their complements one verifies that the minimal elements are

$$S_\alpha(I - S_\beta), \quad S_\beta(I - S_\alpha), \quad S_\alpha S_\beta \quad \text{and} \quad (I - S_\alpha)(I - S_\beta).$$

The first of these represents « species-set α and not species-set β »; the second represents « species-set β and not species-set α »; the remaining two represent « both species-set α and species-set β » and « neither species-set α nor species-set β ». In these terms, a typical minimal element is

$$(3.7) \quad [S_\alpha(I - S_\beta)](x', x) = \sum_{\xi \in M_\alpha} \langle x | \xi_1 \dots \xi_N \rangle \langle \xi_1 \dots \xi_N | x' \rangle - \sum_{\xi \in M_{\alpha\beta}} \langle x | \xi_1 \dots \xi_N \rangle \langle \xi_1 \dots \xi_N | x' \rangle,$$

where $M_{\alpha\beta}$ is the set of values of ξ common to M_α and M_β (*i.e.*, their intersection). This element may be identified with the minimal element σ_α.

It is evident that the elements $S_\alpha S_\beta$ and $(I - S_\alpha)(I - S_\beta)$ represent minimal elements of dubious physical significance, if only two mutually exclusive classifications of the system are desired or deemed necessary. They reflect, of course, the original inadequacies in the criteria employed to characterize the intended classifications. They refer, together, to a « new species-set » required to satisfy the condition of completeness, as discussed in the previous section.

4. – Composition operators and variables.

To this point the description has been directed towards microscopic systems but is entirely general and applies equally well to macroscopic systems. However, the prevalent situation in macroscopic systems is one in which the number of distinct species considered is negligible compared with the number of fundamental particles. The system usually is regarded as having been partitioned into distinct sub-systems of particles and each of the latter is accorded some one of a limited set of species-classifications. Clearly, the limited set is arbitrary but is justifiable pragmatically. In part, the justification relates to the fact that macroscopic systems generally consist of large numbers of identical particles. Ultimately, all partitions which are related to one another by a permutation of identical particles must be regarded as indistinguishable from each other. The set of such partitions evidently is characteristic of a particular *composition* of the macroscopic mixture, and vice versa.

The construction of composition operators can be carried out in terms of the species-classification operators for the subsystems. Considering, for the moment, all particles to be distinguishable one may imagine a particular partition of the system into subsystems which may be classified meaningfully as

α-species, β-species, etc. Inasmuch as each particle is to be regarded as a member of one and only one species (*i.e.*, subsystem), the (macroscopic) operator corresponding to the imagined partition of the system will consist of a product of relevant species-classification operators (the S-operators of the previous section) and complementary species-classification operators (to be referred to as S'-operators). The relevant co-ordinates of each particle of the system appear in one and only one S-operator (*); they appear in more than one S'-operator. The latter refer to those potential subsystems into which the relevant particles have *not* been placed. As a result, the operator which corresponds to the imagined partition may be seen to have the form

$$\chi_{NML} = \{\prod_{i=1}^{N} S_{\alpha_i} \prod_{j=1}^{M} S_{\beta_j} \prod_{k=1}^{L} S_{\gamma_k} \dots\} \{\prod_{i=1}^{N'} S'_{\alpha_i} \prod_{j=1}^{M'} S'_{\beta_j} \dots\}, \tag{4.1}$$

corresponding to N subsystems of the α-species, M subsystems of the β-species, etc. N', M', etc., refer to all potential subsystems corresponding to the α-species, β-species, etc., into which the relevant particles have *not* been placed (**).

By selecting appropriate factors from Eq. (4.1), one may verify that χ_{NLM} generally cannot be expressed simply as the direct product of two χ-operators, each of which depends upon disjoint particle sub-spaces. Thus, for $N = N_1 + N_2$, $M = M_1 + M_2$, $L = L_1 + L_2$, one can obtain

$$\chi_{NML} = \chi_{N_1 M_1 L_1}(1) \chi_{N_2 M_2 L_2}(2) \zeta(1, 2), \tag{4.2}$$

where 1, 2 refer to distinct sets of particles, χ has the form of Eq. (4.1) and $\zeta(1, 2)$ consists entirely of complementary factors from Eq. (4.1), and depends

(*) In this manner stoichiometric relations are maintained automatically. One may note here that the partitioning referred to is not necessarily one involving only the configurational co-ordinates, but refers to those upon which the classification depends.

(**) One may note here that the species-classification operators pertaining to *basic particles*, such as electrons and nuclei in the present context, will have a form different from that implied in Eq. (4.1). The S-operator for a basic particle is simply the identity operator in the appropriate particle subspace, corresponding to the statement that the basic particle is certainly included in the system regardless of the state of the latter. Clearly, however, the complement of the identity operator is the null operator, the presence of which would nullify Eq. (4.1). As a result, Eq. (4.1) will be supposed to refer exclusively to *composite entities*, the species classifications involving basic particles as species being regarded as complementary to those referring to composite entities. In other words, no S-operators or S'-operators depending explicitly upon the co-ordinates of a single basic particle of the system are presumed to be included among the factors of Eq. (4.1).

upon all particles but contains no factors depending upon particle co-ordinates of either set alone (*). To take $\zeta(1, 2)$ equal to the identity is justified for the condition of complete isolation of the two subsystems with respect to particle exchange. The presence of $\zeta(1, 2)$ is necessary to assure one that the partition of the system which corresponds to Eq. (4.2) is distinguishable from any other (considering, for the moment, that all particles are distinguishable from one another). It is evidently symmetric with respect to exchanges of identical particles of each particle set among themselves.

A particular form of Eq. (4.2) which will be useful later refers to a certain microscopic subsystem as well as to the residual macroscopic subsystem. To illustrate,

$$\chi_{NML} = \sigma(\alpha_i, \beta_j)\, \chi_{N-1, M-1, L}\, \zeta_{N-1, M-1, L}(\alpha_i, \beta_j)\,, \tag{4.3}$$

where $\sigma(\alpha_i, \beta_j)$ is one of the minimal elements described in the previous section and depends only upon the particles associated with the pair ot species (α_i, β_j); $\chi_{N-1, M-1, L}$, of the form of Eq. (4.1), depends only upon particle co-ordinates different from the pair (α_i, β_j); $\zeta(\alpha_i, \beta_j)$, as previously described, has no factors depending only upon or independent of the pair (α_i, β_j).

On may note, for a $\chi_{N_1 M_1 L_1}$ of the form of Eq. (4.1) but which depends upon a particle subspace of the original system, that, in accord with Eq. (4.2),

$$\chi_{N_1 M_1 L_1}\, \chi_{NML} = \chi_{N-N_1,\, M-M_1,\, L-L_1}\, \chi_{N_1 M_1 L_1}\, \xi_{(N-N_1,\, M-M_1,\, L-L_1;\, N_1, M_1, L_1)} \qquad \text{or} \qquad \mathbf{0}\,,$$

$$\text{with} \quad N_1 \leqslant N\,, \quad M_1 \leqslant M\,, \quad L_1 \leqslant L\,.$$

The vanishing result occurs for any partition of the system in which the relevant subsystem is not partitioned in precisely the same manner as implied in $\chi_{N_1 M_1 L_1}$. This can be seen to follow from the form of the χ's where each particle (regarded as distinguishable from all others at this point) must occur in corresponding factors in the two χ's for a non-vanishing result to obtain. (See the restriction noted in (*).)

By construction, χ's which correspond to different partitions of the total system, produced either by permutation of identical particles or otherwise, are either orthogonal or identical. The totality of all operators which result from the permutation of the coordinates of identical particles in χ_{NML} characterize a macroscopic system of stated composition. Their union may be termed a *composition operator* and is given by [8]

$$X_{NML\ldots} = \Big(\prod_P \chi'_{NML\ldots}\Big)'\,, \tag{4.4}$$

(*) See preceding page, footnote (**).

the product of the complements extending over all permutations of the co-ordinates of identical particles. By construction, one has

$$X_{NML\ldots} = \sum_P{}' \chi_{NML\ldots}, \tag{4.5}$$

the summation here extending over all « distinguishable » permutations, *i.e.*, those which effectively exchange a particular kind of particle from one subsystem to a different one. Clearly, also by construction,

$$X_{N_1M_1L_1\ldots}X_{N_2M_2L_2\ldots} = X_{N_1M_1L_1\ldots}\delta_{N_1N_2}\delta_{M_1M_2}\delta_{L_1L_2\ldots}, \tag{4.6}$$

this statement asserting the distinguishability of different compositions of the system. The X's (forall possible values of N, M, L, etc.) comprise the physically meaningful minimal elements of the algebra which describes the system precisely in terms of the numbers of α-species, β-species, etc. (*). They obviously satisfy eqs. (2.3) and (2.4).

The remarks concluding Section 3 are relevant here, since the construction given does not generate all possible classifications of the system. Therefore, not all possible « composition » operators have been listed. To see this, note that in the construction of each χ only those partitions have been considered which regard each particle as a member of one and only one subsystem. Clearly, and in spite of their dubious physical significance, classifications which regard some or all of the particles as members of more than a single subsystem must be included for completeness. An indication of the awkwardness introduced by this inclusion arises when one wishes to refer to the composition associated with a corresponding operator. In fact, it is not possible to regard such operators as depending only upon N, M, L, etc. As a result, these operators will be considered collectively and represented by a single projection operator, X^*

(*) From the measurement viewpoint, the expectation values of the X's are to be identified with the probability that a random choice of some portion of the macroscopic system yields the (relative) composition related to the particular composition operator considered. When the system consists of a spatially non-uniform mixture, the information may be presumed to be incorporated in the X's, and specifically in the S-operators and their complements. As a result *different* X's may be envisaged which, nevertheless, correspond to the same macroscopic composition. For uniform, or homogeneous mixtures, the X's and the S'-operators may be expected to depend only upon the relative co-ordinates of the various particles. Alternatively, spatially non-uniform mixtures may be described in terms of *composition-density* operators, referring to a uniform mixture in a small unit volume, together with an appropriate statistical matrix to specify the non-uniformity. This procedure, however, will not be considered since the present considerations refer implicitly to spatially uniform mixtures.

which is orthogonal to each of the X_{NML}. The completeness relations, Eq. (2.5) becomes (*)

$$\sum_{NML} X_{NML} + X^* = I \,. \tag{4.7}$$

The description of a system in terms of mixtures of several species carries with it the tacit implication that many of the properties of the system can be expressed adequately in such terms. If such a property is represented by the operator G, the « composition-description » implies that

$$G \doteq \sum_{NML\ldots} X_{NML\ldots} G X_{NML\ldots} + X^* G X^* \,, \tag{4.8}$$

which generally is satisfied in a least-squares sense (8). Unless there exist some properties of the system which permit the representation implied by eq. (4.8), there is a moot point regarding the validity of a « composition-description ». Clearly, when G commutes with the composition operators the relation is an exact one. Such a property evidently is the number of each species. Thus, one may obtain

$$N \equiv \sum_{N, M, L\ldots} N X_{NML\ldots} + N^*(X^*) \,, \tag{4.9}$$

$$M \equiv \sum_{N, M, L\ldots} M X_{NML\ldots} + M^*(X^*) \,, \quad \text{etc.} \,, \tag{4.10}$$

as the operators corresponding to the numbers of α-species, β-species, etc. The N^* and M^* reflect inadequacies in the normalization of the X_{NML}, as discussed previously. They may be presumed to depend upon the « composition-operators » tacitly included in X^* and possibly upon the time. Unless they are generally small, the composition description will be a poor one.

A simplification occurs with expressions which are linear in the X's and this will be examined here. For definiteness, consider the quantity

$$\mathrm{Tr}\{G X_{NML\ldots}\} = \mathrm{Tr}\{G \sum_{P}{}' \chi_{NML\ldots}\}, \tag{4.11}$$

(*) One should keep in mind that in accord with footnote on page 347 the summation over compositions is actually effected over a set of values of N, M, L, etc., which are consistent with the stoichiometry. Not all values of N, M, L, etc., are included, nor are they generally capable of being changed independently of one another. Clearly, when certain of the species are not convertible to one another, directly or otherwise, these species are stoichiometrically independent of one another. The particle subspaces of such species are disjoint from those of other species and always remain so; as a result every composition operator of the form of Eq. (4.5) separates into factors, with each factor pertaining to the relevant disjoint particle subspace. This situation corresponds to a construction of the composition operators from χ's of the form of Eq. (4.2) in which ζ (1, 2) has been set equal to unity.

making use of eq. (4.5). For G symmetric with respect to permutations of identical particles but otherwise arbitrary it is evident that

$$\mathrm{Tr}\{GX_{NML\ldots}\} = \mathrm{Tr}\{\sum_P{}' GX_{NML\ldots}\}. \tag{4.12}$$

The basis of functions employed to evaluate the trace may be presumed to be appropriately symmetrized with respect to permutations of identical particles (*i.e.* Fermi-Dirac or Bose-Einstein statistics). As a result, each term of the sum indicated in eq. (4.12) will yield an identical value for its trace. The evaluation of eq. (4.12) requires, accordingly, the value obtained for one particular $\chi_{NML\ldots}$ and the number of « distinguishable » permutations of identical particles possible for the identical composition. Clearly the number of such « distinguishable » permutations of identical particles is independent of G so long as the latter is symmetric with respect to such permutations. Hence one may write

$$\frac{\mathrm{Tr}\, GX_{NML\ldots}}{\mathrm{Tr}\, G\chi_{NML\ldots}} = \frac{\mathrm{Tr}\, \varrho X_{NML\ldots}}{\mathrm{Tr}\, \varrho\chi_{NML\ldots}}, \tag{4.13}$$

where ϱ is any other symmetric operator and, in particular, is the density matrix to be employed later. One may note that $\chi_{NML\ldots}$ refers to any particular partition of the system corresponding to the indicated composition.

5. – Equation of motion.

Since the description of a system in terms of various species which consist of collections of the fundamental particles is necessarily approximate, one expects —and confirms experimentally—that such descriptions must change with time. The rates at which changes occur provide, in fact, an important means of characterizing the system.

The basic species-classification operators, for simplicity, have been assumed not to depend explicitly upon the time. As a consequence, the operator corresponding to the time rate of change of X_{NML} is given by Heisenberg's equation of motion (*)

$$i\hbar\dot{X}_{NML} = X_{NML}H - HX_{NML} = [X_{NML}, H], \tag{5.1}$$

where H is the Hamiltonian for the macroscopic system. The expectation value of this operator gives the time rate of change of probability of the system

(*) See, for example, reference (9), pp. 111-116.

having the indicated composition. When the description requires an ensemble of systems, the ensemble average for the same quantity is (noting that $\mathrm{Tr}\,\varrho = 1$)

$$\begin{aligned}(5.2)\qquad \langle \dot{X}_{NML} \rangle &= \mathrm{Tr}\,\varrho \dot{X}_{NML} = \mathrm{Tr}\,\varrho [X_{NML}, H]/i\hbar\,, \\ &= \mathrm{Tr}\, X_{NML}\,[H, \varrho]/i\hbar\,, \\ &= \mathrm{Tr}\, X_{NML} \frac{\partial \varrho}{\partial t}\,,\end{aligned}$$

because of the properties of the trace. As a result, the composition changes which occur can be regarded *equivalently* as either the ensemble average of the time rate of change of the composition operators *or* the composition average of the time rate of change of the statistical matrix. One may note that eq. (5.2) vanishes if any pair of ϱ, H and X_{NML} commute. Accordingly, the description of a *changing* system requires that all the composition operators cannot commute with the Hamiltonian. Similarly, they all cannot commute with the statistical matrix. However, one may elect to adopt criteria of species-classification for which the latter condition is imposed at one instant of time (*); no difficulty ensues thereby, for the temporal evolution of the statistical matrix provides a means of subsequently relaxing this condition (**).

The time rate of change of the average number of α-species is obtained as

$$(5.3)\qquad i\hbar \langle \dot{N} \rangle = \sum_{NML} N\, \mathrm{Tr}\,\varrho [X_{NML}, H] + i\hbar \frac{\mathrm{d}}{\mathrm{d}t} \langle N^* \rangle\,.$$

It is convenient to introduce the normalization equation (4.7), at this point, whereupon

$$\begin{aligned}(5.4)\qquad i\hbar \langle \dot{N} \rangle &= \sum_{NML} N \sum_{N'M'L'} \mathrm{Tr}\,\varrho \{X_{NML} H X_{N'M'L'} - X_{N'M'L'} H X_{NML}\} + \\ &\quad + \sum_{NML} N\, \mathrm{Tr}\,\varrho \{X_{NML} H X^* - X^* H X_{NML}\} + i\hbar \frac{\mathrm{d}}{\mathrm{d}t} \langle N^* \rangle\,, \\ &= \sum_{NML} \sum_{N'M'L'} (N - N')\, \mathrm{Tr}\,\varrho \{X_{NML} H X_{N'M'L'}\} - \\ &\quad - \sum_{NML} N\, \mathrm{Tr}\,\varrho [[X^*, H], X_{NML}]_{(+)} + i\hbar \frac{\mathrm{d}}{\mathrm{d}t} \langle N^* \rangle\,,\end{aligned}$$

(*) One may note that frequently such a restriction corresponds to an initial condition imposed upon a changing system.

(**) A similar situation prevails with regard to the basis employed to evaluate eq. (5.2). Suppose that for a certain instant of time the basis which diagonalizes ϱ consists entirely of real functions. For the special circumstance where X is a real operator, one obtains a null result. This is a situation which will not necessarily persist since the temporal evolution of ϱ generally requires its eigenfunctions to be complex.

the (+) subscript referring to the anti-commutator. To simplify this equation it is possible to *define* N^* of eq. (4.9) so that it satisfies the differential equation

$$i\hbar \frac{\mathrm{d}}{\mathrm{d}t}\langle N^*\rangle = \sum_{NML} N \operatorname{Tr} \varrho[[X^*, H], X_{NML}]_{(+)}\,, \tag{5.5}$$

which yields, upon substitution into eq. (5.4),

$$i\hbar\langle \dot{N}\rangle = \sum_{NML} \sum_{N'M'L'} (N - N') \operatorname{Tr} \varrho\{X_{NML} H X_{N'M'L'}\}\,. \tag{5.6}$$

This expression ostensibly consists entirely of physically significant terms.

With no undue loss of generality, the Hamiltonian of the system may be supposed to depend upon binary particle interactions, *viz.*,

$$H = \sum_i H(i) + \sum_{i>j} \sum_j H(i, j)\,.$$

As a consequence, the Hamiltonian is simply expressed in terms of the various species. For arbitrary composition, as well as partition,

$$H = \sum_{i=1}^{N} H(\alpha_i) + \sum_{j=1}^{M} H(\beta_j) + \ldots + \tfrac{1}{2}\sum_{i\neq j}^{N}\sum_{j=1}^{N} H(\alpha_i, \alpha_j) + \sum_{i=1}^{N}\sum_{j=1}^{M} H(\alpha_i, \beta_j) + \ldots\,, \tag{5.7}$$

α_i, β_j, etc., here standing for the co-ordinates of the particles comprising the respective species. Single particle Hamiltonians are presumed to be included only in $H(\alpha_i)$, $H(\beta_j)$, etc. With this form of the Hamiltonian, a reduction of eq. (5.6) is possible.

For this purpose, consider a typical term of eq. (5.6)

$$\sum_{N'M'L'} (N - N') \operatorname{Tr} \varrho\{X_{NML} H X_{N'M'L'}\} = \tag{5.8}$$

$$= \sum_{N'M'L'} (N - N') \frac{\langle X_{NML}\rangle}{\langle \chi_{NML}\rangle} \operatorname{Tr} \varrho\{\chi_{NML} H X_{N'M'L'}\}\,,$$

where use has been made of eq. (4.13). χ_{NML} refers to a specific partition of the system for which H may be given the form of eq. (5.7). Then a typical term of eq. (5.8) is

$$\sum_{N'M'L'} (N - N') \frac{\langle X_{NML}\rangle}{\langle \chi_{NML}\rangle} \operatorname{Tr} \varrho\{\chi_{NML} H(\alpha, \beta) X_{N'M'L'}\} = \tag{5.9}$$

$$= \sum_{N'M'L'} (N - N') \frac{\langle X_{NML}\rangle}{\langle \chi_{NML}\rangle} \operatorname{Tr} \varrho\{\sigma_i(\alpha, \beta)\, \xi_{\substack{N-1\\M-1\\L}}(\alpha, \beta)\, H(\alpha, \beta)\, \chi_{\substack{N-1\\M-1\\L}} X_{N'M'L'}\}\,,$$

where eq. (4.3) has been used and $\sigma_i(\alpha, \beta)$ is the minimal classification operator of the (α, β) particle subspace which corresponds to an α-species and a β-species. It corresponds to a partition implicit in the original choice taken for χ_{NML} (*).

Now because of the properties of the χ's and the X's it is evident that the right side of eq. (5.9) consists of non-vanishing terms for which

$$\chi_{\substack{N-1\\M-1\\L}} X_{N'M'L'} = \chi_{\substack{N-1\\M-1\\L}} \Big\{ \sum_{(\alpha,\beta)} \sigma_f(\alpha, \beta) \Big\} \zeta_{\substack{N-1\\M-1\\L}}(\alpha, \beta) , \tag{5.10}$$

where $\sigma_f(\alpha, \beta)$ is any one of the minimal classification operators of the indicated particle subspace and the summation extends over the « distinguishable » permutations of the identical particle comprising the pair (α, β) (**).

From eq. (5.10), the changes in composition which may be attributed to the interaction term $H(\alpha, \beta)$ are restricted to those which involve a decomposition or rearrangement of the pair (α, β); and this equation describes the « selection rules » for such changes. It is convenient to introduce the stoichiometry explicitly for these changes. Clearly $\{N', M', L'\}$ is restricted in the illustration considered to

$$\begin{cases} N' = N - \nu_{if}{}^{\alpha\beta} \\ M' = M - \mu_{if}{}^{\alpha\beta} \\ L' = L - \lambda_{if}{}^{\alpha\beta} \end{cases} \tag{5.11}$$

where the ν's, μ's and λ's are integers which depend upon the « initial » and « final » classification of the indicated species subspace. (Note that $\nu_{jk}{}^{\alpha\beta} = -\nu_{kj}{}^{\alpha\beta}$.) With these expressions, eq. (5.9) becomes (using the properties of the trace)

$$\sum_{N'M'L'} (N - N') \frac{\langle X_{NML} \rangle}{\langle \chi_{NML} \rangle} \operatorname{Tr} \varrho \{ \chi_{NML} H(\alpha, \beta) X_{N'M'L'} \} =$$

$$= \sum_f \nu_{if}{}^{\alpha\beta} \frac{\langle X_{NML} \rangle}{\langle \chi_{NML} \rangle} \operatorname{Tr} \Big[\chi_{\substack{N-1\\M-1\\L}} \zeta_{\substack{N-1\\M-1\\L}}(\alpha, \beta) \varrho \zeta_{\substack{N-1\\M-1\\L}}(\alpha, \beta) \chi_{\substack{N-1\\M-1\\L}} \sigma_i(\alpha, \beta) H(\alpha, \beta) \sigma_f(\alpha, \beta) \Big] , \tag{5.12}$$

where the summation over f implicitly includes the distinguishable permutations over $\sigma_f(\alpha, \beta)$.

A further simplification is possible because of the form of the quantity in brackets. Inasmuch as its trace is needed, it is convenient to define a *reduced*

(*) See page 345, footnote (**)

(**) The symmetry of ζ, mentioned previously, permits the permutations to be carried out over $\sigma_f(\alpha, \beta)$ alone.

statistical matrix

$$\bar{\varrho}_{\substack{N-1\\M-1\\L}}(\alpha,\beta) \equiv \frac{\operatorname{Tr}_{\{\substack{N-1\\M-1\\L}\}} \{\chi_{\substack{N-1\\M-1\\L}} \zeta_{\substack{N-1\\M-1\\L}}(\alpha,\beta)\varrho\zeta_{\substack{N-1\\M-1\\L}}(\alpha,\beta)\chi_{\substack{N-1\\M-1\\L}}\}}{\langle\chi_{\substack{N-1\\M-1\\L}}\zeta_{\substack{N-1\\M-1\\L}}(\alpha,\beta)\rangle}, \tag{5.13}$$

the first trace referring to a partial trace over particle co-ordinates different from those comprising the pair (α, β). The reduced statistical matrix evidently is definite when ϱ is definite, and is normalized to unity. For sufficiently large values of $\{N, M, L\}$ it plausibly may be presumed not to depend markedly upon their precise values. Then eq. (5.12) becomes

$$\sum_{N'M'L'}(N-N')\frac{\langle X_{NML}\rangle}{\langle\chi_{NML}\rangle}\operatorname{Tr}\varrho\{\chi_{NML}H(\alpha,\beta)X_{N'M'L'}\} = \tag{5.14}$$

$$= \sum_f \nu_{jf}^{\alpha\beta}\frac{\langle X_{NML}\rangle\langle\chi_{\substack{N-1\\M-1\\F}}\zeta_{\substack{N-1\\M-1\\L}}(\alpha,\beta)\rangle}{\langle\chi_{NML}\rangle}\operatorname{Tr}\bar{\varrho}_{\substack{N-1\\M-1\\L}}(\alpha,\beta)\sigma_i(\alpha,\beta)H(\alpha,\beta)\sigma_f(\alpha,\beta),$$

where the final trace is carried out over particle subspace corresponding to (α, β).

It is evident that the quantity

$$\frac{\langle\chi_{NML}\rangle}{\langle\chi_{\substack{N-1\\M-1\\L}}\zeta_{\substack{N-1\\M-1\\L}}(\alpha,\beta)\rangle} = \frac{\langle\chi_{\substack{N-1\\M-1\\L}}\zeta_{\substack{N-1\\M-1\\L}}(\alpha,\beta)\sigma_i(\alpha,\beta)\rangle}{\langle\chi_{\substack{N-1\\M-1\\L}}\zeta_{\substack{N-1\\M-1\\L}}(\alpha,\beta)\rangle} - \operatorname{Tr}\bar{\varrho}_{\substack{N-1\\M-1\\L}}(\alpha,\beta)\sigma_i(\alpha,\beta), \tag{5.15}$$

may be interpreted as the *conditional probability* that if the system is partitioned so as to consist of a (macroscopic) subsystem containing $(N-1)$ α-species, $(M-1)$ β-species, etc., the total system will consist also of N α-species, M β-species, etc. Hence eq. (5.13) becomes

$$\sum_{N'M'L'}(N-N')\frac{\langle X_{NML}\rangle}{\langle\chi_{NML}\rangle}\operatorname{Tr}\varrho\{\chi_{NML}H(\alpha,\beta)X_{N'M'L'}\} = \tag{5.16}$$

$$= \sum_f \nu_{jf}^{\alpha\beta}\langle X_{NML}\rangle\frac{\operatorname{Tr}\bar{\varrho}_{\substack{N-1\\M-1\\L}}(\alpha,\beta)\{\sigma_i(\alpha,\beta)H(\alpha,\beta)\sigma_f(\alpha,\beta)\}}{\operatorname{Tr}\bar{\varrho}_{\substack{N-1\\M-1\\L}}(\alpha,\beta)\sigma_i(\alpha,\beta)}.$$

Similar terms involving the various $H(\alpha_i, \beta_j)$ from eq. (5.7) will give identical results. Consequently, the total contribution from such terms may be expressed as the product of NM and the right side of eq. (5.16). The resulting expression then is to be summed over all allowed values of $\{N, M, L,$ etc.$\}$.

Before carrying out this operation it is convenient to render eq. (5.16) in

a more symmetrical form than has been given. To do this, one may evaluate the terms of eq. (5.6) by inverting the order of summation over $\{N, M, L\}$ and $\{N', M', L'\}$. The result must be identical with that which has been obtained. Omitting the details, one obtains ultimately for the time rate of change of the average number of α-species:

$$(5.17)\quad \langle \dot{N} \rangle = \frac{1}{2i\hbar} \sum_{NML} \sum_{f} \nu_{if}{}^{\alpha} N \langle X_{NML} \rangle \frac{\operatorname{Tr} \bar{\varrho}_{\substack{N-1 \\ M \\ L}}(\alpha)\{\sigma_i(\alpha) H(\alpha) \sigma_f(\alpha) - \sigma_f(\alpha) H(\alpha) \sigma_i(\alpha)\}}{\operatorname{Tr} \bar{\varrho}_{\substack{N-1 \\ M \\ L}}(\alpha) \alpha \sigma_i(\alpha)} +$$

$$+ \text{analogous terms in } M, L, \text{ etc.} + \frac{1}{2i\hbar} \sum_{NML} \sum_{f} \nu_{if}{}^{\alpha\alpha} \frac{N(N-1)}{2} \langle X_{NML} \rangle \cdot$$

$$\cdot \frac{\operatorname{Tr} \bar{\varrho}_{\substack{N-2 \\ M \\ L}}(\alpha_1, \alpha_2)\{\sigma_i(\alpha_1, \alpha_2) H(\alpha_1, \alpha_2) \sigma_f(\alpha_1, \alpha_2) - \sigma_f(\alpha_1, \alpha_2) H(\alpha_1, \alpha_2) \sigma_i(\alpha_1, \alpha_2)\}}{\operatorname{Tr} \bar{\varrho}_{\substack{N-2 \\ M \\ L}}(\alpha_1, \alpha_2) \sigma_i(\alpha_1, \alpha_2)} +$$

$$+ \text{analogous terms in } M, L, \text{ etc.} + \frac{1}{2i\hbar} \sum_{NML} \sum_{f} \nu_{if}{}^{\alpha\beta} NM \langle X_{NML} \rangle \cdot$$

$$\cdot \frac{\operatorname{Tr} \bar{\varrho}_{\substack{N-1 \\ M-1 \\ L}}(\alpha, \beta)\{\sigma_i(\alpha, \beta) H(\alpha, \beta) \sigma_f(\alpha, \beta) - \sigma_f(\alpha, \beta) H(\alpha, \beta) \sigma_i(\alpha, \beta)\}}{\operatorname{Tr} \bar{\varrho}_{\substack{N-1 \\ M-1 \\ L}}(\alpha, \beta) \sigma_i(\alpha, \beta)} +$$

$$+ \text{analogous terms in } NL, ML, \text{ etc.}$$

Corresponding expressions obtain for the time rate of change of the average number of β-species, etc. Particular note is to be taken of the absence of terms in eq. (5.17) which are (explicitly) not linear or quadratic in $\{N, M, L, \text{etc.}\}$. One may note also that the several ν_{if} vanish for those transitions in which the relevant σ_i and σ_f do not correspond to a change in the number of α-species for the microscopic subsystem.

As noted earlier (*), the summation over $\{N, M, L, \text{etc.}\}$ is complicated somewhat by the fact that these quantities generally depend upon one another for a fixed system. For many purposes it is adequate to restrict one's attention to systems of relatively precise composition (**). Then those terms of eq. (5.7) which correspond to the (ensemble) mean values of $\{N, M, L, \text{etc.}\}$ and the various reduced statistical matrices for the mean composition of this system may be retained. In mathematical terms, such a simplification is pos-

(*) See page 348, fotnote (*).

(**) As shown in Appendix A, this condition implies that the relative rates of change of the number of each species is small.

sible for those mixtures for which

$$(5.18)\qquad \begin{cases} \langle (N-\langle N\rangle)^2\rangle \ll (\langle N\rangle)^2\,, \\ |\langle (N-\langle N\rangle)(M-\langle M\rangle)\rangle| \ll \langle N\rangle\langle M\rangle\,, \quad \text{etc.} \end{cases}$$

As a result, one obtains (restricted for simplicity to α, β and γ species)

$$(5.19)\qquad \langle \dot{N}\rangle \simeq \sum_{n+m+l-1} \frac{\langle N\rangle^n \langle M\rangle^m \langle L\rangle^l}{n!\,m!\,l!} \sum_f \nu_{if}^{(nml)} \frac{\bar{k}_{nml}(i\to f)}{\bar{\sigma}_i(n,m,l)}\,,$$

where n, m, l refer to the number of α, β and γ species, respectively, involved in the initial classification of the relevant microscopic subsystem,

$$(5.20)\qquad \bar{k}_{nml}(i\to f) = \\ = \frac{1}{2i\hbar}\,\mathrm{Tr}\,\bar{\varrho}_i(n,m,l)\,\{\sigma_i(n,m,l)\,H_i(n,m,l)\sigma_f - \sigma_f H_i(n,m,l)\,\sigma_i(n,m,l)\}\,,$$

with $\bar{\varrho}_i(n,m,l)$ the reduced statistical matrix evaluated for a composition corresponding to the (ensemble) mean value of the system, and

$$(5.21)\qquad \bar{\sigma}_i(n,m,l) = \mathrm{Tr}\,\bar{\varrho}_i(n,m,l)\,\sigma_i(n,m,l)\,.$$

σ_f depends upon the same particle subspace as $\sigma_i(n,m,l)$ but the dependence upon the number of species has been suppressed for the sake of clarity. One may note that the summation over f tacitly includes all « distinguishable » permutations of identical particles in σ_f, as described in Section **4**.

The evaluation of eq. (5.19) requires the statistical matrix to be specified in addition to the various classification operators and the Hamiltonian. Since specification of the statistical matrix at one instant of time determines its subsequent values, the equations for $\langle \ddot{N}\rangle$, $\langle \ddot{M}\rangle$, etc., generally are complicated functions of the time since both eqs. (5.20) and (5.21) may be expected to depend upon the time as well as the composition.

6. – Variational considerations.

The problem of formulating expressions for the rate of chemical change necessarily requires for its solutions a knowledge of thes tatistical matrix. However, one may notice from eqs. (5.20) and (5.21) that a specification of the various reduced statistical matrices is sufficient to determine the

$$\frac{k_{nml}(i\to f)}{\bar{\sigma}_i(n,m,l)}$$

(the remaining quantities being presumed known). A knowledge of these quantities permits eq. (5.19) to be evaluated.

As indicated in eq. (5.13), the reduced statistical matrices involve species-classification operators in addition to the statistical matrix for the system. Any alteration of the species-classification operators (*e.g.*, the criteria of species classification) will, consequently, alter the reduced statistical matrices even though the statistical matrix for the system is imagined as fixed in value (as a function of time). It is easy to imagine the reduced statistical matrices as capable of independent and arbitrary variation even if certain of the classification operators remain unchanged. When a proper choice is made of the latter one might suppose that the several $\bar{k}_{nml}(i \to f)$ would not be changed significantly by changes in the reduced statistical matrices of the foregoing sort. Indeed, one might be inclined to adopt such behavior of the $\bar{k}_{nml}(i \to f)$ for the proper choice of the species classification operators.

To that end, consider the conditions under which

$$\delta \operatorname{Tr} \bar{\varrho} A = 0 , \tag{6.1}$$

where $A \equiv (\sigma_i H \sigma_f - \sigma_f H \sigma_i)/i$, $\bar{\varrho} \equiv \tau\tau^\dagger$ with $\operatorname{Tr} \bar{\varrho} = 1$, and

$$\left\{ \begin{array}{l} \delta \operatorname{Tr} \bar{\varrho} \quad = 0 , \\ \delta \operatorname{Tr} \bar{\varrho} \sigma_i = 0 , \\ \delta \operatorname{Tr} \bar{\varrho} \sigma_f = 0 , \end{array} \right. \tag{6.2}$$

subject to otherwise arbitrary variations in τ and τ^+. Inasmuch as the hermitian and anti-hermitian parts of τ (and τ^+) arei ndependent, one readily obtains

$$\operatorname{Tr} \delta \left(\frac{\tau + \tau^+}{2} \right) [(\tau^+ A + A\tau) + \lambda(\tau^+ + \tau) + \alpha(\tau^+ \sigma_i + \sigma_i \tau) + \beta(\tau^+ \sigma_f + \sigma_f \tau)] + \tag{6.3}$$

$$+ \operatorname{Tr} \delta \left(\frac{\tau - \tau^+}{2} \right) [(\tau^+ A - A\tau) + \lambda(\tau^+ - \tau) + \alpha(\tau^+ \sigma_i - \sigma_i \tau) + \beta(\tau^+ \sigma_f - \sigma_f \tau)] = 0 ,$$

where λ, α, β are real constants. With appropriate choices of these constants it is evident that the constraints of eq. (6.2) are satisfied, in which case the variations are indeed arbitrary. Hence one can show that

$$A\tau + \lambda\tau + \alpha\sigma_i \tau + \beta\sigma_f \tau = 0 , \tag{6.4}$$

and the adjoint of this equation. Postmultiplication by τ^+ yields

$$A\bar{\varrho} + \lambda\bar{\varrho} + \alpha\sigma_i \bar{\varrho} + \beta\ \sigma_f \bar{\varrho} = 0 , \tag{6.5}$$

which may be regarded as determining the σ's in terms of $\bar{\varrho}$.

The constants may be determined readily. Taking the trace of eq. (6.5) yields

$$\mathrm{Tr}\,\bar{\varrho}A + \lambda + \alpha\,\mathrm{Tr}\,\bar{\varrho}\sigma_i + \beta\,\mathrm{Tr}\,\bar{\varrho}\sigma_f = 0\,. \tag{6.6}$$

Premultiplying eq. (6.5) by σ_i and adding to the result the adjoint of the result, taking the trace and noting that $\sigma_i A + A\sigma_i = A$, one obtains

$$\mathrm{Tr}\,\bar{\varrho}A + 2(\lambda + \alpha)\,\mathrm{Tr}\,\bar{\varrho}\sigma_i = 0\,. \tag{6.7}$$

Repetition of the previous procedure with σ_f yields

$$\mathrm{Tr}\,\bar{\varrho}A + 2(\lambda + \beta)\,\mathrm{Tr}\,\bar{\varrho}\sigma_f = 0\,. \tag{6.8}$$

Eqs. (6.6)–(6.8) yield the solution

$$\left\{\begin{array}{l} \lambda = 0\,, \\ \alpha = -\,\mathrm{Tr}\,\bar{\varrho}A/2\,\mathrm{Tr}\,\bar{\varrho}\sigma_i\,, \\ \beta = -\,\mathrm{Tr}\,\bar{\varrho}A/2\,\mathrm{Tr}\,\bar{\varrho}\sigma_f \end{array}\right. \tag{6.9}$$

Now, making use of the procedure which led to eqs. (6.7) and (6.8), but using A as the multiplication factor, one readily obtains

$$2\,\mathrm{Tr}\,\bar{\varrho}A^2 + (2\lambda + \alpha + \beta)\mathrm{Tr}\,\bar{\varrho}A = 0\,, \tag{6.10}$$

or, with eqs. (6.9),

$$(\mathrm{Tr}\,\bar{\varrho}A)^2 = \left(\frac{4\bar{\sigma}_i\bar{\sigma}_f}{\bar{\sigma}_i + \bar{\sigma}_f}\right)\mathrm{Tr}\,\bar{\varrho}A^2 = \left(\frac{4\bar{\sigma}_i\bar{\sigma}_f}{\bar{\sigma}_i + \bar{\sigma}_f}\right)(\overline{\sigma_i H\sigma_f H\sigma_i} + \overline{\sigma_f H\sigma_i H\sigma_f})\,, \tag{6.11}$$

where $\bar{\sigma} = \mathrm{Tr}\,\bar{\varrho}\sigma$, etc.

An inequality similar to eq. (6.11) is derived in Appendix B for $\bar{\varrho}$, σ_i, σ_f which need not satisfy eq. (6.5). One may show that, when eq. (6.5) holds the quantity $\mathrm{Tr}\,\bar{\varrho}(\sigma_i H\sigma_f + \sigma_f H\sigma_i)$ vanishes, under which conditions the inequality of the Appendix and eq. (6.11) are identical.

The significance of the variational treatment which has been given may be illuminated by a further examination of eq. (6.5). Clearly, this equation together with its adjoint yields

$$\bar{\varrho}A\sigma_f + \sigma_f A\bar{\varrho} = \frac{\mathrm{Tr}\,\bar{\varrho}A}{2\sigma_f}\,(\sigma_f\bar{\varrho} + \bar{\varrho}\sigma_f)\,. \tag{6.12}$$

In a representation which is diagonal in $\bar{\varrho}$, one may show that

$$A_{nn} = \mathrm{Tr}\,\bar{\varrho}A\frac{(\sigma_f)_{nn}}{\bar{\sigma}_f}\,, \qquad \bar{\varrho}_{nn} \neq 0\,, \tag{6.13}$$

which, since the quantity A_{nn} allows the interpretation of being the rate of transition $(i \to f)$ for the state n, expresses the *Principle of Detailed Balancing* for chemical transitions.

By eq. (6.13), A_{nn} is definite (positive or negative depending upon the sign of $\mathrm{Tr}\,\bar{\varrho}A$) for those $\bar{\varrho}_{nn} \neq 0$. If none of the $\bar{\varrho}_{nn}$ vanishes then $\mathrm{Tr}\,A$ does not vanish. This latter behavior, however, is unexpected: In the representation which diagonalizes the species-classification operators, the diagonal elements of A are null. As a consequence, the previous results for non-null $\mathrm{Tr}\,\bar{\varrho}A$ would appear to pertain to *incomplete ensembles* (*viz.*, some $\bar{\varrho}_{nn} = 0$). For *complete ensembles* (*viz.*, all $\bar{\varrho}_{nn} \neq 0$) consistency is assured if $\mathrm{Tr}\,\bar{\varrho}A$ is null. However, it is to be noted that the aforementioned limitations refer implicitly to discrete distributions of states and may be subject to modification for continuous distributions of states. The ensuing modifications will not be considered at this time.

It is possible to subject eq. (6.1) to even greater variation than that which has been considered. In particular, the σ's may be varied subject to certain conditions of constraint. It may be noted, however, that each $\bar{k}_{nml}(i \to f)$ is invariant to any change in H which leaves $(\sigma_i H\sigma_f + \sigma_f H\sigma_i)$ invariant. As a result it proves convenient to consider

$$\delta\,\mathrm{Tr}\,\bar{\varrho}[\sigma_i(H - \sigma_i^0 H\sigma_i^0 - \sigma_f^0 H\sigma_f^0)\sigma_f - \sigma_f(H - \sigma_i^0 H\sigma_i^0 - \sigma_f^0 H\sigma_f^0)\sigma_i] = 0\,, \tag{6.14}$$

where σ_i^0, σ_f^0 are arbitrary, fixed orthogonal projection operators to be specified subsequently (*). Eq. (6.14) is subject to the following constraints:

$$\begin{cases} \sigma_i\delta\sigma_i + \delta\sigma_i\sigma_i = \delta\sigma_i\,, \\ \sigma_f\delta\sigma_f + \delta\sigma_f\sigma_f = \delta\sigma_f\,, \\ (\sigma_i + \sigma_f)\delta(\sigma_i + \sigma_f) + \delta(\sigma_i + \sigma_f)(\sigma_i + \sigma_f) = \delta(\sigma_i + \sigma_f)\,, \end{cases} \tag{6.15}$$

corresponding to the orthogonal, projection character of the varied σ_i and σ_f. Eqs. (6.2) also are to be invoked. However, since the variations in $\bar{\varrho}$ already

(*) One may note that the effect of the modification in H appearing in eq. (6.14) is to remove certain portions of it which are diagonal in the representation diagonalizing σ_f^0 and σ_f^0. In particular, the subsequent identification of these operators with those involved in the solution of the variational equations has the important effect of removing the effect of any arbitrary constant in H.

have been considered, only the variations in σ_i and σ_f need further investigation. Omitting the details for the sake of brevity, one obtains ultimately (*) the equations

$$(6.16) \quad -i\{(1-\sigma_f)H\sigma_f\bar{\varrho}-\bar{\varrho}\sigma_f H(1-\sigma_f)\}+\gamma_1(\bar{\varrho}\sigma_i+\sigma_i\bar{\varrho})+\mu(\bar{\varrho}\sigma_f+\sigma_f\bar{\varrho}-2\bar{\varrho})=0\,,$$

and

$$(6.17) \quad -i\{\bar{\varrho}\sigma_i H(1-\sigma_i)-(1-\sigma_i)H\sigma_i\bar{\varrho}\}+\gamma_2(\bar{\varrho}\sigma_f+\sigma_f\bar{\varrho})+\mu(\bar{\varrho}\sigma_i+\sigma_i\bar{\varrho}-2\bar{\varrho})=0\,,$$

where γ_1, γ_2 and μ are readily determined constants, and σ_i^0 and σ_f^0 have been set equal to σ_i and σ_f respectively. Eqs. (6.5), (6.16) and (6.17) comprise the necessary conditions to satisfy the general variational problem of eq. (6.14) subject to the constraints of eqs. (6.2) and (6.15).

With straightforward manipulation one again obtains eq. (6.11). Hence that result can be obtained either by independent variations of the reduced statistical matrix or the species-classification operators (subject, of course, to the pertinent constraints). However, one may note that, when eq. (6.11) obtains, alternate equivalent forms are possible. These will not be considered here.

For the present purposes, an important use may be made of form of eq. (6.5). In view of the results of the previous Section, H consists of either of two forms: the partial Hamiltonian of a single species or just the interaction energy between pairs of reactant species. Because of the form of the species-classification operators it is obviously permissible to augment H with the pertinent single-species partial Hamiltonians without any change whatever in the value of A of eq. (6.1) (**). Thus H may be replaced by the partial Hamiltonian for the *entire* microscopic system represented either by σ_i or σ_f (***). Furthermore, while the reduced statistical matrices differ slightly from one set of terms to another (see, for example, eq. (5.17)), it may be supposed that the classification-diagonal quantities $(\sigma_i\bar{\varrho}\sigma_i)$ and $(\sigma_f\bar{\varrho}\sigma_f)$ are quite insen-

(*) To employ eqs. (6.15), they each should be multiplied by an arbitrary operator and the trace should be taken of each of the resultant products. The results may then be combined with the remaining conditions. In the present treatment the arbitrary operators have been taken as scalar multiples of the reduced statistical matrix. Such a choice evidently is suggested heuristically, but permits a solution to be obtained of the variational equations.

(**) See page 345, footnote (**).

(***) Inasmuch as this partial Hamiltonian is symmetric with respect to exchange of identical particles, the line of argument leading to eq. (4.3) may be employed with the result that all σ's may be regarded as properly symmetrized.

sitive to changes corresponding to $\bar{\varrho}$'s which have associated with them the same σ_i and σ_f in eq. (5.17) (*i.e.*, inverse transitions) (*).

From this line of argument one can conclude that

$$\{\bar{k}_{nml}(i \to f)\}^2 = \{\bar{k}_{nml}(f \to i)\}^2 , \tag{6.18}$$

which is an expression of the *Principle of Microscopic Reversibility*.

One serious deficiency of the analysis of the present Section is its incapability of yielding the sign of $\bar{k}_{nml}(i \to f)$. In the form which has been given for the time rate of change of the average number of each species (*i.e.*, eq. (5.19)) these quantities should be negative to correspond to actual physical systems. However, one can show that the $\bar{k}_{nml}$ cannot be negative-definite quantities for arbitrary $\bar{\varrho}$. An examination of the second variation of $\mathrm{Tr}\,\bar{\varrho}A$ does permit one to establish that the magnitude of $\bar{k}_{nml}(i \to f)$ is a maximum when eq. (6.5) is satisfied, although the details will not be given here. Thus, if one could justify the assertion that the $\bar{k}_{nml}(i \to f)$ have their *minimum* value under the conditions which have been considered, one could conclude that they would have negative values.

A second deficiency is related to the temporal dependence of $\bar{\varrho}$, which is presumed lacking in the species-classification operators. Accordingly, one must imagine that $\bar{\varrho}$ is either stationary (or very nearly so) or that some time averaged value of $\bar{\varrho}$ is employed which has a negligible variation in time.

In view of the results which have been obtained, eq. (6.11) may correspond to situations which are stationary in time.

7. – Heuristics.

Apart from a restriction to systems of relatively precise composition, eq. (5.19) generally is applicable to systems undergoing chemical change. However, it is a purely formal expression, utilization of which requires speci-

(*) One can see that this condition corresponds to the assertion that quantities like

$$\mathrm{Tr}\,\chi_{NML}\varrho\chi_{NML}f(\sigma_i) \qquad \text{or} \qquad \mathrm{Tr}\,\chi_{N'M'L'}\varrho\chi_{N'M'L'}f(\sigma_i) ,$$

where $f(\sigma_i)$ commutes with σ_i, are not significantly different. That such a condition could not be introduced earlier, say, in eq. (5.17), can be seen from the fact that the classification-non-diagonal quantities such as $\chi_{NML}\varrho\chi_{N'M'L'}$ and $\chi_{N'M'L'}\varrho\chi_{NML}$ are involved there, the primed quantities being related to the unprimed quantities by the stoichiometric coefficients of eq. (5.11), and $\{N, M, L,$ etc.$\}$ there is the mean composition of the system. For the term of eq. (5.17) which corresponds to the same σ_i and σ_f, but in the inverse sense, the pertinent operators are $\chi_{NML}\varrho\chi_{N''M''L''}$ and $\chi_{N''M''L''}\varrho\chi_{NML}$, where the double-primed quantities have the signs changed in eq. (5.11). For a fixed set $\{N, M, L,$ etc.$\}$ these quantities are clearly very different.

fication of the statistical matrix, the relevant classification operators and the Hamiltonian of the system. Nevertheless, this equation bears a striking resemblance to the Law of Mass Action with the various $\bar{k}_{nml}(i \to f)/\bar{\sigma}_i(n, m, l)$ corresponding to the several « rate constants » of the pertinent elementary mechanisms of chemical change. To make this correspondence perfect the « rate constants » must depend upon the « size » of the system in such a manner as to make $\langle \dot{N} \rangle$ an extensive property of the system.

That such is the case can be seen from the following plausible argument. A diagonal element of a typical $\bar{k}$, in the co-ordinate representation, is $\langle x | \bar{\varrho}_i(\sigma_i H_i \sigma_f - \sigma_f H_i \sigma_i) | x \rangle$, where x stands for all the co-ordinates of the constituent particles of the relevant microscopic subsystem. These diagonal elements can have essentially non-zero values only in a greatly restricted range of small values of the relative co-ordinates of all of the particles (*). This can be seen from the fact that σ_i essentially localizes the particles into several species, in which case H_i gives negligible contributions for configurations of greatly separated species. In comparison, the diagonale lement $\langle x | \bar{\varrho}_i \sigma_i | x \rangle$ will have more-or-less uniform values regardless of the values of relative co-ordinates of the centers of mass of the species. Since the trace of these quantities involves an integration over the configuration space of the microscopic subsystem, it becomes apparent that

$$\bar{k}_{nml}(i \to f)/\bar{\sigma}_i(n, m, l) \propto V^{1-(n+m+l)}, \tag{7.1}$$

where V is the volume of the macroscopic system. This behavior assures one of the extensive property of $\langle \dot{N} \rangle$. The usual expression of chemical kinetics follows if all quantities are referred to a unit of volume, and such will be assumed in what follows.

When one makes use of the results of Section **6**, the imposition of the condition that each mechanism of chemical transition produces no net change in composition (*viz.*, the condition for chemical equilibrium) yields the expected relation between the concentrations of the reactants and products. Thus, if the mechanism be illustrated by

$$n_1\alpha + m_1\beta + l_1\gamma \to n_2\alpha + m_2\beta + l_2\gamma\,, \tag{7.2}$$

one ultimately obtains (for the equilibrium composition)

$$\frac{\langle N \rangle^{n_2} \langle M \rangle^{m_2} \langle L \rangle^{l_2}}{\langle N \rangle^{n_1} \langle M \rangle^{m_1} \langle L \rangle^{l_1}} = \frac{n_2!\, m_2!\, l_2!}{n_1!\, m_1!\, l_1!} \cdot \frac{\mathrm{Tr}\, \bar{\varrho} \left\{ \sum_p{}' \sigma_f(n_2, m_2, l_2) \right\}}{\mathrm{Tr}\, \bar{\varrho} \left\{ \sum_q{}' \sigma_i(n_1, m_1, l_1) \right\}}, \tag{7.3}$$

(*) The dependence upon the location of the center of the mass of the relevant microscopic subsystem may be presumed to be negligible for spacially uniform macroscopic systems. Boundary effects, which can be of considerable importance for heterogeneous reactions, may be regarded as negligible for sufficiently « large » systems.

where $\sum_p'$ refers to the sum over all « distinguishable » permutations of identical particles (as in Section **4**).

It is to be noted, in eq. (7.3), that quantities like $\left(\sum_p' \sigma_i\right)$ and $\left(\sum_p' \sigma_f\right)$ correspond to properly symmetrized species-classification operators of the relevant microscopic subsystem. When $\bar{\varrho}$ has its equilibrium value $\mathrm{Tr}\,\bar{\varrho}\left(\sum_p' \sigma_i\right)$ and $\mathrm{Tr}\,\bar{\varrho}\left(\sum_p' \sigma_f\right)$ each may be identified as *relative partition functions* (for a unit volume) of the reactants or products, respectively (*). Then eq. (7.3) is identical with that obtained from statistical thermodynamics, and

$$\frac{n_2!\,m_2!\,l_2!}{n_1!\,m_1!\,l_1!}\cdot\frac{\mathrm{Tr}\,\bar{\varrho}\left\{\sum_p' \sigma_f(n_2, m_2, l_2)\right\}}{\mathrm{Tr}\,\bar{\varrho}\left\{\sum_p' \sigma_i(n_1, m_1, l_1)\right\}} = \frac{n_2!\,m_2!\,l_2!}{n_1!\,m_1!\,l_1!}\frac{Q_f}{Q_i} = K_e, \tag{7.4}$$

where Q_i, Q_f refer to the partition function for the microscopic subsystem of reactants and products respectively.

In terms of eq. (7.4) it is evident that when $\bar{\varrho}$ is adequately approximated by its stationary value, permitting the use of eq. (6.11),

$$\left|\frac{\bar{k}_{nml}(i \to f)}{\bar{\sigma}_i(n, m, l)}\right| \propto K_e^{\frac{1}{2}}\left\{\frac{\overline{\sigma_i H \sigma_f H \sigma_i} + \overline{\sigma_f H \sigma_i H \sigma_f}}{\bar{\sigma}_i + \bar{\sigma}_f}\right\}^{\frac{1}{2}}, \tag{7.5}$$

indicating an immediate connection between kinetic properties and equilibrium properties for conditions presumably « close » to chemical equilibrium. It is apparent that the quantity in braces has thes ame value for the inverse chemical transition and refers to intrinsic kinetic properties of the mechanism implicit in $(i \leftrightharpoons f)$.

It is further evident that since $\bar{\varrho}$ tacitly depends upon the macroscopic system in which one may regard the microscopic subsystem as immersed, the rate constants may be expected to vary with the concentrations of the several species in the system. This is to be anticipated from the identification which has been made of quantities like $\mathrm{Tr}\,\bar{\varrho}\sigma$. As a consequence, a more simple relation between rates and *activities* than between rates and concentrations is to be anticipated. However, the extent to which such a simplification obtains will depend upon how $\bar{k}_{nml}(i \to f)$ itself is affected. At present this question must be left unanswered.

(*) Because $\bar{\varrho}$ is normalized to unity, rather than to the partition function of the subsystem, only values relative to the value of the latter can be obtained. When they can be expressed in terms of partition functions of the individual species, the relative partition functions of reactants and products will contain factors like $n_1!\,n_2!$, etc., which cancel precisely those in eq. (7.3).

8. – Theories of chemical reaction rates.

Because of the obvious complexity of the formal quantities which have been derived, the necessity of making approximationss eems clear. The generality of the expressions which have been obtained facilitates their use in developing theories of reaction rates corresponding to explicit choices of the criteria of species classification and in assessing the nature of the approximations which may be made.

At the outset, one important limitation suggested by the present analysis is with respect to the molecularity of the elementary mechanisms of chemical change: no mechanism other than unimolecular or bimolecular appear to be necessary for the complete description of the chemical changes of a system (*). This result depends upon the form of the assumed Hamiltonian, in which only binary interactions between fundamental particles occur. When such is not the case, however, the aforementioned result does not obtain. In terms of the Hamiltonians ordinarily ascribed to systems of chemical interest (*i.e.* electrons and nuclei) there is no exception to binary interactions. Nevertheless, in order to assure that the procedure of decomposing the Hamiltonian as in Section 5 does not render the result thereby obtained fortuitous, an alternate decomposition corresponding to k-nary mechanism is considered in Appendix C. It is shown there that the result of such an obviously arbitrary decomposition is, nevertheless, identical with the result that bimolecular mechanisms may not be exceeded.

To examine this result from another aspect, the rate expression may be integrated, subject to stipulated initial conditions on the statistical matrix. This has been done for the condition which initially makes the statistical matrix commute with each of the χ_{NML} of Section 4. The details will be omitted for the sake of brevity. However, the change in composition may be developed as power series in time. Thereupon, expressions similar to those which have been obtained in Section 6 are obtained for the lowest order terms, quadratic in time. These terms have no mechanisms exceeding bimolecular, as discerned from their dependence upon the *initial composition*. It is evident that what are to be regarded as higher order mechanisms (in terms of initial composition) arise for terms corresponding to higher powers of the time. However, these results refer always to *initial compositions* whereas the result obtained in eq. (5.19) refers to instantaneous values of the composition. In this light, the difference perhaps may be understood (**).

(*) See page 345, footnote (**).

(**) To illustrate, consider the simple case in which $\langle \dot{N} \rangle = k \langle N \rangle^p$, where k is a constant. Clearly, in terms of a power series,

$$\langle N \rangle = \langle N \rangle_0 + kt \langle N \rangle_0^p + \tfrac{1}{2} k^2 t^2 p \langle N \rangle_0^{2p-1} + \dots ,$$

Now the limitations of molecularity are intimately connected with the character of species classification. In the sense of the present analysis, it has been implied that the species classification *operators* can be defined in a meaningful way for all configurations of the constituent particles. Since the criteria for such classification generally may be based upon a knowledge of thea sym-p totic configurational behaviour of the system or its subsystems, one may elect to abandon such criteria for certain circumstances of configurational proximity of the particles of the system. In such a case, one may regard such arrangements as comprising classifications which are quite distinct from those based upon asymptotic behaviour. In fact, they may be regarded as an additional species classification of the subsystem, distinct from those which may have been enumerated. From the formal aspect, no problem arises on this account and it has been implicit in the present analysis that such classifications are to be included. Nevertheless, the requirement that the operators pertinent to such classifications be orthogonal to (*i.e.*, distinguishable from) the « isolated » species-classification operators (*) reduces every non-zero rate constant to terms not exceedingly bimolecular (under the conditions that the Hamiltonian of the system is expressible in terms of binary interactions).

Another restriction suggested by the present analysis relates to the choice of criteria of species classification. It is to be noted that if the species classification operators depend upon configurational co-ordinates alone, each of the bimolecular rate constants vanish. A theory which employs such a criterion is the absolute rate theory of Eyring ([2]) and it is to be remarked that only the unimolecular decomposition of the activated complex intrinsic to each elementary mechanism of chemical change is considered as having kinetic importance in this theory. From the present analysis it could not be otherwise. A similar situation prevails with respect to Slater's ([3]) theory of unimolecular decomposition.

By contrast, the Rice-Ramsperger-Kassel theory of unimolecular decomposition ([4]) adopts a different criterion. As has been indicated previously, this criterion relates to the energy associated with certain bonds of a molecule. The incorporation of such a criterion into appropriate species classification operators in a precise manner poses an insurmountable formal problem. This can be seen from the fact that the energy operator (*i.e.* partial Hamiltonian) associated with those particles ostensibly comprising the bonds does not commute with the energy operator resulting from the permutation of any one of the constituent particles with an identical particle not originally considered as a member of the bond system. The problem is rendered perhaps

---

which manifests a higher order dependence of the rate in terms of initial values $\langle N \rangle_0$ than that which is given by the instantaneous expression (for $p > 1$).

(*) See page 345, footnote (**).

less acute but is not resolved by taking the energy operator of the entire molecule into account. In such a case, with an awareness of the lack of preciseness accompanying such criteria, it is to be noted that each of the unimolecular rate constants vanishes. Because of the lack of preciseness, this extreme situation may be anticipated only as an approximation to the actual state of affairs prevailing in chemical reactions. In particular, the choice of the energy criterion which has been described would appear to be reasonably justified when an exchange of identical particles from different chemical species is precluded or considered to be negligible. It is apparent that these matters have some bearing upon the Lindeman-Hinshelwood theory of quasi-unimolecular reactions ([13]), but no further consideration of them will be given here.

Still another important restriction for theories of chemical kinetics dealing with conditions « close » to equilibrium is expressed in eq. (7.5). One has, under these conditions, to recognize an explicit relation between the kinetic rate constant of a specific mechanism and its equilibrium constant. In fact, the rate constant then may be regarded as composed of two factors: one alludes solely to the equilibrium properties of the mechanism, the other alluding to what may be regarded as its transition properties. Such a connection of kinetic properties and equilibrium properties has been well established experimentally and has been emphasized by BRÖNSTED and HAMMETT (*). It is to be noted, however, that the usual theoretical justification offered for the aforementioned connection is based upon arguments which involve explicit reference to the structure of the reactants and products. In the present analysis, the relation obtains in a general manner only as a result of the stationary properties imposed upon the rate constant. It arises as a result of the same conditions which make necessary Detailed Balance and Microscopic Reversibility.

It is to be noted that the expression obtained here is explicit as regards the dependence upon the equilibrium constant of the relevant mechanism. For a set of reactions in which a more-or-less uniform behavior in their transition properties may be justified, eq. (7.5) indicates that the rate constants for such a set should be proportional to the square-root of the relevant equilibrium constant. There are many instances (*) where such a relationship is apparently satisfied to a good approximation, but the equilibrium constant employed is not generally that of the mechanism considered. Instead, a related equilibrium is employed, which may account for certain disparities in the observed correlations.

In spite of the variety of species criteria which may be employed, it is nevertheless possible to render the expressions which have been obtained in a

---

([13]) See, for example, C. N. HINSHELWOOD: *Kinetics of Chemical Change* (Oxford, 1941), pp. 75-79.

(*) See, for example, reference ([1]), pp. 209-223, where additional references may be found.

form which is suggestive of the activated complex theory; the details are given in Appendix D. It is shown there that the quantity $|\mathrm{Tr}\,\bar{\varrho}(\sigma_i H\sigma_f - \sigma_f H\sigma_i)|$ is bounded from above by the ensemble average of the products of the uncertainty in the probability of species classification and the uncertainty in the energy of the system, both uncertainties referring to eigenstates of the equilibrium value of the statistical matrix. It proves possible, further, to obtain the inequality

$$\left|\frac{\bar{k}_{nn'}(i \to f)}{\bar{\sigma}_i(n, m, l)}\right| \leqslant \xi \frac{kT}{\hbar} \frac{\overline{\Delta\sigma_i}}{\overline{\sigma_i}}, \quad \text{with } \sigma_i + \sigma_f = I \text{ and } \xi = O(1), \tag{8.1}$$

where $\overline{\Delta\sigma_i} = \sum_n \varrho_n \{\langle\varphi_n|\sigma_i|\varphi_n\rangle - (\langle\varphi_n|\sigma_i|\varphi_n\rangle)^2\}$ is the ensemble averaged (quantum) uncertainty of species identification. Here φ_n is an eigenfunction of $\bar{\varrho}$. As discussed in Section **7**, $\overline{\sigma_i}$ is proportional to the partition function of the reactants. With $\overline{\Delta\sigma_i}$ related to the ensemble properties of the relevant subsystem when it certainly is *not* either the reactants or products, one has what appears to be equivalent to the (relative) partition function of the activated complex. Because the only approximations involved concern the equilibrium value of the reduced statistical matrix, the relation obtained does not depend upon the specific criterion chosen for species identification.

In the sense of the foregoing result, the activated complex theory of absolute reaction rates appears to furnish a *form* for rate expressions which may be employed with any species criterion to obtain upper bounds to the rate of chemical reactions.

9. – Remarks.

Apart from its formal heuristic aspects, several deficiencies in the present analysis may be noted.

First of all, the sign of the rate constants has not been established in the present analysis. For a physically significant theory, these quantities must be negative definite. However, this condition cannot be assured for all possible statistical matrices. As a result, the precise characteristics of tose statistical matrices which will assure the negative-definite property of the rate constants needs elaboration.

In this connection, a second deficiency in the present analysis is the lack of consideration given to the detailed temporal evolution of the statistical matrix. This behavior, of course, is central to the general problem of the approach of a system to complete equilibrium. In terms of the present analysis, a knowledge of the explicit temporal behavior of the statistical matrix

will yield the temporal behavior of the rate constants. This sort of behavior also is necessary to give a pertinent theoretical description of chemical kinetics under greatly transient circumstances.

Related to such transient behavior is a third deficiency. While the present analysis has, for simplicity, been concerned only with species-classifications which do not depend upon the time explicitly, such a limitation is apt to be unduly restrictive, in spite of its reasonableness. It seems clear that the analysis will differ somewhat from the one which has been given, but to what extent the conclusions will differ thereby is not immediately apparent.

Fourth, one may note that the criteria for species identification need extensive elaboration. In particular, one may like to incorporate in some way criteria which correspond to non-commuting observables. From the present analysis this does not appear possible. However, one may recognize that a given set of species-classification operators enables one to construct operators from any given dynamical variable which approximate the latter when the system is certainly in any one of the original species classifications. Thus, if $\{\sigma_k\}$ is a complete set of species classification operators and O is an arbitrary operator, the set of operators $\{\sigma_k O \sigma_k\}$ are mutually orthogonal and represent approximations to the original O. They may be employed in a construction of species-classification operators related to the original set which, however, involve as well the properties implicit in O.

Finally, the present analysis has been restricted to composite collections of basic particles (*). The results obtained are thus applicablet o situations for which such a description is adequate. However, reactions which do involve the basic particles individually and explicitly require further examination. One can only conjecture at present that these reactions may exhibit certain differences in description from those involving composite entities exclusively.

Appendix A

The condition that the composition of a mixture is relatively precise implies certain restrictions regarding the rates at which the average number of each species are changing. To establish this consider, for example,

$$\text{(A.1)} \qquad \langle \dot{N} \rangle = \operatorname{Tr} \varrho \boldsymbol{N} = \frac{1}{i\hbar} \operatorname{Tr} \varrho (\boldsymbol{N}\boldsymbol{H} - \boldsymbol{H}\boldsymbol{N}) =$$

$$= \frac{1}{i\hbar} \operatorname{Tr} \varrho \{(\boldsymbol{N} - \mu)(\boldsymbol{H} - \lambda) - (\boldsymbol{H} - \lambda)(\boldsymbol{N} - \mu)\},$$

(*) See page 345, footnote (**).

where λ, μ are constants to be determined later. Since ϱ is a positive definite matrix one can show that an application of Schwartz's inequality yields after some manipulation

$$|\langle \dot{N} \rangle|^2 \leqslant \frac{4}{\hbar^2} \{\mathrm{Tr}\, \varrho (N-\mu)^2\} \{\mathrm{Tr}\, \varrho (H-\lambda)^2\} . \tag{A.2}$$

The least upper bound can be had by minimizing the right side of this equation with respect to changes in λ, μ. One obtain that

$$\lambda = \langle H \rangle ,$$

$$\mu = \langle N \rangle .$$

Hence

$$|\langle \dot{N} \rangle|^2 \leqslant \frac{4}{\hbar^2} \langle (\Delta N)^2 \rangle \langle (\Delta H)^2 \rangle , \tag{A.3}$$

the Δ's referring to deviations from the ensemble average values. Hence

$$\frac{\hbar^2 |\langle \dot{N} \rangle|^2}{4 \langle N \rangle^2 \langle (\Delta H)^2 \rangle} \leqslant \frac{\langle (\Delta N)^2 \rangle}{\langle N \rangle^2} , \tag{A.4}$$

which implies that mixtures of relatively precise composition have relatively small rates of change in their composition.

Appendix B

Consider the quantity

$$\mathrm{Tr}\, \varrho A = \mathrm{Tr}\, \varrho \left[\{u - \lambda(u+v)\} \{B - \mu(u+v)\} - \right. \\ \left. - \{B - \mu(u+v)\} \{u - \lambda(u+v)\} \right] , \tag{B.1}$$

where

$$A \equiv uHv - vHu , \qquad \mathrm{B} \equiv uHv + vHu , \qquad u^\dagger = u = u^2 ,$$

$$v^\dagger = v = v^2 , \qquad uv = vu = 0 , \qquad H = H^\dagger .$$

ϱ is definite and λ, μ are real constants. It is evident that

$$|\mathrm{Tr}\, \varrho A| \leqslant |\mathrm{Tr}\, \varrho \{u - \lambda(u+v)\} \{B - \mu(u+v)\}| + \\ + |\mathrm{Tr}\, \varrho \{B - \mu(u+v)\} \{u - \lambda(u+v)\}| . \tag{B.2}$$

With the aid of Schwartz's inequality, the definite character of ϱ and the properties of the trace one may verify that

$$|\mathrm{Tr}\, \varrho A| \leqslant 2 \left[\mathrm{Tr}\, \varrho \{u - \lambda(u+v)\}^2 \cdot \mathrm{Tr}\, \varrho \{B - \mu(u+v)^2\} \right]^{\frac{1}{2}} . \tag{B.3}$$

A least upper bound to $|\mathrm{Tr}\,\varrho A|$ may be found for appropriate values of λ and μ. Omitting the details, one can establish that the minimum value of the right side of eq. (B.3) occurs when

$$\lambda = \overline{u}/(\overline{u}+\overline{v})\,, \tag{B.4}$$

$$\mu = \overline{B}/(\overline{u}+\overline{v})\,, \tag{B.5}$$

where $\overline{u} = \mathrm{Tr}\,\varrho u$, etc.

For these values

$$|\mathrm{Tr}\,\varrho A| \leqslant 2\left[\left(\frac{\overline{u}\,\overline{v}}{\overline{u}+\overline{v}}\right)\left(B^2 - \frac{(\overline{B})^2}{\overline{u}+\overline{v}}\right)\right]^{\frac{1}{2}}. \tag{B.6}$$

The similarity of this equation with eq. (6.11) is apparent.

Now, nothing precludes the utilization of eq. (B.6) for situations in which u, v refer to the most general sort of projection operators. It is instructive to examine the case where (in terms of its representative)

$$\begin{cases} u \equiv \langle x|\psi_n\rangle\langle\psi_n|x'\rangle\,, \\ v = I - u\,, \end{cases} \tag{B.7}$$

and ψ_n is a member of a complete, orthonormal set of eigenfunctions of an approximate Hamiltonian, H_0. The quantity H above may be regarded as the perturbation of H_0. Also it is convenient to regard ϱ as depending upon the time,

$$\varrho(t) = \sum_{k=0}^{\infty} \frac{t^k}{k!}\,\varrho_k(0)\,, \qquad \mathrm{Tr}\,\varrho(t) = 1\,, \tag{B.8}$$

with the initial value such that $\mathrm{Tr}\{\varrho_0(0)u\} = 1$. It is evident that

$$u(t) = \sum_{k=0}^{\infty} \frac{t^k}{k!}\,\mathrm{Tr}\{\varrho_k(0)u\} = \sum_{k=0}^{\infty} \frac{t^k}{k!}\,\overline{u}_k\,, \tag{B.9}$$

with corresponding expressions for the other quantities of eq. (B.6).

When multiplied by the factor $(1/h)^2$, eq. (B.6) becomes an expression for the transition probability $\dot{\overline{u}}$ from the initial state $\psi_n(x)$ to any other. Squaring both sides of eq. (B.6), one can write for the present case (assuming the equality to hold),

$$(\dot{\overline{u}})^2 = \frac{4\overline{u}\,\overline{v}}{\hbar^2}\left[\mathrm{Tr}\,\varrho(t)\{uH(1-u)Hu + (1-u)HuH(1-u)\} - \right.$$
$$\left. - \left(\mathrm{Tr}\,\varrho(t)\{uH(1-u) + (1-u)Hu\}\right)^2\right]. \tag{B.10}$$

Both sides of this equation may be expressed as a power series in t, making use of the foregoing relations. It is then possible to determine the $\overline{u}_k$. For

the first few values, one obtains

$$\text{(B.11)} \qquad \begin{cases} \overline{u}_0 = 1 \,, \\ \overline{u}_1 = 0 \,, \\ \overline{u}_2 = -\dfrac{2}{\hbar^2} \sum\limits_{k \neq n} |\langle \psi_k | H | \psi_n \rangle|^2 \,. \end{cases}$$

Higher order $\overline{u}_k$ require a knowledge of $\varrho_k(0)$, $k \geqslant 1$, which can be obtained only by a solution of the equation of motion of the density matrix. This will not be attempted here.

From eq. (B.11), one obtains for small values of t

$$\text{(B.12)} \qquad \dot{\overline{u}}(t) \doteq -\frac{2t}{\hbar^2} \sum_{k \neq n} |\langle \psi_k | H | \psi_n \rangle|^2 \,, \qquad (t \text{ small}),$$

which may be recognized as the usual result for sufficiently small times obtained from first order time-dependent perturbation theory of quantum mechanics. As a consequence, eq. (B.6) appears to yield results which bridge the behavior for short intervals of time with those obtained under stationary conditions. (See Section **6**).

Appendix C

The result of Section **5** that no elementary mechanisms of chemical transition need be considered which will exhibit a composition dependence greater than bimolecular may be traced to the decomposition of the Hamiltonian given in eq. (5.7). It is of interest, therefore, to examine the effect of some other decomposition of the same Hamiltonian. For simplicity, consider a set of terms involving only k-nary combinations of α-species. No undue loss of generality is introduced thereby.

Consider, therefore, those terms of eq. (5.7)

$$\text{(C.1)} \qquad H_{\alpha\alpha} \equiv \tfrac{1}{2} \sum_{i \neq j}^{N} \sum_{j=1}^{N} H(\alpha_i, \alpha_j) = \sum_{\{i, j, \ldots k\}} H'(\alpha_i, \alpha_j, \ldots, \alpha_k) \,,$$

where the summation excludes those terms for which two members of $\{i, j, \ldots, k\}$ are the same. Each $H'(\alpha_i, \alpha_j, \ldots, \alpha_k)$ will be supposed to have the same form, independent of $\{i, j, \ldots, k\}$, and will consist of $k!/(k-2)!\,2!$ binary terms $H(\alpha_m, \alpha_n)$. Moreover, there will be $(N-2)!/(k-2)!\,(N-k)!k$ -nary terms which contain the same binary term, say, $H(\alpha_p, \alpha_q)$. Accordingly, each binary term of a specific k-nary term will be multiplied by a factor $(k-2)!\,(N-k!)/(N-2)!$ since the terms with a common binary term must sum to yield that binary term. In other words,

$$\text{(C.2)} \qquad H'(\alpha_i, \alpha_j, \ldots, \alpha_k) = \frac{(k-2)!\,(N-k)!}{(N-2)!} H(\alpha_i, \alpha_j, \ldots, \alpha_k) \,,$$

where $H(\alpha_i, \alpha_j, ..., \alpha_k)$ is the sum of all binary terms $H(\alpha_m, \alpha_n)$ for a specified set $\{i, j, ..., k\}$ and corresponds to what one would ordinarily regard as the interaction between the k α-species. Hence

$$H_{\alpha\alpha} \equiv \frac{(k-2)!\,(N-k)!}{(N-2)!} \sum_{\{i,j,\ldots k\}} H(\alpha_i, \alpha_j, ..., \alpha_k)\,. \tag{C.3}$$

The sum evidently consists of $N!/(N-k)!k!$ terms.

If the procedure employed in Section 5 is carried through with eq. (C.3), one obtains the contribution that is made by $H_{\alpha\alpha}$ to $\langle \dot{N} \rangle$. It can be seen that this contribution,

$$\langle \dot{N} \rangle_{\alpha\alpha} \propto \frac{N!}{(N-k)!\,k!} \cdot \frac{(k-2)!\,(N-k)!}{(N-2)!} = \frac{N(N-1)}{k(k-1)}\,, \tag{C.4}$$

the constant of proportionality ostensibly containing the k-nary rate constant. Therefore, no concentration dependence greater than second-order is exhibited by such terms. As one might anticipate, although this will not be demonstrated here, a detailed evaluation of the k-nary rate constant will yield $k!/(k-2)!\,2!$ identical terms which correspond to the binary rate constant (*). Thus the result of eq. (5.19) is obtained in spite of a different form taken for $H_{\alpha\alpha}$.

Appendix D

The results of Appendix B apply for any normalized reduced statistical matrix and, thus, may be seen to apply for each eigenstate of that quantity. Accordingly, one may obtain (noting, as discussed in Section 6, that H is Hamiltonian of the subsystem of particles comprising the species-classifications involved)

$$|\langle \varphi_n | \sigma_i H \sigma_f - \sigma_f H \sigma_i | \varphi_n \rangle|^2 \leqslant 4\, \frac{\langle \varphi_n | \sigma_i | \varphi_n \rangle \langle \varphi_n | \sigma_f | \varphi_n \rangle}{\langle \varphi_n | \sigma_i + \sigma_f | \varphi_n \rangle} \cdot \left[\langle \varphi_n | \sigma_i H \sigma_f H \sigma_i + \sigma_f H \sigma_i H \sigma_f | \varphi_n \rangle - \frac{|\langle \varphi_n | \sigma_i H \sigma_f + \sigma_f H \sigma_i | \varphi_n \rangle|^2}{\langle \varphi_n | \sigma_i + \sigma_f | \varphi_n \rangle} \right], \tag{D.1}$$

where $\{\varphi_n\}$ is any complete orthonormal set. It will simplify matters to restrict the analysis to the case where

$$\sigma_i + \sigma_f = I \tag{D.2}$$

(*) See page 345, footnote (**).

with no severe limitations upon the generality of the results. Then

$$(D.3)\qquad |\langle\varphi_n|\sigma_i H\sigma_f - \sigma_f H\sigma_i|\varphi_n\rangle|^2 \leqslant 4\langle\varphi_n|\sigma_i|\varphi_n\rangle\langle\varphi_n|1-\sigma_i|\varphi_n\rangle\cdot \cdot[\langle\varphi_n|(H-H_0)^2|\varphi_n\rangle - |\langle\varphi_n|(H-H_0)|\varphi_n\rangle|^2],$$

where $H_0 \equiv \sigma_i H\sigma_i + (1-\sigma_i)H(1-\sigma_i)$, corresponding to the « unperturbed » Hamiltonian of the reactants σ_i and products $(1-\sigma_i)$.

Hence, taking $\{\varphi_n\}$ to be the eigenfunctions of $\bar{\varrho}$, one obtains

$$(D.4)\qquad |\operatorname{Tr}\bar{\varrho}(\sigma_i H\sigma_f - \sigma_f H\sigma_i)| \leqslant 2\sum_n \bar{\varrho}_n\{\Delta_n\sigma_i\}\{\Delta_n(H-H_0)\},$$

where the quantity

$$(D.5)\qquad (\Delta_n\chi)^2 \equiv \langle\varphi_n|(\chi - \langle\varphi_n|\chi|\varphi_n\rangle)^2|\varphi_n\rangle .$$

is the square of fluctuation, or uncertainty, in χ for the state φ_n: Now, one may suppose that for situations « close » to equilibrium $\bar{\varrho}$ reasonably may be approximated by its equilibrium value in which case $\{\varphi_n\}$ may be taken to be eigenfunctions of H. Then

$$(D.6)\qquad |\operatorname{Tr}\bar{\varrho}(\sigma_i H\sigma_f - \sigma_f H\sigma_i)| \leqslant 2\sum_n \bar{\varrho}_n\{\Delta_n\sigma_i\}\{\Delta_n H_0\}.$$

One may anticipate, for an appropriately chosen species criterion, that many φ_n will give negligibly small values of $\{\Delta_n\sigma_i\}$. Such will be the case, for example, when the appropriate φ_n represent the eigenfunctions of the reactants or products of a chemical reaction, but not both, with considerable accuracy. Then, the sum in eq. (D.6) extends over those n for which $\{\Delta_n\sigma_i\}$ differs appreciably from zero.

The right side of eq. (D.6) may be simplified, with the aid of Schwartz's inequality. One obtains

$$(D.7)\qquad \sum_n \bar{\varrho}_n\{\Delta_n\sigma_i\}\{\Delta_n H_0\} \leqslant \Big(\sum_n \bar{\varrho}_n\{\Delta_n\sigma_i\}\Big)^{\frac{1}{2}}\Big(\sum_n \bar{\varrho}_n\{\Delta_n\sigma_i\}\{\Delta_n H_0\}^2\Big)^{\frac{1}{2}}.$$

Since

$$(\Delta_n H_0)^2 = \langle\varphi_n|H_0^2|\varphi_n\rangle - |\langle\varphi_n|H_0|\varphi_n\rangle|^2,$$

and

$$\sum_n \bar{\varrho}_n\{\Delta_n\sigma_i\}|\langle\varphi_n|H_0|\varphi_n\rangle|^2 \geqslant \frac{|\sum_n \bar{\varrho}_n\{\Delta_n\sigma_i\}\langle\varphi_n|H_0|\varphi_n\rangle|^2}{\sum_n \bar{\varrho}_n\{\Delta_n\sigma_i\}},$$

one obtains

$$(D.8)\qquad |\operatorname{Tr}\bar{\varrho}(\sigma_i H\sigma_f - \sigma_f H\sigma_i)| \leqslant 2\Big(\sum_n \bar{\varrho}_n\{\Delta_n\sigma_i\}\Big)\cdot \cdot\left[\frac{\sum_n \bar{\varrho}_n\{\Delta_n\sigma_i\}\langle\varphi_n|H_0^2|\varphi_n\rangle}{\sum_n \bar{\varrho}_n\{\Delta_n\sigma_i\}} - \left|\frac{\sum_n \bar{\varrho}_n\{\Delta_n\sigma_i\}\langle\varphi_n|H_0|\varphi_n\rangle}{\sum_n \bar{\varrho}_n\{\Delta_n\sigma_i\}}\right|^2\right]^{\frac{1}{2}}\cdot$$

The term in brackets may be identified as the (ensemble) uncertainty in the energy of the reactants or products, averaged over those states of the subsystem for which the (quantum) uncertainty in regarding the subsystem as consisting of either reactants or products (but not both) differs appreciably from zero. For systems distributed canonically with respect to energy no great error is incurred by neglect of the difference between H and H_0, so that the term in brackets may be approximated (*) by a number of the order of magnitude of (kT), where T is the absolute temperature of the system and k is Boltzmann's constant.

The quantity $\sum_n \overline{\varrho}_n\{\Delta_n\sigma_i\}$ is the ensemble average of the (quantum) uncertainties in regarding the system as consisting of either reactants or products (but not both) and will be represented by $\Delta\sigma_i$. Hence, combining the previous results with the definition eq. (5.20), one obtains the following expression for the « rate constant ».

$$\left|\frac{k_{nml}(i \to f)}{\overline{\sigma}_i(n, m, l)}\right| \leqslant \xi \frac{kT}{\hbar} \frac{\overline{\Delta\sigma_i}}{\overline{\sigma_i}}, \qquad \xi = O(1). \tag{D.9}$$

The similarity of this expression with that of the activated complex theory (2) is reinforced when $\overline{\sigma}_i$ is related to the partition function of the reactants, as indicated in Section 7. For the present purpose it suffices to note that $\overline{\Delta\sigma_i}$ (which is the same as $\overline{\Delta\sigma_f}$ for the case considered) assumes the role of the partition function of the activated complex.

(*) This may be done by comparing with the expression for the fluctuation in energy for a canonical distribution. See, for example, T. L. Hill: *Statistical Mechanics* (New York, 1956), p. 101. In the present case, the distribution clearly is modified by the weights $\{\Delta_n\sigma_i\}$, but this should not alter the conclusions appreciably. For, if $\{\Delta_n\sigma_i\}$ is essentially zero, one may anticipate that the corresponding eigenvalue of the energy is less than some fixed value. In that case, the distribution may be rendered more nearly canonical by an appropriate change of the energy origin.

SUPPLEMENTO AL VOLUME XV, SERIE X
DEL NUOVO CIMENTO

N. 3, 1960
1° Trimestre

Characteristics of Fuji Nuclear Emulsion Type ET-7A.

K. IMAEDA (*)

Department of Physics, Yamanashi University - Kofu

(ricevuto il 21 Settembre 1959)

CONTENTS. — **1. Introduction. – 2. Experimental procedure. – 3. Results.** 1. Density and stopping power. 2. Sensitivity of the emulsion. 3. Grain spacing.

1. – Introduction.

Recently, a number of emulsions which are capable of recording minimum ionizing particles have been reported (1).

The aim of this paper is to report on one of such emulsions FUJI ET-7A.

In order to improve the characteristics of the emulsion, the close collaboration between user and manufacturer is necessary. For that purpose, the characteristics of the emulsion were investigated from the following point of view.

1) Physical properties of the emulsion.

2) Emulsion as a detector.

3) Emulsion as an analyser.

The fundamental characters so far examined are as follows.

a) The size of the developed grains.

b) The specific gravity of the emulsion under atmospheres of different humidity.

(*) Now at Dublin Institute for Advanced Studies, Dublin, Ireland.

(1) G. F. DENISENKO, N. S. IVAHOVA, N. R. NOVIKOVA, N. A. PERFILOV, E. I. PROKOFIEVA and V. P. SHAMOV: *Phys. Rev.*, **109**, 1779 (1958).

c) Stopping power determined by the μ-meson range of the π-μ decay.

Nuclear emulsion is used by the research worker for two purposes, either for the detection of particles, *i.e.* as a particle detector, or for the kinematic analysis of events, *i.e.* as a particle analyser.

The smaller the grain size in the emulsion, the more information can be obtained with regard to the grain density, the scattering and the residual range of tracks, *i.e.* the better analyser it becomes. At the same time, the detecting properties deteriorate since it becomes difficult to recognize minimum tracks when a nuclear emulsion is used as a particle detector. For in a detector, all events, even minimum tracks, should be easy to see and locate. Thus, the better the analysing power of the emulsion, the worse becomes the recognition of the minimum track and *vice versa*.

As a measure of the detecting power of the emulsion we have adopted the scheme of Berriman (2), *i.e.* we have estimated the visibility of a track produced by a plateau ionizing particle, by plotting blob density *versus* background fog density of the emulsion.

The visibility of the track of a minimum ionizing particle under specified conditions of scanning (*i.e.* the field magnification of the microscope and the velocity of scanning by a scanner, etc., having been defined) depends upon the character of the emulsion, the exposure conditions and the development agents.

We have investigated the characteristics of the emulsion as regards the visibility of plateau ionizing particle tracks, by changing the development conditions and the exposure conditions, and we have tested the gap length distribution along tracks.

2. – Experimental procedures.

The emulsions were exposed as follows:

1) At sea level to the γ-rays of ^{60}Co or the electrons from ^{90}Sr.

2) At Mt. Fuji (3776 meters) for 35 days.

3) At an altitude of 30000 meters for 6 hours by free balloon.

The emulsions used in the experiment were FUJI ET-7A electron sensitive nuclear emulsions. The plates were 200 μm and 50 μm thick and pellicles were 370 μm and 600 μm thick.

The emulsion was exposed immediately after it was produced by the manufacturer. Special care was paid to the moisture and temperature during the time of exposure. After the exposure, part of the emulsion was developed by

(2) R. W. Berriman: *Photographic Sensitivity* (London, 1951).

the amidol-bisulphite temperature method (pH = 6.7) ([3]) and another part by the amidol-bisulphite temperature method (pH = 10.0) ([3]), varying the temperature and the time of development.

3. – Results.

3·1. *Density and stopping power.* – Samples of emulsion pellicles, each weighing about 2 mg were kept in various relative humidities and the specific gravity measured. The atmosphere of a required humidity was obtained by the mixture of water and glycerine ([5]). After a certain period of time in those atmospheres, the pellicles were weighed in air and in CCl_4. In this way, after the emulsion was in equilibrium with an atmosphere of a given humidity, we could estimate how the density of the emulsion varied with the atmospheric humidity to which it had been exposed.

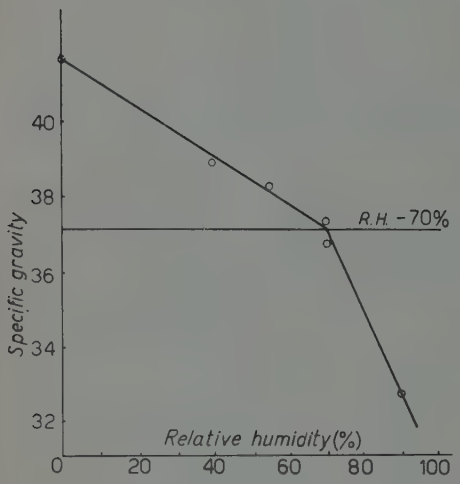

Fig. 1. – Density of emulsion Fuji ET7A as a function of atmospheric relative humidity (temperature between (30÷40) °C).

The density of the emulsion pellicles is shown in Fig. 1.

The stopping power of the emulsion was estimated by measurement of the range of five μ-mesons from π-μ decay in the plates of 200 μm thickness. The value of the mean range of μ-mesons is 608.7 μm and the straggling is 32.7 μm.

The result shows that though the 7A emulsion is produced by a different process from that of Ilford's their density and stopping power are nearly equal. So the range-energy relation is similar to that of Ilford G-5, provided that the relative humidity at the time of exposure is taken into account.

3·2. *Sensitivity of the emulsion.* – In order to obtain the characteristics of the emulsion ET7A for development, the amidol-bisulphite temperature method was applied. The details of the composition and the process applied are shown in Table I and Table II.

The plates and the pellicles used in the experiment were picked out of the

([3]) A. D. Dainton, A. R. Gattiker and W. O. Lock: *Phil. Mag.*, **42**, 396 (1951).
([4]) M. Blau and A. J. De Fellice: *Phys. Rev.*, **74**, 1198 (1947).
([5]) A. J. Oliver: *Rev. Sci. Instr.*, **25**, 326 (1954).

TABLE I. – *Development procedure (amidol bisulphite).*

(1)	Immersion in water	5 °C	30 min
(2)	Cold stage in developer	5 °C	50 min
(3)	Hot stage (dry)	(15÷30) °C	(15÷120) min
(4)	Stop bath (acetic acid 0.2%)	5 °C	30 min
(5)	Fixing	5 °C	17 h
(6)	Washing	15 °C	10 h

TABLE II. – *Developer* (pH = 6.7).

(1)	Amidol	3.0 g
(2)	Anhydrous sodium sulphite	6.7 g
(3)	Sodium bisulphite liquor, S.G.=1.34	1.4 ml
(4)	Distilled water	930 ml

same batch of emulsion. The temperature and the time of the development were varied. All the other variables in the developing agents were kept constant for all the plates used in the development. In raising the temperature of a plate from the cold stage to the hot stage, the equilibrium with the temperature of the hot stage was attained in all cases within three minutes.

The blob density of a plateau ionizing particle in a plate was obtained by the weighted mean of the blob density of five to fifteen tracks as thin as electron tracks. If the value of the blob density of a track deviated from the mean value by more than four times the standard deviation the track was discarded, as it must have been produced by a particle of ionization different from plateau. The mean values obtained for the blob density of plateau ionizing particles were checked against the blob density of the electron tracks of μ-e decay and cascade shower particles in the same plate. It should be noticed that blob density of plateau ionizing particles (electrons of μ-e decay and those of cascade showers) lies at all development conditions between 20 and 40 blobs per 100 μm and thus lies in a region of good recognition.

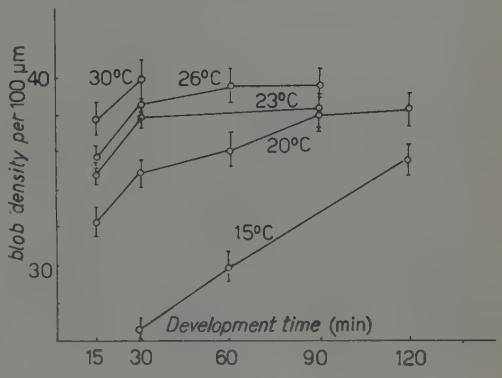

Fig. 2. – Blob density of plateau ionizing particle tracks as a function of developing time and temperature (amidol bisulphite temperature development).

The dependence of the blob density of a track of a plateau ionizing particle on the development time and temperature are shown in Fig. 2. The

development time is measured from the time when the plates are placed on a hot metal plate in the hot stage to the time when they are taken out of the hot stage and immersed in the stop bath.

The grain density increases with the development time and temperature. The dependence of the blob density on the temperature of development is large for short developing time and small for long developing time. The saturation value of the blob density ($\sim$ 40 blobs-100 μm) is nearly the same for all the developing temperatures. At 30 °C, the blob density saturates at about 30 minutes of developing time. For shorter developing time and lower temperatures, the blob density is rather sensitive to temperature and time of development.

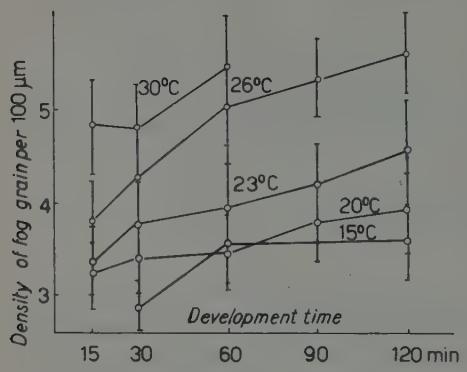

Fig. 3. – Density of fog grains as a function of developing time and temperature (amidol bisulphite temperature development).

The density of background for grains was measured using a microscopic magnification of 1500 times. In the measurement, care was taken for not counting those grains which were due to background slow electron tracks.

The number of fog grains is 0.5 ÷ 5.0 per 1000 cubic microns of the processed emulsion. The dependence of fog grain density on the temperature and time of the development are shown in Fig. 3.

Contrary to the blob density of tracks which saturates at about 40 blobs per 100 μm, the fog density increases almost linearly with the developing times and temperatures so far examined and shows no saturation.

This result indicates that there is an optimum development time and temperature. From the practical point of view, there are different criteria for the optimum development. In this experiment, we studied the visibility of minimum ionizing particle tracks. Though the visibility of a track of a minimum ionizing particle depends upon many factors: microscopic conditions, velocity of scanning, the experience and fatigue of the scanner and so on, it is chiefly determined by the grain density of the track and the background fog density of the emulsion when the above factors have been fixed.

The result on the visibility of a plateau ionizing particle track in each plate is shown in Fig. 4. In the figure, we plotted blob density against to fog density ([2]). « Good recognition curve » and « fair recognition curve » are shown after Berriman's definition. But the real visibility curve obtained visually is different from those given by BERRIMAN in our emulsion. The curve cor-

responding to equal visibility obtained by the visual comparison of the tracks of different plates is shown in Fig. 4 by curve *C*.

It can be seen from Fig. 4 that a temperature lying betweed 20 °C and 23 °C, and a developing time of between 15 minutes and 30 minutes, give the best results in our long exposure time.

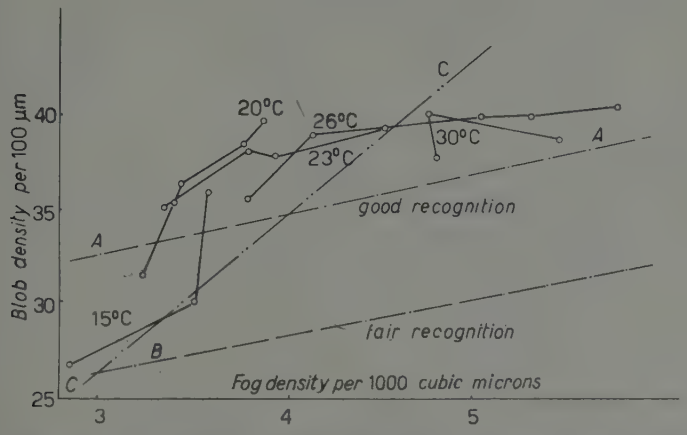

Fig. 4. – Visibility of a plateau ionizing particle in Fuji ET7A emulsion by various temperatures and times of development (*A*, *B*: Berriman's curve; *C*: curve of good recognition obtained by visual comparison).

3·3. *Grain spacing.* – The finite size of the developed grain introduces errors in measurements of ionization, scattering and range of tracks.

We have estimated the distribution of the diameters (d_i) of grains along the plateau ionizing particle tracks in ET7A as well as in Ilford G-5, and we have got an arithmetic mean ($\bar{d}$) (0.60 ± 0.02) μm for 7A and (0.58 ± 0.02) μm for G-5. The dispersion $\sqrt{\sum_{i=1}^{N} (\bar{d} - d_i)^2/(N-1)}$ is 0.19 μm in both emulsions. The result is plotted in Fig. 5.

The result of the measurement of the gap length distribution along the tracks of protons, μ-mesons and electrons confirmed the power law distribution of gaps ([6]):

$$g = B \exp[-gl],$$

where B denotes the blob density, g denotes the density of the gaps greater than l μm.

([6]) C. O'Ceallaigh: *Proc. Bagnères Conf.* (1953), p. 74.

The normalized coefficient g^* defined by FOWLER-PERKINS (7) was obtained from the blob density of μ-mesons and their decay electrons. In Fig. 6 and Fig. 7, the gap distribution in the tracks of a μ-meson and an electron are shown. The blob densities of μ-mesons were normalized by 1) the

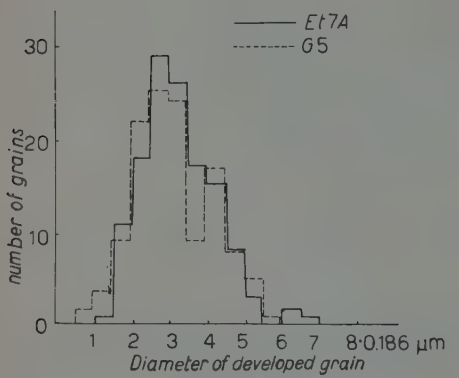

Fig. 5. – Distribution of grain diameters in the track of a plateau ionizing particle.

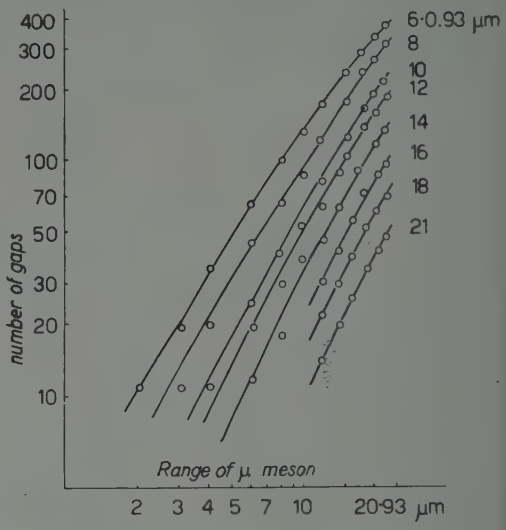

Fig. 6. – Number of gaps ($\geqq l$ microns) in the track of a μ-meson as a function of its range.

associated decay electron, 2) the unassociated electron from the decay electron of a different μ-meson. We, thus, obtained blob densities normalized to minimum, assuming that plateau blob density is 10% higher than minimum blob density. The result shows that in the case 1), the value of the g^* given by Fowler-Perkins' for Ilford G-5 emulsion agrees with that of a μ-meson track normalized by g_0

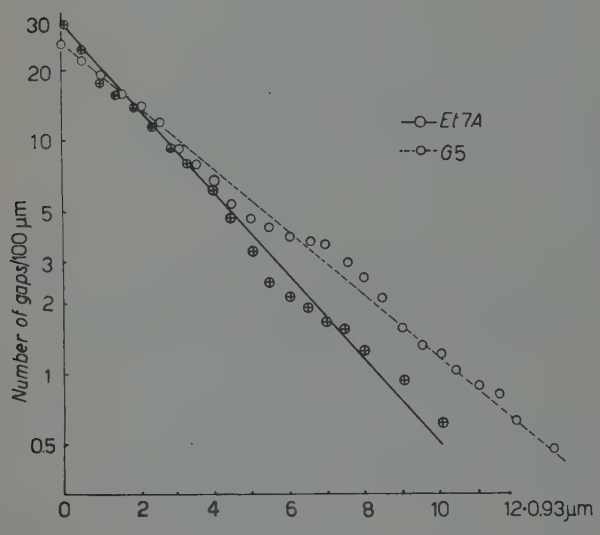

Fig. 7. – Gap length distribution in an electron track in ET7A and in a track of 4.3 GeV π^--meson in G5.

(7) P. H. FOWLER and D. H. PERKINS: *Phil. Mag.*, **46**, 587 (1955).

derived from that of the electron which is the decay product of the same μ-meson. But in the case 2), the value of the track of the μ-mesons normalized by that of the other electron track do not agree with the curve. The reason

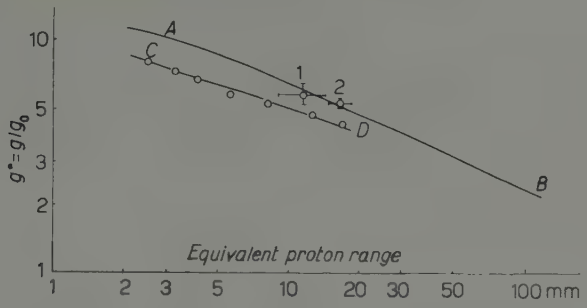

Fig. 8. - g^* values defined by Fowler-Perkins in ET7A emulsion. Curve AB: Fowler-Perkins' curve. 1, 2: denotes g^* of the track without fading effect; CD: denotes g^* of the track with fading effect.

for this is that the exposure to cosmic rays was so long in duration that the fading effect was considerable in some tracks. An example which exhibits a remarkable deviation from the Fowler-Perkins' curve in shown in Fig. 8.

* * *

I wish to thank Miss Mitsuko Kazuno for her great help, Dr. Yasuo Koseki and Dr. Yoshito Takao who supplied emulsions which were in the testing stage in perfect condition with relevant data, and the members of the Research Laboratory of Fuji Photo Film Co. Ltd. for their promptness in supplying the emulsions. I am also grateful to Mr. Toshio Higuchi and Mr. Issei Otagiri for their assistance in the experiment.

SUPPLEMENTO AL VOLUME XV, SERIE X
DEL NUOVO CIMENTO

N. 3, 1960
1° Trimestre

Efficiency in Area-Scanning for Events in Nuclear Emulsions.

Y. K. LIM

Physics Department, University of Malaya - Singapore

J. E. LABY and V. D. HOPPER

Physics Department, University of Melbourne - Victoria

(ricevuto l'8 Ottobre 1959)

In scanning nuclear emulsions, it is often desired to obtain the absolute number of a certain type of event in a given area, or to compare the number of events in emulsions of different sensitivities. This involves an estimation of the scanning efficiency. In general, high efficiency can be achieved by using high magnification lenses, but this involves great physical effort and, due to the diminished field of view, large systematic errors might be introduced by a slight displacement of the plate relative to the moving holder. It is often more advantageous to scan with some lower magnification, which still gives good visibility, and then correct for the scanning loss.

The efficiency of scanning for a given type of event under a given set of conditions can be determined by a simple method similar to those used by GEIGER and WERNER [1] in counting scintillations and by PETERS [2] in track tracing. A test volume is scanned twice. Let N be the true number of events present, and $n+n_1$ and $n+n_2$ be respectively the numbers found in the first and second scans, where n_1 and n_2 are respectively the numbers found in the first and second scans but otherwise missed. Assuming that the scanning efficiency is constant throughout each scan, one has for the corresponding scanning

---

(1) See E. RUTHERFORD, J. CHADWICK and C. D. ELLIS: *Radiations from Radioactive Substances* (1930) p. 548.

(2) B. PETERS: *Proc. Ind. Acad. Sci.*, A **40**, 230 (1954).

efficiencies f_1 and f_2 the simultaneous equations

$$Nf_1 = n + n_1 \tag{1}$$

$$Nf_2 = n + n_2 \tag{2}$$

$$N(1 - f_1)f_2 = n_2 \tag{3}$$

$$N(1 - f_2)f_1 = n_1 \tag{4}$$

with the solution

$$f_1 = \frac{n}{n + n_2}, \tag{5}$$

$$f_2 = \frac{n}{n + n_1}, \tag{6}$$

$$N = \frac{(n + n_1)(n + n_2)}{n}. \tag{7}$$

Fluctuation in the values obtained for the efficiencies can be obtained by a simple consideration. The efficiency f, assumed constant throughout a scan, can be regarded as the probability of an event being found in the process. In an area where there are N events, the number found may be expected to fluctuate according to binomial distribution with a standard deviation $\sqrt{Nf(1-f)}$. This fluctuation is reflected in the estimated value of f. Thus

$$\frac{\Delta f}{f} = \frac{\sqrt{Nf(1-f)}}{Nf} = \sqrt{\frac{1-f}{Nf}}. \tag{8}$$

For example, if the efficiency is 90%, to reduce the percentage fluctuation to 5%, one requires $Nf = 40$, or one has to duplicate-scan a sample area containing 44 events for estimating f. In practice, scanning efficiency does vary during a scan and the fluctuation may be somewhat larger.

If the whole area is duplicate-scanned and events found in both scans are included, the « combined efficiency » is

$$F = \frac{n + n_1 + n_2}{N} = 1 - (1 - f_1)(1 - f_2), \tag{9}$$

which can be very close to unity as the inefficiency involved is of the second order of magnitude. Fluctuation in F is given by

$$\Delta F = \sqrt{[(1 - f_2)\,\Delta f_1]^2 + [(1 - f_1)\,\Delta f_2]^2}. \tag{10}$$

Three 600 μm thick Ilford G-5 plates, belonging to the same batch, were exposed to cosmic rays at mean atmospheric depth 20 g cm^{-2} over Melbourne (geomagnetic latitude 47° S) for 3.9 h. Two of these, 3G1 and 3G3 were loaded with water to 2.61 times the original thickness before exposure, and the other, 1G1, was exposed in the normal state. Areas in each of the plates have been duplicate area-scanned for stars produced by neutral or singly charged particles with three or more heavy prongs, which were defined as prongs with a range $\geqslant 5$ μm in the loaded emulsions or $\geqslant 4$ μm in the normal emulsion, and a grain density > 1.4 times the plateau grain density, σ-stars being excluded. The scanning was carried out under 20 × or 45 × objectives and the two scans in each efficiency determination were performed by the same observer or by different observers. Since the efficiency was found higher for larger stars, stars with more than 6 heavy prongs and stars with 6 or less heavy prongs are treated separately. However, the estimated total numbers of events are not significantly different whether the large and small stars are treated separately or together. Stars which occur in layers close to either emulsion surface were excluded and their loss corrected for on assumption of uniform depth distribution. Values for N given in Table I have been corrected for this loss.

TABLE I. – *Results of area-scanning in normal and loaded emulsions.*

Plate		3G1	3G3	1G1	1G1
Area scanned (mm^2)		400	587	205	899
Large stars	f_1 %	89 ± 4*	98 ± 2*	78 ±8$^\Delta$	98 ± 2*
	f_2 %	91 ± 4$^\Delta$	90 ± 4$^\Delta$	91 ±5$^\Delta$	97 ± 2*
	F %	99 ± 1	100	98 ±2	100
	N	57 ± 8	64 ± 8	32 ±6	126 ±13
Stars/mm^2		.14± .02	.11± .01	.15± .03	.14± .01
Small stars	f_1 %	65 ± 4*	84 ± 2*	68 ±7$^\Delta$	82 ± 3*
	f_2 %	53 ± 4$^\Delta$	59 ± 3$^\Delta$	92 ±4$^\Delta$	84 ± 3*
	F %	83 ± 2	93 ± 1	97 ±2	97 ± 1
	N	176 ±14	273 ±17	55 ±8	268 ±19
Stars/mm^2		.44± .04	.47± .03	.27± .04	.30± .02

* Scanning done by observer A $^\Delta$ Scanning done by observer B

The scans reported here were performed in 1957 and in 1959. The efficiencies for the earliest scans were significantly lower. These are the values given for observer A in column 1 and the upper values in column 3. Allowing for the possible time variation, there appears to be reasonably good consistency

in the scanning efficiencies obtained for an observer for each type of emulsion.

The star density is subject to two sources of error, the statistical fluctuation in the true number of stars occurring in the area scanned, and the uncertainty in the scanning efficiency estimated. The former has a standard deviation given by $\sqrt{N}$, while the latter depends on the area duplicate-scanned. For the densities given in Table I, which were obtained by duplicate-scanning the entire area, errors arising from efficiency determination were those of the combined efficiencies. As these are small, errors quoted for N are those due entirely to the true star number fluctuation.

Calculation shows that to within 3% accuracy the same number of star-producing particles has passed through each plate. One would expect the same number of disintegrations per unit area to have occurred in the Ag and Br nuclei of each plate and more light nucleus disintegrations in the loaded emulsions due to the extra amount of light elements traversed. With our selection criteria, these extra stars must have occurred in the oxygen nuclei introduced by water loading.

It is possible to correct for the number of stars from the data which were produced prior to the flight in the normal emulsion by counting the number of stars in the loaded emulsions which were produced in the dry state. These show a much heavier grain density near the end of a prong. The correction was found to be 10% of the observed star density in the normal emulsion, giving the weighted mean star density in the normal emulsion as $(.39 \pm .02)$ stars mm^{-2}. The weighted mean star density in the loaded emulsions is $(.58 \pm .02)$ stars mm^{-2}, giving $(.18 \pm .03)$ stars mm^{-2} as the density of stars arising from the disintegration of the loaded oxygen nuclei.

The ratio of the number of stars in the loaded oxygen nuclei to the number of stars in the original emulsion nuclei is $.46 \pm .09$. If it is assumed that the cross-section for star production is proportional to the geometrical cross-section, the calculated value (excluding the contribution of hydrogen nuclei) of this ratio is .60. This indicates that light nuclei are more transparent than heavy nuclei in their interaction with cosmic rays in producing stars of three or more prongs. Defining k as the ratio of the interaction cross-section to the geometrical cross-section, the above data give the opacity of an oxygen nucleus relative to a heavy emulsion nucleus, $\varrho = k_0/k_H$ as $.72 \pm .14$; if it is assumed that this ratio applies to the gelatin nuclei as well. The present result suggests that (21 ± 4)% of the stars satisfying the selection criteria in a normal emulsion are due to the disintegration of the gelatin nuclei.

Interpolation of the data [3] on the absorption cross-section of various

[3] Among others: N. E. Booth, G. W. Hutchinson and B. Ledley: *Proc. Phys. Soc.*, **71**, 293 (1958); T. Coor, D. A. Hill, W. F. Hornyah, L. N. Smith and G. Snow: *Phys. Rev.*, **98**, 1369 (1955); J. M. Cassels and J. D. Lawson: *Proc. Phys. Soc.*, A **67**, 125 (1954).

elements for protons and neutrons shows that the corresponding relative opacity ϱ for absorption is insensitive to incident energy up to at least 1.4 GeV and has a value of about 0.8. This however cannot be compared immediately with the value obtained in the present experiment since in the latter only interactions which gave rise to stars having at least three heavy prongs are considered. BLAU *et al.* [4] have obtained $.71 \pm 11$ for ϱ or 21% of the stars produced by 300 MeV neutrons in normal emulsions with at least two heavy prongs as due to the gelatin nuclei. The percentage of light nucleus stars expected on geometrical cross-section is 27%.

* * *

This work was carried out with the aid of a Nuffield Foundation Grant. One of the authors (Y.K.L.) also received assistance from an IGY Analysis Grant.

[4] M. BLAU, A. R. OLIVER and J. E. SMITH: *Phys. Rev.*, **91**, 949 (1953).

SUPPLEMENTO AL VOLUME XV, SERIE X
DEL NUOVO CIMENTO

N. 3, 1960
1° Trimestre

Elementary Particle Reactions - II.

H. C. MEYER, III and W. G. HOLLADAY (*)

Physics Department, Vanderbilt University - Nashville, Tenn.

(ricevuto il 12 Novembre 1959)

1. – Introduction.

On the basis of present ideas concerning conservation of the relevant quantum numbers of elementary particles, BEASLEY and HOLLADAY (1) presented a procedure for determining the different final sets of known elementary particles of mass equal to or greater than the pion mass that can be produced from a given pair of colliding initial particles. By this procedure they determined all the two, three, and four particle final states that can be produced (or that conserve the relevant quantum numbers) by a γ, e, π, K, $\overline{\text{K}}$, $\mathcal{N}$, or $\overline{\mathcal{N}}$ incident upon a target nucleon. The threshold energy for each of these reactions was calculated for both the case of the target nucleon at rest and the target nucleon in motion in a nucleus with 25 MeV of kinetic energy and momentum toward the projectile.

The present paper constitutes a continuation of this work. In Section **2**, a different and perhaps more natural procedure than that of Ref. (1) is presented for determining the possible reactions for the elementary particles.

(*) On leave for the year 1959-1960 at the University of Wisconsin, Madison, Wis.

(1) C. O. BEASLEY jr. and W. G. HOLLADAY: *Suppl. Nuovo Cimento*, **10**, 77 (1958).

Section **3** presents Tables of the two, three, and four particle final states that arise from a Λ, $\overline{\Lambda}$, Σ, $\overline{\Sigma}$ Ξ, and $\overline{\Xi}$ incident on a nucleon together with the threshold energy for the reaction when the target nucleon is stationary and in motion in a nucleus. Thresholds for multistage reactions are discussed in Section **4**, and the problem of determining the total number of reactions as a function of the number of particles produced for a given set of initial particles is mentioned but not satisfactorily solved in Section **5**.

2. – Determination of all possible reactions.

Each particle can be represented by a pair of numbers, namely its A and B quantum numbers (1) which are given in Table I. Here $q = (A/2) + T_3$ and

TABLE I. – *Quantum numbers and masses* (GeV) *for elementary particles* (*).

		A		
		1	0	−1
B	1	p n 0.939	Λ^0 1.115 Σ^+ Σ^0 Σ^- 1.190	Ξ^- Ξ^0 1.320
	0	K^0 K^+ 0.494	π^+ π^0 π^- 0.139	K^- K^0 0.494
	−1	$\overline{\Xi}^-$ $\overline{\Xi}^0$ 1.320	$\overline{\Lambda}^0$ 1.115 $\overline{\Sigma}^+$ $\overline{\Sigma}^0$ $\overline{\Sigma}^-$ 1.190	$\overline{\mathrm{p}}$ $\overline{\mathrm{n}}$ 0.939

(*) A bar over a particle indicates that it is an antiparticle.

B is the baryon number. For instance, the K particle is represented by

$$\begin{matrix} A \\ B \end{matrix} = \begin{matrix} 1 \\ 0 \end{matrix}.$$

This representation for the elementary particles is not unique in the case of the pairs

$$\begin{matrix} 0 \\ 1 \end{matrix} \quad \text{and} \quad \begin{matrix} 0 \\ -1 \end{matrix},$$

which correspond to the Λ or Σ and $\overline{\Lambda}$ or $\overline{\Sigma}$, respectively.

A reaction can then be represented by two sets of these pairs of quantum numbers, one set for the initial particles and one for the final particles. When we ask the question: what are all the final sets of n particles for a given pair of initial particles, we are asking: what are all the possible different sets of n pairs of the A and B quantum numbers such that

$$\sum_{i=1}^{2} A_i = \sum_{f=1}^{n} A_f,$$

$$\sum_{i=1}^{2} B_i = \sum_{f=1}^{n} B_f;$$

the i and f refer to initial and final sets of particles. We can find all these possible sets by writing down all the possible combinations of the numebrs 1, 0, and -1 taken n at a time such that the sum of these n numbers equals the sum of the A of the initial particles. The similar combinations for the B quantum number are written down. All the possible combinations that equal the sum of the initial A can easily be found by taking as few of the numbers 1, 0, and -1 that equal the sum of the initial A and adding as many 0's as are necessary to have n numbers in the sum. Then by successively replacing each pair of 0's by 1 and -1 all the combinations are found.

Now we group each of the combinations for the A with each of the combinations for the B forming sets of n pairs, which pairs each consist of an A and a B quantum number. Then we permute either the A or the B quantum numbers for each of these sets to obtain all the different possible sets. Replacing the pairs of quantum numbers by the particles they represent, we have all the possible reactions with n product particles for the given pair of initial particles.

As an example let us find all the possible reactions with three product particles for the case of the initial particles being the Ξ and $\mathcal{N}$. Here $\sum A_i = 0$ and $\sum B_i = 2$. The possible combinations for the A's are

$$0+0+0 \quad \text{and} \quad 0+1-1.$$

For the B's we have

$$1+1+0\,.$$

Grouping each of the combinations for the A's with each of the combinations for the B's, we have the two groupings

$$(1)\qquad \begin{matrix}[0 & 0 & 0]\\ (1 & 1 & 0)\end{matrix}$$

$$(2)\qquad \begin{matrix}[0 & 1 & -1]\\ (1 & 1 & 0)\end{matrix};$$

where the A's are in the brackets and the B's are in parentheses. To obtain all the different sets of pairs of each grouping, we permute the B's and find no new sets for the first grouping. For the second grouping we have two differents sets:

$$(3)\qquad \begin{matrix}[0 & 1 & -1]\\ (1 & 0 & 1)\end{matrix}$$

$$(4)\qquad \begin{matrix}[0 & 1 & -1]\\ (0 & 1 & 1)\end{matrix}.$$

These sets of pairs correspond to the eight reactions with three product particles listed in Table II for the initial particles being a Ξ and a $\mathcal{N}$. Once again we note that some of these sets correspond to more than one possible reaction because of the pairs

$$\begin{matrix}0\\1\end{matrix}\qquad\text{and}\qquad\begin{matrix}0\\-1\end{matrix}$$

that appear in the product sets represent Λ, Σ and $\overline{\Lambda}$, $\overline{\Sigma}$ respectively.

This method has been used to find all the possible reactions with up to four product particles for the initial particles being those heavier than muons and the target being a nucleon.

Those reactions not given in Ref. [1] are listed in Table II. The particles at the top of the columns are the initial particles, and the product particles follow in groups of two, three, and four product particles.

TABLE II. – *Threshold energies.*

Reaction products	Threshold energy (GeV)			
	$\Sigma+\mathcal{N}\rightarrow$		$\Lambda+\mathcal{N}\rightarrow$	
	$\mathcal{N}$(*)	$\overleftarrow{\mathcal{N}}$	$\mathcal{N}$	$\overleftarrow{\mathcal{N}}$
$\mathcal{N}+\Lambda$	Exothermic		—	—
$\mathcal{N}+\Sigma$	—	—	0.167	0.0542
$\mathcal{N}+\Lambda+\pi$	0.146	0.0412	0.314	0.145
$\mathcal{N}+\Sigma+\pi$	0.325	0.148	0.492	0.266
$2\mathcal{N}+\overline{K}$	0.582	0.324	0.749	0.452
$2\Lambda+K$	1.54	1.04	1.70	1.18
$\mathcal{N}+\Xi+K$	1.62	1.11	1.79	1.24
$\Lambda+\Sigma+K$	1.76	1.21	1.93	1.35
$2\Sigma+K$	1.98	1.39	2.15	1.53
$\mathcal{N}+\Lambda+2\pi$	0.482	0.254	0.649	0.379
$\mathcal{N}+\Sigma+2\pi$	0.671	0.389	0.839	0.518
$2\mathcal{N}+\pi+\overline{K}$	0.944	0.589	1.11	0.723
$2\Lambda+K+\pi$	1.95	1.36	2.12	1.50
$\mathcal{N}+\Xi+K+\pi$	2.04	1.43	2.21	1.57
$\Lambda+\Sigma+K+\pi$	2.18	1.54	2.35	1.68
$2\Sigma+K+\pi$	2.42	1.72	2.59	1.87
$\mathcal{N}+\Lambda+K+\overline{K}$	2.51	1.80	2.68	1.94
$\mathcal{N}+\Sigma+K+\overline{K}$	2.76	1.99	2.93	2.13
$\Lambda+\Xi+2K$	3.83	2.83	3.99	2.97
$\Sigma+\Xi+2K$	4.10	3.04	4.27	3.19
$2\mathcal{N}+\Lambda+\overline{\mathcal{N}}$	5.82	4.40	5.99	4.55
$2\mathcal{N}+\Sigma+\overline{\mathcal{N}}$	6.14	4.65	6.30	4.80
$\mathcal{N}+2\Lambda+\overline{\Lambda}$	7.36	5.62	7.53	5.77
$2\mathcal{N}+\Xi+\overline{\Lambda}$	7.49	5.73	7.66	5.87
$\mathcal{N}+2\Lambda+\overline{\Sigma}$	7.70	5.89	7.87	6.04
$\mathcal{N}+\Lambda+\Sigma+\overline{\Lambda}$	7.70	5.89	7.87	6.04
$2\mathcal{N}+\Xi+\overline{\Sigma}$	7.84	6.00	8.01	6.15
$\mathcal{N}+\Lambda+\Sigma+\overline{\Sigma}$	8.06	6.17	8.22	6.32
$\mathcal{N}+2\Sigma+\overline{\Lambda}$	8.06	6.17	8.22	6.32
$\mathcal{N}+2\Sigma+\overline{\Sigma}$	8.41	6.45	8.58	6.60
$3\Lambda+\overline{\Xi}$	9.17	7.06	9.34	7.20
$\mathcal{N}+\Lambda+\Xi+\overline{\Xi}$	9.32	7.17	9.49	7.32
$2\Lambda+\Sigma+\overline{\Xi}$	9.55	7.36	9.72	7.50
$\mathcal{N}+\Sigma+\Xi+\overline{\Xi}$	9.70	7.47	9.86	7.62
$\Lambda+2\Sigma+\overline{\Xi}$	9.93	7.66	10.1	7.81
$3\Sigma+\overline{\Xi}$	10.3	7.97	10.5	8.11

(*) The column labeled $\mathcal{N}$ is for the target at rest, and the column labeled $\overleftarrow{\mathcal{N}}$ is for the target with 25 MeV of kinetic energy moving toward the projectile.

TABLE II (*continued*).

Reaction products	Threshold energy (GeV)			
	$\bar{\Lambda}+\mathcal{N}\rightarrow$		$\bar{\Sigma}+\mathcal{N}\rightarrow$	
	$\mathcal{N}$	$\bar{\mathcal{N}}$	$\mathcal{N}$	$\bar{\mathcal{N}}$
$K+\pi$	Exothermic		Exothermic	
$\mathcal{N}+\bar{\Lambda}$	—	—	Exothermic	
$\mathcal{N}+\bar{\Sigma}$	0.167	0.0542	—	—
$\Lambda+\bar{\Xi}$	0.911	0.572	0.744	0.441
$\Sigma+\bar{\Xi}$	1.11	0.721	0.941	0.587
$2K+\bar{K}$	Exothermic		Exothermic	
$K+2\pi$	Exothermic		Exothermic	
$\mathcal{N}+\pi+\bar{\Lambda}$	0.314	0.145	0.147	0.0412
$\mathcal{N}+\pi+\bar{\Sigma}$	0.492	0.266	0.325	0.148
$\mathcal{N}+K+\mathcal{N}$	0.749	0.452	0.582	0.324
$\Lambda+\pi+\bar{\Xi}$	1.28	0.853	1.11	0.717
$\Sigma+\pi+\bar{\Xi}$	1.49	1.01	1.32	0.876
$\Lambda+K+\bar{\Lambda}$	1.70	1.18	1.54	1.04
$\mathcal{N}+\bar{K}+\bar{\Xi}$	1.79	1.24	1.62	1.11
$\Lambda+K+\bar{\Sigma}$	1.93	1.35	1.76	1.21
$\Sigma+K+\bar{\Lambda}$	1.93	1.35	1.76	1.21
$\Sigma+K+\bar{\Sigma}$	2.15	1.53	1.98	1.39
$\Xi+K+\bar{\Xi}$	2.98	2.18	2.82	2.03
$K+3\pi$	Exothermic		Exothermic	
$2K+\pi+\bar{K}$	Exothermic		Exothermic	
$\mathcal{N}+2\pi+\bar{\Lambda}$	0.649	0.379	0.482	0.254
$\mathcal{N}+2\pi+\bar{\Sigma}$	0.839	0.518	0.671	0.389
$\mathcal{N}+K+\pi+\bar{\mathcal{N}}$	1.11	0.723	0.944	0.589
$\Lambda+2\pi+\bar{\Xi}$	1.67	1.15	1.51	1.02
$\Sigma+2\pi+\bar{\Xi}$	1.89	1.32	1.73	1.18
$\Lambda+K+\pi+\bar{\Lambda}$	2.12	1.50	1.95	1.36
$\mathcal{N}+\pi+\bar{K}+\bar{\Xi}$	2.21	1.57	2.04	1.43
$\Lambda+K+\pi+\bar{\Sigma}$	2.35	1.68	2.18	1.54
$\Sigma+K+\pi+\bar{\Lambda}$	2.35	1.68	2.18	1.54

TABLE II (*continued*).

Reaction products	Threshold energy (GeV)			
	$\bar{\Lambda}+\mathcal{N}\rightarrow$		$\bar{\Sigma}+\mathcal{N}\rightarrow$	
	$\mathcal{N}$	$\bar{\mathcal{N}}$	$\mathcal{N}$	$\bar{\mathcal{N}}$
$\Sigma + K+\pi+\bar{\Sigma}$	2.59	1.87	2.42	1.72
$\mathcal{N}+ K+\bar{K}+\bar{\Lambda}$	2.68	1.94	2.51	1.80
$\Lambda +2K+\bar{\mathcal{N}}$	2.68	1.94	2.51	1.80
$\mathcal{N}+ K+\bar{K}+\bar{\Sigma}$	2.93	2.13	2.76	1.99
$\Sigma +2K+\bar{\mathcal{N}}$	2.93	2.13	2.76	1.99
$\Xi + K+\pi+\bar{\Xi}$	3.46	2.55	3.29	2.41
$\Xi +2K+ \bar{\Lambda}$	3.99	2.97	3.83	2.83
$\Lambda + K+ \bar{K}+\bar{\Xi}$	3.99	2.97	3.83	2.83
$\Xi +2K+ \bar{\Sigma}$	4.27	3.19	4.10	3.04
$\Sigma + K+ \bar{K}+\bar{\Xi}$	4.27	3.19	4.10	3.04
$2\mathcal{N}+ \bar{\Lambda}+ \bar{\mathcal{N}}$	5.99	4.55	5.82	4.40
$2\mathcal{N}+ \bar{\Sigma}+ \bar{\mathcal{N}}$	6.30	4.80	6.14	4.65
$\mathcal{N}+ \Lambda+2\bar{\Lambda}$	7.53	5.77	7.36	5.62
$\mathcal{N}+ \Lambda+ \bar{\Xi}+\bar{\mathcal{N}}$	7.66	5.87	7.49	5.73
$\mathcal{N}+ \Lambda+ \bar{\Sigma}+\bar{\Lambda}$	7.87	6.04	7.70	5.89
$\mathcal{N}+ \Sigma+2\bar{\Lambda}$	7.87	6.04	7.70	5.89
$\mathcal{N}+ \Sigma+ \bar{\Xi}+\bar{\mathcal{N}}$	8.01	6.15	7.84	6.00
$\mathcal{N}+ \Lambda+2\bar{\Sigma}$	8.22	6.32	8.06	6.17
$\mathcal{N}+ \Sigma+ \bar{\Sigma}+\bar{\Lambda}$	8.22	6.32	8.06	6.17
$\mathcal{N}+ \Sigma+2\bar{\Sigma}$	8.58	6.60	8.41	6.45
$2\Lambda + \bar{\Xi}+ \bar{\Lambda}$	9.34	7.20	9.17	7.06
$\mathcal{N}+ \Xi+ \bar{\Lambda}+\bar{\Xi}$	9.49	7.32	9.32	7.17
$2\Lambda + \bar{\Xi}+\bar{\Sigma}$	9.72	7.50	9.55	7.36
$\Lambda + \Sigma+ \bar{\Xi}+\bar{\Lambda}$	9.72	7.50	9.55	7.36
$\mathcal{N} + \Xi+ \bar{\Xi}+\bar{\Sigma}$	9.86	7.62	9.70	7.47
$\Lambda + \Sigma+ \bar{\Xi}+\bar{\Sigma}$	10.1	7.81	9.93	7.66
$2\Sigma + \bar{\Xi}+ \bar{\Lambda}$	10.1	7.81	9.93	7.66
$2\Sigma + \bar{\Xi}+ \bar{\Sigma}$	10.5	8.11	10.3	7.97
$\Lambda + \bar{K}+2\bar{\Xi}$	11.5	8.89	11.3	8.75
$\Sigma + \Xi+2\bar{\Xi}$	11.9	9.22	11.7	9.07

TABLE II (*continued*).

Reaction products	Threshold energy (GeV) $\Xi + \mathcal{N} \rightarrow$	
	$\mathcal{N}$	$\bar{\mathcal{N}}$
2Λ	Exothermic	
$\Lambda + \Sigma$	0.112	0.0211
2Σ	0.299	0.124
$2\Lambda + \pi$	0.271	0.107
$\mathcal{N} + \Xi + \pi$	0.345	0.153
$\Lambda + \Sigma + \pi$	0.463	0.232
$2\Sigma + \pi$	0.661	0.371
$\mathcal{N} + \Lambda + \bar{K}$	0.740	0.427
$\mathcal{N} + \Sigma + \bar{K}$	0.946	0.579
$\Lambda + \Xi + K$	1.85	1.27
$\Sigma + \Xi + K$	2.09	1.45
$2\Lambda + 2\pi$	0.632	0.350
$\mathcal{N} + \Xi + 2\pi$	0.710	0.406
$\Lambda + \Sigma + 2\pi$	0.835	0.497
$2\Sigma + 2\pi$	1.04	0.652
$\mathcal{N} + \Lambda + \pi + \bar{K}$	1.13	0.714
$\mathcal{N} + \Sigma + \pi + \bar{K}$	1.34	0.878
$2\mathcal{N} + 2\bar{K}$	1.66	1.12
$\Lambda + \Xi + K + \pi$	2.29	1.61
$\Sigma + \Xi + K + \pi$	2.54	1.80
$2\Lambda + K + \bar{K}$	2.80	2.00
$\mathcal{N} + \Xi + K + \bar{K}$	2.90	2.08
$\Lambda + \Sigma + K + \bar{K}$	3.06	2.20
$2\Sigma + K + \bar{K}$	3.32	2.41
$2\Xi + 2K$	4.92	3.17
$\mathcal{N} + 2\Lambda + \bar{\mathcal{N}}$	6.27	4.73
$2\mathcal{N} + \Xi + \bar{\mathcal{N}}$	6.40	4.84
$\mathcal{N} + \Lambda + \Sigma + \bar{\mathcal{N}}$	6.60	5.00
$\mathcal{N} + 2\Sigma + \bar{\mathcal{N}}$	6.94	5.26
$3\Lambda + \bar{\Lambda}$	7.87	6.01
$\mathcal{N} + \Lambda + \Xi + \bar{\Lambda}$	8.01	6.12
$3\Lambda + \bar{\Sigma}$	8.23	6.29
$2\Lambda + \Sigma + \bar{\Lambda}$	8.23	6.29
$\mathcal{N} + \Lambda + \Xi + \bar{\Sigma}$	8.37	6.40
$\mathcal{N} + \Sigma + \Xi + \bar{\Lambda}$	8.37	6.40
$2\Lambda + \Sigma + \bar{\Sigma}$	8.60	6.58
$\Lambda + 2\Sigma + \bar{\Lambda}$	8.60	6.58
$\mathcal{N} + \Sigma + \Xi + \bar{\Sigma}$	8.74	6.69
$\Lambda + 2\Sigma + \bar{\Sigma}$	8.97	6.87
$3\Sigma + \bar{\Lambda}$	8.97	6.87
$3\Sigma + \bar{\Sigma}$	9.35	7.17
$2\Lambda + \Xi + \bar{\Xi}$	9.91	7.62
$\mathcal{N} + 2\Xi + \bar{\Xi}$	10.1	7.74
$\Lambda + \Sigma + \Xi + \bar{\Xi}$	10.3	7.93
$2\Sigma + \Xi + \bar{\Xi}$	10.7	8.25

TABLE II (*continued*).

Reaction products	Threshold energy (GeV)	
	$\bar{\Xi}+\mathcal{N}\rightarrow$	
	$\mathcal{N}$	$\bar{\mathcal{N}}$
2K	Exothermic	
$2K+\pi$	Exothermic	
$\mathcal{N}+\pi+\bar{\Xi}$	0.345	0.153
$\mathcal{N}+K+\bar{\Lambda}$	0.740	0.427
$\mathcal{N}+K+\bar{\Sigma}$	0.946	0.579
$\Lambda+K+\bar{\Xi}$	1.85	1.27
$\Sigma+K+\bar{\Xi}$	2.09	1.45
$2K+2\pi$	Exothermic	
$3K+\bar{K}$	Exothermic	
$\mathcal{N}+2\pi+\bar{\Xi}$	0.710	0.406
$\mathcal{N}+K+\pi+\bar{\Lambda}$	1.13	0.714
$\mathcal{N}+K+\pi+\bar{\Sigma}$	1.34	0.878
$\mathcal{N}+2K+\bar{\mathcal{N}}$	1.66	1.12
$\Lambda+K+\pi+\bar{\Xi}$	2.29	1.61
$\Sigma+K+\pi+\bar{\Xi}$	2.54	1.80
$\Lambda+2K+\bar{\Lambda}$	2.80	2.00
$\mathcal{N}+K+\bar{K}+\bar{\Xi}$	2.90	2.08
$\Lambda+2K+\bar{\Sigma}$	3.06	2.20
$\Sigma+2K+\bar{\Lambda}$	3.06	2.20
$\Sigma+2K+\bar{\Sigma}$	3.32	2.41
$\Xi+2K+\bar{\Xi}$	4.29	3.17
$2\mathcal{N}+2\bar{\Lambda}$	6.27	4.73
$2\mathcal{N}+\bar{\Xi}+\bar{\mathcal{N}}$	6.40	4.84
$2\mathcal{N}+\bar{\Sigma}+\bar{\Lambda}$	6.60	5.00
$2\mathcal{N}+2\bar{\Sigma}$	6.94	5.26
$\mathcal{N}+\Lambda+\bar{\Xi}+\bar{\Lambda}$	8.01	6.12
$\mathcal{N}+\Lambda+\bar{\Xi}+\bar{\Sigma}$	8.37	6.40
$\mathcal{N}+\Sigma+\bar{\Xi}+\bar{\Lambda}$	8.37	6.40
$\mathcal{N}+\Sigma+\bar{\Xi}+\bar{\Sigma}$	8.74	6.69
$2\Lambda+2\bar{\Xi}$	9.91	7.62
$\mathcal{N}+\Xi+2\bar{\Xi}$	10.1	7.74
$\Lambda+\Sigma+2\bar{\Xi}$	10.3	7.93
$2\Sigma+2\bar{\Xi}$	10.7	8.25

3. – Threshold energies.

The threshold energies for the reactions listed in Ref. [1] and those in Table II were calculated with the « Oracle », an electronic digital computer at the Oak Ridge National Laboratory. The threshold energies which deviated

by more than 2% from those given in Ref. [1] are given in Table III. In Table II the column labeled $\mathcal{N}$ is for the target at rest and the column labeled $\overleftarrow{\mathcal{N}}$ for the target with 25 MeV of energy moving toward the projectile.

TABLE III. – *Corrected threshold energies.*

Reaction	Threshold energy (GeV)	
	BEASLEY and HOLLADAY	« Oracle »
$\pi + \overleftarrow{\mathcal{N}} \rightarrow \mathcal{N} + \Sigma + \bar{\Lambda}$	4.07	3.93
$\bar{K} + \overleftarrow{\mathcal{N}} \rightarrow \Xi + K + 2\pi$	0.80	0.898
$\bar{\mathcal{N}} + \overleftarrow{\mathcal{N}} \rightarrow 2\mathcal{N} + 2\bar{\mathcal{N}}$	4.384	4.298

Figs. 1 and 2 give the threshold energy for a given production process as a function of the total mass of the product particles. The threshold energy as a function of the total mass of the produced particles for an antiparticle incident upon a given particle is the same function as that for the corresponding

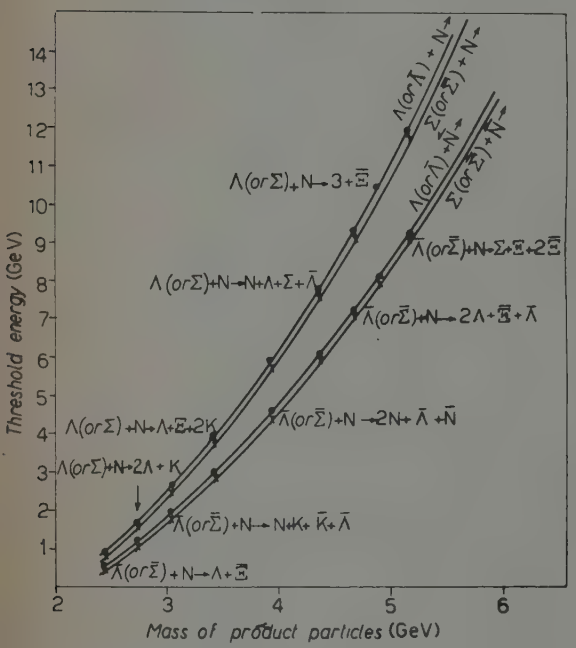

Fig. 1. – Threshold energies for various production processes.

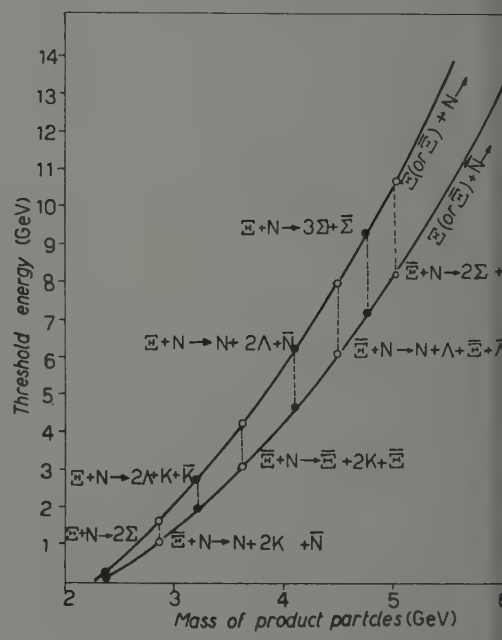

Fig. 2. – Threshold energies for various production processes.

particle incident on the same target. Of course, the specific product particles will be different for the two situations. The lines of constant mass of some typical particles in the two situations are shown.

The masses [2] of the particles used in all the claculations are given in Table I.

4. – Multistage reations.

Frequently it is of interest to know the threshold energy required to produce a given particle in a multistage process. For instance, given the reactions $\mathcal{N}+\mathcal{N}\to 3\mathcal{N}+\overline{\mathcal{N}}$, and $\overline{\mathcal{N}}+\mathcal{N}\to \Xi+\overline{\Xi}$, we might ask what energy the incident nucleon must have in order to produce a $\overline{\Xi}$ by this process. We can answer this question if we know what energy the incident nucleon must have to produce an $\overline{\mathcal{N}}$ of sufficient energy to initiate the latter reaction. A relation, therefore, is required for the maximum energy of the $\overline{\mathcal{N}}$ terms in terms of the energy of the incident nucleon. In general, this relation for the maximum kinetic energy of the produced intermediate particle (subscript I) which serves as a projectile in the second state of the reaction is

$$T_I=\frac{qS}{2}+\frac{r}{2}\sqrt{S^2-\frac{4M_I^2}{s}}-M_I\,, \tag{5}$$

where

$$\begin{aligned} q &= E_p+E_t\,,\\ r &= |p_p-p_t|\,,\\ s &= q^2-r^2\,,\\ S &= 1-\frac{M^2-M_I^2}{s}\,. \end{aligned}$$

The subscripts p and t designate the projectile and target in the first stage of the reaction and M is the total mass of all the particles produced in the final state of the first stage of the reaction aside from particle I. The symbols p and E represent momentum and total energy, respectively.

Particle I will receive maximum kinetic energy only if its momentum is parallel to that of the projectile, and the rest of the product particles leave the reaction center together with the same velocity either parallel or antiparallel to the projectile. It is also assumed that the target momentum is toward the projectile.

---

[2] M. Gell-Mann and A. H. Rosenfeld: *Ann. Rev. Nucl. Sci.*, **7**, 411 (1957).

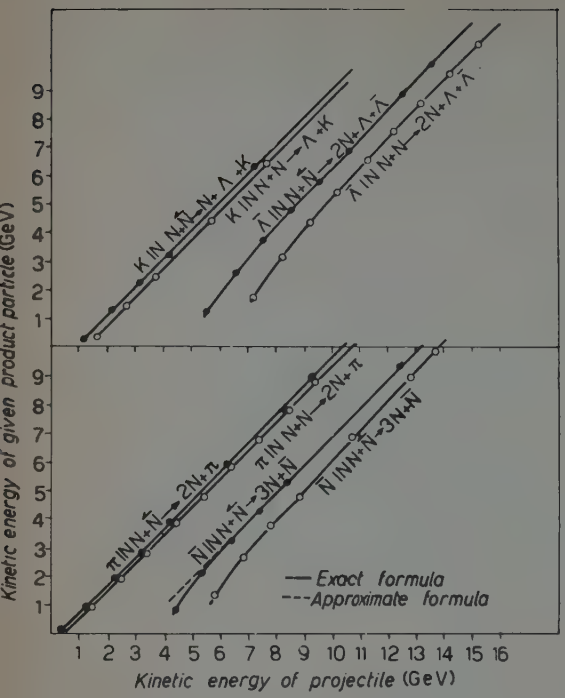

Fig. 3. – Maximum energies for various processes.

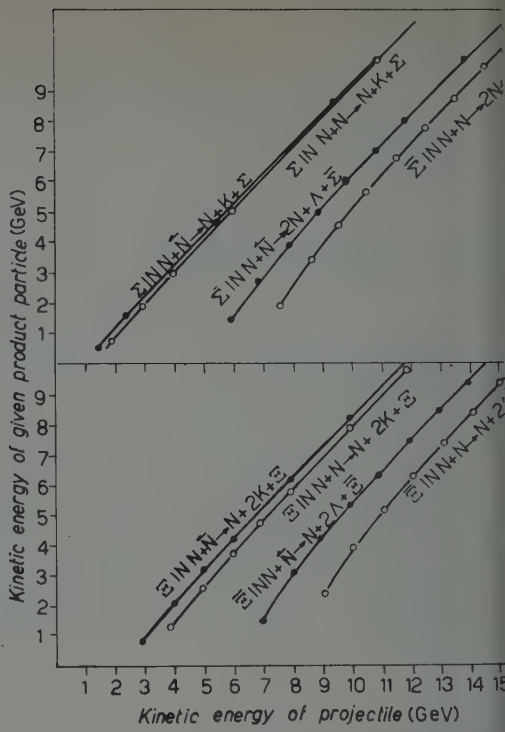

Fig. 4. – Maximum energies for various proc

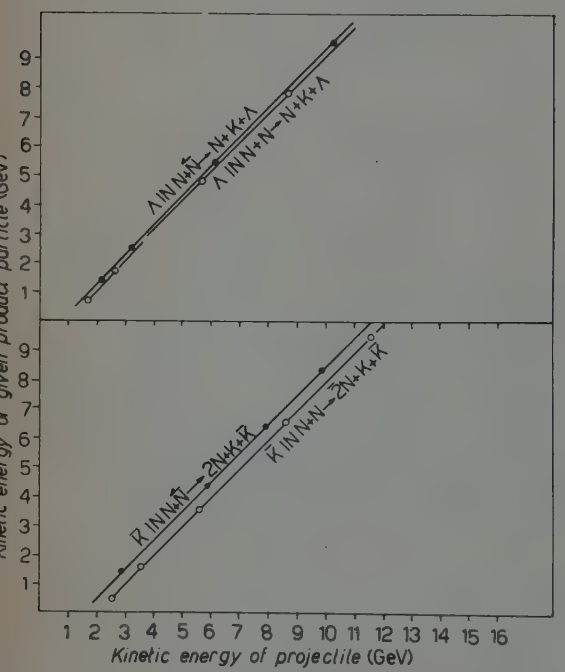

Fig. 5. – Maximum energies for various processes.

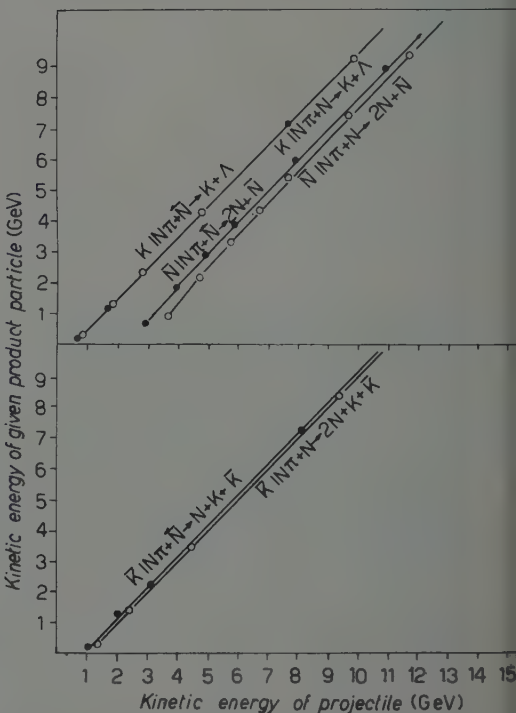

Fig. 6. – Maximum energies for various proc

From this equation the maximum laboratory kinetic energy that each of the particles listed in Table I can have when it is produced by a nucleon and a pion incident on a nucleon, has been calculated as a function of the laboratory kinetic energy of the projectile. The results of these calculations are

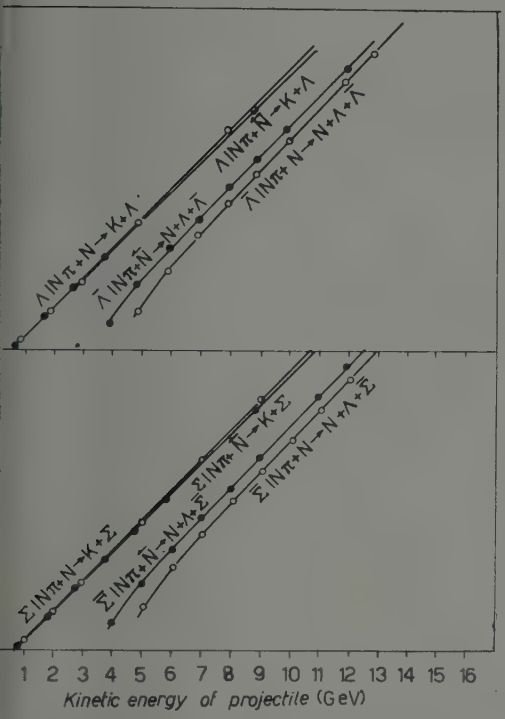

Fig. 7. – Maximum energies for various processes.

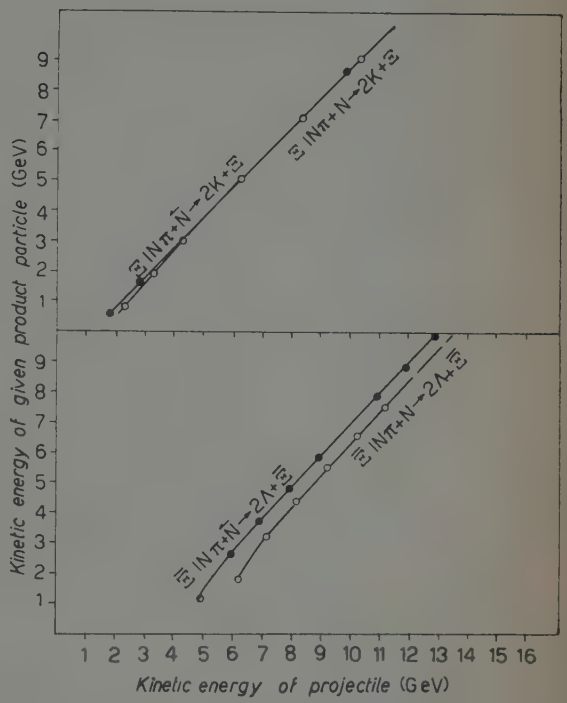

Fig. 8. – Maximum energies for various processes.

plotted in Figs. 3-8. An inspection of Figs. 3-8 shows that the dependence of the maximum energy of a given product particle on the energy of the projectile becomes practically linear for high energies of the projectile. This linear dependence may be obtained by an asymptotic expansion of equation (5) and is

$$T_I \simeq E_p + \frac{(E_t - p_t)}{2} - \frac{M^2}{2(E_t + p_t)} - M_I \,. \tag{6}$$

A comparison of equations (5) and (6) is shown in Fig. 3.

Table IV presents some interesting threshold energies obtained in this way.

TABLE IV. – *Thresholds for several two stage processes.*

Process	Threshold energy (GeV)			
	$\mathcal{N}_1\,\mathcal{N}_2$ (*)	$\overleftarrow{\mathcal{N}}_1\,\mathcal{N}_2$	$\mathcal{N}_1\,\overleftarrow{\mathcal{N}}_2$	$\overleftarrow{\mathcal{N}}_1\,\overleftarrow{\mathcal{N}}_2$
$\mathcal{N}+\mathcal{N} \rightarrow \mathcal{N}+\Lambda+\mathrm{K}$ (then)				
$\mathrm{K}+\mathcal{N} \rightarrow 2\mathcal{N}+\bar{\Lambda}$	4.93	4.60	4.06	3.74
(or) $2\mathcal{N}+\bar{\Sigma}$	5.16	4.83	4.26	3.93
$\mathcal{N}+\Lambda+\Xi$	6.23	5.90	5.10	4.77
$\mathcal{N}+\mathcal{N} \rightarrow \mathcal{N}+\mathcal{N}+\mathcal{N}+\mathcal{N}$ (then)				
$\mathcal{N}+\mathcal{N} \rightarrow \Sigma+\bar{\Lambda}$	5.63 (**)	4.29	5.63	4.29
$\Lambda+\bar{\Sigma}$	5.63	4.42	5.63	4.29
$\Sigma+\bar{\Sigma}$	5.63	4.52	5.63	4.29
$\Xi+\bar{\Xi}$	6.08	5.08	5.72	4.67

(*) The labels $\mathcal{N}_1$ and $\mathcal{N}_2$ refer respectively to the target nucleons of the first and second stage at rest. The labels $\overleftarrow{\mathcal{N}}_1$ and $\overleftarrow{\mathcal{N}}_2$ refer to these same targets with 25 MeV of kinetic energy and momentum toward the projectile.

(**) The recurrence of thresholds 5.63 GeV and 4.29 GeV is due to the threshold of the second stage of each of these reactions being lower than the maximum energy of the product particle of the first stage (the projectile of the second stage) when this product particle is produced at the threshold of the first stage.

5. – Additional comments.

When two particles collide whose total A and B quantum numbers are A_T and B_T, then a total of N different reactions (not counting the different electric charge states) with n particles in the final state can be initiated. It is clear that N is a well defined function, $N(A_T, B_T, n)$, of A_T, B_T, and n. We have sought an explicit representation of this function and have not succeeded in finding one. The knowledge of this function would be valuable in determining the feasibility of writing down all the possible reactions having a large number of product particles and in providing a check on whether one has indeed written down all the possible reactions with n particles in the final state which may be produced by a given pair of initial particles. One can, of course, determine N by writing down all the various reactions that are involved by the method of this paper and simply count them. In this way it has been determined that for $A_T = 1$, $B_T = 1$ (π+nucleon), $N(1, 1, 2) = 3$, $N(1, 1, 3) = 14$, $N(1, 1, 4) = 32$, $N(1, 1, 5) = 83$, $N(1, 1, 6) = 179$, and $N(1, 1, 7) = 379$.

6. – Conclusion.

A method has been developed for finding all possible reactions for a given pair of initial particles. By this method and, also, by means of the « Oracle », all possible reactions for a Λ, Σ, Ξ, Ξ, $\bar{\Sigma}$ and $\bar{\Lambda}$ incident on a nucleon at rest and with 25 MeV of kinetic energy and momentum toward the projectile were determined. The thresholds for these reactions were calculated by the « Oracle ». The results are given in Table II.

The possible reactions with three product particles are of particular interest because in many cases they may be used to study the interaction between two of the product particles

A formula for the maximum laboratory kinetic energy of one of the particles produced in a given reaction, as a function of the laboratory kinetic energy of the initial particles, has been derived. From this formula, the maximum energy that each of the particles of Table I can have when it is produced by a pion or a nucleon incident on a nucleon at rest and in motion toward the projectile with 25 MeV of kinetic energy, has been calculated on the « Oracle ». The results are plotted in Figs. 3-8.

* * *

We are grateful to the Oak Ridge National Laboratories for the use of the « Oracle » and to Mr. C. T. Fike and C. W. Nestor for their work in coding the problem.

SUPPLEMENTO AL VOLUME XV, SERIE X
DEL NUOVO CIMENTO

N. 3, 1960
1° Trimestre

Statistical Weights of Many-Particle Systems in Spin or Isospin Space.

F. CERULUS
CERN - Geneva

(ricevuto il 19 Novembre 1959)

1. – Introduction.

It has been pointed out earlier [1] that in many cases one does not need to know all quantum numbers characterizing the end-state of a production process, in order to check certain properties of the interaction, and that it is useful to know the statistical weights of states characterized by an incomplete set of parameters.

We shall develop the theory with the example in mind of the high-energy nucleon-nucleon collisions, where the end-particles have to combine to yield states of given total isospin and charge.

We shall use the notation j_i, m_i for the (iso)spin and the projection along a given direction of the i-th particle.

2. – The formalism.

Experimentally one observes end-states which one describes by stating the number and the charges of each kind of particle ($\mathcal{N}$, π, K, etc.).

It is therefore natural to describe the (iso)spin dependence of such end-

[1] Y. YEIVIN and A. DE-SHALIT: *Nuovo Cimento*, **1**, 1147 (1955).

states by a product wave function

$$|j_1, m_1\rangle |j_2, m_2\rangle \ldots |j_n, m_n\rangle \equiv |m_1, m_2, \ldots, m_n\rangle , \tag{1}$$

where in the r.h.s. notation the j_i's are supposed to be given.

(Iso)spin conservation states, however, that

$$J^2 = \left(\sum j_i\right)^2$$

is a good quantum number, and to put this property in evidence one should use a system of base-vectors in (iso)spin space where J is diagonal. The choice of such a base is equivalent to the choice of a coupling scheme for the j_i [2]; we can choose, *e.g.*, a system where

$$j_{12}^2 = (j_1 + j_2)^2$$

$$j_{123}^2 = (j_1 + j_2 + j_3)^2$$

.....

are diagonal.

A base-vector of this scheme is denoted by

$$|j_{12}, j_{123}, \ldots, J, M\rangle , \tag{2}$$

where the j_1, j_2, etc., are assumed to be known. If it is wished to state the j_1, j_2, etc., explicitly, (2) is written

$$|\{[(j_1 j_2) j_{12} j_3] j_{123} \ldots\rangle$$

or, more simply

$$|j_1 j_2 (j_{12}) j_3 (j_{123}) j_4 \ldots\rangle .$$

Both systems (1) and (2) are complete, and a unitary transformation

$$|j_{12}, \ldots, J, M\rangle = \sum_{m_1 \ldots m_n} \langle m_1, m_2, \ldots, m_n | j_{12}, \ldots, J, M\rangle |m_1, \ldots, m_n\rangle \tag{3}$$

leads from the one to the other [2]. The coefficient $\langle m_1, m_2, \ldots | j_{12}, \ldots, J, M\rangle$ is called a recoupling coefficient. The recoupling coefficient is a product of Clebsch-Gordan coefficients

$$\langle j_{12}, \ldots, J, M | m_1, \ldots, m_n\rangle = C^{j_1 j_2 j_{12}}_{m_1 m_2 m_1 + m_2} \ldots C^{j_{12 \ldots n-1} j_n J}_{m_1 + \ldots + m_{n-1} m_n M} . \tag{4}$$

---

[2] U. Fano and G. Racah: *Irreducible Tensorial Sets* (New York, 1959). We shall follow closely the notation of these authors in this report.

In a statistical theory of production, where nothing is known about the dynamics of the production, it is assumed that all end-states of n specified particles and with a given J, M have equal probability. The probability to observe an end-state $|m_1 \dots m_n\rangle$ is then

$$(5) \qquad \sum_{j_{12}\dots j_{12\dots n-1}} |\langle j_{12}, \dots, J, M | m_1 \dots m_n\rangle|^2 .$$

3. – The charge distribution coefficients: their properties.

To shorten the notation, let us define

$$j_{12\dots i} = J_i ,$$

$$m_1 + m_2 + \dots + m_i = M_i .$$

The probability (5) is then given by

$$(6) \qquad P^J_{m_1,\dots,m_n} \equiv \sum_{J_2, J_3, \dots, J_{n-1}} |\langle J_2, J_3, \dots, J_{n-1}, J, M | m_1, m_2, \dots, m_n\rangle|^2$$

$$(7) \qquad = \sum_{J_2, J_3, \dots, J_{n-1}} (C^{j_1 j_3 J_2}_{m_1 m_2 M_2} C^{J_2 j_3 J_3}_{M_2 m_3 M_3} \dots C^{J_{n-1} j_n J}_{M_{n-1} m_n M})^2 .$$

These coefficients can be calculated by a recurrence relation, using the known values of the Clebsch-Gordan coefficients, which follows at once from (7), *viz.*:

$$(8) \qquad P^J_{m_1,\dots,m_n} = \sum_{J_{n-1} = J - j_n}^{J + j_n} P^{J_{n-1}}_{m_1,\dots,m_{n-1}} (C^{J_{n-1} j_n J}_{M_{n-1} m_n M})^2 .$$

A more general formula, which follows again from (7) is:

$$(9) \qquad P^J_{m_1,\dots,m_n} = \sum_{J_r} {}^{(j_a)}P^{J_r}_{m_1,\dots,m_r} {}^{(j_b)}P^J_{M_r, m_{r+1},\dots,m_n}$$

(j_a) is shorthand for the suppressed indices $j_1, \dots, j_r$,

(j_b) is shorthand for the suppressed ineices $J_r, j_{r+1}, \dots, j_n$.

This allows to calculate the $P^J_{m_1,\dots,m_n}$ for a system of particles composed of two other systems, if the $P^J_{m_1,\dots}$ for each of these are known.

A few properties of these coefficients can be stated:

$$(10) \quad a) \qquad P^J_{m_1,\dots,m_n} = P^J_{-m_1,\dots,-m_n}$$

because of the property $C^{j_1 j_2 j}_{m_1 m_2 m} = (-1)^{j_1+j_2-j} C^{j_1 j_2 j}_{-m_1,-m_2,-m}$ and the recurrence relation (8).

b) The P coefficients are independent of the order in which the particles occur

$$(11) \qquad {}^{(j_1,\ldots,j_i,j_{i+1},\ldots)}P^{J}_{m_1,\ldots,m_i,m_{i+1},\ldots} = {}^{(j_1,\ldots,j_{i+1},j_i,\ldots)}P^{J}_{m_1,\ldots,m_{i+1},m_i,\ldots}.$$

One goes from the l.h.s. of (8) to the r.h.s. by interchanging the particles i and $i+1$. This means going over from the coupling scheme

$$(12) \qquad [(J_i j_i) J_{i+1} j_{i+1}] J_{i+2}, \ldots$$

to the alternate scheme

$$(13) \qquad [(J_i j_{i+1}) J'_{i+1} j_i] J_{i+2}, \ldots$$

and from

$$j_1, m_1, \ldots, j_i, m_i, j_{i+1}, m_{i+1}, \ldots$$

to

$$j_1, m_1, \ldots, j_{i+1}, m_{i+1}, j_i m_i, \ldots .$$

The latter involves only a trivial permutation of columns in the transformation matrix from the $|j_1 m_i, \ldots, j_n m_n\rangle$ to the $|j_1, j_2(J), \ldots, J, M\rangle$ system. The relation between (12) and (13) is given by a recoupling coefficient:

$$\langle \ldots (J_{i-1}) j_i (J_i) j_{i+1} (J_{i+1}) \ldots | = \sum_{J'_i} \langle \ldots (J_{i-1}) j_i (J_i) J_{i+1} (J_{i+1}) \ldots | \ldots (J_{i-1}) j_{i+1} (J'_i) j_i (J_{i+1}) \ldots \rangle \cdot$$
$$\cdot \langle \ldots (J_{i-1}) j_{i+1} (J'_i) j_i (J_{i+1}) \ldots | .$$

The $P^{J}_{m_1,\ldots,m_i,m_{i+1},\ldots}$ is then equal to

$$\sum_{J_1,\ldots,J_{n-1}} | \sum_{j_{12}} \langle j_{12}, j_3 | j_{13}, j_2 \rangle^{j_4} \langle \ldots (J_{i-1}) j_{i+1} (J'_i) j_i (J_{i+1}) | m_1, \ldots, m_n \rangle |^2 ,$$

where we have put

$$j_1 = J_{i-1} \qquad j_3 = j_{i+1} \qquad j_{13} = J'_i$$
$$j_2 = j_i \qquad j_{12} = J_i \qquad j_4 = J_{i+1}$$

in order to show that we need only a three-vector recoupling coefficient.

Taking only the sum over $J_i = j_{12}$ and writing the square as a product

of two sums with indices j_{12} and j'_{12}, we have

$$\sum_{j_{12}}\sum_{j_{13}}\sum_{j'_{13}}\langle j_{12}, j_3 | j_{13}, j_2\rangle^{j_4}\langle j_{12}, j_3 | j'_{13}, j_2\rangle^{j_4}\cdot$$

$$\cdot\langle\ldots (j_{13})j_2(i_4)\ldots | m_1, \ldots, m_n\rangle\langle\ldots (j'_{13})j_2(j_4)\ldots | m_1, \ldots, m_n\rangle =$$

$$= \sum_{j_{13}}\sum_{j'_{13}}\langle\ldots (j_{13})\ldots | m_1, \ldots, m_n\rangle\langle\ldots (j'_{13})\ldots | m_1, \ldots, m_n\rangle\sqrt{(2j_{12}+1)(2j'_{13}+1)}\cdot$$

$$\cdot\sum_{j_{12}}(2j_{12}+1)\,\overline{W}\begin{pmatrix} j_1 & j_2 & j_{12}\\ j_4 & j_3 & j_{13}\end{pmatrix}\,\overline{W}\begin{pmatrix} j_1 & j_2 & j_{12}\\ j_4 & j_3 & j'_{13}\end{pmatrix},$$

where $\overline{W}$ are the Racah coefficients, as defined in [2]. The last sum, because of one of the sum rules for the $\overline{W}$ reduces to $1/(2j_{13}+1)\ \delta(j_{13}, j'_{13})\ \delta(j_1, j_2, j_{13})\cdot$ $\cdot\delta(j_4, j_2, j_{13})$ and the triple sum reduces to

$$\sum_{j_{13}}|\langle\ldots (j_{13})j_2(j_4)\ldots | m_1, \ldots, m_n\rangle|^2\,.$$

Performing the other summation, over J_1 to J_{n-1} (except $J'_i = j_{13}$) one gets the P coefficient with the order of the particles interchanged.

Therefore ${}^{(j,j,\ldots,j)}P^J_{m_1,\ldots,m_n}$, *i.e.* the P^J coefficient for a system of n equal particles, is independent of the order of the $m_1, \ldots, m_n$ and depends only on their set of values. If the particles have $j=1$, $P^J_{m_1,\ldots,m_n}$ can be written as $P^J_{n_-,n_0,n_+}$ where n_-, n_0, n_+ are the numbers of particles with $m=-1,\ 0,+1$ respectively.

4. – Orthogonality properties.

In the following Tables one will find P^J coefficients for systems composed of spin $\frac{1}{2}$, 1 and $\frac{3}{2}$ and all possible combinations of m's. They have been prepared for use in statistical theories of meson production. The number of spin $\frac{1}{2}$ and $\frac{3}{2}$ particles is at most two, the number of spin 1 particles is at most 8.

The Tables for spin 1 particles were computed using formula (8) and the well known formulae for the Clebsch-Gordan coefficients. The Tables for mixed systems ($\frac{1}{2}$ and $\frac{3}{2}$ plus spin 1) using formula (9) are derived from the former.

There exist two simple checks as to the accuracy of the Tables. Both stem from the fact that the recoupling transformation is orthogonal. Suppose we label the columns of the transformation matrix by the sets of numbers $m_1, \ldots, m_n$, and the rows by $J_1, J_2, \ldots, J, M$ The transformation is unitary and real and therefore orthogonal. This property can easily be checked on formula (4), using the orthogonality of the Clebsch-Gordan coefficients.

As a first consequence, the sum of the squares of the elements in a column is one:

$$\sum_{J_1,\ldots,J_{n-1},J,M} (\langle J_1, J_2, \ldots, j_n(J), M \,|\, m_1, \ldots, m_n\rangle)^2 = 1 .$$

Because the coefficients are zero, unless $M = m_1 + \ldots + m_n$, the M-summation is trivial, and the equation can be written, because of (6):

$$\sum_J P^J_{m_1,\ldots,m_n} = 1 \qquad \text{for every set of } m_1, \ldots, m_n . \tag{14}$$

Doing the sum of the squares of the elements of a row we get (provided the $j_1, \ldots, j_n, J_1, \ldots, J_n$ are such that all triangular conditions on the vector couplings are satisfied)

$$\sum_{(m)_M} (\langle J_1\, J_2, \ldots, J, M \,|\, m_1, \ldots, m_n\rangle)^2 = 1 ,$$

where the summation is over all combinations of $m_1, \ldots, m_n$ whose sum is M.

Summing this further over $J_1, J_2, \ldots, J_{n-1}$, we get

$$\sum_{(m)_M} P^J_{m_1,\ldots,m_n} = \varrho(J) , \tag{15}$$

where $\varrho(J)$ is the number of independent (product) spin functions of n particles which can be constructed, and which yield a total spin J. $\varrho(J)$ depends on the spin of the particles, and on their number, but is independent of M. The $\varrho(J)$ have been tabulated elsewhere [1,3].

In applying the check (15) to a Table of $P^J_{m_1,\ldots,m_n}$ one has to keep in mind that each set of $m_1, \ldots, m_n$ is listed only once, although there are as many columns in the transformation matrix labelled by the numbers of this set (in different orders) as there are permutations of $m_1, \ldots, m_n$. One can alternatively sum over different sets of m_1 only, and use as terms in the sum the numbers

$$^*P^J_{m_1,\ldots,m_n} = P^J_{m_1,\ldots,m_n} \times (\text{nr. of permutations of } m_1, \ldots, m_n) .$$

For systems composed of spin 1 particles one has *e.g.*

$$^*P^J_{n_-,n_0,n_+} = \frac{n!}{n_-!\, n_0!\, n_+!}\, P^J_{n_-,n_0,n_+} .$$

---

[3] V. S. Barašenkov and B. M. Barbašev: *Suppl. Nuovo Cimento*, **7**, 19 (1957).

Tables of the ${}^*P^J$ are also given, because one needs precisely those numbers in analysing the probabilities for multiple meson production into different charge states. As these ${}^*P^J$ are likely to be used for computational purposes they are listed in decimal form.

For systems of two baryons (spins $\frac{1}{2}$ or $\frac{3}{2}$) we give Tables of the coefficients

$$ {}^{(j_1,j_2,j_3)}P^1_{m_1,m_2(1-m_1-m_2)} \,, $$

and

$$ {}^{(j_1,j_2,j_3)}P^{0 \text{ or } 1}_{m_1,m_2,(-m_1-m_2)} \,, $$

because these are more useful in calculating the P^J coefficients for composite systems of baryons and pions, according to formula (9), *e.g.*

$$ {}^{(1,1,\ldots,1,j_1,j_2)}P^1_{n_+,n_0,n_-;m_1,m_2,} = \sum_{j_3} {}^{(1,\ldots,1)}P^{j_3}_{n_+,n_0,n_-} \, {}^{(j_1j_2j_3)}P^1_{m_1,m_2,n_+-n_-} \,. $$

As a check on these Tables one can use the following property

$$ \sum_{j_3} (2j_3+1) \, {}^{(j_1,j_2,j_3)}P^J_{m_1,m_2,m_3} = 2J+1 \,. \tag{16} $$

This is easily proved:

$$ {}^{(j_1,j_2,j_3)}P^J_{m_1,m_2,m_3} = \sum_{J_2} (C^{j_1j_2J_2}_{m_1m_2M_2} \, C^{J_2j_3J}_{M_2m_3M})^2 = \frac{2J+1}{2j_3+1} \sum_{J_2} (C^{j_1j_2J_2}_{m_1m_2M_2} \, C^{J_2j_3j_3}_{M_2-M-m_3})^2 = \tag{17} $$

$$ = \frac{2J+1}{2j_3+1} \, {}^{(j_1j_2J)}P^{j_3}_{m_1,m_2,-M} \,, $$

multiplying both sides with $(2j_3+1)$ and summing over j_3 one gets (17) because of the orthogonality property (14).

Composite systems of two baryons and n pions ($0 \leqslant n \leqslant 5$) have been considered with $J=1$, $M=1$, corresponding to meson production in p-p collisions: the corresponding Tables are given.

* * *

The author has profited from valuable advice by Dr. DE-SHALIT. He is very much indebted to Mr. W. KLEIN who carried out all the numerical work and whose collaboration was most pleasant and most efficient.

TABLE I. – $P^J_{m_1,m_2}$ *for* 2 *spin* 1 *particles.*

M	m_1	m_2	J		
			0	1	2
2	+	+	0	0	1
1	+	0	0	1/2	1/2
0	0	0	1/3	0	2/3
	+	−	1/3	1/2	1/6

TABLE II. – $P^J_{n_+,n_0 n_-}$ *for* 3 *spin* 1 *particles.*

M	n_+	n_0	n_-	J			
				0	1	2	3
3	3	0	0	0	0	0	1
2	2	1	0	0	0	2/3	1/3
1	2	0	1	0	3/5	1/3	1/15
	1	2	0	0	2/5	1/3	4/15
0	1	1	1	1/6	2/5	1/3	1/10
	0	3	0	0	3/5	0	2/5

TABLE III. – $P^J_{n_+,n_0,n_-}$ *for* 4 *spin* 1 *particles.*

M	n_+	n_0	n_-	J				
				0	1	2	3	4
4	4	0	0					1
3	3	1	0				3/4	1/4
2	3	0	1			5/7	1/4	1/28
	2	2	0			11/21	1/3	1/7
1	2	1	1		2/5	8/21	11/60	1/28
	1	3	0		3/10	5/14	1/5	1/7
0	0	4	0	1/5	0	4/7	0	8/35
	1	2	1	2/15	3/10	13/42	1/5	2/35
	2	0	2	1/5	2/5	2/7	1/10	1/70

TABLE IV. – $P^J_{n_+,n_0,n_-}$ *for 5 spin 1 particles.*

M	n_+	n_0	n_-	J					
				0	1	2	3	4	5
5	5	0	0						1
4	4	1	0					4/5	1/5
3	4	0	1				7/9	1/5	1/45
	3	2	0				11/18	3/10	4/45
2	3	1	1			15/28	1/3	4/35	1/60
	2	3	0			3/7	1/3	6/35	1/15
1	3	0	2		3/7	5/14	1/6	3/70	1/210
	2	2	1		11/35	1/3	7/30	1/10	2/105
	1	4	0		9/35	2/7	4/15	4/35	8/105
	2	1	2	2/15	11/35	13/42	8/45	2/35	1/126
	1	3	1	1/10	9/35	2/7	19/90	4/35	2/63
	0	5	0	0	3/7	0	4/9	0	8/63

TABLE V. – $P^J_{n_+,n_0,n_-}$ *for 6 spin 1 particles.*

M	n_+	n_0	n_-	J						
				0	1	2	3	4	5	6
6	6	0	0							1
5	5	1	0						5/6	1/6
4	5	0	1					9/11	1/6	1/66
	4	2	0					37/55	4/15	2/33
3	4	1	1				28/45	16/55	7/90	1/110
	3	3	0				31/60	69/220	2/15	2/55
2	4	0	2			5/9	14/45	6/55	1/45	1/495
	2	4	0			23/63	14/45	78/385	4/45	16/495
	3	2	1			55/126	59/180	53/308	1/18	4/495
1	3	1	2		9/28	85/252	2/9	36/385	29/1260	1/396
	2	3	1		9/35	19/63	43/180	213/1540	17/315	1/99
	1	5	0		3/14	5/18	2/9	2/11	4/63	4/99
0	3	0	3	1/7	9/28	25/84	1/6	9/154	1/84	1/924
	2	2	2	11/105	9/35	2/7	19/90	81/770	2/63	1/231
	1	4	1	3/35	3/14	11/42	2/9	52/385	4/63	4/231
	0	6	0	1/7	0	10/21	0	24/77	0	16/231

TABLE VI. – $P^J_{n_+,n_0,n_-}$ *for 7 spin 1 particles.*

M	n_+	n_0	n_-	J = 0	1	2	3	4	5	6	7
7	7	0	0								1
6	6	1	0							6/7	1/7
5	6	0	1						11/13	1/7	1/91
	5	2	0						28/39	5/21	4/91
4	5	1	1					15/22	10/39	13/231	1/182
	4	3	0					32/55	19/65	8/77	2/91
3	5	0	2				7/11	3/11	1/13	1/77	1/1001
	4	2	1				259/495	17/55	76/585	13/385	4/1001
	3	4	0				74/165	17/55	32/195	24/385	16/1001
2	4	1	2			4/9	161/495	9/55	32/585	38/3465	1/1001
	3	3	1			31/84	103/330	151/770	71/780	32/1155	4/1001
	2	5	0			20/63	29/99	16/77	14/117	32/693	16/1001
1	4	0	3		1/3	1/3	7/33	1/11	1/39	1/231	1/3003
	3	2	2		11/42	19/63	47/198	103/770	212/4095	17/1386	4/3003
	2	4	1		23/105	17/63	118/495	61/385	328/4095	20/693	16/3003
	1	6	0		4/21	5/21	8/33	12/77	32/273	8/231	64/3003
0	3	1	3	3/28	11/42	2/7	9/44	31/308	3/91	1/154	1/1716
	2	3	2	3/35	23/105	11/42	12/55	52/385	11/182	4/231	1/429
	1	5	1	1/14	4/21	5/21	43/198	12/77	68/819	8/231	4/429
	0	7	0	0	1/3	0	14/33	0	8/39	0	16/429

TABLE VII. – $P_{n_+,n_0,n}$ *for 8 spin 1 particles.*

M	n_+	n_0	n_-	J						
				0	1	2	3	4	5	6
6	7	0	1							13/15
	6	2	0							79/105
5	6	1	1						66/91	8/35
	5	3	0						115/182	19/70
4	6	0	2					9/13	22/91	2/35
	5	2	1					84/143	157/546	233/2310
	4	4	0					367/715	136/455	52/385
3	5	1	2				35/66	87/286	34/273	8/231
	4	3	1				224/495	4/13	263/1638	13/210
	3	5	0				157/396	171/572	148/819	20/231
2	5	0	3			5/11	7/22	45/286	5/91	1/77
	4	2	2			37/99	14/45	138/715	361/4095	97/3465
	3	4	1			74/231	193/660	4159/20020	157/1365	8/165
	2	6	0			65/231	3/11	213/1001	12/91	16/231
1	4	1	3		4/15	10/33	7/30	37/286	2/39	16/1 155
	3	3	2		31/140	251/924	13/55	783/5005	11/140	131/4620
	2	5	1		4/21	170/693	91/396	683/4004	82/819	158/3465
	1	7	0		1/6	5/22	7/33	27/143	4/39	4/55
0	4	0	4	1/9	4/15	28/99	98/495	14/143	4/117	4/495
	3	2	3	11/126	31/140	727/2772	107/495	12/91	193/3276	23/1260
	2	4	2	23/315	4/21	166/693	43/198	1523/10010	68/819	118/3465
	1	6	1	4/63	1/6	305/1386	7/33	162/1001	4/39	172/3465
	0	8	0	1/9	0	40/99	0	48/143	0	64/495

TABLE VIII. – $^*P^J_{m_1,m_2}$ *for 2 spin 1 particles.*

M	m_1	m_2	J			$2!$
			0	1	2	$n_+!\,n_0!\,n_-!$
2	+	+			1.0000	1
1	+	0		1.0000	1.0000	2
0	0	0	0.3333	0.0000	0.6666	1
	+	−	0.6666	1.0000	0.3333	2
	$\varrho(J)$		1	1	1	

TABLE IX. – $^*P^J_{n_+,n_0,n_-}$ *for 3 spin 1 particles.*

M	n_+	n_0	n_-	J				$3!$
				0	1	2	3	$n_+!\,n_0!\,n_-!$
3	3	0	0				1.0000	1
2	2	1	0			2.0000	1.0000	3
1	2	0	1		1.8000	1.0000	0.2000	3
	1	2	0		1.2000	1.0000	0.8000	3
0	1	1	1	1.0000	2.4000	2.0000	0.6000	6
	0	3	0	0.0000	0.6000	0.0000	0.4000	1
	$\varrho(J)$			1	3	2	1	

TABLE X. – $^*P^J_{n_+,n_0,n_-}$ *for 4 spin 1 particles.*

M	n_+	n_0	n_-	J					$4!$
				0	1	2	3	4	$n_+!\,n_0!\,n_-!$
4	4	0	0					1.0000	1
3	3	1	0				3.0000	1.0000	4
2	3	0	1			2.8571	1.0000	0.1429	4
	2	2	0			3.1429	2.0000	0.8571	6
1	2	1	1		4.8000	4.5714	2.2000	0.4286	12
	1	3	0		1.2000	1.4286	0.8000	0.5714	4
0	2	0	2	1.2000	2.4000	1.7143	0.6000	0.0857	6
	1	2	1	1.6000	3.6000	3.7143	2.4000	0.6857	12
	0	4	0	0.2000	0.0000	0.5714	0.0000	0.2286	1
	$\varrho(J)$			3	6	6	3	1	

TABLE XI. – ${}^*P^J_{n_+,n_0,n_-}$ *for 5 spin 1 particles.*

M	n_+	n_0	n_-	J						$\frac{5!}{n_+!\,n_0!\,n_-!}$
				0	1	2	3	4	5	
5	5	0	0						1.0000	1
4	4	1	0					4.0000	1.0000	5
3	4	0	1				3.8889	1.0000	0.1111	5
	3	2	0				6.1111	3.0000	0.8889	10
2	3	1	1			10.7143	6.6667	2.2857	0.3333	20
	2	3	0			4.2857	3.3333	1.7143	0.6667	10
1	3	0	2		4.2857	3.5714	1.6667	0.4286	0.0476	10
	2	2	1		9.4286	10.0000	7.0000	3.0000	0.5714	30
	1	4	0		1.2857	1.4286	1.3333	0.5714	0.3810	5
0	2	1	2	4.0000	9.4286	9.2857	5.3333	1.7143	0.2381	30
	1	3	1	2.0000	5.1429	5.7143	4.2222	2.2857	0.6349	20
	0	5	0	0.0000	0.4286	0.0000	0.4444	0.0000	0.1270	1
$\varrho(J)$				6	15	15	10	4	1	

TABLE XII. – ${}^*P_{n_+,n_0,n_-}$ *for 6 spin 1 particles.*

M	n_+	n_0	n_-	J							$\frac{6!}{n_+!\,n_0!\,n_-!}$
				0	1	2	3	4	5	6	
6	6	0	0							1.0000	1
5	5	1	0						5.0000	1.0000	6
4	5	0	1					4.9091	1.0000	0.0909	6
	4	2	0					10.0909	4.0000	0.9091	15
3	4	1	1				18.6667	8.7273	2.3333	0.2727	30
	3	3	0				10.3333	6.2727	2.6667	0.7273	20
2	4	0	2			8.3333	4.6667	1.6363	0.3333	0.0303	15
	3	2	1			26.1905	19.6667	10.3247	3.3333	0.4848	60
	2	4	0			5.4762	4.6667	3.0390	1.3333	0.4848	15
1	3	1	2		19.2857	20.2381	13.3333	5.6104	1.3810	0.1515	60
	2	3	1		15.4286	18.0952	14.3333	8.2987	3.2380	0.6061	60
	1	5	0		1.2857	1.6667	1.3333	1.0909	0.3810	0.2424	6
0	3	0	3	2.8571	6.4286	5.9524	3.3333	1.1688	0.2381	0.0216	20
	2	2	2	9.4286	23.1429	25.7143	19.0000	9.4675	2.8571	0.3896	90
	1	4	1	2.5714	6.4286	7.8571	6.6667	4.0519	1.9048	0.5195	30
	0	6	0	0.1429	0.0000	0.4762	0.0000	0.3117	0.0000	0.0693	1
$\varrho(J)$				15	36	40	29	15	5	1	

TABLE XIII. – ${}^{*}P^{J}_{n_+,n_0,n_-}$ *for 7 spin 1 particles.*

M	n_+	n_0	n_-	J = 0	1	2	3	4	5	6	7	$7!/(n_+!\,n_0!\,n_-!)$
7	7	0	0								1.0000	1
6	6	1	0							6.0000	1.0000	7
5	6	0	1						5.9230	1.0000	0.0769	7
	5	2	0						15.0769	5.0000	0.9230	21
4	5	1	1					28.6364	10.7692	2.3636	0.2308	42
	4	3	0					20.3636	10.2308	3.6364	0.7692	35
3	5	0	2				13.3636	5.7273	1.6154	0.2727	0.0210	21
	4	2	1				54.9394	32.4545	13.6410	3.5454	0.4196	105
	3	4	0				15.6970	10.8181	5.7436	2.1818	0.5594	35
2	4	1	2			46.6667	34.1515	17.1818	5.7436	1.1515	0.1049	105
	3	3	1			51.6667	43.6970	27.4546	12.7436	3.8788	0.5594	104
	2	5	0			6.6667	6.1515	4.3636	2.5128	0.9697	0.3357	21
1	4	0	3		11.6667	11.667	7.4242	3.1818	0.8974	0.1515	0.0117	35
	3	2	2		55.0000	63.3333	49.8485	28.0909	10.8718	2.5758	0.2797	210
	2	4	1		23.0000	28.3333	25.0303	16.6364	8.4104	3.0303	0.5594	105
	1	6	0		1.3333	1.6667	1.6970	1.0909	0.8204	0.2424	0.1492	7
0	3	1	3	15.0000	36.6667	40.0000	28.6364	14.0909	4.6154	0.9091	0.0816	140
	2	3	2	18.0000	46.0000	55.0000	45.8182	28.3637	12.6923	3.6364	0.4895	210
	1	5	1	3.0000	8.0000	10.0000	9.1212	6.5454	3.4872	1.4545	0.3916	30
	0	7	0	0.0000	0.3333	0.0000	0.4242	0.0000	0.2051	0.0000	0.0373	1
		$\varrho(J)$		36	91	105	84	49	21	6	1	

TABLE XV. – $^{(j_1 j_2 j_3)}P^0_{m_1,m_2,m_3}\left(\sum m_i = 0\right)$.

j_1	j_2	m_1	m_2	m_3	j_3			
					0	1	2	3
1/2	1/2							
		1/2	1/2	— 1		1/3		
		1/2	— 1/2	0	1/2	1/6		
3/2	1/2							
		3/2	1/2	— 2			1/5	
		3/2	— 1/2	— 1		1/4	1/20	
		1/2	1/2	— 1		1/12	3/20	
		1/2	— 1/2	0		1/6	1/10	
3/2	3/2							
		3/2	3/2	— 3				1/7
		3/2	1/2	— 2			1/10	1/14
		3/2	— 1/2	— 1		1/10	1/10	1/35
		3/2	— 3/2	0	1/4	3/20	1/20	1/140
		1/2	1/2	— 1		2/15	0	3/35
		1/2	— 1/2	0	1/4	1/60	1/20	9/140

TABLE XVI. – $^{(j_1 j_2 j_3)*}P^0_{m_1 m_2 m_3}\left(\sum m_i = 0\right)$.

j_1	j_2	m_1	m_2	m_3	j_3				permut.
					0	1	2	3	
1/2	1/2								
		1/2	1/2	— 1		0.3333			1
		1/2	— 1/2	0	1.0000	0.3333			2
3/2	1/2								
		3/2	1/2	— 2			0.2000		1
		3/2	— 1/2	— 1		0.2500	0.0500		1
		1/2	1/2	— 1		0.0833	0.1500		1
		1/2	— 1/2	0		0.1667	0.1000		1
3/2	3/2								
		3/2	3/2	— 3				0.1429	1
		3/2	1/2	— 2			0.2000	0.1429	2
		3/2	— 1/2	— 1		0.2000	0.2000	0.0572	2
		3/2	— 3/2	0	0.5000	0.3000	0.1000	0.0143	2
		1/2	1/2	— 1		0.1333	0.0000	0.0857	1
		1/2	— 1/2	0	0.5000	0.3333	0.1000	0.1286	2

TABLE XIV. – ${}^{*}P^{J}_{n_+ n_0 n_-}$ *for 8 spin 1 particles.*

M	n_+	n_0	n_-	J							$\frac{8!}{n_+!\, n_0!\, n_-!}$
				0	1	2	3	4	5	6	
6	7	0	1							6.9333	8
	6	2	0							21.0667	28
5	6	1	1						40.6154	12.8000	56
	5	3	0						35.3846	15.2000	56
4	6	0	2					19.3846	6.7692	1.6000	28
	5	2	1					98.6853	48.3077	16.9455	168
	4	4	0					35.9301	20.9231	9.4545	70
3	5	1	2				89.0909	51.1049	20.9231	5.8182	168
	4	3	1				126.7071	86.1538	44.9572	17.3333	280
	3	5	0				22.2020	16.7413	10.1197	4.8485	56
2	5	0	3			25.4546	17.8182	8.8112	3.0769	0.7272	56
	4	2	2			156.9697	130.6667	81.0629	37.0256	11.7576	420
	3	4	1			89.6970	81.8788	58.1678	32.2051	13.5758	280
	2	6	0			7.8788	7.6363	5.9581	3.6923	1.9394	28
1	4	1	3		74.6667	84.8484	65.3333	36.2238	14.3590	3.8788	280
	3	3	2		124.0000	152.1212	132.3636	87.6084	44.0000	15.8788	560
	2	5	1		32.0000	31.2121	38.6061	28.6573	16.8205	7.6607	168
	1	7	0		1.3333	1.8182	1.6970	1.5105	0.8025	0.5818	8
0	4	0	4	7.7778	18.6667	19.7980	13.8586	6.8531	2.3932	0.5656	70
	3	2	3	48.8889	124.0000	146.8687	121.0506	73.8462	32.9914	10.2222	560
	2	4	2	30.6667	80.0000	100.6061	91.2121	63.9021	34.8718	14.3030	420
	1	6	1	3.5556	9.3333	12.3232	11.8788	9.0629	5.7436	2.7798	56
	0	8	0	0.1111	0.0000	0.4040	0.0000	0.3357	0.0000	0.1293	1
		$\varrho(J)$		91	232	284	238	154	76	28	

TABLE XVII. – ${}^{(j_1 j_2 j_3)}P^1_{m_1 m_2 m_3}$ $\left(\sum m_i = 0\right)$.

j_1	j_2	m_1	m_2	m_3	j_3				
					0	1	2	3	4
1/2	1/2								
		1/2	1/2	— 1		1/2	3/10		
		1/2	— 1/2	0	1/2	1/2	1/5		
3/2	1/2								
		3/2	1/2	— 2			2/5	1/7	
		3/2	— 1/2	— 1		9/20	1/4	2/35	
		1/2	1/2	— 1		21/60	3/20	6/35	
		1/2	— 1/2	0	1/2	1/5	1/5	9/70	
3/2	3/2								
		3/2	3/2	— 3				9/28	1/12
		3/2	1/2	— 2			19/70	1/7	1/14
		3/2	— 1/2	— 1		3/10	13/70	17/140	1/28
		3/2	— 3/2	0	9/20	7/20	27/140	9/140	1/105
		1/2	1/2	— 1		1/5	9/35	3/140	3/28
		1/2	— 1/2	0	1/20	7/20	19/140	9/140	3/35

TABLE XVIII. – ${}^{(j_1 j_2 j_3)*}P^1_{m_1 m_2 m_3}$ $\left(\sum m_i = 0\right)$.

j_1	j_2	m_1	m_2	m_3	j_3					permut.
					0	1	2	3	4	
1/2	1/2									
		1/2	1/2	— 1		0.5000	0.3000			1
		1/2	— 1/2	0	1.0000	1.0000	0.4000			2
3/2	1/2									
		3/2	1/2	— 2			0.4000	0.1429		1
		3/2	— 1/2	— 1			0.2500	0.0571		1
		1/2	1/2	— 1		0.3500	0.1500	0.1714		1
		1/2	— 1/2	0	0.5000	0.2000	0.2000	0.1286		1
3/2	3/2									
		3/2	3/2	— 3					0.0833	1
		3/2	1/2	— 2			0.5428	0.2857	0.1429	2
		3/2	— 1/2	— 1		0.6000	0.3714	0.2429	0.0714	2
		3/2	— 3/2	0	0.9000	0.7000	0.3857	0.1286	0.0190	2
		1/2	1/2	— 1		0.2000	0.2571	0.0214	0.1071	1
		1/2	— 1/2	0	0.1000	0.7000	0.2714	0.1286	0.1714	2

TABLE XIX. – $^{(j_1 j_2 j_3)}P^{1}_{m_1 m_2 m_3}$ $\left(\sum m_i = 1\right)$.

j_1	j_2	m_1	m_2	m_3	j_3				
					0	1	2	3	4
1/2	1/2								
		1/2	1/2	0	1	1/2	1/10		
		1/2	– 1/2	1		3/4	3/20		
		– 1/2	– 1/2	2			3/5		
3/2	1/2								
		3/2	1/2	– 1		3/5	1/5	1/35	
		3/2	– 1/2	0	3/4	9/20	3/20	3/140	
		1/2	1/2	0	1/4	7/20	1/4	9/140	
		1/2	– 1/2	1		3/10	3/10	3/35	
		– 1/2	1/2	1		3/10	3/10	3/35	
		– 1/2	– 1/2	2			3/10	3/14	
		– 3/2	1/2	2			1/2	1/14	
		– 3/2	– 1/2	3				3/7	
3/2	3/2								
		3/2	3/2	– 2			3/7	3/28	1/84
		3/2	1/2	– 1		3/10	17/70	29/280	1/56
		3/2	– 1/2	0	3/10	3/10	3/14	3/35	1/70
		3/2	– 3/2	1		1/2	3/14	3/56	1/168
		1/2	1/2	0	2/5	1/5	1/7	9/70	3/70
		1/2	– 1/2	1		3/10	9/70	39/280	3/56
		– 1/2	– 1/2	2			9/35	3/28	3/28
		3/2	1/2	2			2/7	5/28	1/28
		– 3/2	– 1/2	3				15/56	1/8
		– 3/2	– 3/2	4					1/3

TABLE XX. $^{(j_1 j_2 j_3)*}P^{1}_{m_1 m_2 m_3}\left(\sum m_i - 1\right)$.

j_1	j_2	m_1	m_2	m_3	j_3				
					0	1	2	3	4
1/2	1/2								
		1/2	1/2	0	1.0000	0.5000	0.1000		
		1/2	−1/2	1		1.5000	0.3000		
		−1/2	−1/2	2			0.6000		
3/2	1/2								
		3/2	1/2	−1		0.6000	0.2000	0.0286	
		3/2	−1/2	0	0.7500	0.4500	0.1500	0.0214	
		1/2	1/2	0	0.2500	0.3500	0.2500	0.0643	
		1/2	−1/2	1		0.6000	0.6000	0.1714	
		1/2	−1/2	2			0.3000	0.2142	
		−3/2	1/2	2			0.5000	0.0714	
		−3/2	−1/2	3				0.4285	
3/2	3/2								
		3/2	3/2	−2			0.4286	0.1071	0.0119
		3/2	1/2	−1		0.6000	0.4857	0.2071	0.0357
		3/2	−1/2	0	0.6000	0.6000	0.4286	0.1714	0.0286
		3/2	−3/2	1		1.0000	0.4286	0.1071	0.0119
		1/2	1/2	0	0.4000	0.2000	0.1429	0.1286	0.0429
		1/2	1/2	1		0.6000	0.2571	0.2786	0.1071
		1/2	−3/2	2			0.5714	0.3571	0.0714
		−1/2	−1/2	2			0.2571	0.1071	0.1071
		−1/2	−3/2	3				0.5357	0.2500
		−3/2	−3/2	4					0.3333

TABLE XXI. – $^*P^1$ *for 2 spin* $\frac{1}{2}$ *and n spin 1 particles.*

n	m_1	m_2	n_+	r_0	n_-	$^*P^1_{m_1,m_2;n_+,n_0,n_-}$ (fractional)	(decimal)
0	1/2	1/2	0	0	0	1	1.000
1	1/2	1/2	0	1	0	1/2	0.500
	1/2	−1/2	1	0	0	3/2	1.500
2	1/2	1/2	0	2	0	2/5	0.400
			1	0	1	6/5	1.200
	1/2	−1/2	1	1	0	9/5	1.800
	−1/2	−1/2	2	0	0	3/5	0.600
3	1/2	1/2	1	1	1	12/5	2.400
			0	3	0	3/10	0.300
	1/2	−1/2	1	2	0	21/10	2.100
			2	0	1	3	3.000
	−1/2	−1/2	2	1	0	6/5	1.200
4	1/2	1/2	2	0	2	18/7	2.572
			1	2	1	132/35	3.771
			0	4	0	9/35	0.257
	1/2	−1/2	1	3	0	78/35	2.229
			2	1	1	60/7	8.571
	−1/2	−1/2	2	2	0	66/35	1.886
			3	0	1	12/7	1.714
5	1/2	1/2	2	1	2	135/14	9.643
			1	3	1	36/7	5.143
			0	5	0	3/14	0.214
	1/2	1/2	1	4	0	33/14	2.357
			2	2	1	120/7	17.142
			3	0	2	15/2	7.500
	1/2	−1/2	2	3	0	18/7	2.571
			3	1	1	45/7	6.429

TABLE XXII. – $^{*}P^{1}$ *for* 1 *spin* $\frac{3}{2}$, 1 *spin* $\frac{1}{2}$ *and* n *spin* 1 *particles.*

n	m_1	m_2	n_+	n_0	n_-	$^{(\frac{3}{2},\frac{1}{2},1,\ldots)}{}^{*}P^{1}_{m_1,m_2;n_+,n_0,n_-}$ (fractional)	(decimal)
0	3/2	– 1/2	0	0	0	3/4	0.750
	1/2	1/2	0	0	0	1/4	0.250
1	3/2	1/2	0	0	1	3/5	0.600
	3/2	– 1/2	0	1	0	9/20	0.450
	1/2	1/2	0	1	0	7/20	0.350
	1/2	– 1/2	1	0	0	3/5	0.600
2	3/2	1/2	0	1	1	4/5	0.800
	3/2	– 1/2	0	2	0	7/20	0.350
			1	0	1	1	1.000
	1/2	1/2	0	2	0	1/4	0.250
			1	0	1	3/5	0.600
	1/2	– 1/2	1	1	0	6/5	1.200
	– 1/2	– 1/2	2	0	0	3/10	0.300
	– 3/2	1/2	2	0	0	1/2	0.500
3	3/2	1/2	1	2	0	33/35	0.943
			2	0	1	9/7	1.286
	3/2	– 1/2	0	3	0	39/140	0.279
			1	1	1	15/7	2.143
	1/2	1/2	0	3	0	33/140	0.236
			1	1	1	57/35	1.629
	1/2	– 1/2	1	2	0	51/35	1.457
			2	0	1	12/7	1.714
	– 1/2	– 1/2	2	1	0	57/70	0.814
	– 3/2	1/2	2	1	0	15/14	1.071
	– 3/2	– 1/2	3	0	0	3/7	0.429

TABLE XXII (*continued*).

n	m_1	m_2	n_+	n_0	n_-	$(\frac{3}{2},\frac{1}{2},1,\ldots)*P^1_{m_1,m_2;n_+,n_0,n_-}$ (fractional)	(decimal)
			1	3	0	36/35	1.029
	3/2	1/2	2	1	1	27/7	3.857
			0	4	0	33/140	0.236
	3/2	−1/2	1	2	1	24/7	3.429
			2	0	2	9/4	2.250
			0	4	0	27/140	0.193
	1/2	1/2	1	2	1	96/35	2.743
4			2	0	2	45/28	1.607
			1	3	0	12/7	1.714
	1/2	−1/2	2	1	1	6	6.000
			2	2	0	48/35	1.371
	−1/2	−1/2	3	0	1	15/14	1.071
			2	2	0	12/7	1.714
	−3/2	1/2	3	0	1	3/2	1.500
	−3/2	−1/2	3	1	0	9/7	1.286
			1	4	0	23/21	1.095
	3/2	1/2	2	2	1	55/7	7.857
			3	0	2	10/3	3.333
			0	5	0	17/84	0.202
	3/2	−1/2	1	3	1	100/21	4.762
			2	1	2	35/4	8.750
			0	5	0	5/28	0.179
	1/2	1/2	1	3	1	4	4.000
			2	1	2	195/28	6.964
			1	4	0	13/7	1.857
5	1/2	−1/2	2	2	1	90/7	12.857
			3	0	2	5	5.000
			2	3	0	2	2.000
	−1/2	−1/2	3	1	1	65/14	4.642
			2	3	0	50/21	2.379
	−3/2	1/2	3	1	1	35/6	5.833
			3	2	0	55/21	2.619
	−3/2	−1/2	4	0	1	5/3	1.667

TABLE XXIII. – $^*P^1$ *for 2 spin* $\frac{3}{2}$ *and n spin 1 particles.*

n	m_1	m_2	n_+	n_0	n_-	$^*P^1_{m_1,m_2;\,n_+,n_0,n_-}$ (fractional)	$^*P^1_{m_1,m_2;\,n_+,n_0,n_-}$ (decimal)
0	3/2	– 1/2	0	0	0	3/5	0.600
	1/2	1/2	0	0	0	2/5	0.400
1	3/2	1/2	0	0	1	3/5	0.600
	3/2	– 1/2	0	1	0	3/5	0.600
	3/2	– 3/2	1	0	0	1	1.000
	1/2	1/2	0	1	0	1/5	0.200
	1/2	– 1/2	1	0	0	3/5	0.600
2	3/2	3/2	0	0	2	3/7	0.429
	3/2	1/2	0	1	1	38/35	1.086
	3/2	– 1/2	0	2	0	17/35	0.486
			1	0	1	8/7	1.143
	3/2	– 3/2	1	1	0	10/7	1.429
	1/2	1/2	0	2	0	8/35	0.229
			1	0	1	18/35	0.514
	1/2	– 1/2	1	1	0	6/7	0.857
	1/2	– 3/2	2	0	0	4/7	0.571
	– 1/2	– 1/2	2	0	0	9/35	0.257
3	3/2	3/2	2	1	0	27/28	0.964
	3/2	1/2	1	2	0	48/35	1.371
			2	0	1	45/28	1.607
	3/2	– 1/2	0	3	0	3/7	0.429
			1	1	1	3	3.000
	3/2	– 3/2	1	2	0	12/7	1.714
			2	0	1	9/4	2.250
	1/2	1/2	0	3	0	6/35	0.171
			1	1	1	87/70	1.243
	1/2	– 1/2	1	2	0	6/5	1.200
			2	0	1	39/28	1.393
	1/2	– 3/2	2	1	0	3/2	1.500
	– 1/2	– 1/2	2	1	0	87/140	0.622
	– 1/2	– 3/2	3	0	0	15/28	0.536
4	3/2	3/2	2	2	0	11/7	1.571
			3	0	1	4/3	1.333
	3/2	1/2	1	3	0	8/5	1.600
			2	1	1	39/7	5.571

TABLE XXIII (*continued*).

n	m_1	m_2	n^+	n_0	n^-	$^*P^1_{m_1,m_2;n_+,n_0,n_-}$ (fractional)	(decimal)
			0	4	0	13/35	0.371
	3/2	− 1/2	1	2	1	36/7	5.142
			2	0	2	3	3.000
	3/2	− 3/2	1	3	0	40/21	1.905
			2	1	1	7	7.000
			0	4	0	6/35	0.171
	1/2	1/2	1	2	1	78/35	2.228
			2	0	2	9/7	1.286
4			1	3	0	48/35	1.371
	1/2	− 1/2	2	1	1	33/7	4.714
			2	2	0	18/7	2.571
	1/2	3/2	3	0	1	2	2.000
			2	2	0	39/35	1.114
	1/2	1/2	3	0	1	6/7	0.857
	1/2	− 3/2	3	1	0	13/7	1.857
	3/2	− 3/2	4	0	0	1/3	0.333
			2	3	0	31/14	2.214
	3/2	3/2	3	1	1	16/3	5.333
			1	4	0	37/21	1.762
	3/2	1/2	2	2	1	169/14	12.071
			3	0	2	14/3	4.666
			0	5	0	1/3	0.33
	3/2	− 1/2	1	3	1	158/21	7.524
			2	1	2	13	13.000
			1	4	0	43/21	2.048
	3/2	− 3/2	2	2	1	29/2	14.500
			3	0	2	6	6.000
			0	5	0	1/7	0.143
5	1/2	1/2	1	3	1	23/7	3.286
			2	1	2	39/7	5.571
			1	4	0	11/7	1.571
	1/2	− 1/2	2	2	1	21/2	10.500
			3	0	2	4	4.000
			2	3	0	79/21	3.762
	1/2	3/2	3	1	1	26/3	8.666
			2	3	0	23/14	1.643
	− 1/2	− 1/2	3	1	1	26/7	3.714
			3	2	0	169/42	4.024
	− 1/2	− 3/2	4	0	1	7/3	2.333
	− 3/2	3/2	4	1	0	4/3	1.333

INDICE DEL SUPPLEMENTO

AL VOLUME XV, SERIE X, DEL

NUOVO CIMENTO

Anno 1960

Fine del *Supplemento* al Vol. XV, Serie X
del *Nuovo Cimento*, 1960

Direttore responsabile: G. POLVANI Tipografia Compositori - Bologna

Questo Fascicolo del *Supplemento* è stato licenziato dai torchi il 14-III-1960